GFZ

Helmholtz Centre
POTSDAM

HELMHOLTZ CENTRE POTSDAM
GFZ GERMAN RESEARCH CENTRE
FOR GEOSCIENCES

Marco Pilz, Cecilia Nievas, Fabrice Cotton, Karsten Prehn, Hoby Razafindrakoto, Danijel Schorlemmer, Graeme Weatherill, Thomas Spies, Thomas Lege

Seismic risk analysis in Germany: an example from the Lower Rhine Embayment

- Final report -

Scientific Technical Report STR20/02

www.gfz-potsdam.de

HELMHOLTZ
RESEARCH FOR GRAND CHALLENGES

Recommended citation

Marco Pilz, Cecilia Nievas, Fabrice Cotton, Karsten Prehn, Hoby Razafindrakoto, Danijel Schorlemmer, Graeme Weatherill, Thomas Spies, Thomas Lege (2020), Seismic risk analysis in Germany: an example from the Lower Rhine Embayment. Final report. Scientific Technical Report STR 20/02, Potsdam: GFZ German Research Centre for Geosciences.
DOI: https://doi.org/10.2312/GFZ.b103-20026

Supplementary data

Schwarz, J., H. Maiwald (2019). Bevölkerungsschutz Bund – Risikoanalyse 2019 – Szenario "Erdbeben": Vorschlag zur Schadenmodelierung im Referenzgebiet Köln (inklusive Anlage zur Altersstruktur). Bauhaus-Universität Weimar, Earthquake Damage Analysis Center (EDAC).

Imprint

Helmholtz Centre Potsdam
GFZ German Research Centre for Geosciences

Telegrafenberg
D-14473 Potsdam

Published in Potsdam, Germany
May 2020

DOI: https://doi.org/10.2312/GFZ.b103-20026
URN: urn:nbn:de:kobv:b103-20026

This work is published in the GFZ series Scientific Technical Report (STR) and electronically available at GFZ website https://www.gfz-potsdam.de

Seismic risk analysis in Germany: an example from the Lower Rhine Embayment

- Final report -

Marco Pilz[1], https://orcid.org/0000-0002-8575-579X
Cecilia Nievas[1], https://orcid.org/0000-0001-9260-9590
Fabrice Cotton[1,2], https://orcid.org/0000-0002-9242-3996
Karsten Prehn[1]
Hoby Razafindrakoto[1], https://orcid.org/0000-0002-7717-280X
Danijel Schorlemmer[1]
Graeme Weatherill[1], https://orcid.org/0000-0001-9347-2282
Thomas Spies[3]
Thomas Lege[3]

[1] GFZ German Research Centre for Geosciences, Potsdam, Germany
[2] Universität Potsdam, Institut für Geowissenschaften, Potsdam, Germany
[3] Bundesanstalt für Geowissenschaften und Rohstoffe BGR, Hannover, Germany

GFZ
Helmholtz-Zentrum
POTSDAM

Table of contents

Abstract

The Lower Rhine Embayment in western Germany is one of the most important areas of earthquake recurrence north of the Alps, facing a moderate level of seismic hazard in the European context but a significant level of risk. This study deals with the impact of a scenario earthquake with a moment magnitude of 6.5 occurring along the Erft fault system south-west to the city of Cologne, the fourth largest German city with more than one million inhabitants and accommodating important industrial facilities. Since the city is located on thick layers of Quarternary sediments, the geological discontinuities at depth will have a significant influence on the duration and the amplification of ground-motion. Based on a new, harmonized and spatially highly resolved, model of the sedimentary cover, the sensitivity of spectral intensity measures to the site response analysis method is assessed employing random vibration theory approaches. Corresponding damage calculations are conducted in terms of European Macroseismic Scale (EMS-98) damage grades. Residential buildings and buildings with mixed residential and commercial occupancy are included in the corresponding calculations only, in line with most seismic risk assessment studies which have traditionally focused on residential typologies. Results from the damage calculations are presented in terms of number of buildings exposed to bands of EMS-98 intensity levels and probabilities of EMS-98 damage grades for residential buildings and buildings with mixed residential and commercial occupancy. Casualties in the city and the neighboring districts are estimated by means of the PAGER empirical method using population counts at the quartier (“Stadtviertel”) level in Cologne, the “Bezirk” level in Bonn and Aachen and at the municipality (“Gemeinde”) level for the surrounding areas, all of these comprised within the district (“Regierungsbezirk”) of Cologne.

STR 20/02. GFZ German Research Centre for Geosciences.
DOI: 10.2312/GFZ.b103-20026

1. Introduction

The German Federal Office for Civil Protection and Disaster Assistance (Bundesamt für Bevölkerungsschutz und Katastrophenhilfe BBK) carries out the federal tasks of civil protection, planning and preparation of measures to provide emergency supplies, emergency planning as well as preparation of cooperation between the Federation and the federal states. A particular focus lies on hazard assessment, planning/conceptual prevention for the protection of critical infrastructures and informing the population. Since 2004, the federal states created individual hazard estimations following a uniform structure based on the "New strategy for the protection of the population in Germany". In 2019, the focus has been on earthquakes and the corresponding risks.
For this purpose, BBK has created a working group of geoscientists, engineers from various disciplines, planning scientists, local and federal authorities and disaster management representatives. Herein, the German Federal Institute for Geosciences and Natural Resources (BGR) in Hanover and the German Research Center for Geosciences (GFZ) in Potsdam serve as leading institutes for seismic risk assessment. Following BBK's guidelines, the analysis should represent a scientifically reasonable worst case scenario with a high level of risk due to a high population density and the existence of important economic and industrial sectors in the studied region.
Earthquake hazard in Germany is relatively low on a global scale but not negligible. In the Rhine Basin, on the Swabian Alb and in eastern Thuringia and western Saxony with the Vogtland earthquake-swarm area, minor earthquakes occur frequently (on average, there is one earthquake with a magnitude of 3.8 per year). However, earthquakes which are perceptible or even might cause damage are rare events in Germany. Nevertheless, as high-value assets are concentrated in these regions, strong events may result in major losses. In 1356, the historically strongest earthquake north of the Alps occurred in Basel close to today's border with Germany (moment magnitude M_w between 6.7 and 7.1, Fäh et al. 2009). In the Lower Rhine Embayment, the 1756 Düren event (moment magnitude according to various sources ranges from 5.6 to 5.9), the strongest event reported in Germany to date, occurred as a culmination of a multi-year long series of earthquakes in Germany. Geological investigations have shown that even events of magnitudes around 7 have occurred in this region (Grützner et al. 2016).
One should keep in mind that the level of risk (i.e. potential losses) will not only depend on the level of hazard but also on the exposure and the vulnerability of assets located in the hazard prone areas. Therefore, the risk analysis and risk management should include considerations of all relevant contributing factors.
To minimize seismic risk, the first seismic building code, DIN 4149 (German Institute for Standardization DIN), was already released in July 1957, following the 1951 Euskirchen earthquake. However, at that time it was only formulated as a recommendation and its application was considered optional. Following the 1969 and 1970 earthquakes on the Swabian Alb, in 1971, DIN 4149:1957-07 was introduced as a legally binding regulation in the state of Baden-Württemberg. In 1981, a revised earthquake standard was presented by DIN 4149-1:1981-04 although the introduction of the standard by the building authorities in some federal states did not follow until 1998. In the state of North Rhine-Westphalia the standard has never been officially introduced in the building code. Only in 2005, a completely revised version of the DIN 4149:2005 was introduced and approved by the building authorities in all

STR 20/02. GFZ German Research Centre for Geosciences.
DOI: 10.2312/GFZ.b103-20026

affected federal states without any transitional regulation (for an overview of the historical development see, for example, Keintzel 2005).
In this document, we will describe the risk analysis for the Lower Rhine Embayment that is focusing on a severe scenario earthquake occurring close to the city of Cologne. The levels of ground-motions and corresponding macroseismic intensities will be presented together with the expected consequences for the building and human environment.

STR 20/02. GFZ German Research Centre for Geosciences.
DOI: 10.2312/GFZ.b103-20026

2. Seismic hazard assessment in Germany and in the Lower Rhine Embayment

2.1. Seismicity of Germany and earthquake catalogue harmonization

The seismicity in Germany and neighboring countries is shown in the epicenter map of Figure 2.1 The study area encompasses all seismic-source regions that can generate earthquakes with shaking in Germany, i.e. from a distance of up to 250 km. The seismicity exhibits higher levels along the Alps, on the Swabian Alb, around the Vogtland and along the Rhine river.
Although earthquakes with moment magnitudes larger than 6 are not known to have occurred within Germany in the historical past, they have struck the immediate surroundings (like the 1356 Basel event) and can be expected within the country as well. The probability of such event within Germany is comparatively low, however, the impact would be important if critical regions like conurbations or specific industrial plants were to be affected.
In this case where the study region overlaps national boundaries, earthquake catalogues covering different regions need to be harmonized and combined into a composite catalogue. Because magnitudes can differ substantially between national seismological agencies, any harmonization procedure needs to be conducted carefully. The harmonization and conversion of local magnitude scales to a uniform moment magnitude scale M_w as used here is described in detail in Grünthal et al. (2009).
In this study, we will use only the moment magnitude scale (Hanks and Kanamori 1979), a measure of an earthquake's "energy" based on the seismic moment. M_w is considered the authoritative magnitude scale because it is more directly related to the released energy and does not saturate, i.e. it does not underestimate magnitudes of very large earthquakes, as other scales do under certain conditions. Nowadays, M_w is the standard magnitude scale, replacing the use of local (country-specific) magnitude scales (such as the generally known Richter local magnitude M_L) and various surface-wave magnitude scales.

2.2. Occurrence rates of major earthquakes

Any seismicity-rate estimation needs to also consider its uncertainties to be propagated into uncertainties for the resulting hazard. To reduce the rate uncertainties, historic and even paleoseismic data are usually combined with instrumentally recorded seismicity through a harmonization approach. To account for all possible sources of ground-motions in the study area, all earthquakes that are expected to have effects in the target region have to be included.

STR 20/02. GFZ German Research Centre for Geosciences.
DOI: 10.2312/GFZ.b103-20026

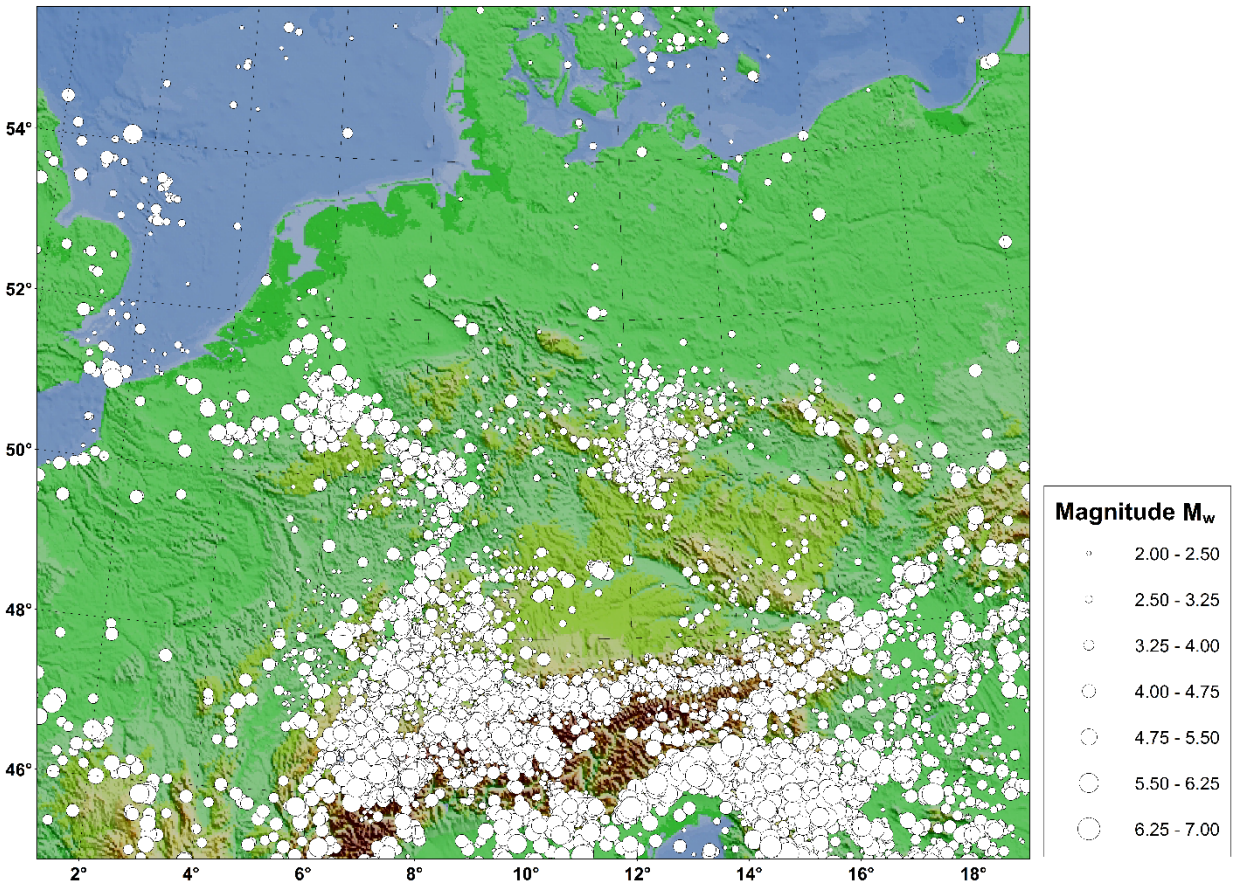

Figure 2.1: Seismicity (tectonic) in central Europe based on an updated database by Leydecker (2011), Grünthal and Wahlström (2012) and Grünthal et al. (2018). Mainshocks are shown as white circles, scaled by moment magnitude. Fore- and aftershocks are not displayed.

To estimate the seismicity rates, Grünthal et al. (2018) used a double-truncated exponential frequency function, so that the cumulative seismicity rates can be split up into a number of different magnitude-frequency relations capturing the uncertainties of the seismicity rates. Further details can be found in Grünthal et al. (2018). Figure 2.2 presents the weighted M_{max}-dependent uncertainty modeling for the Lower Rhine zone. The discretized distributions of seismicity rates (black dots in Figure 2.2) can thus be calculated for each of the discretized value of M_{max}.

STR 20/02. GFZ German Research Centre for Geosciences.
DOI: 10.2312/GFZ.b103-20026

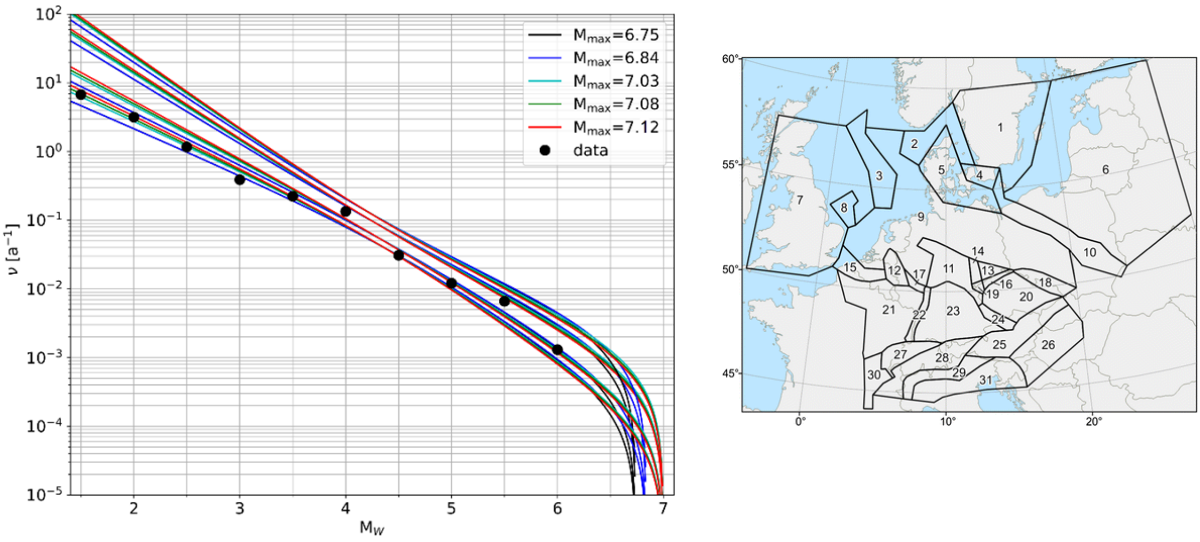

Figure 2.2: (left) Observed cumulative seismicity rates (circles) and magnitude-frequency distributions with equal weights for five different M_{max} capturing the uncertainties of the estimated seismicity rate by a four-point discretization of the resulting distribution of source zone 12 (Lower Rhine). To the right, the turquoise, the green and the red curves overlap. (right) Seismic zonation (large-scale seismic source zones) of Grünthal et al. (2018) for assessing the seismic hazard in Germany. The model represents the large-scale geological structure and tectonic architecture. The Lower Rhine area corresponds to A12 in Grünthal et al. (2018).

Thereon, a mean recurrence period of earthquakes with given moment magnitude can be assessed (for details see Grünthal et al. 2018). Figure 2.2 indicates for the Lower Rhine area that earthquakes of moment magnitude around 5.5 can be expected with a recurrence period of around 100 to 300 years while earthquakes of moment magnitude around 6.5 have a recurrence period of around 500 to 3000 years (annual frequency of $\nu \approx 1 \cdot 10^{-3}$). However, the model does not provide any spatial details of historical and modern seismicity in the area but rather it assumes the occurrence of seismicity at any place within the larger zone, including places other than those with historically known activity concentrations.

2.3. Tectonic settings of the Lower Rhine area and locations of major known active faults

The Lower Rhine area is the north-western branch of the Rhine Graben system in the border area of the Netherlands, Germany, and Belgium, which is part of the European Cenozoic rift system extending from west of the Alps to the North Sea. It extends over a distance of around 200 km between the city of Bonn in the southeast and the confluence area of the Rhine and Meuse Rivers in the northwest, and a width (measured perpendicular to the axis) of up to 75 km. During Oligocene through Pliocene, fluviatile and marginal marine sediments were deposited in the Lower Rhine Embayment. Several normal faults divide the eastern part of the Lower Rhine Embayment into blocks. Herein, the Erft fault system (ERF in Figure 2.3) is a NW-SE trending normal fault zone at the western border of the Ville mountain range and

STR 20/02. GFZ German Research Centre for Geosciences.
DOI: 10.2312/GFZ.b103-20026

separates the Erft Block in the west from the Cologne Block in the east. Its total lateral extension is around 50 km with a closest distance to the center of Cologne of 15 to 20 km. The complex system consists of several sections (10 to 15 km long). The movement history of the Erft fault system shows ongoing activities since early Tertiary times. Nowadays, the total vertical movement sums up to more than 700 m. While the bottom of the lower Pleistocene main terrace is at maximum displaced by 140 m, the top of this layer shows vertical movements of up to 60 m. The youngest sediments from late Pleistocene show a vertical offset of a few meters. The average geological slip rate is in the range of 0.05 to 0.10 mm/a (Ahorner 1962, 1988).

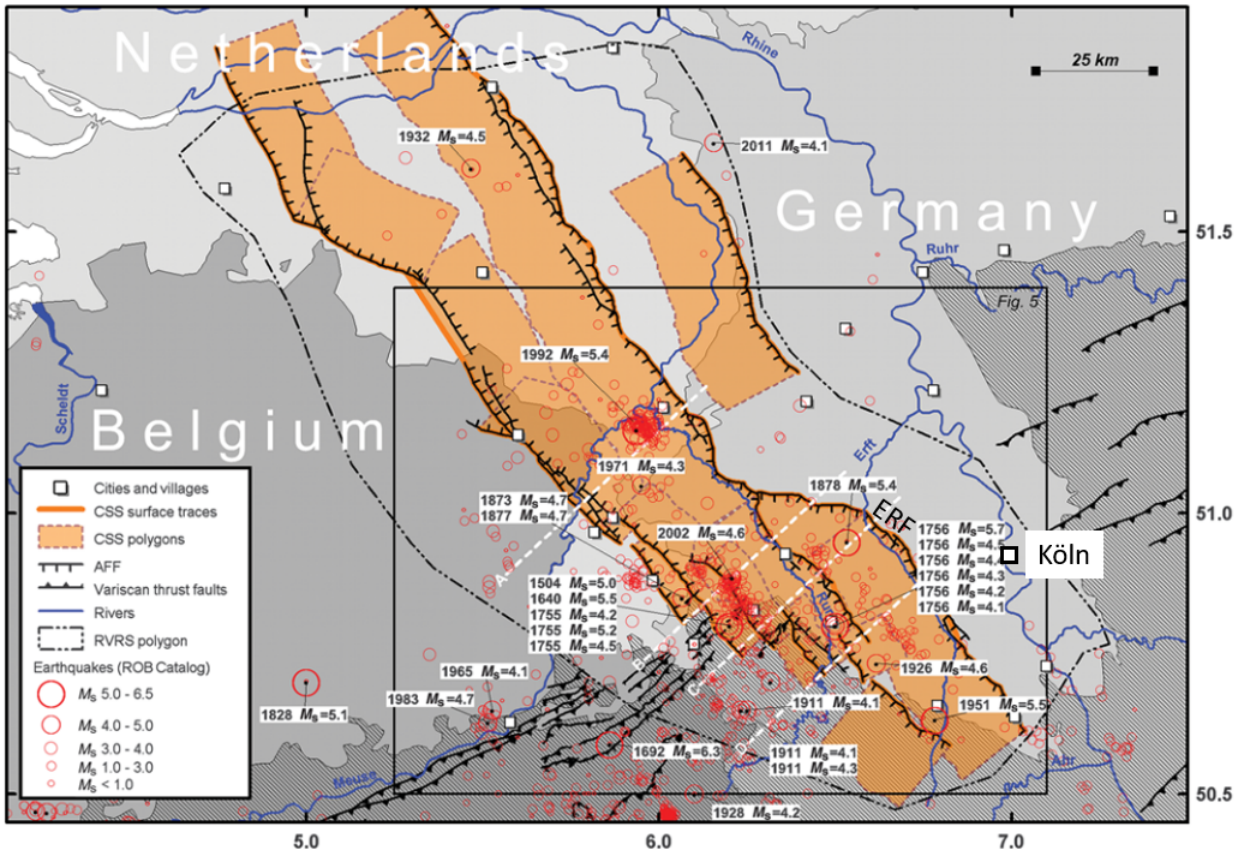

Figure 2.3: Seismotectonic setting of the northern Rhine area including the Lower Rhine Embayment represented by the dashed-dotted line. Red circles represent seismic events, scaled by magnitude. For stronger earthquakes, magnitude and year of occurrence are given. Active faults are shown as black lines. ERF represents the Erft fault system (Figure taken from Vanneste et al. 2013 and slightly modified).

2.4. Recent probabilistic seismic hazard assessment for the city of Cologne

For every spatial point, hazard calculations can be accomplished. As an example, for the city of Cologne the level of seismic hazard was assessed for soft rock conditions with an average S-wave velocity in the uppermost 30 m of the soil column of 760 m/s and for the hazard levels of occurrence, or exceedance probabilities, of 10, 5 and 2%

STR 20/02. GFZ German Research Centre for Geosciences.
DOI: 10.2312/GFZ.b103-20026

within 50 years, which correspond to the mean return periods of 475, 975 and 2475 years. Grünthal et al. (2018) computed horizontal 5%-damped Uniform Hazard response Spectra (UHS) for the spectral range of periods between 0.02 and 3.0 s. The basic hazard results are the occurrence or exceedance rates for each of the logic tree end branches for a given acceleration or site intensity at a grid point. Combinations of results for several given accelerations are derived from hazard curves for each grid point. As an example, Figure 2.4 shows a typical hazard curve for all percentiles from the 1st, 2nd, 3rd, … to the 99th for the city of Cologne. The 50th and the 84th percentile as well as the mean are highlighted.

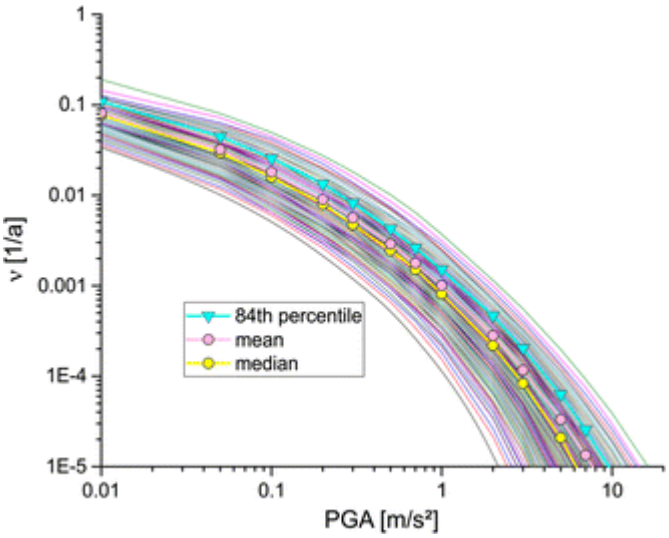

Figure 2.4: Hazard curve for peak ground acceleration (PGA) for Cologne (50.94°N, 6.96°E) for all percentiles from the 1st up to the 99th. Median, mean and the 84th percentile are highlighted

For a better understanding of the predominant sources of the hazard in the Cologne area, we created a deaggregation of the seismic hazard for this location. Deaggregations (see McGuire 1995, Bazzurro and Cornel 1999) are a different representation of the hazard model, dividing the total hazard for the site of interest into contributions based on distance and magnitude. Identifying the predominant sources of hazard can allow proper choices for the design earthquake's characteristics and for the modeling of time histories.
Figure 2.5 shows the deaggregation for the seismic hazard in Cologne. The pattern of contributions to the hazard of Cologne is rather complex, governed by a broader range of magnitudes M_w between 4.5 to 6 and distances of 10 to 40 km, with only a minor impact of Mw > 6.5 events up to around 100 km.

STR 20/02. GFZ German Research Centre for Geosciences.
DOI: 10.2312/GFZ.b103-20026

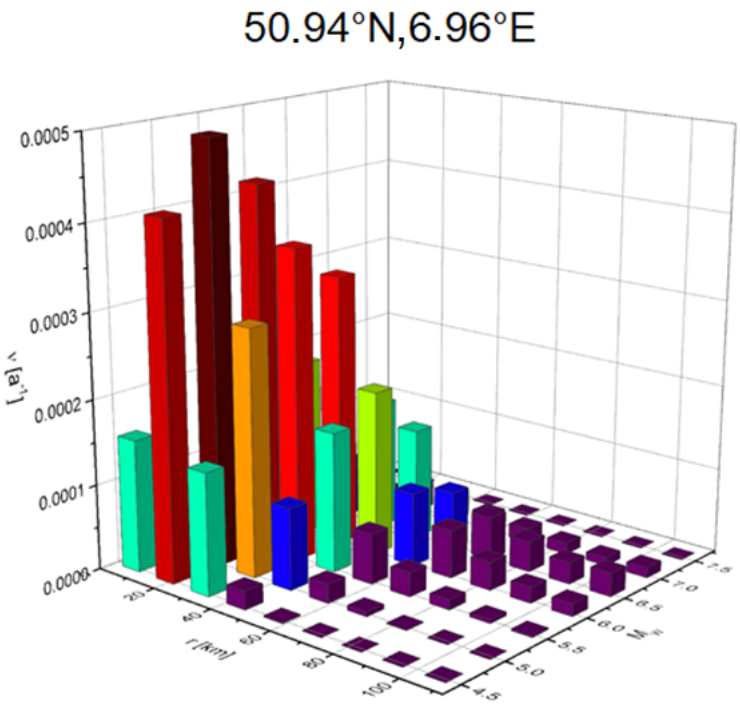

Figure 2.5: Deaggregations of peak ground acceleration (PGA) for the center of Cologne (soft rock conditions with an average S-wave velocity in the uppermost 30 m of the soil column of 760 m/s). The height of the columns is color-coded. The deaggregation is given for a return period of 475 years as rates of magnitude-distance bins as they contribute to the hazard. *v* describes the cumulative annual frequency for magnitudes $M_w > 4$.

STR 20/02. GFZ German Research Centre for Geosciences.
DOI: 10.2312/GFZ.b103-20026

3. Characterization of the sedimentary layers in the Lower Rhine Embayment

In general, seismic hazard analyses are carried out for reference site conditions. These conditions generally comprise soft/firm rock, defined as having an average S-wave velocity of 760 to 800 m/s in the top 30 meters (V_{s30}). A value of 760 m/s corresponds to the boundary between NEHRP (US National Earthquake Hazards Reduction Program) site classes B and C (BSSC 2003). On the European site, the Eurocode 8 (CEN 2003) refers to reference site conditions as sites with V_{s30} = 800 m/s.

The local subsurface geological conditions, the 3D geometry of the basin, and the surrounding outcropping bedrock as well as the geotechnical characteristics of the soil strata, however, will have a strong influence on the duration and on the level of ground-motions. This issue was first noticed already after earthquake in Istanbul in 1509. Following the 1906 San Francisco, USA, and the 1923 Kanto, Japan, earthquakes, a large number of studies were carried out indicating that there is strong correlation between subsurface geology and the strength of ground-motions and local amplification characteristics. Such characteristics, now widely known as seismic site effects, have been used to describe the influence of local geology on ground-motions.

We use the geological and geophysical 3D model of the sedimentary cover model of Weber (2007) to quantify the site effects in the southern Lower Rhine Embayment. This model is based on a hydrogeological map (Breddin 1963) covering a territory of around 3,500 km² between the cities of Aachen, Cologne, and Bonn. Weber (2007) combined different hydrogeological models with different lateral and vertical resolutions. The large-scale model (internal name A3, Breddin 1963) consists of vertical profiles reaching a depth of up to several 100 m with a lateral distance of 2 km. It was created for assessing the consequences of large open pit lignite mines on groundwater conditions. For assessing the near-surface properties with a higher spatial resolution, the model A1 consists of shallow profiles on a 1 km grid reaching a maximum depth of 100 m. Additionally, numerous boreholes for assessing ground-water levels and deeper boreholes of the Rheinische Braunkohlewerke AG (present name RWE Power AG) reaching the bedrock (depth up to 1,300 m for the Erft Block) were included in Weber's 3D model. Further details can be found in the respective publication of Weber (2007).

Weber (2007) further modeled the depth of the sediment-bedrock interface and the stratigraphic layering using borehole data, data on hard rock material properties from the hydrogeological maps of Breddin (1954), and further information on the regional stratigraphy taken from the North Rhine-Westphalia Geological Survey (Hilden 1988a, 1988b, Knapp 1988, Knauff 1988). Boreholes sites used for constructing the 3D geophysical model of the sedimentary cover in the southern Lower Rhine Embayment are shown in Figure 3.1. Figure 3.2 shows a sample drill hole (not to scale).

STR 20/02. GFZ German Research Centre for Geosciences.
DOI: 10.2312/GFZ.b103-20026

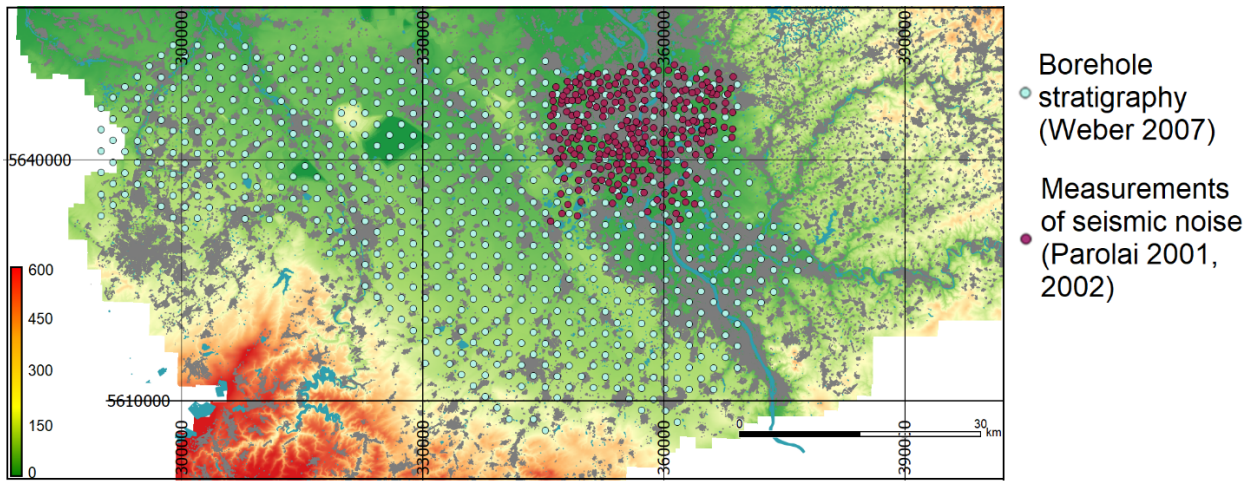

Figure 3.1: Boreholes sites across the southern Lower Rhine Embayment for which stratigraphic information are available (turquoise circles, Weber 2007). The red circles represent the sites in and around Cologne at which measurements for seismic noise have been carried out by Parolai (2001, 2002). Built-up areas are shown in gray. UTM coordinates are given for UTM zone 32.

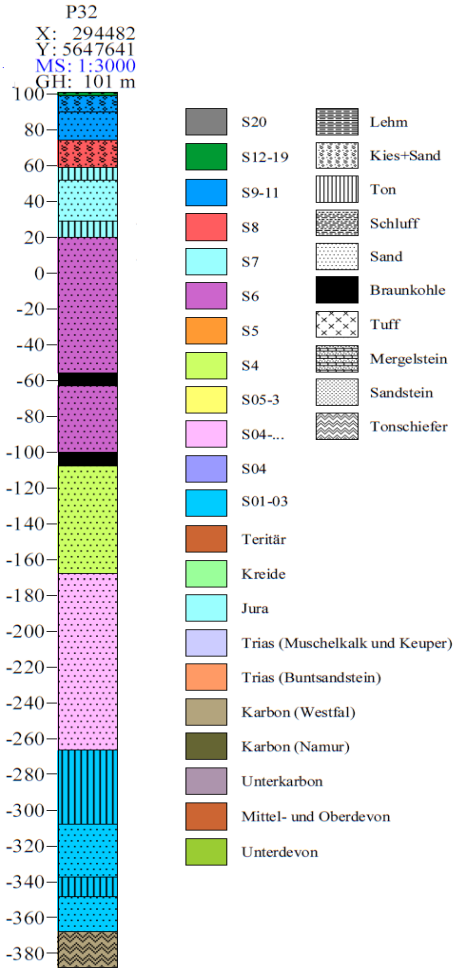

Figure 3.2: Borehole sample (here P32) taken from the original publication of Weber (2007). X and Y represent UTM coordinates in UTM zone 32. MS represents the vertical scale. GH indicates the elevation above sea level. Notation similar to Schneider and Thiele (1965). Capital letter S represents quaternary sediments.

STR 20/02. GFZ German Research Centre for Geosciences.
DOI: 10.2312/GFZ.b103-20026

The oldest stratigraphic units in the Lower Rhine Embayment are partly marine, partly brackish, limnic, and terrestrial Lower Devonian deposits on the former coastal and shelf area of the Old Red continent consisting of a monotonous succession of predominantly grey claystones, siltstones, sandstones, and quartzites. In the Tertiary, significant volcanism took place in the southeast of today's Lower Rhine Embayment accompanied by the extraction of tuffs. The tuffs cover Middle Oligocene clays, sands and gravel, and they are generally covered by tertiary sands and clays (some exceptions, however, exist). The rather thick most recent Oligocene sediments were created in an extended succession of subsidence and sedimentation leading to a wide penetration of the water level and a correspondingly long sedimentation period.
For characterizing the different stratigraphic units, Budny (1984) carried out downhole measurements at 36 sites in and in close vicinity of the Lower Rhine Embayment. For the downhole velocity survey, Budny (1984) measured the travel times of signals from an impulsive source of energy at the surface to a sequence of measurement points in the borehole. Based on Budny's measured S-wave velocities, Weber (2007) derived generalized velocity-depth relationships for various kinds of sedimentary and rock stratigraphy, further distinguishing sediment type and age of the sediments.
For all stratigraphic materials, the corresponding velocity-depth relationship can be described by a simple exponential equation

$$V_S = A\ (1 + Z)^B\ . \qquad (1)$$

Herein, A represents the reference velocity at the surface, Z represents the depth below the surface, and B is an exponential parameter for the correlation between depth and S-wave velocity V_S.
Correspondingly, while carrying out velocity measurements, Budny (1984) could similarly derive density information for sedimentary materials and rock. Weber (2007) converted the corresponding data to density-depth relationships, i.e.

$$\rho = \rho_0 + \varepsilon \ln(1 + Z). \qquad (2)$$

ρ represents the density at a depth Z below the surface, ρ_0 describes the density at the Earth's surface, and ε is a material parameter. Table 3.1 provides an overview of the material-specific parameters used of Equations 1 and 2. Please note that for Equation 2, literature parameters of Brüstle and Stange (1999) and Mason et al. (2004) have been proposed by Weber (2007) for tuff and clay because too few measurements were available for these materials in the Lower Rhine Embayment. Correspondingly, ε is set to 0 for these materials.

STR 20/02. GFZ German Research Centre for Geosciences.
DOI: 10.2312/GFZ.b103-20026

Table 3.1: Material parameters used in Equations (1) and (2) for sediments and rocks in the Lower Rhine Embayment according to Weber (2007). The coefficient of determination R^2, describing the proportion of the variance in the dependent variable that is predictable from the independent variables, can serve as an indicator for assessing the quality of the velocity and density equations.

Material	**Series / Epoch**	***A* [m/s]**	***B***	***R*²**		**ρ₀ [kg/m³]**	**ε [kg/m³]**	***R*²**		***Q*S**
Sand	Tertiary	143	0.315	0.76		1783	75.6	0.62		3-22
Clay	Tertiary	203	0.171	0.53		1942	17.4	0.02		5-22
Gravel	Quarternary & Tertiary	157	0.287	0.70		1744	70.7	0.34		2-22
Loam	Quarternary	187	0.212	0.18		1900	0	-		2-5
Silt	Tertiary	202	0.178	0.50		1802	54.9	0.49		10-24
Brown coal	Tertiary	70	0.306	0.91		1068	91.6	0.47		3-10
Tuff	Tertiary	566	0.106	0.25		2200	0	-		
Sand / Marl	Trias & Cretaceous	409	0.231	0.91		1978	57.1	0.95		5-41
Clay shale	Paleozoic	767	0.203	0.67		2281	80.3	0.65		20-85

The quality factor for various stratigraphic units has been determined by Budny (1984) for SH-waves (Q_S) only. Due to the small number of measurements, the corresponding results are not well constrained. Therefore, Budny (1984) proposed the use of the low values given in Table 3.1 only for near-surface layers (down to depths of less than 10 m). For deeper layers (> 100 m), only values larger than 10 should be used. We follow this recommendation. Because no information on the qualify factor for P-waves (Q_P) is available, we follow the empirical relationship $Q_P = 2Q_S$ (Xia et al. 2012).

Besides the studies of Weber (2007), Parolai et al. (2001, 2002) had previously carried out measurements of seismic noise at around 270 sites in the city of Cologne and to the west (measurement sites are shown in Figure 3.1), aiming at deriving a velocity model of the sedimentary cover below the city. Seismic noise is caused by a variety of spatially distributed, mostly unrelated and often continuous sources of both natural (e.g. weather, tides) as well as artificial/human noise.

Since Parolai et al. (2002) further collected information on the thickness of the sedimentary cover in the investigated area, for each measurement site, 1D-S wave velocity profiles have been calculated based on the H/V inversion method of Fäh et al. (2001, Figure 3.3). While the large-scale velocity model of Weber (2007) has been derived from a grid with a lateral resolution of 2 km (see Figure 3.1), the measurements of seismic noise allow for a much higher spatial resolution in the urban area (see Figure 3.4). The velocity model along the cross-section is constrained by 20 single 1D velocity profiles. In turn, the agreement between the stratigraphic layers and the S-wave velocity model is remarkable. Both vertical and lateral velocity variations can be clearly observed.

STR 20/02. GFZ German Research Centre for Geosciences.
DOI: 10.2312/GFZ.b103-20026

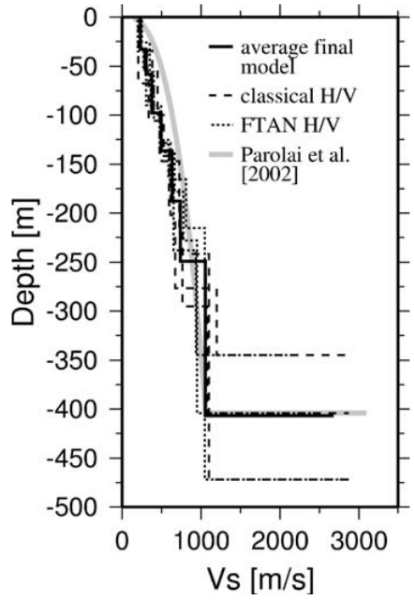

Figure 3.3: Final S-wave velocity profile using H/V-ratio inversion for the Cologne site. The thickness of the sedimentary cover was fixed while different methods were applied for the inversion. Figure taken from Parolai et al. (2006).

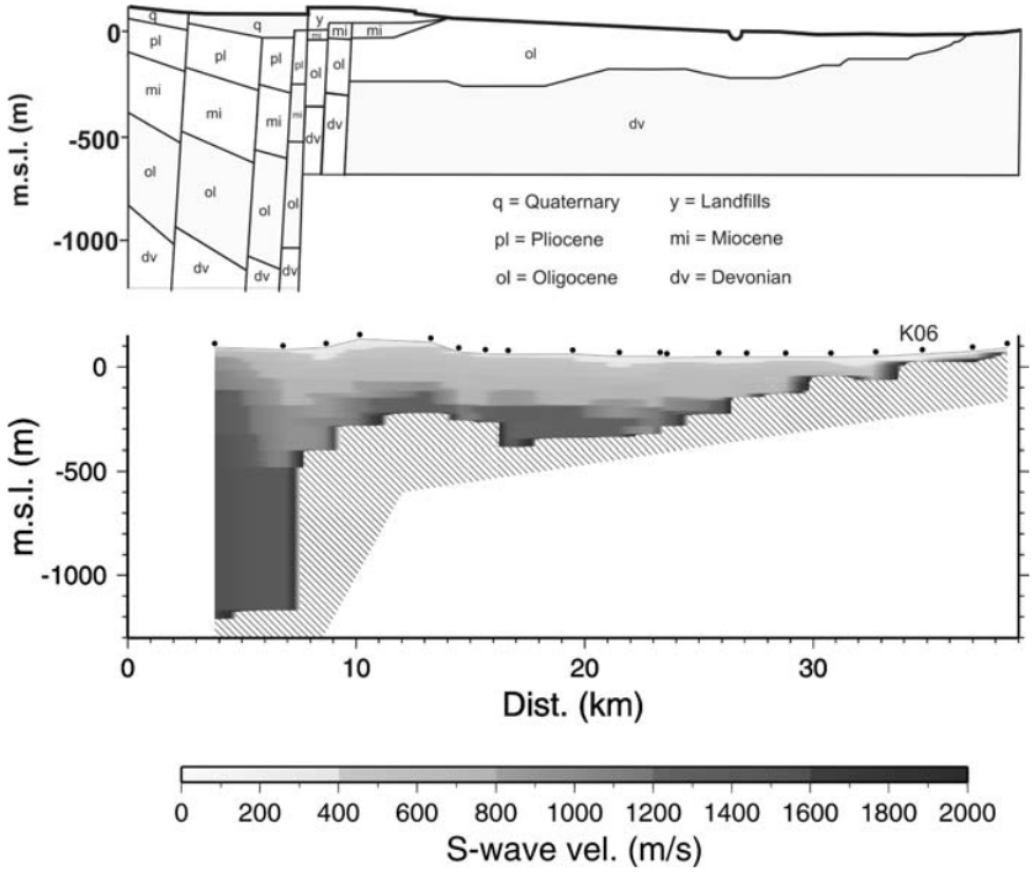

Figure 3.4: (top) Geological cross-section through the sedimentary cover in the southern Lower Rhine Embayment along the line Kerpen-Cologne-Bergisch Gladbach (Von Kamp 1986). (bottom) 2D-S-wave velocity model, generated through interpolation between 1D-velocity profiles after inversion of seismic noise measurements (black circles). The hatched area represents the Devonian bedrock. Figure taken from Parolai et al. (2006).

STR 20/02. GFZ German Research Centre for Geosciences.
DOI: 10.2312/GFZ.b103-20026

4. Quantification of site effects and their influence on the level of ground-shaking

Site response analyses help modeling the influence of near-surface layers on earthquake ground-motions. These near-surface layers act as a filter that can amplify/de-amplify the seismic waves coming from an earthquake source. Based on the complexity of the near-surface geometry and the characteristics of the layers, several approaches are possible.
In a general sense, one can distinguish between two types of subsurface geometries: flat horizontally-layered sites and valleys/canyons. Each of them requires a specific approach for a site-response analysis. A one-dimensional analysis is used whenever the stratigraphy and/or the geometry of the soil deposit is flat. In the Lower Rhine Embayment, no significant lateral stratigraphy/velocity variations are present (see Figure 3.4 and Weber (2007)), allowing for a simplification using a single multi-layered column with known material properties and assuming that the influence of 3D site effects such as basin-induced surface waves or topographic effects is minor and negligible.
We performed linear 1D-SH simulations using the available datasets (i.e. seismic velocities, density and quality factor, see Chapter 3), to calculate the theoretical transfer functions with respect to a reference velocity of V_S = 760 m/s (A transfer function describes the ratio of the output signal of a system to the input signal of a system depending on the frequency). The reason for using a reference velocity of 760 m/s is described in the following chapter. Here, we follow the classical Knopoff layer matrix description (Knopoff 1964). The model is based on an optimized form of the Thomson-Haskell formalism (Thomson 1950, Haskell 1953), which develops transfer-matrix methods quantifying the displacement and stress at the top and at the bottom of each layer in the multi-layered soil column. The corresponding waves passing vertically through a soil column are described by increasing and decreasing exponential values which should cancel each other. In reality, however, for a finite number of layers, there is no complete elimination. This problem has been solved by Knopoff (1964) by reformulating the subdeterminants. Details can be found in the respective publications.
We have calculated 1D-SH transfer functions for all sites with given velocity and attenuation information, as shown in Figure 3.1. An example transfer function for a site in Cologne is shown in Figure 4.1.

STR 20/02. GFZ German Research Centre for Geosciences.
DOI: 10.2312/GFZ.b103-20026

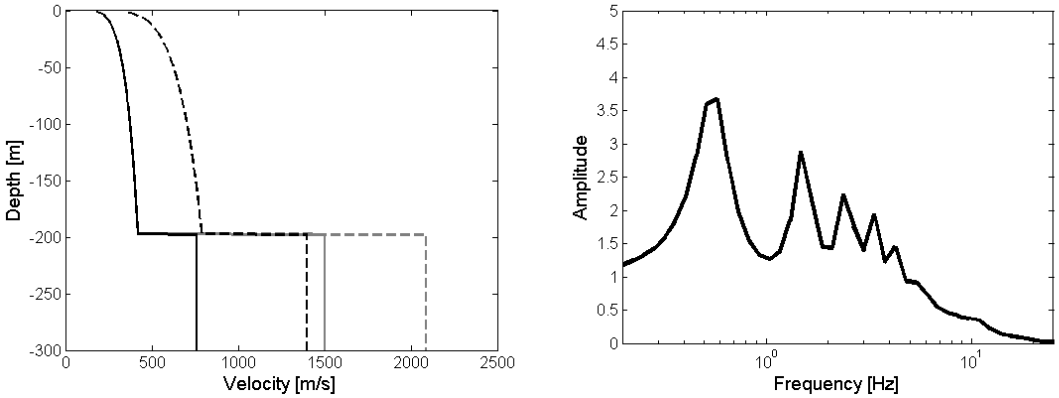

Figure 4.1: (left) Velocity profile for V_S (bold lines) and V_P (dashed lines) for a site in Cologne-Deutz (50.93° N, 7.01° E). The gray lines represent the unaltered velocity profiles as described in Chapter 3. The black lines represent velocity profiles confined at V_S = 760 m/s and V_P = 1400 m/s. (right) Corresponding 1D SH transfer function with respect to velocity profiles limited to V_S = 760 m/s and V_P = 1400 m/s.

As can be seen in Figure 4.1, the level of ground-motion is amplified significantly over a wide frequency range between approximately 0.2 and 5 Hz. The amplification, i.e. the fundamental resonance of the entire soil column, occurs at around 0.5 Hz. In this frequency range, the level of ground-motion will be amplified by a factor of six. On the contrary, high frequencies (f > 5 Hz) are significantly attenuated due to the very low quality factors of the shallow materials (see material parameters in Chapter 3).

STR 20/02. GFZ German Research Centre for Geosciences.
DOI: 10.2312/GFZ.b103-20026

5. Ground-motion modeling

There are different methodologies for site-specific modeling of ground-motion (Figure 5.1). Standard practice estimates scalar ground-motion intensity measures using empirical ground-motion prediction equations (GMPEs). As an alternative, 3D physics-based numerical simulations can serve as an appropriate tool for earthquake ground-motion prediction and for its application to seismic hazard assessment studies. While the use of GMPEs is well consolidated in the engineering community, physics-based ground-motion modeling have not been used yet for practical application. Indeed, ground-motions probability distributions for any desired seismicity scenario can easily be generated by using empirical ground-motion model through predictive relationships. The use of numerical modeling implies knowledge of the probability distribution of rupture and wave propagation properties which have not been fully calibrated yet. Therefore, our modeling of spectral intensities will be based on the use of GMPEs only (left and central part in Figure 5.1).

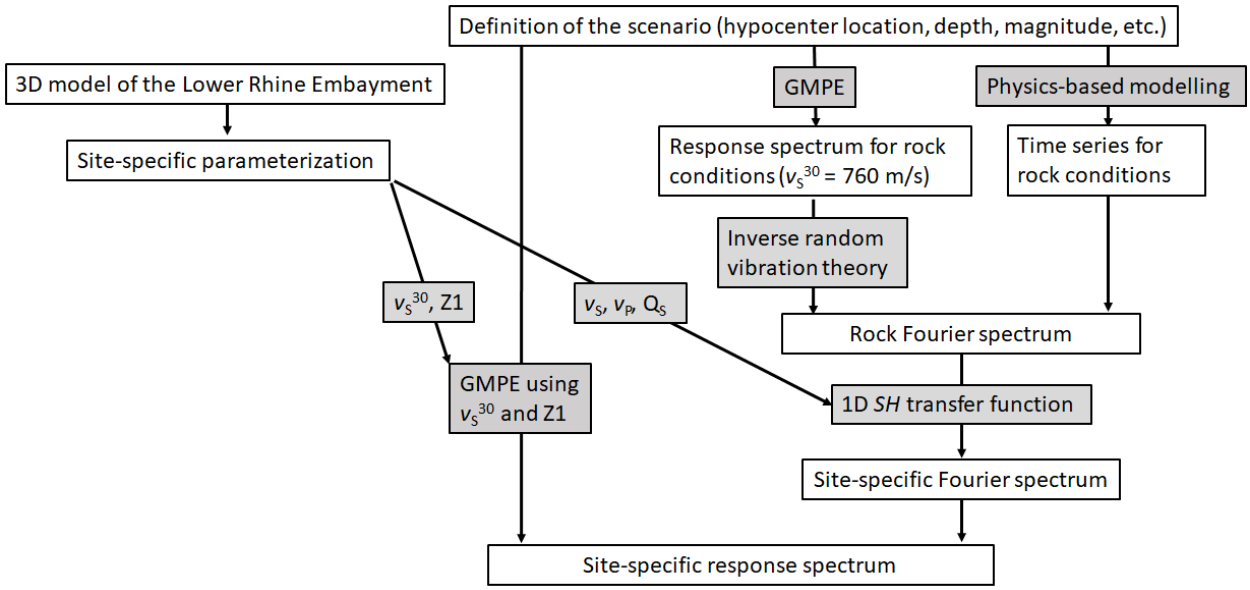

Figure 5.1: Overview of the methodologies used in this study for obtaining site-specific ground-motion intensity measures.

GMPEs relate a ground-motion spectral intensity measure, e.g. peak ground acceleration (PGA) or spectral acceleration (SA), at a given period to a set of explanatory variables describing the earthquake source, wave propagation path and the local site conditions. These independent variables include magnitude, style of faulting mechanism, source-to-site distance and some parameterization of local site conditions. More recent models also account for other factors affecting earthquake ground-motions, e.g., hanging wall effects.
In the past five decades, many hundreds of GMPEs for the prediction of PGA and linear elastic response spectrum ordinates have been published. Nowadays, more than 600 GMPEs are available worldwide (an overview is given in Douglas 2019). Since 2003, the Pacific Earthquake Engineering Research Center (PEER) is conducting a large research program to develop the next generation of ground-motion prediction

STR 20/02. GFZ German Research Centre for Geosciences.
DOI: 10.2312/GFZ.b103-20026

equations (GMPEs) for shallow crustal earthquakes in active tectonic regions (the Lower Rhine Embayment can be considered an active tectonic region). The second phase of this project (called NGA-West2, see Bozorgnia et al. 2014) concluded in 2014 and provided important results, including a strong motion database of recorded ground-motions and a set of peer-reviewed GMPEs (Gregor et al. 2014). Several recent hazard projects have shown that the models developed by the NGA-West and NGA-West2 projects may be of interest not only for highly seismically active regions but also for non-cratonic and lower seismicity regions like Germany (see also Mak et al. 2018). In turn, the NGA-West ground-motion models have been selected as part of ground-motion logic tree to compute recent probabilistic seismic hazard assessments in Europe (Delavaud et al. 2012), Switzerland (Edwards et al. 2016) and Germany (Grünthal et al. 2018). Moreover, while in most modern ground-motion models site effects are modeled through V_{s30}, only NGA-West2 ground-motion models account for additional factors characterizing the influence of deep basins which cannot be captured by V_{s30} alone.
In the following, we encounter the application of the NGA-West 2-equations proposed by Abrahamson et al. (2014), Boore et al. (2014) and Campbell and Bozorgnia (2014) due to their simple functional form. For testing the suitability of the model of Boore et al. (2014) for ground-motion modeling in the Lower Rhine Embayment, we have analyzed recordings of 16 small and moderate events ($3.1 \leq M \leq 4.4$) that occurred since January 2000 with distances to site of up to 150 km and have been recorded by at least three stations (Table 5.1). Due to the limited number of stronger events, we did not take into account the remaining NGA-West 2 equations by Chiou and Youngs (2014) and Idriss (2014) since they can be applied only for larger magnitudes (M > 3.5 for the Chiou and Youngs 2014 model, M ≥ 5 for the Idriss model).

Table 5.1: List of earthquakes for testing the NGA-West 2 ground-motion models.

Time (UTC)	Magnitude	Latitude	Longitude	Depth [km]
2016-05-28 03:37:23	3.4	51.60	6.85	5.0
2011-06-28 09:58:23	3.2	51.50	6.59	1.0
2011-02-07 16:06:44	3.3	51.48	6.55	1.0
2011-02-02 17:23:45	3.4	51.49	6.60	1.0
2011-01-05 08:33:41	3.7	51.49	6.58	2.0
2010-08-10 09:25:50	3.6	51.49	6.72	5.0
2010-06-01 10:43:30	3.5	51.52	6.56	5.0
2009-11-06 17:23:24	3.5	51.40	6.50	5.0
2009-10-07 09:32:25	3.3	51.50	6.50	5.0
2009-09-05 09:30:27	3.6	51.50	6.60	5.0
2009-07-31 11:03:15	3.9	51.40	6.60	1.0
2009-07-24 02:58:06	3.9	51.40	6.60	10.0
2008-02-17 11:07:21	3.8	51.50	6.50	10.0
2008-01-24 03:30:08	3.8	51.50	6.40	5.0
2007-12-12 14:52:34	3.7	51.30	6.80	1.0
2007-08-03 02:58:09	4.4	50.40	7.20	10.0

We have downloaded all data from the EIDA (European Integrated Data Archive) data centers and processed using the stream2segment software (Zaccarelli et al. 2018,

STR 20/02. GFZ German Research Centre for Geosciences.
DOI: 10.2312/GFZ.b103-20026

2019). EIDA currently offers uniform access via standard FDSN (Federation of Digital Seismograph Networks) protocols to unrestricted data from 10 European nodes, hosting data from about 100 permanent and several hundreds of temporary networks.
Instead of using the local magnitudes as the input, moment magnitudes are taken from the European-Mediterranean Earthquake Catalogue (EMEC, Grünthal and Wahlström 2012) with its temporal extension as described in Stromeyer and Grünthal (2015). We calculated response spectra with 5%-damping in a frequency range between 0.5 and 20 Hz, using the geometrical mean between the two horizontal components. For the analyzed sites for which V_{S30} is not available, its V_{S30} is derived from the topographic slope following Wald and Allen (2007). As a GMPE represents average properties of ground-motions in a given region, the residual ground-motion represents any unmodeled but also aleatory variations in regional parameters. Results for a period range between PGA and 1 s are shown in Figure 5.2.

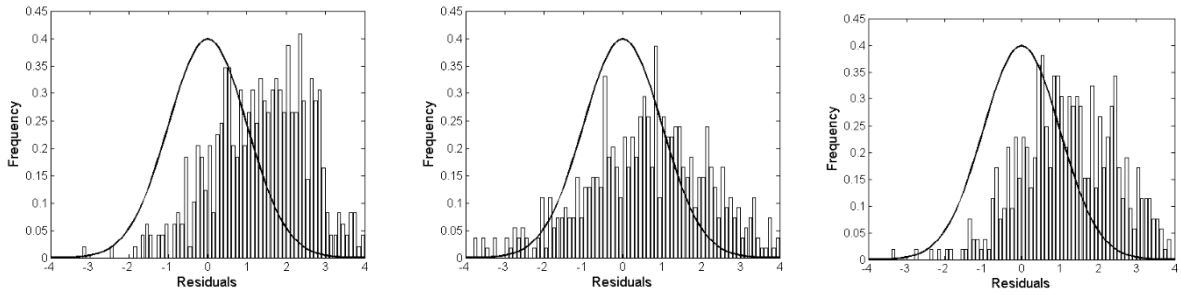

Figure 5.2: Residuals (PGA ≤ T ≤ 1 s) using different NGA-West2 ground-motion models (left: Abrahamson et al. 2014, middle: Boore et al. 2014, right: Campbell and Bozorgnia 2014) compared to a Gaussian distribution with unit variance (black line).

The central tendency is underestimated, meaning that all models more or less underpredict the ground-motion tendency. This might mainly be caused by an insufficient consideration of site effects due to the thick sedimentary cover (since the use of V_{s30} based on the topography does take into account potential the effect of thick sediments). Only for the model of Boore et al. (2014), this trend is less significant and only this model seems to be compatible with the observations. For this equation the distribution tends to be Gaussian although with a large variance.
This indicates that the equation of Boore et al. (2014) can be considered appropriate for modeling ground-motion in the Lower Rhine Embayment. The corresponding prediction is of the following form

$$\ln Y = F_E(\mathbf{M}, mech) + F_P(R_{JB}, \mathbf{M}, region) + F_S(V_{S30}, R_{JB}, \mathbf{M}, region, z_1) + \varepsilon_n \sigma(\mathbf{M}, R_{JB}, V_{S30}) \quad (3)$$

Herein, ln Y represents the natural logarithm of a ground-motion intensity measure (PGA or SA). F_E, F_P and F_S represent functions for source ("E" for "event"), path ("P"), and site ("S") effects. ε_n is the fractional number of standard deviations of a single predicted value of ln Y away from the mean and σ is the total standard deviation of the model. The predictor variables are the earthquake magnitude M, the Joyner-

STR 20/02. GFZ German Research Centre for Geosciences.
DOI: 10.2312/GFZ.b103-20026

Boore distance R_{JB} (i.e. the shortest distance from a site to the surface projection of the rupture surface), the region (i.e. regional corrections for some variables), V_{s30} and Z1, the depth at which V_S exceeds a threshold of 1.0 km/s. Of all NGA-West2 models, only the model of Boore et al. (2014) uses R_{JB} as distance metric, implicitly accounting for hanging-wall features. Because R_{JB} is the closest horizontal distance of the site to the surface projection of the fault, rupture depth is explicitly not considered in this equation.

The site function is composed of various factors accounting for the linear and nonlinear component of site amplification. Herein, the linear component of the site amplification model describes the scaling of ground-motion with Vs_{30} with respect to the site condition for which the amplification is unity (i.e. reference site conditions, here taken as Vs_{30} = 760 m/s and Z1=0). More details on the actual form of the model can be found in Boore et al. (2014). Since a detailed underground model of the area of investigation is available, ground-motion are derived for reference site conditions (taken as Vs_{30} equal to 760 m/s). As outlined in Boore et al. (2014), this is a reasonable default condition.

STR 20/02. GFZ German Research Centre for Geosciences.
DOI: 10.2312/GFZ.b103-20026

6. Earthquake scenario and modeling choices

On 20 November 2018, the working group in BBK has decided to study a single earthquake scenario on the Erft fault as defined in the German National PSHA (DECS003, Grünthal et al. 2018). The expected maximum magnitude on the Erft fault is M_w 7.1 as outlined in Chapter 2. To model a more frequent event, a moment magnitude M_w 6.5 event along the Erft fault system on a Monday morning in May was chosen to be studied.
Because a normal-sized *M*w 6.5 mainshock can occur on various locations along the Erft fault without extending it, we had to choose a location that will provide useful results in our study. We assumed a multi-planar rupture (see Chapter 2) with an aspect ratio of 1.5 (i.e. length to height of the fault 1.5 according to Leonard 2010; this corresponds to a length of the fault of about 20 km and a vertical extent of the fault of about 14 km for the rupture plane following Wells and Coppersmith 1994). We placed all possible hypocenters on a regular grid with a horizontal and vertical spacing of 2 km, resulting in 161 possible hypocentral positions on the fault plane.
To account for more conservative approach, we choose a relatively unfavorable location (according to the findings of Mai et al. 2005), in which the rupture begins in the middle of the Erft fault (50.79°N, 6.74°E, see Figure 6.1) at a shallow depth of approximately 4 km. Although rather shallow, such hypocenter depth will not cause any permanent deformation in the sedimentary layers. The choice of the shallow hypocenter depth is based on the assumption of the "reasonable worst case scenario". Such depths, however, should not be considered unrealistic because earthquakes with similar magnitudes and similar rupture mechanisms have already occurred in various locations at depths of less than 6 km. Reamer and Hinzen (2004) have further observed very shallow seismic events in the Lower Rhine Embayment, albeit with smaller magnitudes.

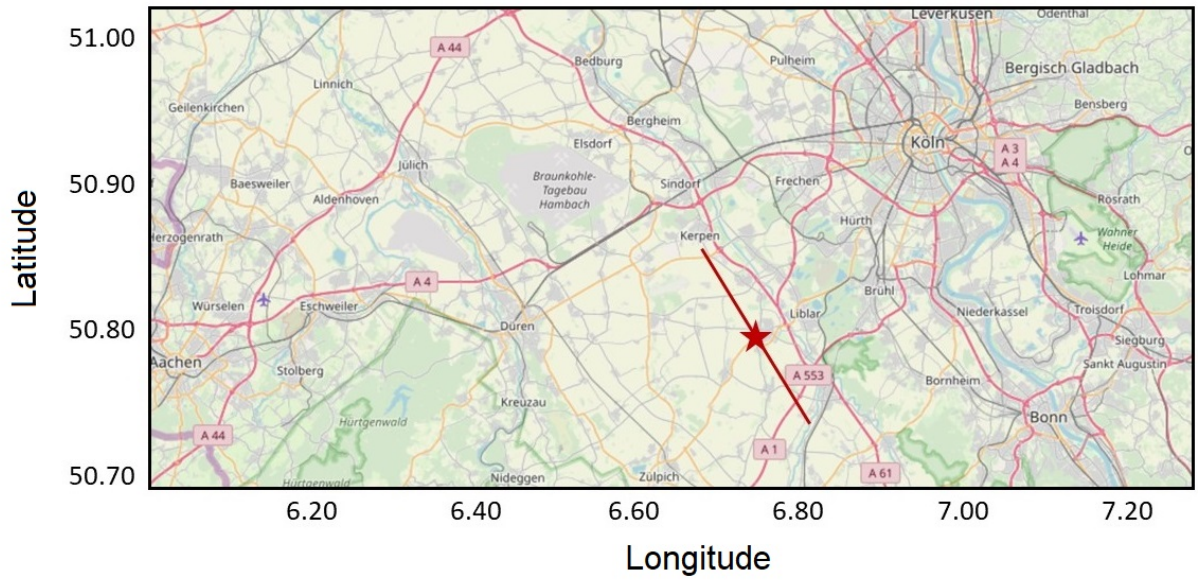

Figure 6.1: Epicenter (red star) and fault rupture (red line) for the scenario event (red star).

We performed all analyses using the OpenQuake engine (https://www.globalquakemodel.org/oq-get-started, last accessed in September

STR 20/02. GFZ German Research Centre for Geosciences.
DOI: 10.2312/GFZ.b103-20026

2019). The fundamental motivations for using the OpenQuake engine, the hazard and risk software developed by the Global Earthquake Model (GEM), are reproducibility, testing, and community-based development process. Reproducibility, one of the main pillars of the scientific process, is an expanding requirement in the scientific software development. Pagani et al. (2014) provides an overview of the main features of the OpenQuake engine.

STR 20/02. GFZ German Research Centre for Geosciences.
DOI: 10.2312/GFZ.b103-20026

7. Ground-motion modeling results

As outlined in Chapter 5, there are two GMPE-based methods for assessing ground-motions. On the one hand, the site function of the ground-motion model can be directly assessed using available V_{S30} and Z1 information (see Equation 3). On the other hand, ground-motions are calculated for reference site conditions (taken as V_{S30} = 760 m/s and Z1 = 0). As outlined in Boore et al. (2014), this is a "reasonable default condition". Site effects are then added through 1D-SH amplification functions (see Figure 4.1 for an example) anchored at a reference velocity of 760 m/s for any site of interest using a detailed 3D-velocity model for the southern Lower Rhine Embayment. The corresponding results of both methods are described below.

7.1. Ground-motion modeling results based on Vs_{30} and Z1

Figures 7.1 provides a summary of the ground-motion distributions (PGA, SA at T = 0.3s, and SA at T = 0.6s) over the ground-motion model of Boore et al. (2014) for the scenario event. For the site term of the ground-motion model, site-specific V_{s30} and Z1 are directly considered.
For the urban area, the modeled spectral accelerations are in the order of 0.15 g to 0.25 g. Because both V_{s30} and Z1 do not vary significantly laterally, the largest ground-motions are modeled for the south-western districts (i.e. towards the Erft fault system) and there is a steady decrease with increasing distance from the fault. Lateral variations of ground-motions due to site effects are almost not present because V_{s30} and Z1 do not fully allow for the influence of thick sediment layers to be taken into account.

STR 20/02. GFZ German Research Centre for Geosciences.
DOI: 10.2312/GFZ.b103-20026

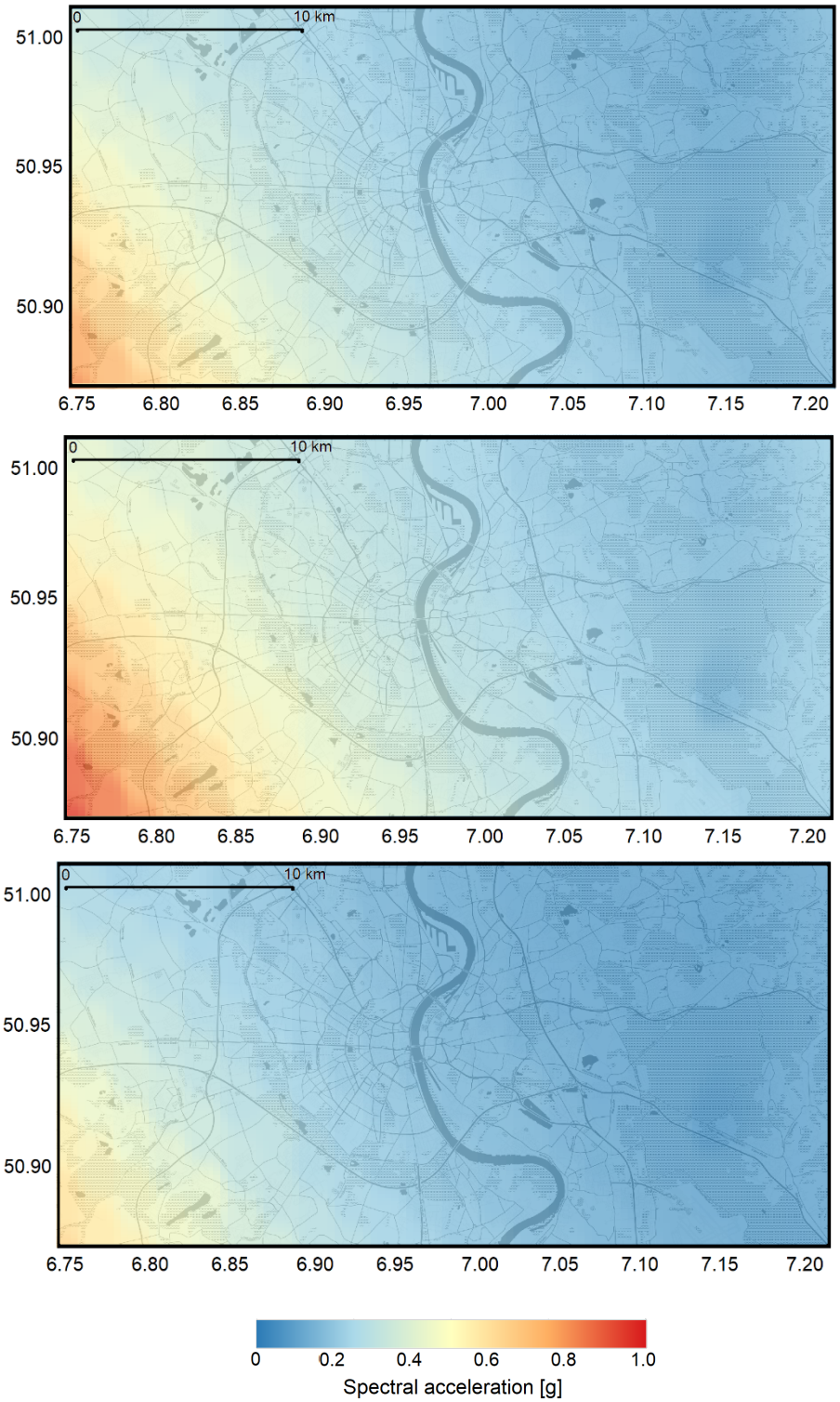

Figure 7.1: Spatial variation of PGA (top), SA at T = 0.3s (center) and SA at T = 0.6s (bottom) for the scenario earthquake using Boore et al. (2014) with site-specific V_{S30} and Z1.

STR 20/02. GFZ German Research Centre for Geosciences.
DOI: 10.2312/GFZ.b103-20026

7.2. Ground-motion modeling for soft rock (V_{S30} = 760 m/s) and corresponding integration of site effects

As described by Boore et al. (2014), the coefficients of the site term are calibrated for reference conditions (i.e. soft rock conditions with V_{s30} = 760m/s and Z1 = 0). Corresponding spectral accelerations for soft-rock conditions are illustrated in Figure 7.2. PGA values are in the order of (0.1 ± 0.05) g at distances of 15 km to 25 km from the Erft fault. For SA at 0.3 s, ground-motions are in the order of (0.15 ± 0.08) g and around (0.1 ± 0.05) g at T = 0.6s.

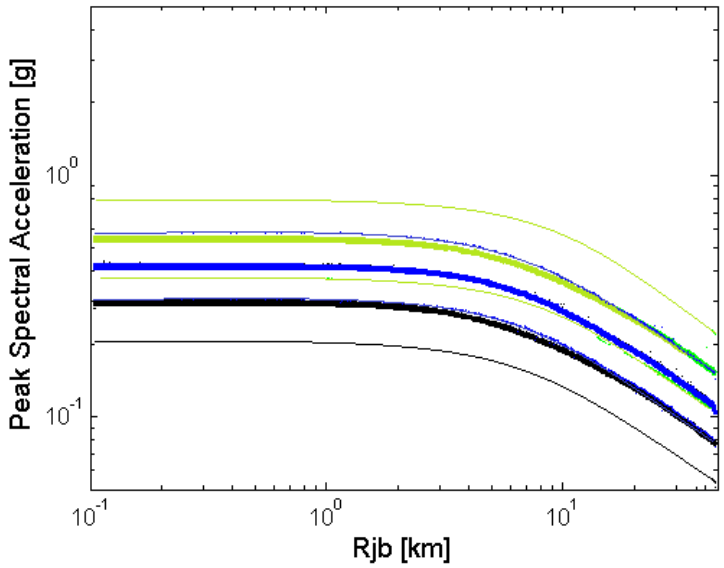

Figure 7.2: Distance scaling of ground-motion intensities as a function of R_{JB} (PGA: black, SA for T = 0.3 s: green, SA for T = 0.6 s: blue) using the ground-motion model of Boore et al. (2014) for soft rock conditions (Vs_{30} = 760 m/s, Z1 = 0). The thick black line represents the median, the thin lines represent plus/minus one standard deviation.

We have made site-specific adjustments of the ground-motion accelerations for correctly assessing the influence of the shallow sedimentary cover. Site-specific amplification functions are available as Fourier amplitude spectra (FAS), however GMPEs are defined as response spectra, rendering simple inclusions of site effects impossible. In a more complex approach (e.g. Rodriguez-Marek et al. 2014), ground-motion accelerations are calculated for hard-rock conditions and then convolved with 1D site-effects. Such an approach is not straightforward in practice because (1) GMPEs are generally well calibrated for soft rock conditions (i.e. V_{s30} = 760m/s to 800m/s) only but not for higher V_{s30}; (2) V_{s30}-κ adjustments (from soft to hard rock) are not yet fully understood (κ is the high-frequency spectral decay of the acceleration spectrum), (3) it is not clear what is the main impedance contrast and the true "bedrock" depth and (4) 1D models are mostly well calibrated only at shallow depths.
Therefore, we follow the method proposed by Al Atik et al. (2013) which is based on the Random Vibration Theory (RVT, Cartwright and Longuet-Higgins 1956) and on

STR 20/02. GFZ German Research Centre for Geosciences.
DOI: 10.2312/GFZ.b103-20026

the Inverse Random Vibration Theory (IRVT, Vanmarcke and Gasparini 1976) and allows for calculating Fourier amplitude spectra (FAS) that are compatible with predefined acceleration response spectra.
While it is straightforward to generate a response spectrum from a given FAS, an iterative procedure is required in the opposite direction. This is mainly due to two problems: Firstly, the spectral acceleration for a given frequency is influenced by a range of frequencies in the FAS, meaning that the spectral acceleration for a given period does not only depend on the Fourier amplitude for that period. To solve this problem, the IRVT method relies on the narrow-band properties of slightly damped single-degree-of-freedom (SDOF) oscillator transfer functions. Secondly, the response amplitude scaling cannot be determined a-priori because it is based on the initially unknown FAS but it can be assessed in an iterative procedure. In this way, the corresponding FAS can be used to constrain the scaling factors for the inversion.

STR 20/02. GFZ German Research Centre for Geosciences.
DOI: 10.2312/GFZ.b103-20026

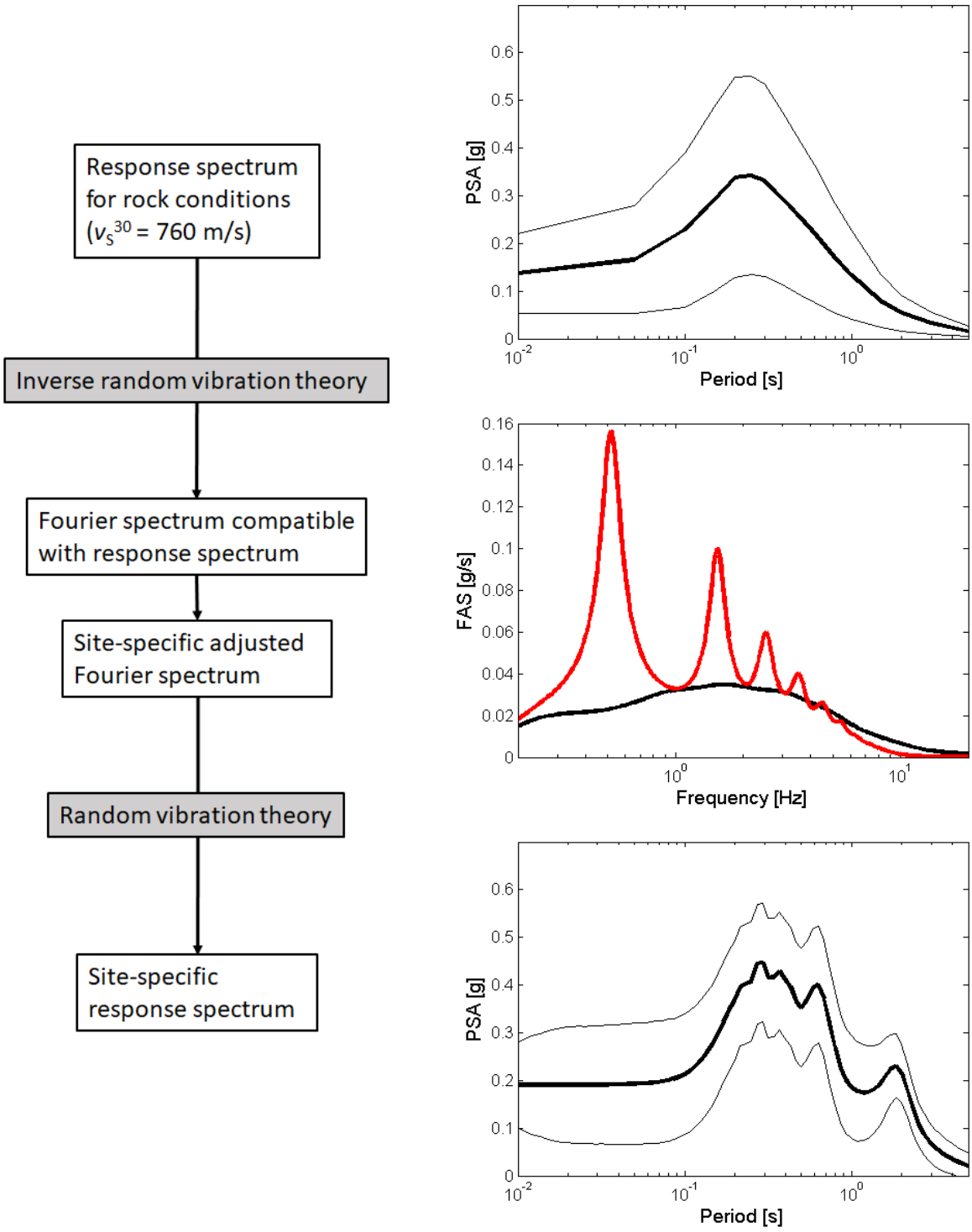

Figure 7.3: (left) Flowchart for assessing site conditions in the response spectrum domain. (right) Example for obtaining spectral intensity for the site Cologne-Deutz (50.93° N, 7.01° E). Top: Response spectrum for rock conditions (Vs_{30} = 760 m/s). The black line corresponds to the median plus/minus one standard deviation. Middle: Corresponding Fourier spectrum for soft rock conditions (black line) and site-specific adjusted Fourier spectrum (red line). The respective transfer function is shown in Figure 4.1. Bottom: Site-specific response spectrum plus/minus one standard deviation.

STR 20/02. GFZ German Research Centre for Geosciences.
DOI: 10.2312/GFZ.b103-20026

We follow the classical procedure (see Figure 7.3 for an overview and an example, for details see Rathje et al. 2005 and Al Atik et al. 2013):

1. For the given scenario, we calculate the target response spectrum for soft-rock conditions (V_{s30} = 760m/s).
2. We use the IRVT to calculate the FAS for each site that is compatible with the response spectrum defined in step 1 and implemented in the computer program *Strata* (Kottke and Rathje 2008). We address the problem of converting a response spectrum to a corresponding Fourier spectrum by using single-degree-of-freedom transfer functions which are narrow-band for lightly damped systems and converging to zero for frequencies larger than the site's fundamental frequency. In this way, we minimize the frequency range that contributes to the spectral acceleration for each single frequency. Further details of this procedure can be found in Rathje et al. (2005). More recently, Wang and Rathje (2016) showed that the performance can be improved if the Vanmarcke (1975) peak factor model is used as an alternative to the Cartwright and Longuet-Higgins (1956) model. The Vanmarcke peak factor considers the statistical dependence between peaks, which is important for narrow-band processes associated with site response and oscillator responses. A critical part of this approach is computing the root-mean square (rms) error of the oscillator response from the FAS through the duration of the oscillator response. While various models are available for defining rms duration models, these models do not consider the influence of the site response. Therefore, our analysis is based on the empirical ground-motion model of Kempton and Stewart (2006) which considers both the source duration as well as the increase in duration through V_{S30} and Z1.5 (i.e. the depth at which V_S exceeds 1.5 km/s).
3. For each site, we multiply the FAS by the site-specific adjusted FAS (an example can be found in Figure 4.1) to take the site effects into account. Herein, the velocity profile is truncated at the soil depth at which the velocity exceeds 760 m/s. Below that depth, we use an average crustal velocity model (Reamer and Hinzen 2004). Because the attenuation is stronger for the near-surface sediments than for the underlying solid rock due to the relatively low values for Q, no additional scaling is required (Al Atik et al. 2013).
4. We obtain the adjusted response spectrum for each site by applying the RVT to the FAS obtained in step 3.

Figure 7.4 provides a summary of the ground-motions following the scheme outlined above.

STR 20/02. GFZ German Research Centre for Geosciences.
DOI: 10.2312/GFZ.b103-20026

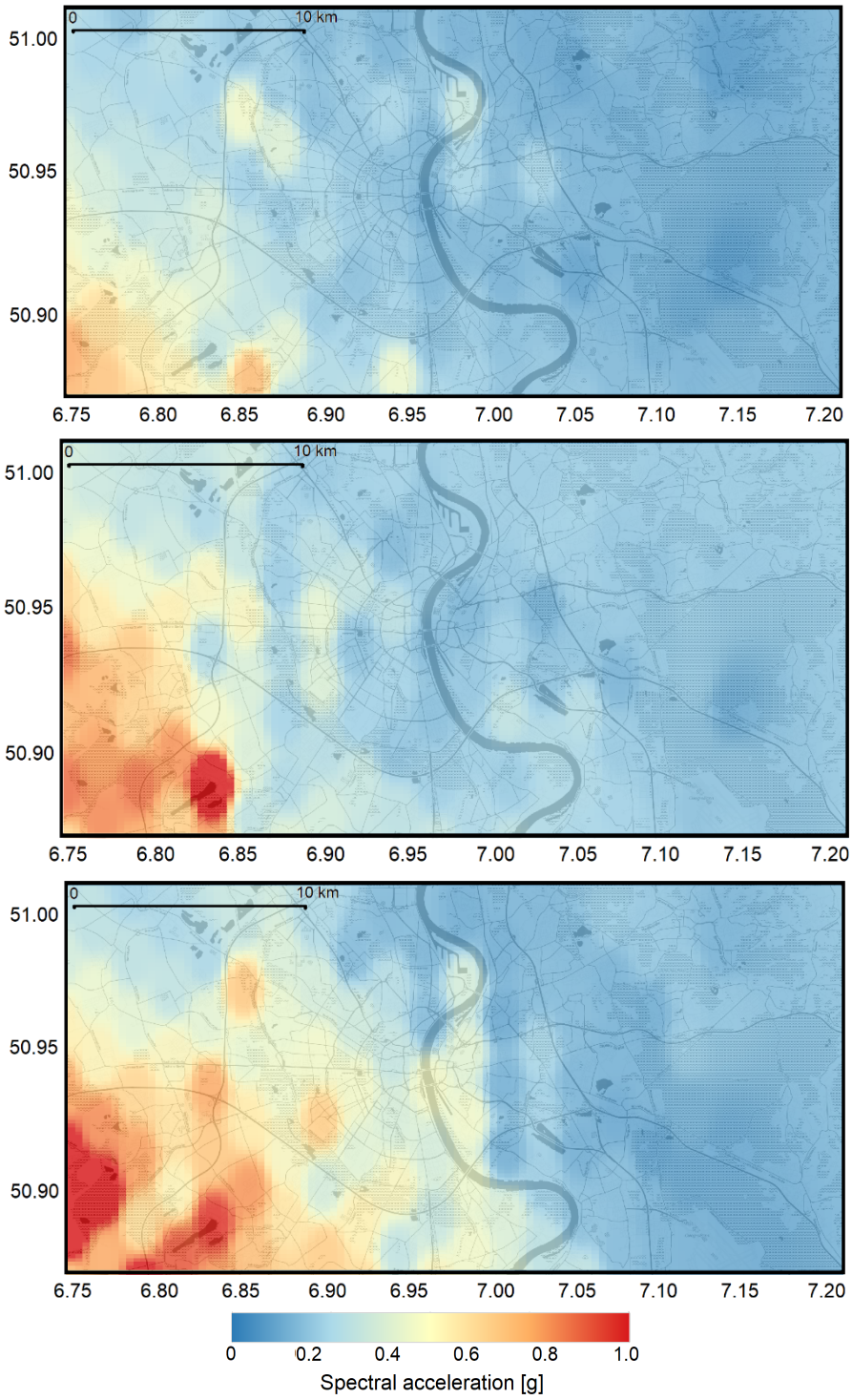

Figure 7.4: Spatial variation of PGA (top), SA at T = 0.3 s (center) and SA at T = 0.6 s (bottom) for the scenario earthquake using Boore et al. (2014) for soft rock followed by an integration of site effects.

Comparing Figures 7.1 and 7.4 clearly emphasizes the influence of the shallow sedimentary layers. When taking site effects fully into account, slightly lower PGA values (compared to the Boore et al. 2014 model) are calculated for the city center

STR 20/02. GFZ German Research Centre for Geosciences.
DOI: 10.2312/GFZ.b103-20026

and the eastern districts of Cologne. Only for some selected spots, we observe higher spectral intensities. This is mainly due to the strong attenuation (low values of Q) of the sedimentary layers, meaning that high frequencies (i.e. small periods) are significantly attenuated (see also Figure 4.1: For high frequencies f > 5 to 7 Hz, the transfer function takes values of less than 1, i.e. the level of ground-motion is reduced).
On the contrary, for higher periods, the values mapped in Figure 7.4 are significantly higher than the results presented above. This trend, caused by the resonance of the sedimentary layers, can be seen particularly well for T = 0.6 s. For the south-western districts of the city, ground-motions of 0.4 g are reached and partly exceeded.

7.3. Comparison of the two ground-motion modeling approaches and discussion

Figure 7.5 illustrates the modelled site-specific ground-motion spectral amplitudes for four different periods as a function of R_{JB}. We further compare the results with the ground-motion model of Boore et al. (2014) in which the influence of site effects, as described in Chapter 7.1, is taken into account through a standard parameterization.

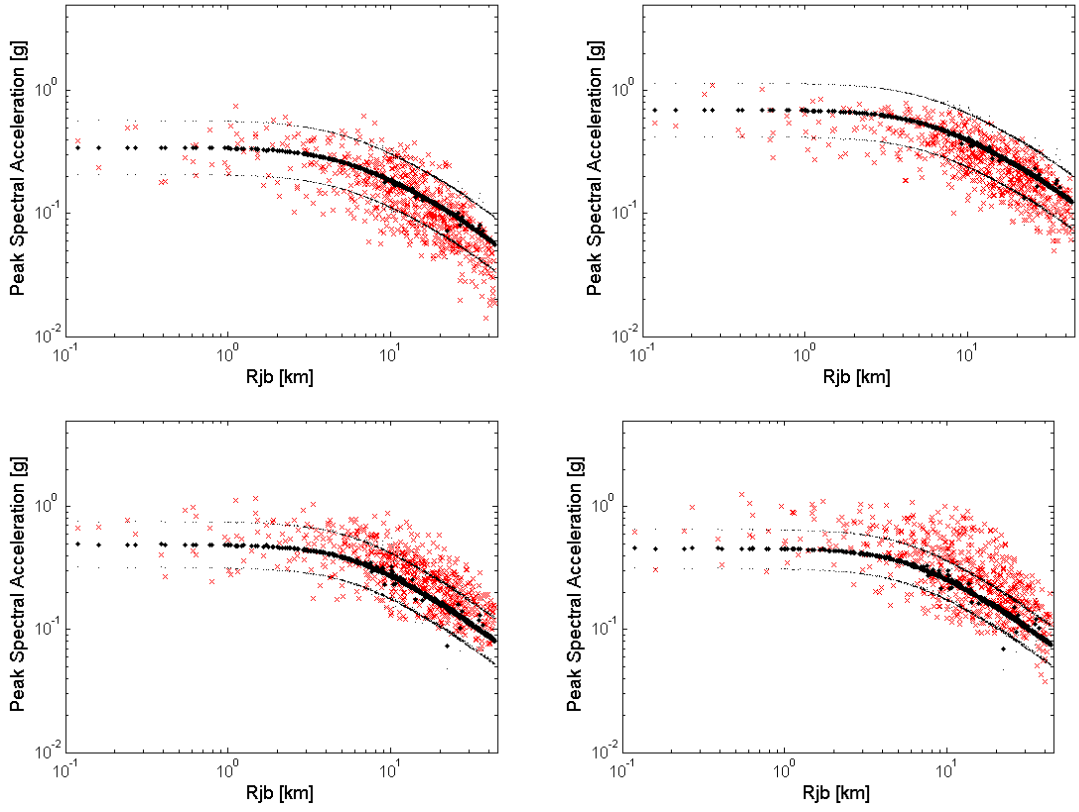

Figure 7.5: Empirically predicted mean ground-motion spectral parameters for PGA (top left), SA (T = 0.3 s, top right), SA (T = 0.6 s, bottom left) and SA (T = 1.0 s, bottom right) as a function of the Joyner-Boore distance. Black dots represent the ground-motion model of Boore et al. (2014) with site-specific parameterization using V_{S30} and Z1 from the velocity model of the LRE (Chapter 3). Red crosses represent results of the RVT approach as

STR 20/02. GFZ German Research Centre for Geosciences.
DOI: 10.2312/GFZ.b103-20026

For small spectral periods, the agreement between the ground-motion model with the standard parameterization and the site-specific approach is acceptable for short distances, the RVT approach attenuates faster at larger distances. This is mainly due to the high attenuation of ground-motion (low values of Q_S) in the thick sedimentary cover of the Lower Rhine Embayment. For increasing periods, the GMPE with V_{S30} and Z1 tends to slightly underestimate the site-specific RVT approach. This feature is most prominent for the highest period. Since most of the sites are located in the basin (i.e. not on outcropping rock) and since the sedimentary cover can reach thicknesses of several hundred meters, the influence of the soft soil layers on ground-motion is covered only when fully accounting the deeper site effects.
Moreover, as the duration has been found to be the most critical parameter for RVT predictions (Kottke and Rathje 2013, Wang and Rathje 2016), our approach explicitly considers the increase in duration due to the soft soil layers with respect to soft rock reference conditions. Similar findings have recently been made by Chi-Mirando and Montejo (2017). Moreover, our approach of using the Vanmarcke (1975) peak model leading has been shown to be advantageous over other peak factor models (Wang and Rathje 2016).
While the influence of the thick sedimentary cover and the corresponding extension of duration of ground-motion have been sufficiently considered, a critical plea is the degree to which near-fault effects are well established in the empirical GMPE model and whether ground-shaking may be particularly strong due to a peculiar kinematics of the source process (e.g. large stress-drop). This could be indicated by the amount of data which are available to constrain those portions of the empirical models. Physics-based modeling approaches have highlighted that the variability caused by the rupture directivity and the rupture model can be comparable to the influence of site effects (Bradley et al. 2017). Fully accounting for this apparent aleatory variability requires the use of physics-based modeling approaches (as shown in Figure 5.1).
It has to be noted that no analysis on the possible occurrence of nonlinear effects (i.e. liquefaction potential) has been carried out. Although there are various methods for determining the liquefaction potential of soils based on empirically established relationships from laboratory measurements and from sites where data are available, we decided to not include such considerations because they usually come with large uncertainties. The unknown site-specific soil characteristics make it difficult to choose a suitable empirical equation for regression analysis.

STR 20/02. GFZ German Research Centre for Geosciences.
DOI: 10.2312/GFZ.b103-20026

8. Macroseismic intensities (EMS-98) considering site effects

Macroseismic intensity scales categorize the intensity or severity of ground shaking resulting from an earthquake in a given region in terms of its effects on the built environment and/or the population. In particular, the European Macroseismic Scale (EMS-98, Grünthal et al. 1998) defines levels of intensity based on the shaking felt by humans, the movement/oscillation/shaking of ordinary objects and damage to buildings. The EMS-98 is the first intensity scale designed to encourage co-operation between engineers and seismologists, rather than being for use by seismologists alone. The scale comes with a detailed manual, which includes guidelines, illustrations, and application examples. More details on background information on establishing the EMS-98 can be found in the introduction to the scale (Grünthal et al. 1998). Table 8.1 provides an overview of the EMS-98.

Table 8.1: Short form of the European Macroseismic Scale (EMS-98) following Grünthal (1998).

EMS intensity	Definition	Description of typical observed effects (abstracted)
I	**Not felt**	Not felt.
II	**Scarcely felt**	Felt only by very few individual people at rest in houses.
III	**Weak**	Felt indoors by a few people. People at rest feel a swaying or light trembling.
IV	**Largely observed**	Felt indoors by many people, outdoors by very few. A few people are awakened. Windows, doors and dishes rattle.
V	**Strong**	Felt indoors by most, outdoors by few. Many sleeping people awake. A few are frightened. Buildings tremble throughout. Hanging objects swing considerably. Small objects are shifted. Doors and windows swing open or shut.
VI	**Slightly damaging**	Many people are frightened and run outdoors. Some objects fall. Many houses suffer slight non-structural damage like hair-line cracks and fall of small pieces of plaster.
VII	**Damaging**	Most people are frightened and run outdoors. Furniture is shifted and objects fall from shelves in large numbers. Many well built ordinary buildings suffer moderate damage: small cracks in walls, fall of plaster, parts of chimneys fall down; older buildings may show large cracks in walls and failure of fill-in walls.
VIII	**Heavily damaging**	Many people find it difficult to stand. Many houses have large cracks in walls. A few well built ordinary buildings show serious failure of walls, while weak older structures may collapse.
IX	**Destructive**	General panic. Many weak constructions collapse. Even well built ordinary buildings show very heavy damage: serious failure of walls and partial structural failure.
X	**Very destructive**	Many ordinary well built buildings collapse.
XI	**Devastating**	Most ordinary well built buildings collapse, even some with good earthquake resistant design are destroyed.
XII	**Completely devastating**	Almost all buildings are destroyed.

There are two approaches for mapping the estimated distribution of macroseismic intensities, either through intensity attenuation equations (equations which are similar to GMPEs) or by converting ground-motion spectral or peak ground accelerations to macroseismic intensities by means of empirical models. Stromeyer and Grünthal (2009) have proposed an intensity attenuation relationship for Central

STR 20/02. GFZ German Research Centre for Geosciences.
DOI: 10.2312/GFZ.b103-20026

Europe but this equation is explicitly not valid for the magnitude range considered here. Moreover, the influence of the thick sedimentary cover, as outlined in the previous chapter, cannot be fully considered by using such empirically derived equations.
In order to be able to make use of the wealth of data on site characterization available for Cologne, we opted for converting the peak ground accelerations calculated as described in Chapter 7.2 into macroseismic intensity using the model of Faenza and Michelini (2010). A 1:1 relation between the Mercalli-Cancani-Sieberg (MCS) scale used by Faenza and Michelini (2010) and the EMS-98 values required for the application of the fragility models for the calculation of damage was assumed, following Cua et al. (2010), who found the deviations between the two intensity scales to be very minor (less than 0.2 macroseismic intensity units). Moreover, the MCS values lie within one standard deviation of the equation of Kaestli and Fäh (2006) based on the EMS-98.
Macroseismic intensities are thus estimated as

$$I = a + b \log_{10}[\mathrm{PGA}] \qquad (4)$$

where, I represents the macroseismic EMS-98 intensity. Following Faenza and Michelini (2010), we use $a = 1.68 \pm 0.22$ and $b = 2.58 \pm 0.14$ as regression parameters. For PGA values in Equation 4, we used the values shown in Figure 7.4 and rounded the final results to integers.
Figure 8.1 illustrates the macroseismic intensity distribution for the scenario earthquake. The standard deviation covers both uncertainties for the PGA on soft rock and uncertainties arising from the conversion model (equation 4) but no additional uncertainty stemming from accounting for site amplification has been incorporated. For the studied event, macroseismic intensities between VI (slightly damaging, such as small cracks and falling objects) and VIII (heavily damaging, i.e. large cracks in and serious failure of walls) are calculated for the urban area with an average intensity of VII (damaging, i.e. moderate damage for most buildings). Although there is some decrease in intensity from west to east, higher macroseismic intensities are further estimated for some districts east of the Rhine river, especially for the southern districts.

STR 20/02. GFZ German Research Centre for Geosciences.
DOI: 10.2312/GFZ.b103-20026

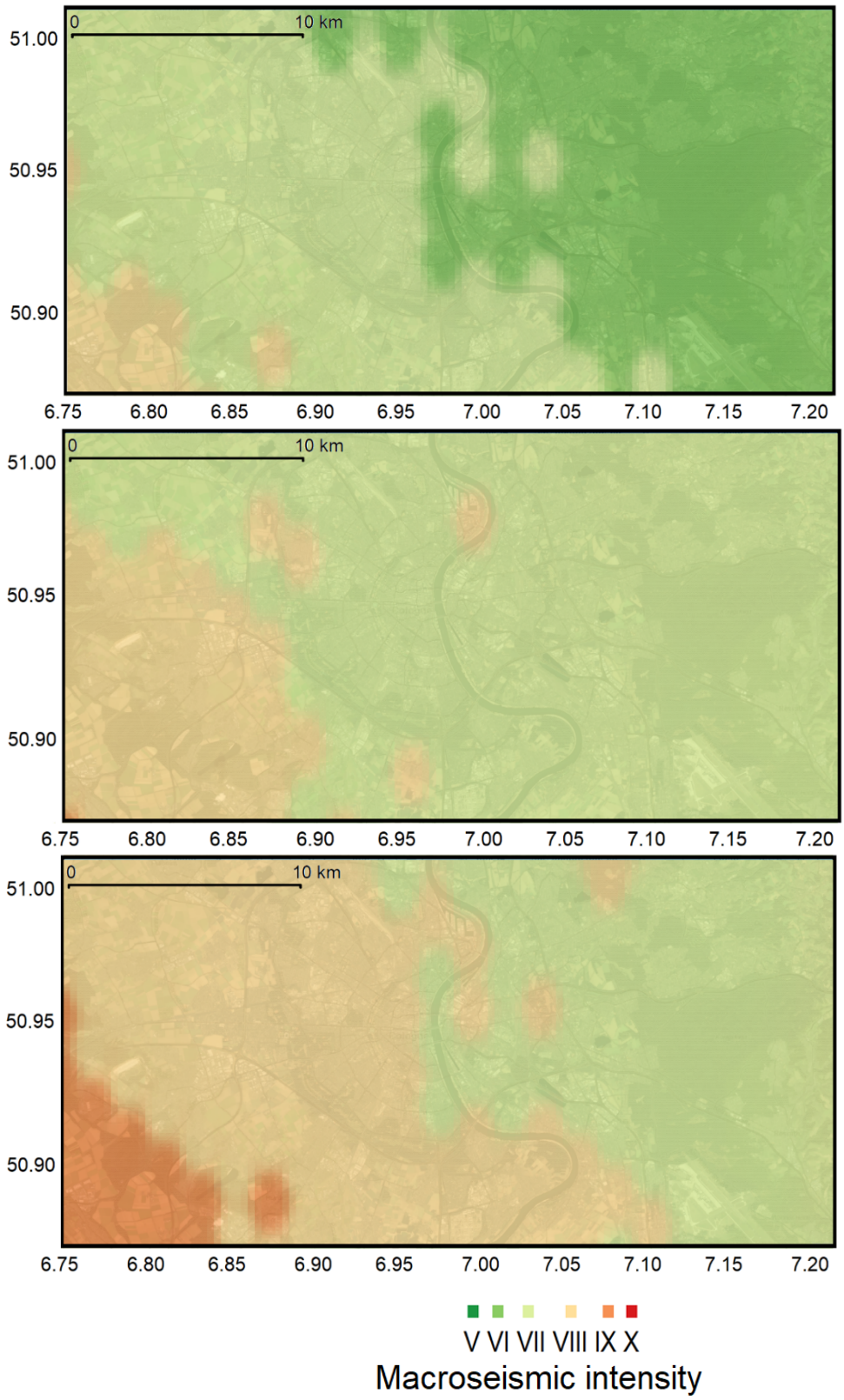

Figure 8.1: Modelled minimum (median minus one standard deviation, top), median (center) and maximum (median plus one standard deviation, bottom) EMS-98 intensities for the scenario event following Equation (4).

STR 20/02. GFZ German Research Centre for Geosciences.
DOI: 10.2312/GFZ.b103-20026

Having detailed site characterizations for only a limited number of sites, the final intensity fields used for the estimation of consequences in a larger area were defined by combining the intensity field stemming from the sites for which detailed site-response analyses were carried out (sites are shown in Figure 3.1, results are shown in Figure 8.1) and the intensity field stemming from applying the GMPE of Boore et al. (2014) with the site term on and using the slope-derived proxy V_{s30} values of Wald and Allen (2007) over a 30 arc-second uniform grid.
In order to carry out the merging of intensity fields stemming from the implementation of two different methods, we compared results from the two within the region in which they overlap. As can be observed in Figure 8.2 (left), the means and medians of the binned data (5-km bins) are in relatively good agreement for R_{JB} distances shorter than 20 km but the difference increases for larger distances, with those of the detailed site response case (red and green lines) resulting slightly higher than those of the uniform grid (lilac and light blue lines). Individual data points from the detailed site response case present larger median intensity values than those of the grid, with the overall dispersion of the plot being larger for the former set. The opposite is true for the standard deviations (plot on the right), for which both mean and median values of the uniform grid are slightly larger than those of the detailed site response case.

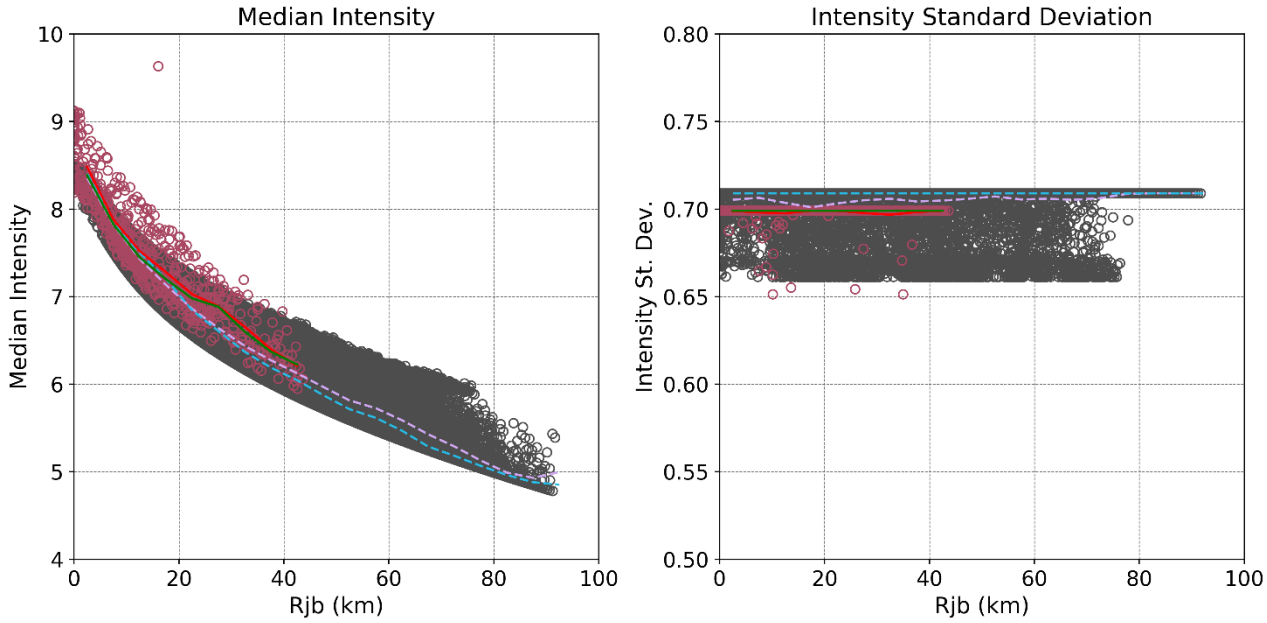

Figure 8.2: Median (left) and standard deviation (right) of EMS-98 intensities against R_{JB} for the sites for which we carried out detailed site-response analyses (burgundy points) and a 30-arc second grid for which ground-motions were calculated only with the GMPE of Boore et al. (2014) with the site term on (black points). The continuous red and green lines indicate mean and median of the former, respectively, while the dashed lilac and light blue lines are the mean and median of the 30-arc second grid (in both cases we binned the data in 5-km bins; smaller bins were observed to be noisy). The outlier at $R_{JB}\approx18$ km is caused by site-specific data at the open pit mine Hambach.

Based on these findings, we generated the final regional macroseismic intensity field by merging the two alternative fields as follows:

STR 20/02. GFZ German Research Centre for Geosciences.
DOI: 10.2312/GFZ.b103-20026

- The intensity field (both median and standard deviation) stemming from the sites for which we carried out detailed site response analyses (see chapters above) was adopted within an imaginary polygon encompassing this area. Through linear interpolation we obtained a field from these sites over a uniform 30-arc second grid.
- Outside of the imaginary polygon, the field of median intensities was adopted, scaled up by a factor of 1.031 for sites at R_{JB} greater than or equal to 20 km and not scaled at closer distances. The scale factor results from the ratio of the median values of the two fields at R_{JB} between 20 km and 45 km. The field of standard deviation of intensities was adopted without any scaling.

Figure 8.3 illustrates the results of this merging procedure while Figure 8.4 indicates the composition of the final field of median intensities. For the damage calculation, we interpolated the macroseismic intensity field (median and standard deviation) to retrieve the values corresponding to the centroids of the buildings' footprints. For the estimation of casualties, we determined the median and standard deviation of intensity of each administrative unit by means of averaging the values at the points of the grid that fall within the boundaries of the unit, if these were at least two, and by interpolating the field to obtain the values at the centroids of the administrative units otherwise. The minimum of two points was defined in order to ensure that if only a single point is available then it will correspond to the centroid (instead of a random location). The method is described in detail in the following chapters.

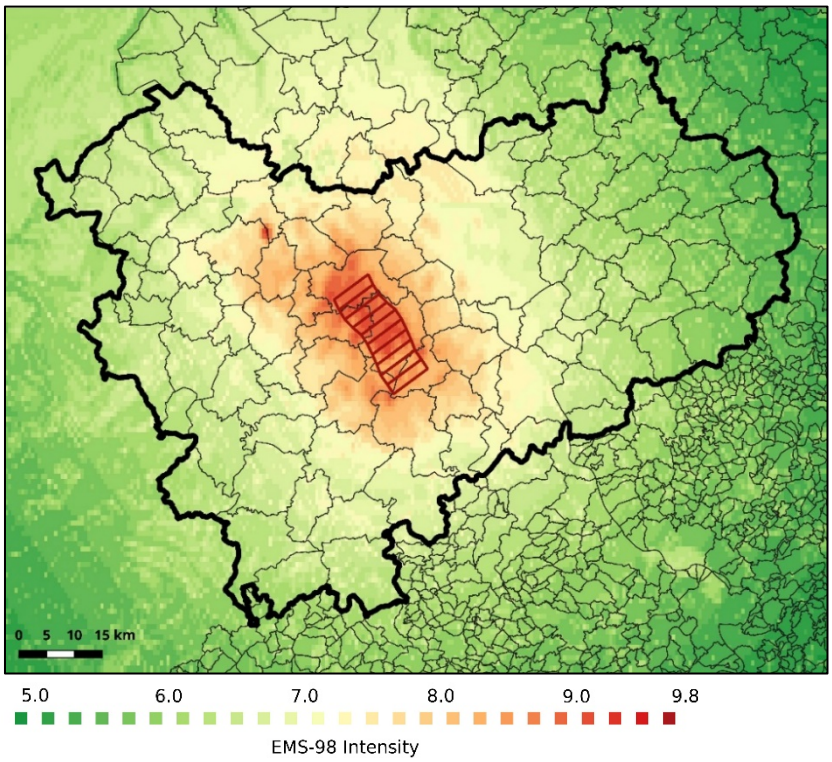

Figure 8.3: Final field of median macroseismic intensities for the whole Regierungsbezirk Köln marked by the thick black line. Thin lines represent local administrative units ("Gemeinde"). The outlier in the north-west is caused by site-specific data at the open pit mine Hambach.

STR 20/02. GFZ German Research Centre for Geosciences.
DOI: 10.2312/GFZ.b103-20026

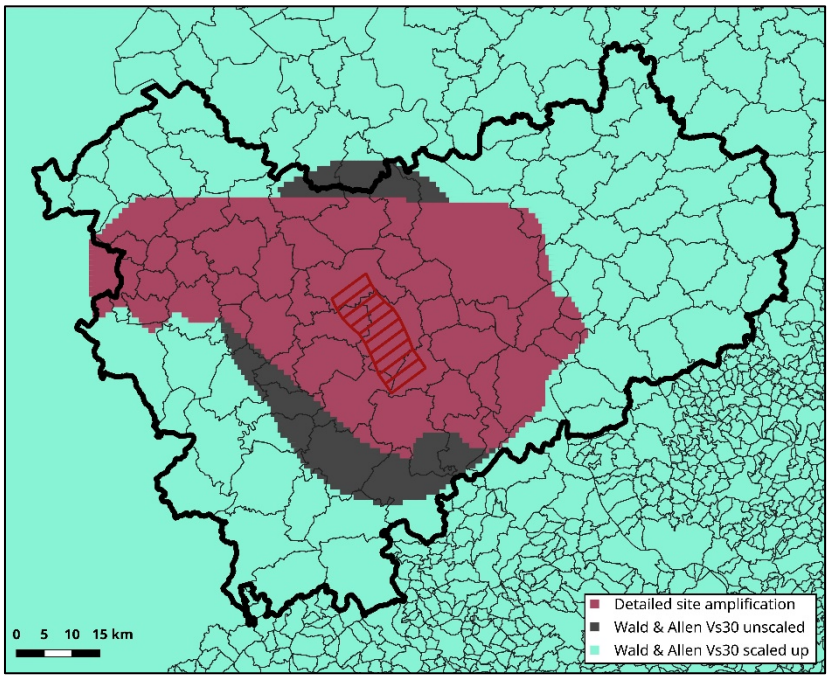

Figure 8.4: Composition of the final field of median intensities for the whole Regierungsbezirk Köln marked by the thick black line. Thin lines represent local administrative units ("Gemeinde").

STR 20/02. GFZ German Research Centre for Geosciences.
DOI: 10.2312/GFZ.b103-20026

9. Building damage assessment

The calculation of damage to buildings due to a scenario earthquake requires the characterization of the three components of seismic risk: hazard, vulnerability and exposure. While the expected ground shaking has already been discussed in Chapters 7 and 8, the present chapter focuses on the latter two and the calculation of the resulting damage itself.

Section 9.1 describes the vulnerability of the buildings in Cologne in terms of the EMS-98 vulnerability classes. Following the recommendations of Schwarz and Maiwald (2019), buildings were assigned a distribution of vulnerability classes (i.e., a probability of the building having vulnerability class A, B, C, etc.) based on their year of construction. The fragility models of Raschke (2003) used herein subsequently defined the expected damage based on the EMS-98 vulnerability class and the number of stories of each particular building. As each building was characterized by a probability of belonging to any particular vulnerability class, all of these were considered with their respective probabilities to estimate the final likelihood of observing different damage grades.

Requiring knowledge on both year of construction and number of stories to define the vulnerability of buildings, the building exposure model needs to contain such information. The kind of exposure model used for seismic risk calculations depends mostly on the data availability for the site of interest. It is quite common for exposure models to be aggregated at the level of a certain administrative unit, as this is how statistics on population, dwellings and/or buildings are often provided by official/governmental institutions (e.g. Yepes-Estrada et al. 2017). Detailed information on structural classes may sometimes be available for relatively small areas such as cities or districts within cities (e.g. Beinersdorf et al. 2013, Schwarz et al. 2004). The kind of data required to use the fragility models of Raschke (2003) and the availability of three open datasets of relevance for the area rendered the city of Cologne as a perfect test-case within the broader development of the OpenBuildingMap (OBM), a service that aims at combining the strengths of crowd-sourced data collection with the knowledge of experts in the fields of structural engineering to produce high-resolution building-by-building exposure models. Chapter 9.2.1 discusses the process of merging the three available open datasets to produce a building-by-building exposure model for Cologne in which each building is characterized by its year of construction, number of stories and occupancy type (i.e. purpose/use). As the year of construction and number of stories were not available for every single building, Chapter 9.2.2 explains the procedure followed to enrich this building-by-building exposure model with statistics available at the "Stadtviertel" (also called Viertel in the following) level.

We calculated damage only for residential buildings and buildings with mixed residential and commercial occupancy, as the fragility curves used herein are appropriate only for these kinds of structures. This is in line with most seismic risk assessment studies, which have traditionally focused only on residential building classes. This is due not only to the difficulties associated with retrieving data on industrial and commercial buildings, but also to the fact that the former have been, in general terms, the most broadly studied. Special buildings such as historical constructions and monuments are even more difficult to characterize, as each individual structure might be unique and thus deserve a detailed analysis of its own, though simplified studies aiming at analyzing large sets of such buildings exist and

STR 20/02. GFZ German Research Centre for Geosciences.
DOI: 10.2312/GFZ.b103-20026

can be useful to establish priorities for the allocation of resources for further studies (Despotaki et al. 2018). A small comparison with damage grades recorded for the 3 September 1978 Albstadt (Baden-Württemberg) earthquake is presented as well.

9.1. Fragility

9.1.1. Vulnerability classes and damage grades according to EMS-98

For the present work, we have classified the buildings of the city of Cologne according to the European Macroseismic Scale EMS-98 vulnerability classes (Grünthal 1998) ranging from A (most vulnerable) to F (least vulnerable), also using intermediate subdivisions such as AB, BC, etc. in line with the recommendations of Schwarz and Maiwald (2019).
According to Grünthal (1998), vulnerability class A is the most likely class of masonry buildings constructed with rubble stone, fieldstone or adobe (earth brick), while class B is the most likely class of those built in simple stone and unreinforced masonry of manufactured stone units. Masonry buildings constructed with massive stone, unreinforced masonry with reinforced concrete (RC) floors, or RC frames or walls without earthquake-resistant design are all most likely of vulnerability class C. Vulnerability class D, the least vulnerable found in Cologne according to Schwarz and Maiwald (2019), is assigned as the most likely class of reinforced or confined masonry, RC frames and walls with moderate level of earthquake-resistant design, or timber structures. It should be noted, however, that Grünthal (1998) defines not only most likely vulnerability classes but also ranges of probable and less probable classes for each type of structure.
Table 9.1 summarizes the EMS-98 damage scale, which we used for the present work as well. It is noted that, in practice, each damage grade represents a range and not an unequivocally defined state. This is particularly important for understanding the meaning of damage grade (DG) 5. As pointed out by Coburn et al. (1992) and implicitly stated in the EMS-98 definition ("total or near total collapse" and "collapse of ground floor or parts of buildings"), the volumetric reduction of the building can vary significantly within a set of buildings classified as suffering DG 5. This has a large influence on the casualties that may result from such damage (Coburn et al. 1992, So and Pomonis 2012). It is also noted that injuries and deaths can be associated with slight damage too, particularly when loose stones or bricks detach from buildings, or chimneys collapse.

STR 20/02. GFZ German Research Centre for Geosciences.
DOI: 10.2312/GFZ.b103-20026

Table 9.1: Definition of EMS-98 damage grades after Grünthal et al. (1998). Detailed descriptions are summaries of the original definition.

DG	General description	Kind of damage		Detailed description	
		Structural	Non-struct.	Masonry	Reinforced concrete
1	Negligible to slight damage	None	Slight	- Hair-line cracks in very few walls - Fall of small pieces of plaster - Fall of loose stones from buildings: very few	- Fine cracks in plaster, partitions and infills
2	Moderate damage	Slight	Moderate	- Cracks in many walls - Fall of fairly large pieces of plaster - Partial collapse of chimneys	- Cracks in structural elements - Cracks in partitions and infills - Fall of brittle cladding and plaster - Fall of mortar from joints of wall panels
3	Substantial to heavy damage	Moderate	Heavy	- Large and extensive cracks in most walls - Roof tiles detach - Chimneys fracture at roof line - Failure of non-structural elements (partitions, gable walls, etc.)	- Cracks in structural elements - Spalling of concrete cover - Buckling of rebars - Large cracks in partitions and infills - Failure of individual infills
4	Very heavy damage	Heavy	Very heavy	- Serious failure of walls - Partial structural failure of roofs and floors	- Large cracks in structural elements - Failure of concrete in compression - Fracture of rebars - Bond failure of beam rebars - Tilting of columns - Collapse of a few columns or a single upper floor
5	Destruction	Very heavy	Very heavy	- Total or near total collapse	- Collapse of ground floor or parts (e.g. wings) of buildings

9.1.2. Distribution of vulnerability classes per ranges of year of construction

We assigned EMS-98 vulnerability classes based on the year of construction of each building following the recommendations of Schwarz and Maiwald (2019) for the city of Cologne. Table 9.2 reproduces the distribution of vulnerability classes for each range.

STR 20/02. GFZ German Research Centre for Geosciences.
DOI: 10.2312/GFZ.b103-20026

Table 9.2: Distribution of EMS-98 vulnerability classes per range of year of construction in the city of Cologne according to Schwarz and Maiwald (2019).

Year of construction	EMS-98 vulnerability class						
	A	AB	B	BC	C	CD	D
Before 1918	4.5%	4.5%	91.0%	0%	0%	0%	0%
1919-1948	0%	0%	70.0%	0%	30.0%	0%	0%
1949-1962	0%	0%	5.4%	5.4%	89.2%	0%	0%
1963-1975	0%	0%	1.5%	1.5%	89.1%	6.3%	1.6%
1976-1989	0%	0%	0%	8.2%	82.2%	8.2%	1.4%
After 1990	0%	0%	0%	0%	88.9%	11.1%	0%

9.1.3. Fragility of buildings

We calculated damage due to the scenario earthquake to the residential buildings by means of functions that estimate the mean damage grade as a function of EMS-98 intensity and EMS-98 vulnerability. The functions used were those recommended by Schwarz and Maiwald (2019) based on the work of Raschke (2003) and can be written as

$$d_m = \frac{tanh[0.0088 \cdot f^2 + 0.2227 \cdot f - 2.4167]}{2} + 0.5 \quad (5)$$

Herein, the factor *f* is calculated as

$$f = I + \frac{tanh(3.3 \cdot I - 3.3 \cdot 6.5)}{2} + 0.5 - C \quad (6)$$

I represents the EMS-98 intensity and C is a vulnerability index tabulated as a function of the EMS-98 vulnerability class and the number of stories (values are provided as well for the case of unknown number of stories).
The mean damage d_m that results from the expressions above belongs to a damage scale d in the 0 to 1 domain that is later transformed into a damage scale D in the 0 to 5 domain (equivalent to the EMS-98 damage scale) through

$$D_m = 6 \cdot (d_m - 1/12) \quad (7)$$

As D_m needs to be a number between 0 and 5, whenever d_m lies below 1/12, a value of 1/12 is imposed, as a value of 11/12 is imposed on d_m whenever it lies above 11/12. The resulting values of the mean damage grade D_m are depicted in Figure 9.1 for the vulnerability classes of interest for the present work and the number of stories-independent vulnerability indices provided by Schwarz and Maiwald (2019).

STR 20/02. GFZ German Research Centre for Geosciences.
DOI: 10.2312/GFZ.b103-20026

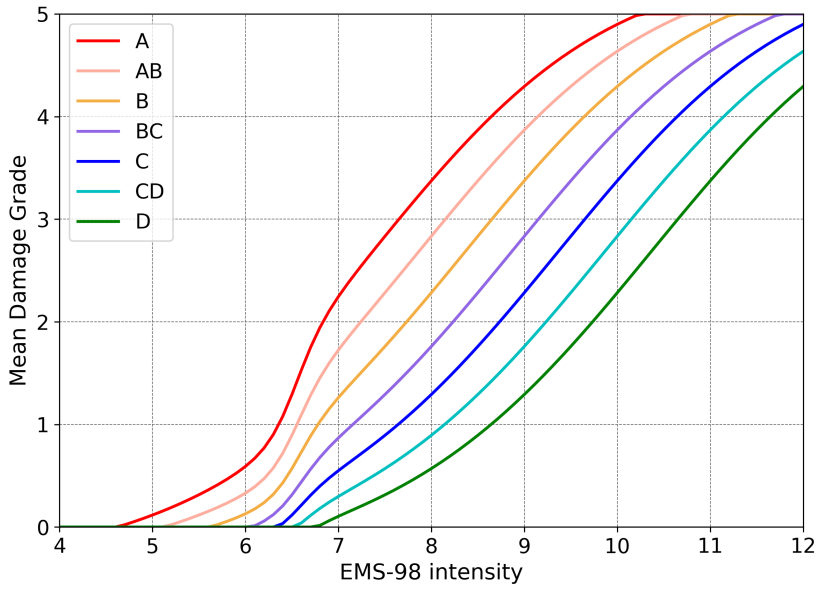

Figure 9.1: Mean damage grades for different EMS-98 vulnerability classes (color scale) and vulnerability indices C independent of number of stories.

We converted the mean damage grade into probabilities of occurrence of individual damage grades using a Beta distribution as recommended by Raschke (2003). Raschke (2003) uses the Beta distribution in its standard [0,1] domain and establishes an equivalence between d_m in the [0,1] domain and D_m in the [0,5] domain (see Table 9.3). The two shape parameters *b* and *c* are calculated from the mean (d_m) and standard deviation (σ_d) of the damage grade *d* in the [0,1] domain. In order to calculate the latter, first the standard deviation of the damage grade *D* in the [0,5] domain is calculated as

$$\sigma_D = 0.4401 \cdot [D_m \cdot (5 - D_m)]^{0.4358} \quad (8)$$

The standard deviation, σ_d, of the damage grade *d* in the [0,1] domain is:

$$\sigma_d = \sqrt{0.00212461 \cdot {\sigma_D}^4 + 0.02296389 \cdot {\sigma_D}^2} \quad (9)$$

The shape parameters *b* and *c* are calculated as:

$$b = d_m \cdot \left[\frac{d_m}{\sigma_d^2} \cdot (1 - d_m) - 1\right] \quad (10)$$

$$c = (1 - d_m) \cdot \left[\frac{d_m}{\sigma_d^2} \cdot (1 - d_m) - 1\right] \quad (11)$$

As σ_d appears in the denominator of *b* and *c*, σ_D was capped to be 0.0001 the lowest.

STR 20/02. GFZ German Research Centre for Geosciences.
DOI: 10.2312/GFZ.b103-20026

Table 9.3: Equivalence between the damage grade *d* in the [0,1] domain and EMS-98 damage grades *D* in the [0,5] domain according to Raschke (2003).

EMS-98 damage grade		**0**	**1**	**2**	**3**	**4**	**5**
damage grade in [0,1] domain	upper bound	1/6	2/6	3/6	4/6	5/6	1
	lower bound	0	1/6	2/6	3/6	4/6	5/6

Finally, the probability of observing a given damage grade is calculated as the probability of the damage grade lying in between the lower and upper bounds defined in Table 9.3, which is calculated as a simple subtraction between the cumulative density function (CDF) of a Beta distribution with shape parameters *b* and *c* at both values. For example, the probability of observing damage grade 2 is calculated as:

$$P[DG2] = CDF_\beta\left[\frac{3}{6}, b, c\right] - CDF_\beta\left[\frac{2}{6}, b, c\right] \quad (12)$$

Figure 9.2 depicts the probabilities of occurrence of each damage grade as a function of the mean damage grade D_m that result from these assumptions.

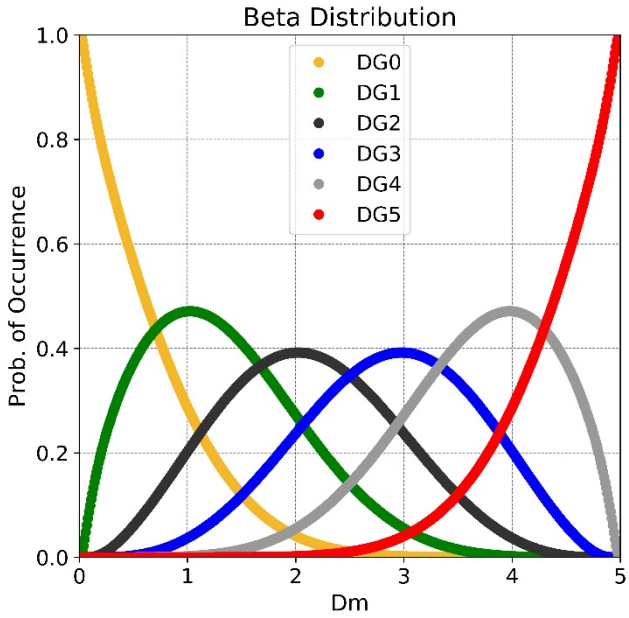

Figure 9.2: Probability of occurrence of each damage grade (color scale) as a function of the mean damage grade under the assumptions of a Beta distribution and the equivalences defined by Raschke (2003).

Figure 9.3 shows the resulting probabilities of exceedance of each EMS-98 damage grade (fragility curves) for four different vulnerability classes, obtained using the vulnerability indices *C* for unknown number of stories. As can be observed, these curves provide the link between the building's vulnerability class, the EMS-98 intensity level and the resulting damage. The number of stories can have a significant impact on the fragility within the model considered herein. For example, the

STR 20/02. GFZ German Research Centre for Geosciences.
DOI: 10.2312/GFZ.b103-20026

vulnerability index of a 7-story building of vulnerability class C is, according to Schwarz and Maiwald (2019), the same as that of a 2-store building of vulnerability class B, the latter being the generic vulnerability index assigned to class B when the number of stories is unknown.

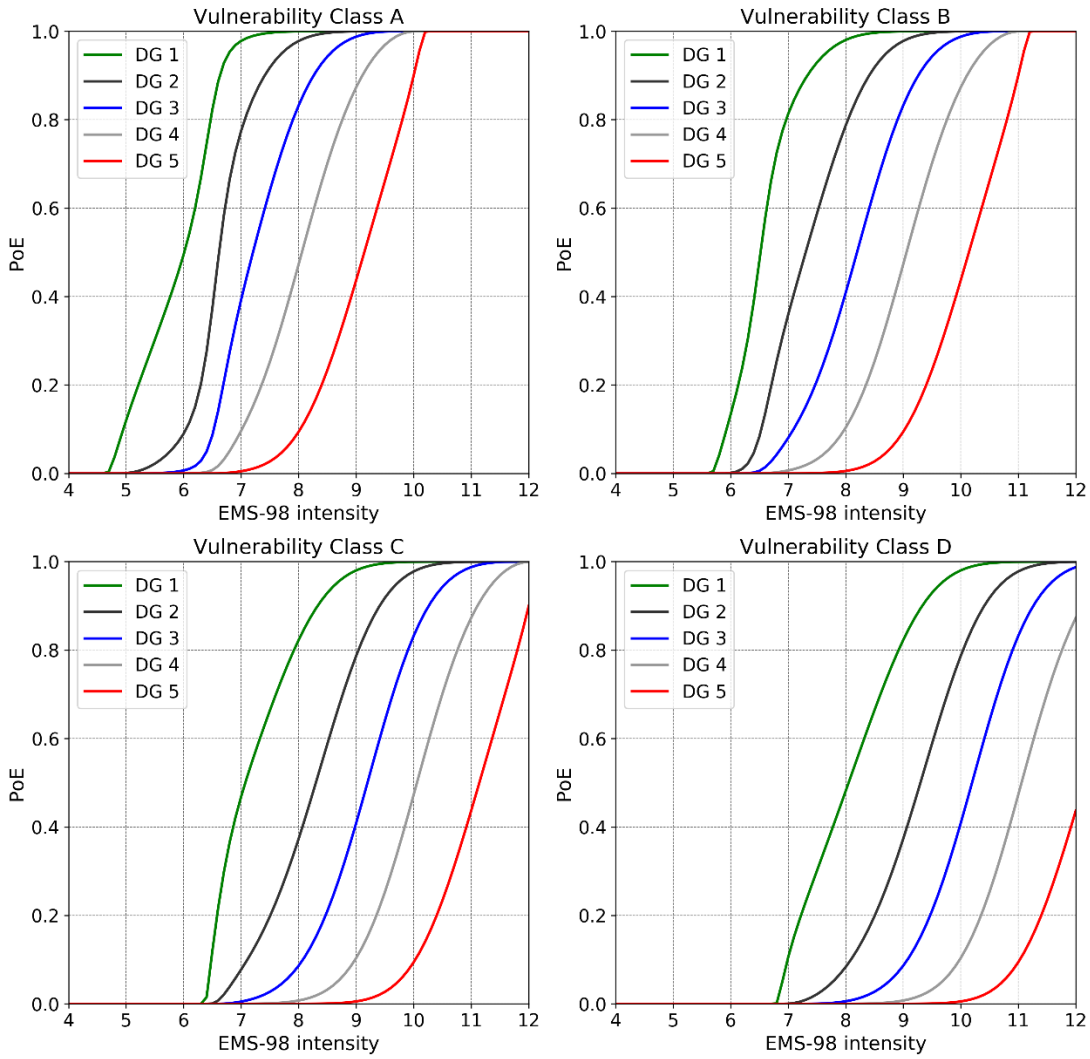

Figure 9.3. Probabilities of exceedance (PoE) of each EMS-98 damage grade resulting from the mean damage grade functions and the assumption of a Binomial distribution as described in the main text.

9.1.4. Calculation of Damage

The distributions of vulnerability classes per year of construction defined by Schwarz and Maiwald (2019) and reproduced herein as Table 9.2 were not sampled but fully used for the calculation of the probability of a building observing a particular damage grade. We thus calculated the probability of observing damage grade *i* as

$$P[DG_i] = \sum_j \sum_k P\left[I_{EMS-98_j}\right] \cdot P[V_k] \cdot P\left[DG_i | I_j, V_k\right] \quad (13)$$

STR 20/02. GFZ German Research Centre for Geosciences.
DOI: 10.2312/GFZ.b103-20026

where $I_{EMS\text{-}98,j}$ indicates a particular value of intensity with a certain probability $P[I_{EMS\text{-}98,j}]$ of occurring (discretization of the distribution of seismic intensity at a site resulting from considering both median intensity and its associated uncertainty), V_k refers to vulnerability class k, with probability $P[V_k]$ (according to Table 9.2 for the relevant year of construction), and $P[DG_i \mid I_{EMS\text{-}98,j}, V_k]$ is the probability of a building with vulnerability class k subject to intensity $I_{EMS\text{-}98,j}$ suffering damage grade i (according to the fragility curves).

9.2. Building exposure model

The building exposure model used for the estimation of damage due to the earthquake scenario considered herein was defined at the building-by-building level, thanks to the existence of three particularly relevant open datasets that allowed for such a resolution, namely

(i) OpenStreetMap (OSM),

(ii) a dataset (ODK hereafter) containing information on years of construction, available from Offene Daten Köln (Stadt Köln 2019b), an open-contribution web service from the city of Cologne, and

(iii) a second dataset containing information on the number of stories and the occupancy, available from the Nordrhein-Westfalen Web Feature Service (2019) that provides cadastral information for the whole state according to the European Union INSPIRE directive (NRW-WFS hereafter).

Decisions on how to combine these three datasets were informed by imagery from Google Maps/Google Earth/Google Street View and Mapillary.

As information regarding the year of construction of buildings is not available for all buildings in the ODK dataset and this is fundamental for the assignment of vulnerability classes according to Table 9.2, we enriched the building-by-building exposure model by data aggregated at the city and Viertel levels, namely the 2011 German National Census and the distribution of year of construction per Viertel surveyed by the city of Cologne in the year 2000 and summarized by Schwarz and Maiwald (2019).

Table 9.4 lists the main data sources used to build the building exposure model for Cologne. Details regarding the generation of the model are provided in Chapter 9.2.1., whose outcome is a building-by-building model in which each building is characterized by its year of construction, number of stories and occupancy type. Not all buildings have information on year of construction and number of stories at this stage. Chapter 9.2.2. then explains how we used additional aggregated data to assign the year of construction and/or numbers of stories to the cases in which these data were missing, following a Monte Carlo approach. Figure 9.4 schematically represents, in broad terms, the procedure followed.

STR 20/02. GFZ German Research Centre for Geosciences.
DOI: 10.2312/GFZ.b103-20026

Table 9.4: Data sources used to build the building exposure model for Cologne.

Source	Acronym	Contents	Last accessed
OpenStreetMap	OSM	Footprints, location, occupancy type of buildings. Buildings represented as geolocated polygons.	20 August 2019
Offene Daten Köln (Stadt Köln 2019b)	ODK	Years of construction and addresses of buildings. Data in terms of Lon-Lat of a point.	24 August 2018
Nordrhein-Westfalen Web Feature Service (2019)	NRW-WFS	Number of stories, occupancy type and addresses of buildings. Buildings represented as geolocated polygons.	20 August 2019
German National Census 2011	Census 2011	Number of buildings in the city of Cologne in the year 2011.	6 October 2018
Schwarz and Maiwald (2019)	SM19	Distribution of ranges of year of construction per Viertel of Cologne, based on data from the city of Cologne for the year 2000.	-
Google Maps / Google Earth / Google Street View	-	3D models and photos of buildings.	Indicated case-by-case
Mapillary	-	Photos of buildings.	Indicated case-by-case

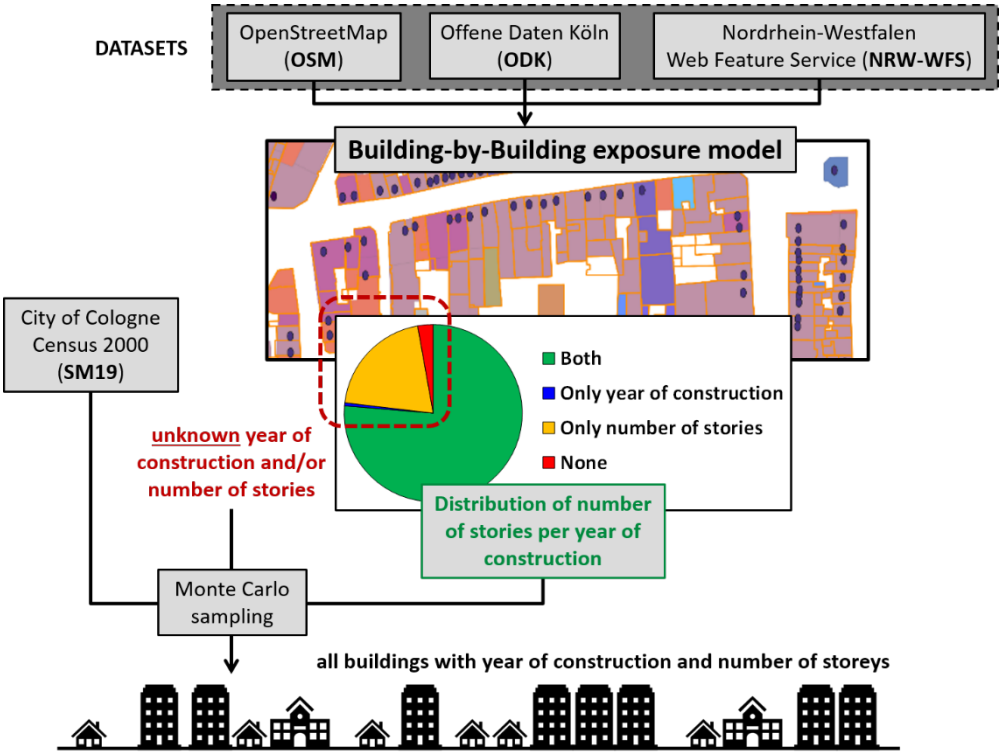

Figure 9.4: Schematic (simplified) representation of the process followed to generate the building exposure model for Cologne with year of construction and number of stories. An extensive description is given in the text.

STR 20/02. GFZ German Research Centre for Geosciences.
DOI: 10.2312/GFZ.b103-20026

9.2.1. OpenBuildingMap (OBM): Building-by-building exposure

OpenBuildingMap (OBM) is a service that aims at combining the strengths of crowd-sourced data collection with the knowledge of experts in the fields of building exposure and structural engineering with the purpose of generating a high-resolution global building exposure model. Its main source of information is OpenStreetMap (OSM), a community-based open-data mapping project in which contributors all over the world voluntarily map and characterize geographic features. OSM is ever-growing, with around 150,000 building footprints being added to the database in average every day. OBM retrieves data from OSM in real-time and combines it with other external open-data sources that help improving the amount of information known for any particular building. While OBM is being developed independently of the work presented herein, the process carried out to merge data from OSM, ODK and NRW-WFS can be considered a test case for the way in which data other than OSM is incorporated into OBM. We use the name OBM in this report to represent the merging of the three aforementioned open datasets together with the implicit existing machinery behind OBM.

9.2.1.1. Data sources

While the level of coverage is variable around the globe, OSM is quite complete within the administrative unit of Cologne in terms of the existence of most (if not all) building footprints. However, other kinds of information about buildings are often scarce in OSM, reason for which the latter has been complemented with two external datasets: ODK, containing years of construction, and NRW-WFS, which contains information on number of stories and occupancy type.
In the ODK dataset, the year of construction of buildings is provided in terms of latitude-longitude of a point representing the building as well as its corresponding address. Due to it stemming from an open-contribution web service, the origin of this data is not known, though random visual checks through images available from Google Maps, Google Street View and Mapillary suggest an overall reasonable agreement between what can be observed and the reported years, albeit some identified inconsistencies.
The NRW-WFS consists of polygons with assigned properties stored as a GeoJSON file. These properties include the address, number of stories and a string describing the building use, from which the occupancy type can be inferred.
The ODK dataset comprises 159,994 points with known year of construction for the administrative unit of Cologne, while the NRW-WFS dataset consists of 301,120 polygons classified as “Gebäude” (building) or “Bauwerk oder Anlage für Industrie und Gewerbe” (building or plant for industry and commerce) for the administrative unit of Cologne as well.

9.2.1.2. Generation

To merge the information stemming from the three different datasets, we matched points from ODK with polygons from OSM, which we in turn matched with polygons from NRW-WFS. For this purpose, both the OKD and the NRW-WFS datasets were compared against OSM first by means of geospatial intersection and then through

STR 20/02. GFZ German Research Centre for Geosciences.
DOI: 10.2312/GFZ.b103-20026

the addresses retrieved from both datasets. The latter allows, for example, to match a point from OKD that falls slightly outside of an OSM polygon through the address of the NRW-WFS polygon that has been matched with the OSM target, and vice versa. Figure 9.5 shows an example of the overlap of the three datasets.

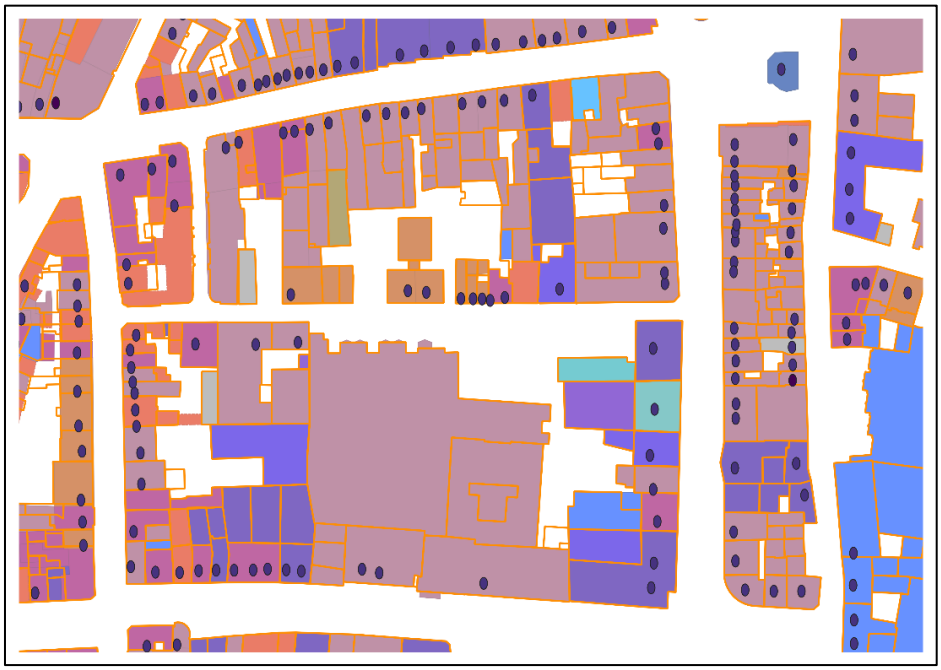

Figure 9.5: Example of overlap of the three datasets used to generate OpenBuildingMap for Cologne: OpenStreetMap (filled polygons), NRW-WFS (orange polygon contours) and ODK (blue dots).

As there is not a one-to-one match across the datasets, there are cases in which conflicts arise. For example, when more than one OKD point is matched with an OSM polygon, and these points are associated with different years of construction, the year of construction that is repeated the most, if repetition of certain values occurs, or the older of all years was adopted. This last case produces the most fragile building and thus lies on the conservative side. Conflicts regarding NRW-WFS can be more complex, as several polygons from NRW-WFS might intersect one OSM polygon. This might be due to many reasons, including the fact that sometimes two or more polygons appear to have been used in NRW-WFS to define a building for which only one polygon has been used in OSM, but also because small misalignments between the datasets lead to small intersections on the edges. In order to deal with such sites, we applied the following criteria:

- If the area of intersection between an OSM and a NRW-WFS polygon is less than 5% of the area of the OSM polygon, it will be discarded
- unless the NRW-WFS polygon is fully contained within the OSM polygon (fully contained is defined as at least 95% of the area of the NRW-WFS polygon lying within the OSM polygon).

Figure 9.6 shows a hypothetical example of how these criteria work. In this case, both NRW 4 and NRW 5 polygons get discarded because of their overlap area being less than 5% of the area of the OSM polygon, but NRW 3 does not, because it is fully contained within the latter.

STR 20/02. GFZ German Research Centre for Geosciences.
DOI: 10.2312/GFZ.b103-20026

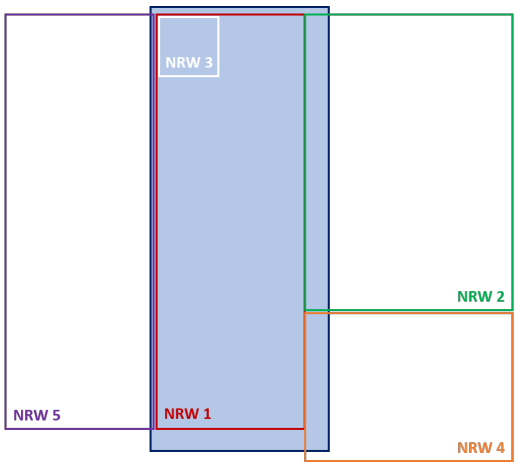

Polygon	L1 (m)	L2 (m)	A (m²)	A overlap (m²)	% overlap of OSM	% overlap of itself	A_{mean}-A	Outcome
OSM	6	15	90	90.0	-	-	-	-
NRW 1	5	14	70	70.0	77.8%	100.0%	-27.00	Keep
NRW 2	7	10	70	8.0	8.9%	11.4%	35.00	Keep
NRW 3	2	2	4	4.0	4.4%	100.0%	39.00	Keep
NRW 4	7	5	35	3.7	4.1%	10.6%	-	Discard
NRW 5	5	14	70	1.8	2.0%	2.6%	-	Discard

Mean	43.00
StDev	43.53

Figure 9.6: Example of decisions made when matching OSM polygons (blue filled rectangle) with NRW-WFS polygons. *A* stands for area, *L*1 and *L*2 represent length and width of the rectangle.

If after applying these criteria more than one NRW-WFS polygon remained within the set of potential matches of the OSM polygon under consideration, all the areas of overlap were gathered and their mean and standard deviation was calculated (see example in Figure 9.6). NRW-WFS polygons were discarded if the difference between their overlap area A and the mean A_{mean} was larger than the standard deviation σ_A (the comparison was carried out with sign so as to only eliminate cases of too little overlap, *i.e.*, $A_{mean} - A > \sigma_A$ → discard). We considered all remaining NRW-WFS polygons for retrieving addresses and number of stories, the largest of all numbers conservatively selected for the latter if discrepancy existed.
The assignment of occupancy types is of relevance to be able to classify buildings from OSM into residential and non-residential. For this, we used several data sources, namely

- NRW-WFS occupancy strings: the NRW-WFS polygons contain a string (in German) that describes the function of the building; we created a mapping dictionary to assign occupancy type from these strings.
- OSM points of interest: tagged (a tag in OSM is a key-value pair) OSM nodes indicating the existence of, for example, a bakery, a medical surgery, a school, etc.
- OSM tags on the building polygon: they describe a mixture of type and use of the building (e.g. apartments, house, restaurant, bank, train station).
- OSM land use polygons: OSM polygons describing the predominant land use in usually high resolution.
- CORINE Land Cover project of the European Environmental Agency (EEA): areas of land use derived from satellite imagery, aerial photos, digital elevation data etc.

The hierarchy of these sources was as listed, with NRW-WFS occupancy strings taking precedence over all other alternatives. Our use of occupancy classes was based on GEM's Building Taxonomy v2.0 (Brzev et al. 2013), which was expanded to separate categories that we deemed to deserve their own separate status. For example, we introduced a separate category (labeled MED) for health-care related building uses with subcategories hospitals (MED1) and sanatoria (MED2). As a consequence, we

STR 20/02. GFZ German Research Centre for Geosciences.
DOI: 10.2312/GFZ.b103-20026

abandoned COM4, a subcategory of "commercial and public", intended in the GEM taxonomy to gather all hospitals and medical clinics. Moreover, the decision of dropping the code "99" to imply unknown subcategory taken within the GED4ALL project (Silva et al. 2018) was adopted as well (e.g. RES99, which used to refer to "residential, unknown type", became simply RES).
We also modified the mixed use category (MIX). In the present work, MIX1 refers to any combination of residential (RES and subclasses) and commercial/public (COM and subclasses), while MIX gathers any other possible combination, including, for example, a mixture of MIX, COM and IND. This is a simplification from the GEM Taxonomy, which uses MIX1 for "mostly residential and commercial" and MIX2 for "mostly commercial and residential", as it is not possible for us to quantify the meaning of "mostly" within building use information from the datasets used to generate the exposure model. The full list of occupancy types is shown in the upcoming section, while the mapping of NRW-WFS occupancy strings into occupancy classes can be found in the appendix.

9.2.1.3. Resulting exposure model

By 21 August 2019, 286,373 buildings were identified in OpenStreetMap within the administrative boundaries of the city of Cologne. Combining the different data sets listed above, the complete classification of these 286,373 buildings according to their occupancy is shown in Table 9.5.

Table 9.5: Number of buildings in OpenBuildingMap within the administrative boundaries of the city of Cologne classified by occupancy type. Shaded areas correspond to unknown properties within each category.

Code	Description	Number
AGR	Agriculture, unknown type	157
AGR1	Agricultural storage	31
AGR2	Animal shelter (barn, stable, zoo building)	249
AGR3	Agricultural processing	1,273
ASS	Assembly, unknown type	183
ASS1	Religious gathering (church, monastery)	968
ASS2	Arena	3
ASS3	Auditorium, cinema, concert hall	57
ASS5	Club house	245
ASS6	Cemetery	89
ASS7	Exhibition hall	40
COM	Commercial and public, unknown type	23,664
COM1	Retail trade	3,018
COM2	Wholesale trade and storage (warehouse)	1,479
COM3	Offices, professional/technical services	4,648
COM5	Entertainment	82
COM6	Public building	138
COM7	Parking	1,304
COM9	Railway station	35
COM11	Recreation and leisure	611

STR 20/02. GFZ German Research Centre for Geosciences.
DOI: 10.2312/GFZ.b103-20026

Code	Description	Number
COM14	Hotel	616
COM15	Restaurant	344
COM16	Bank	79
COM17	Post	5
COM18	Gas station	198
EDU	Education and research, unknown type	252
EDU1	Pre-school	922
EDU2	School	820
EDU3	College and university, offices and/or classrooms	853
EDU4	Research facilities and/or labs	47
EME	Emergency, unknown type	146
EME1	Police	24
EME2	Firefighters	68
GOV	Government, unknown type	2
GOV1	Administration	129
GOV3	Town hall	9
GOV4	Diplomatic mission	4
GOV6	Court house	7
GOV7	Tax and customs	47
GOV8	Prison	55
IND	Industrial, unknown type	663
IND1	Heavy industrial (oil, petrochemical, timber etc)	22
IND2	Light industrial (factories, textiles, breweries etc)	1,662
IND3	Company building within industrial complex	50
IND6	Container	6
LIF	Buildings related to lifelines, unknown type	23
LIF1	Water	73
LIF2	Electricity	1,434
LIF4	Sewage treatment	103
LIF5	Waste disposal	90
MED	Healthcare, unknown	247
MED1	Hospital	114
MED2	Sanatorium	17
MIX	Mixed occupancy: any mixed that is not MIX1	5,565
MIX1	Mixed occupancy: residential and commercial	22,083
OTH	Other occupancy type	38
OTH1	Non-occupied	18
OTH2	Garage	63,372
RES	Residential, unknown type	11,674
RES1	Single dwelling	134,363
RES3	Temporary	1,024
RES4	Institutional housing	327
TRA	Buildings related to traffic and transportation	2
TRA1	Maritime traffic	33
TRA2	Bus traffic	2
TRA3	Railway traffic	163
TRA4	Subway line	17
TRA5	Flight traffic	36
TRA6	Road	22
TRA7	Ropeway	3
UNK	Unknown	226

STR 20/02. GFZ German Research Centre for Geosciences.
DOI: 10.2312/GFZ.b103-20026

Of these, we classified 147,388 (51.5%) as residential while 22,083 (7.7%) were identified as MIX1. All following damage calculations were carried out over these 169,471 buildings. Information on both year of construction and number of stories is known for 129,349 of these 169,471 residential plus MIX1 buildings. Of the remaining 40,122 buildings, a great majority is associated only with data on the number of stories, as shown in Figure 9.7.

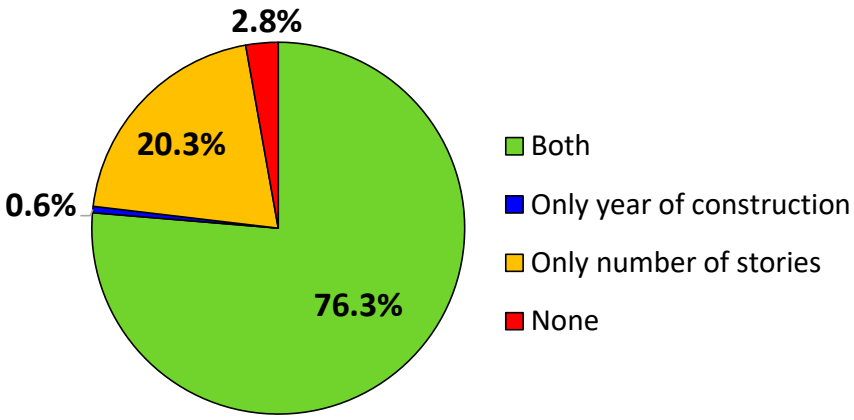

Figure 9.7: Proportions of the 169,471 residential plus MIX1 buildings with associated year of construction and number of stories (green), only year of construction (blue), only number of stories (yellow) and none of the two (red).

The map in Figure 9.8 shows the number of residential plus MIX1 buildings in each Viertel of the city of Cologne, while the map in Figure 9.9 indicates the corresponding number of buildings with unknown year of construction. The buildings in the colored Viertel account for 165,073 of the total 169,471 buildings, while the remaining 4,398 are distributed within the boundaries of the city but outside all Viertel boundaries available from Schwarz and Maiwald (2019). We used these boundaries to maintain the consistency with the statistics on the distribution of year of construction per Viertel surveyed by the city of Cologne in the year 2000, whose use for the enrichment of the building-by-building model is explained in Section 9.2.2.

STR 20/02. GFZ German Research Centre for Geosciences.
DOI: 10.2312/GFZ.b103-20026

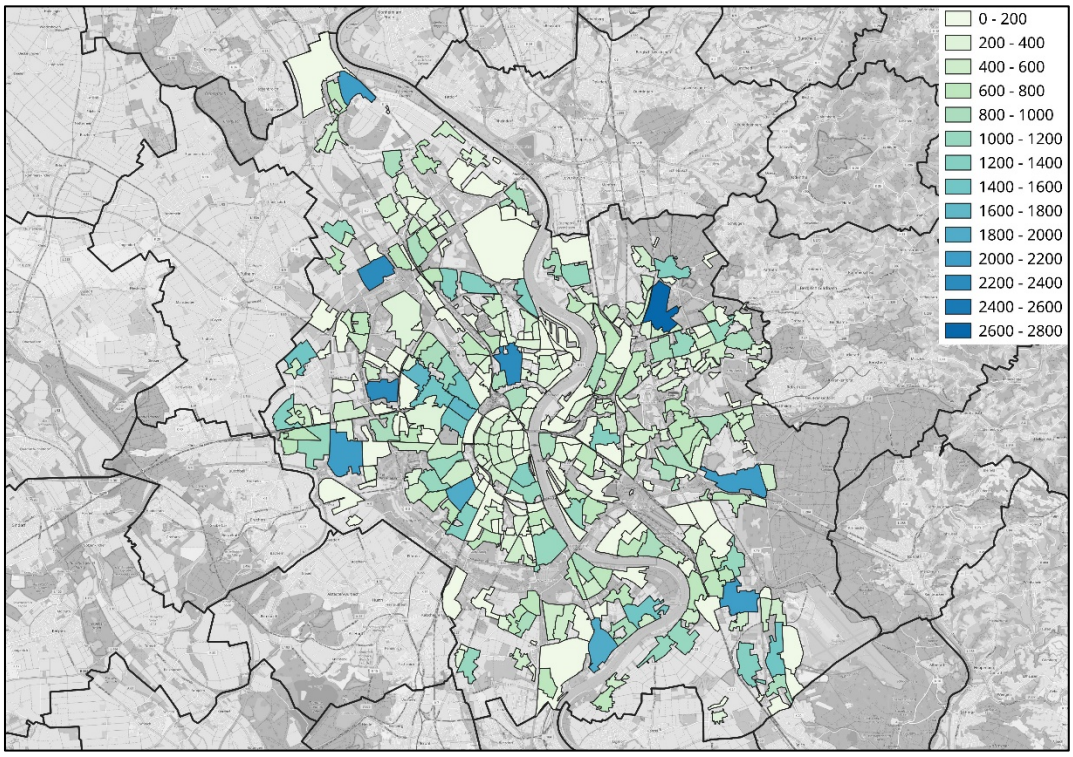

Figure 9.8: Number of residential plus MIX1 buildings per Viertel in the city of Cologne. Shapefile with Cologne Viertel boundaries courtesy of Schwarz and Maiwald (2019).

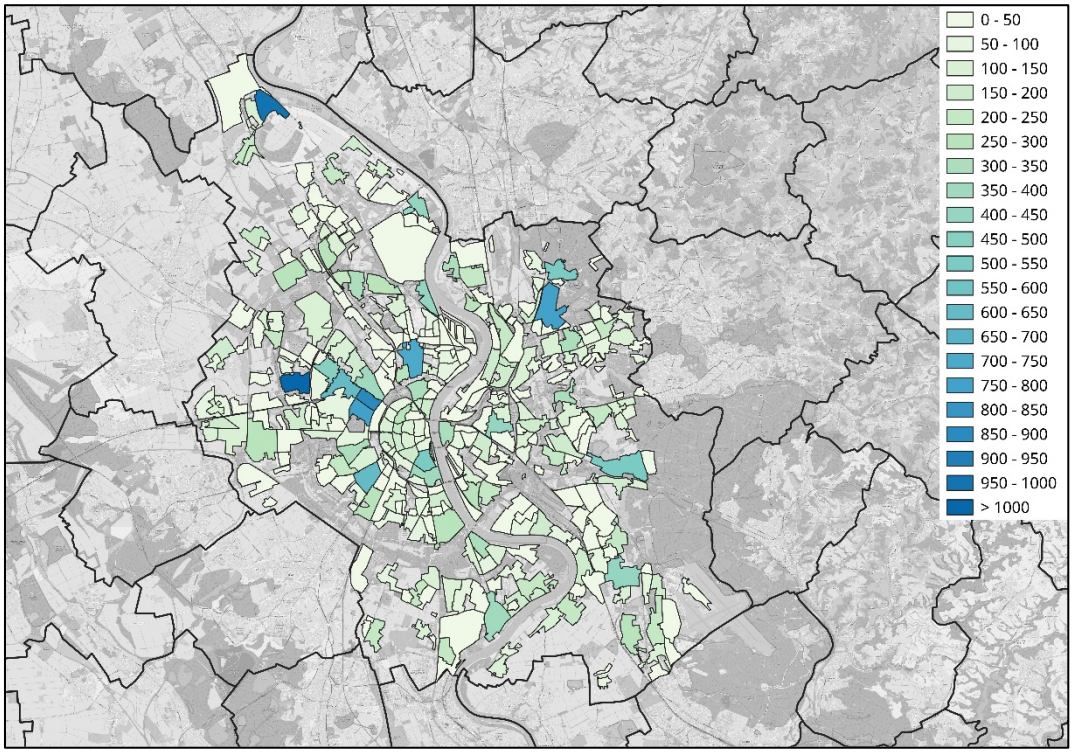

Figure 9.9: Number of residential plus MIX1 buildings with unknown year of construction per Viertel in the city of Cologne. Shapefile with Cologne Viertel boundaries courtesy of Schwarz and Maiwald (2019).

STR 20/02. GFZ German Research Centre for Geosciences.
DOI: 10.2312/GFZ.b103-20026

9.2.1.4. Limitations

Availability of data at the building-by-building level for the development of exposure models suitable for seismic risk assessment is not usual. For this reason, seismic risk studies are usually carried out in an aggregated fashion, either in terms of administrative units for which information regarding the characteristics of the building stock might exist or uniform grid cells (e.g. GED4GEM, Gamba 2014). In this sense, the OpenBuildingMap approach represents a relevant advance as it allows for the computation of risk at a more refined resolution which enables the variability of ground-motion, site response and building exposure within a region as small as Cologne to be taken into account.
Despite this clear advantage, the procedure is not free of limitations, some of which are for the case of Cologne:

- The OKD dataset is retrieved from an open-contribution web service from the city of Cologne. The origin of the information regarding the year of construction within the dataset is not known. Visual inspections using Google Street View, Google Maps 3D view and Mapillary suggest the existence of cases of agreement as well as disagreement with respect to what can be observed and/or inferred from photos.
- Matching of different datasets, that is, establishing a relationship of equivalence between elements of one dataset and those of another is a challenging task and requires that decisions be made when the agreement is not perfect. Several OKD points being enclosed by one OBM polygon or several NRW-WFS polygons intersecting one OBM polygon are examples of the difficulties entailed. A case-by-case human-based decision is not possible when dealing with large datasets.
- It is not uncommon to find buildings that look like separate entities in photos (e.g. Google Street View) but are represented as one polygon in OBM and/or NRW-WFS. It appears that sometimes a polygon represents one structure while in other cases it represents one address. This leads to the number of buildings in OBM potentially not matching that found in other sources of information, such as censuses.
- Along the same line, there appears to be inconsistency with respect to how vertical irregularities (i.e. structures whose height is not the same for the whole of the building) are treated. These parts are sometimes described in a more complex manner within one building polygon, but are often represented as two separate polygons corresponding to the two sections of the building with different height.
- Automatic processing of verbal descriptions of the buildings' functions for the purpose of assigning occupancy types is based on criteria that establish a relationship between keywords and the occupancy finally assigned. In many cases the description is not enough to fully and unequivocally interpret the kind of building under analysis.

Examples of these limitations are given along this report.

STR 20/02. GFZ German Research Centre for Geosciences.
DOI: 10.2312/GFZ.b103-20026

9.2.2. Enrichment of building-by-building exposure with aggregated statistics

As information on the year of construction is not known for around a quarter of the 169,471 (residential) buildings and this data point is fundamental for the assignment of vulnerability classes according to Table 9.2, the building-by-building exposure model was enriched by data aggregated at the city and Viertel levels. The two main sources of these data were the 2011 German National Census and the distribution of year of construction per Viertel surveyed by the city of Cologne in the year 2000 and summarized by Schwarz and Maiwald (2019) in the form of a spreadsheet. These were complemented with knowledge on the distribution of number of stories for each range of year of construction stemming from the three quarters of the buildings for which both parameters were known in OBM. The ultimate goal was to be able to assign years of construction (and numbers of stories, when necessary) to the remaining buildings. As the available sources only add information in an aggregated manner, this assignment was carried out by means of Monte Carlo simulations. In this way, we randomly assigned years of construction (and numbers of stories) to buildings lacking these data from the theoretical distributions derived for each Viertel from the sources mentioned above. The importance of assigning a particular combination of years of construction and number of stories to each building is given by the spatial variability of ground-motions and, therefore, intensities, as different locations of these buildings can lead to different kinds of damage.

9.2.2.1. Distribution of year of construction per district

As the year of construction of each individual building is available on OpenBuildingMap for only around three quarters of the buildings in Cologne, the age distribution of buildings per district was used to assign years of construction to those buildings for which the information is unknown. The age distributions for each district, surveyed by the city of Cologne in the year 2000 and summarized by Schwarz and Maiwald (2019) in the form of a spreadsheet (of which Figure 9.10 is an example) were used for this purpose. The total number of buildings in this dataset is 128,971.

STR 20/02. GFZ German Research Centre for Geosciences.
DOI: 10.2312/GFZ.b103-20026

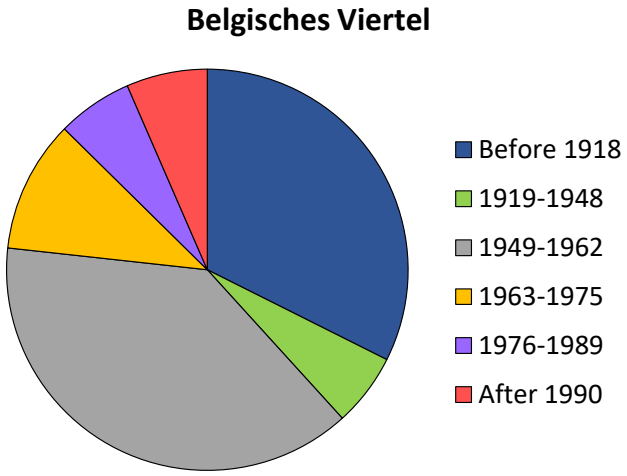

Figure 9.10: Age distribution of buildings in the Belgisches Viertel of Cologne by 31 December 2000 according to data from the city of Cologne as summarized by Schwarz and Maiwald (2019).

According to data from the 2011 German national census, in 2011 there were 132,789 residential buildings ("Wohngebäude") and 4,936 buildings with residential space ("sonstige Gebäude mit Wohnraum") in the city of Cologne (Statistische Ämter des Bundes und der Länder 2018) which add up to a total of 137,725. These numbers imply that 96.4% of the buildings used as residences are purely residential while 3.6% are used both for residential and other purposes.
According to statistics released in 2016 (Stadt Köln 2016), the total number of residential buildings ("Wohngebäuden") in the city of Cologne in the year 2000 was 125,179. Being this number smaller than 128,971, it may be inferred that the total number of residential buildings plus buildings with residential space was 128,971 of which 125,179 represents the 97.1%, while the remaining 2.9% of the 128,971 would correspond to buildings with residential space ("sonstige Gebäude mit Wohnraum").
From the description of the meaning of the Viertel/Stadtviertel as a spatial unit available from Offene Daten Köln (2018), Viertel whose names start with the acronyms GE or GI are business districts and industrial areas, respectively. The dataset provided by Schwarz and Maiwald (2019) includes such districts. However, from the aforementioned considerations we conclude that the buildings enumerated by Schwarz and Maiwald (2019) within GE and GI Viertel are residential or with residential space, as removing the GE and GI Viertel from the entire dataset would lead to a final number of buildings that could not be matched with the other available statistics. Moreover, there are residential (RES) and other buildings with residential space (MIX1) in these Viertel in the OBM data set, a fact that corroborates that GE and GI might refer only to an overall predominant use of the land.
Table 9.6 shows the total number of buildings in the city of Cologne at different points in time and according to the different sources mentioned. Data from OBM is only provided as a total, given that the year of construction is not available for all buildings. The total reduction from the year 2000 to the 2011 Census of 1.4% of the number of buildings built before 1990 may be due to demolitions but also to potential imprecisions in the data sources.

STR 20/02. GFZ German Research Centre for Geosciences.
DOI: 10.2312/GFZ.b103-20026

The statistics regarding numbers of residential buildings available from Stadt Köln (2016) for the period 2000 to 2015 allows to infer an average annual increase of around 0.6%. However, an increase from 137,725 buildings in 2011 to 169,471 buildings in 2019 is equivalent to a much larger average annual increase of over 2.6%. It is unlikely that this dramatic change in annual increase is real. Furthermore, it may be reflecting the existence of more than one OSM polygon per building as well as the difficulties associated with determining the occupancy type of each building. This last statement points not only at the cases in which a misalignment between the OSM and NRW-WFS polygons may result in an OSM polygon being classified as MIX1 when it was, in fact, only commercial but also at the potential discrepancies in the interpretation of what phrases such as "mostly residential" or "building with residential space" mean. Moreover, when importing building data from Stadt Köln (2016) into OSM, mistakes in the official data were found as outlined below.

Table 9.6: Number of buildings with residential space in the city of Cologne.

	Before 1990	**After 1990**	**Total**
Year 2000 as provided by Schwarz and Maiwald (2019)	116,279	12,692	128,971
2011 Census	114,607	23,118	137,725
2019 OBM	-	-	169,471

Apart from 359 easily-identifiable Viertel, the data provided by Schwarz and Maiwald (2019) include an entry for unknown location ("Nicht zugewiesen", referred to as Viertel 0 hereafter) and 61 entries labelled "Zuordnung X", where X is the name of a Stadtteil, an administrative division larger than the Viertel. As these 61 entries contained only 319 buildings overall (i.e. an average of a bit over 5 buildings), we merged them with Viertel 0. When using these data later on, OBM buildings that could not be assigned to any of the 360 Viertel (359 Viertel plus Viertel 0) were treated as a group and we used the distribution resulting from considering all 360 Viertel together as the theoretical distribution for this group.
As the data available from Schwarz and Maiwald (2019) refers to the situation in 2000, we adjusted the age distribution to reflect the increase in the number of buildings during the last two decades. For this purpose, we retrieved from OBM the number of RES plus MIX1 buildings in each Viertel. We then carried out a comparison between the distributions of years of construction per Viertel stemming from each of the two datasets. One of the factors that renders this comparison challenging is clearly the fact that years of construction are not available for OBM buildings, and this is the exact same reason for which the data from the year 2000 is of use and such comparison is needed.
While carrying out this comparison, we observed the following:

- In many Viertel, the total number of buildings in OBM is much smaller than that in the dataset surveyed by the city of Cologne and summarized by Schwarz and Maiwald (2019) (despite the overall sum being larger, as shown in Table 9.6).

STR 20/02. GFZ German Research Centre for Geosciences.
DOI: 10.2312/GFZ.b103-20026

- Distributions of years of construction from the city of Cologne/Schwarz and Maiwald (2019) and the known OBM buildings can be quite different.

Based on these observations and the detailed manual analysis of a few selected Viertel as described below, we determined the adopted *theoretical* distributions of years of construction as depicted in Figure 9.11. This means that for each Viertel, a first decision was made whether the Schwarz and Maiwald (2019) (SM19 hereafter, referring to data surveyed by the city of Cologne in the year 2000) or the OBM distribution should be used. This decision is based on two criteria: (1) the ratio of change from in the total number of buildings from 2000 to 2019 (r_{change}), and (2) the number of OBM buildings for which the year of construction is known ($N_{\text{b known}}^{\text{OBM}}$). The basic assumption behind this is that if the number of OBM buildings is much smaller than that of SM19 buildings (represented by the -15% limit in Figure 9.11), then the use of the SM19 distribution may not be justified. We decided for thresholds of -15% change (i.e. the number of OBM buildings is smaller than that of SM19 buildings by at least 15%) and at least 20 OBM buildings for which the year of construction is known. Out of 360 Viertel, eight were finally assigned the OBM distribution, 97 the SM19 distribution, and 255 and adjusted version of the SM19 distribution, to be used as their corresponding theoretical distributions.

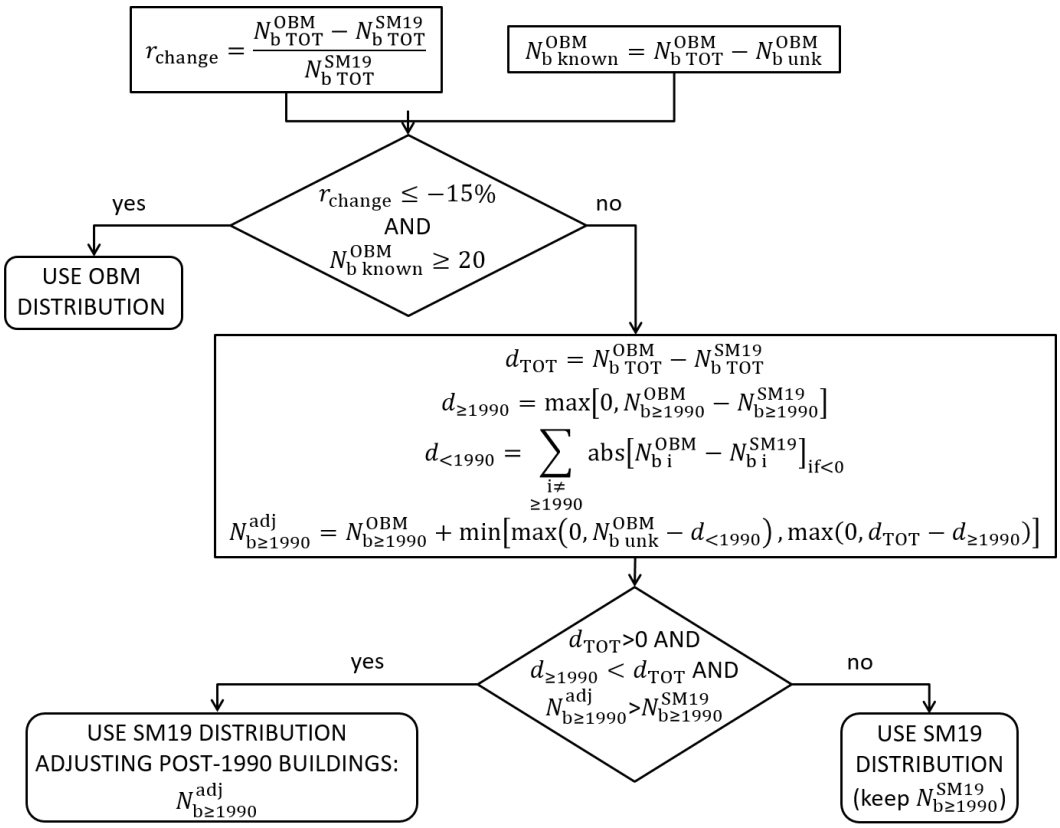

Figure 9.11: Flowchart depicting how the theoretical distributions of year of construction to use were defined for any particular Viertel. SM19 stands for the information for the year 2000 available from Schwarz and Maiwald (2019).

STR 20/02. GFZ German Research Centre for Geosciences.
DOI: 10.2312/GFZ.b103-20026

For those Viertel for which the criterion defined above was not satisfied (*i.e.*, r_{change} > -15% or $N_{b\ known}^{OBM}$ < 20), the SM19 distribution was used. However, as the two distributions stem from datasets gathered 19 years apart, the passage of time and construction of new buildings needed to be taken into consideration. If the data were perfect, no demolitions occurred and the year of construction is known for all OBM buildings. The difference between the number of OBM and SM19 buildings should then correspond to buildings built after the year 2000 and, thus, after 1990, which is the last category considered by Schwarz and Maiwald (2019) for the assignment of vulnerability classes (see Table 9.2).
However, having a proportion of OBM buildings with unknown years of construction and reductions in the number of buildings built before 1990 rendered inferences more complicated. The criterion used was based first on checking (1) if the number of OBM buildings was larger than that of SM19 buildings (i.e. $d_{TOT} > 0$) and (2) if the difference in the number of buildings between OBM and SM19 was larger for the total than for those built after 1990 ($d_{\geq 1990} < d_{TOT}$). If these conditions were met, then the number of buildings built after 1990 was adjusted ($N_{b\geq 1990}^{adj}$), otherwise, the number of buildings built after 1990 was taken as that from SM19 ($N_{b\geq 1990}^{SM19}$). We carried out the adjustment (*i.e.*, the calculation of $N_{b\geq 1990}^{adj}$) accounting not only for those OBM buildings known to have been built after that date but also the largest number of buildings with unknown year of construction that could be allocated to the post-1990 category without contradicting the OBM observations. This last part means the following: if we assume that all additional buildings d_{TOT} were built after 1990, we need to account for the fact that some of those may be already counted in $d_{\geq 1990}$ while some others might remain unknown. Therefore, we cannot assume that the number of post-1990 buildings can be increased with respect to the OBM value more than by the number of buildings with unknown year of construction. Moreover, some of the OBM buildings for which the year of construction is not known may correspond as well to other ranges of year of construction other than after 1990, if the number of buildings in these other ranges is smaller in OBM than in SM19. The summation of the absolute value of the differences between the OBM and the SM19 number of buildings for all ranges other than post-1990 across the cases in which the difference is negative, designated as $d_{<1990}$ in Figure 9.11, accounts for this. Finally, this adjusted value should not be smaller than the number of buildings built after 1990 according to SM19. In our algorithm and, consequently, Figure 9.11, this last condition (*i.e.*, $N_{b\geq 1990}^{adj} > N_{b\geq 1990}^{SM19}$) was verified together with the previous two (see the bottom-most rhombus), though it was left until the end of this explanation for clarity.
Situations in which the number of buildings built before 1990 increased in OBM with respect to SM19 were not solved at this stage but rather during the process of assigning vulnerability classes to buildings as will be explained in the following. Such cases are clearly a problem of inconsistency between datasets and are potentially related to whether a polygon in OBM represents one or more buildings or one building is represented by one or more polygons, and how buildings were counted by the city of Cologne when carrying out the census in the year 2000 (for example, is one building equivalent to one address or one structure?).
Figure 9.12 depicts, as an example, the case of Kuniberts-Viertel. As can be observed, the number of OBM buildings is larger than the number of SM19 buildings by 80 ($=d_{TOT}$), while the number of buildings built after 1990 decreases from 15 to 13 ($d_{\geq 1990}$ = max [0,-2] = 0). With these parameters it is clear from Figure 9.11 that this

STR 20/02. GFZ German Research Centre for Geosciences.
DOI: 10.2312/GFZ.b103-20026

is a situation in which the SM19 distribution was applied with an adjustment for the buildings built after 1990. Assuming all d_{TOT}=80 buildings were built after 1990, and given that there are 167 OBM buildings with unknown year of construction, 80 of which could have been built after 1990, the number of post-1990 buildings is adjusted to be 13 + 80 = 93. Thirteen is taken and not 15 because those two buildings could be within the 167 unknown. The final proportions thus consider 78, 21, 108, 59, 19 and 93 buildings in each category and result in the values shown in the bottom of the plot on the right of Figure 9.12. It is interesting to see how the final adopted distribution keeps the overall signature of the SM19 distribution, while still increasing the proportion of post-1990 buildings (compare 26%-7%-36%-20%-6%-5% against 21%-6%-29%-16%-5%-25%).

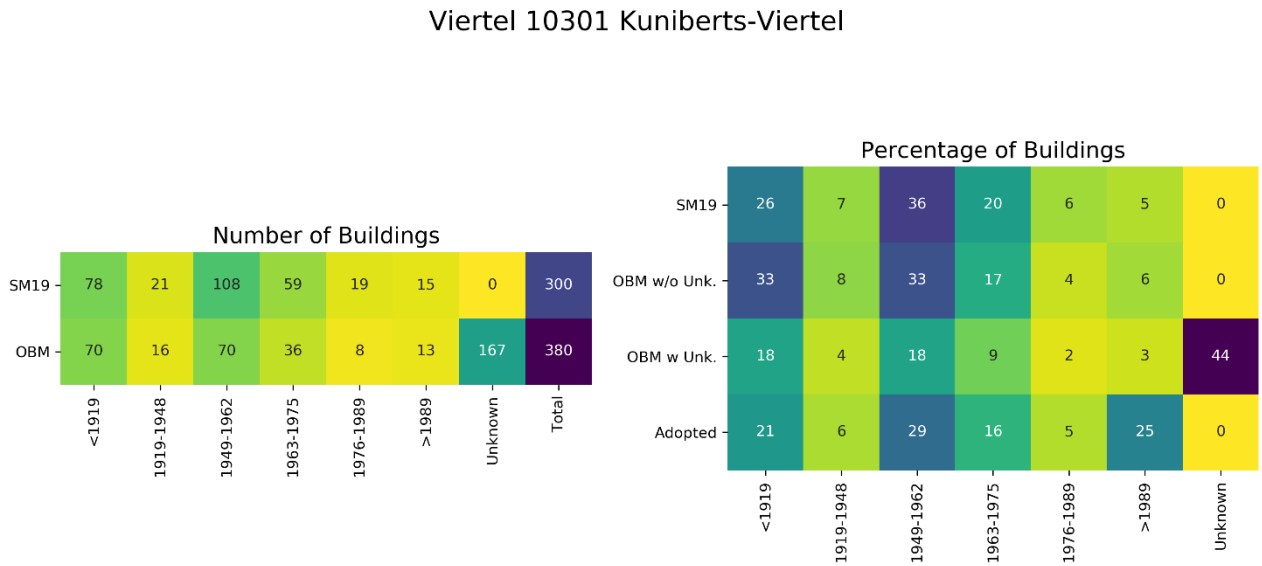

Figure 9.12: Number (left) and percentage (right) of OBM and SM19 buildings by category of year of construction for the Kuniberts-Viertel. In the plot on the right, rows correspond, from top to bottom, to SM19, OBM buildings with known year of construction ("OBM w/o Unk."), all OBM buildings (including those with unknown year of construction; "OBM w Unk."), and the final adopted distribution ("Adopted").

The final distributions adopted by means of these criteria became one of the inputs of the procedure followed to assign vulnerability classes. Two case studies are outlined below.

Case Study 1: Rheinauhafen (Viertel 10107)

A series of photos retrieved from Google Maps 3D view and Mapillary were particularly useful to assess the situation. As shown in Photos 1 and 2 (Figures 9.15 and 9.16), the waterfront is quite modern and thus fits the post-1990 label well. However, Photo 1 also suggests the existence of a building between the modern [H2] and [H3] in Figure 9.13 that appears to be older than the rest. This building can be better observed on the left-hand side of Photo 3 (Figure 9.17). While the ODK dataset indicates 2010 as the year of construction for this building, it is possible that the building was older but renovated and/or refurbished in the reported date. One could

STR 20/02. GFZ German Research Centre for Geosciences.
DOI: 10.2312/GFZ.b103-20026

keep in mind that something similar occurs with the building to the north of H3, which is depicted in Photo 4 (Figure 9.18) and on the right-hand side of Photo 5 (Figure 9.19). A Google Street View photo from 2008 (not shown herein) indicates this building under construction, supporting the idea that the aged appearance of both buildings might be an architectural choice and not a reflection of their year of construction. However, from the available photos and information it is not fully clear whether the two pre-1990 buildings identified in the dataset from the year 2000 were demolished and replaced by more modern ones or renovated and reassigned the refurbishing year as construction year. If the latter were the case, it would not be possible to know from the available data whether or not the structure of the buildings was modified during the renovation. The buildings on the left-hand side of Photo 5 are visibly modern.

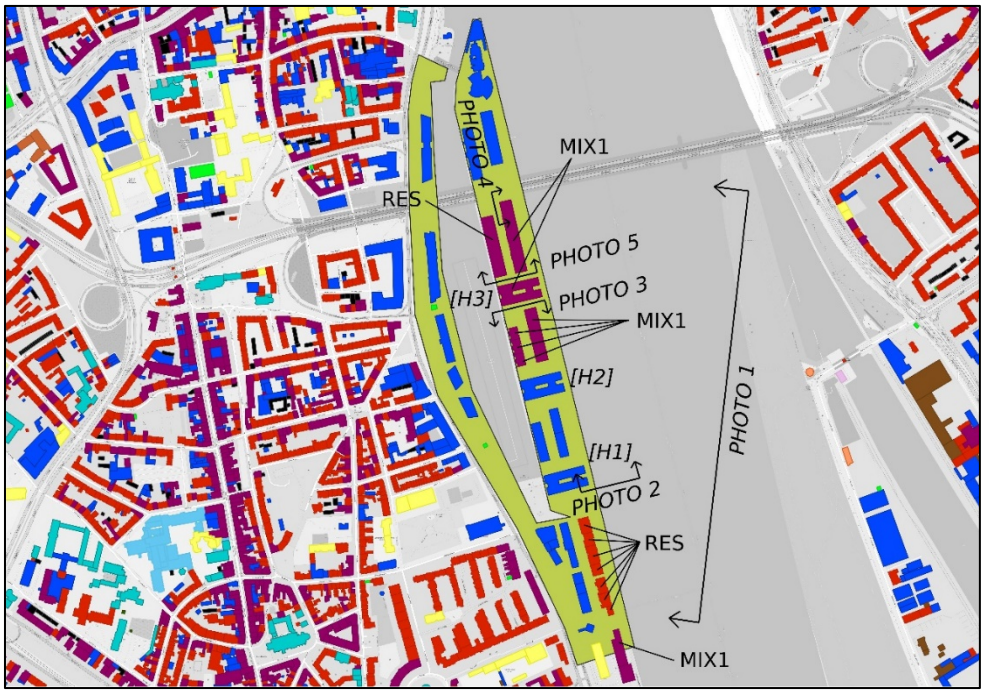

Figure 9.13: Buildings in OBM for Viertel 10107 (Rheinauhafen), which is indicated in green. Buildings colored by occupancy type represent commercial (blue), assembly (turquoise), lifeline-related buildings (green), residential (red), mixed occupancy (burgundy) and industrial (brown). RES and MIX1 buildings are marked.

STR 20/02. GFZ German Research Centre for Geosciences.
DOI: 10.2312/GFZ.b103-20026

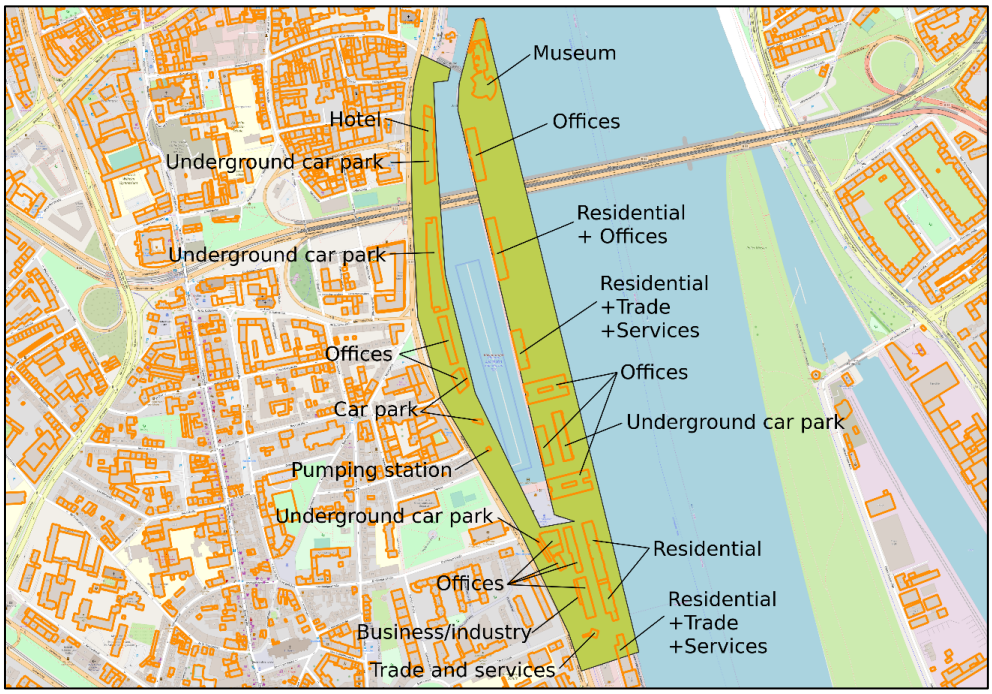

Figure 9.14: Buildings in the NRW-WFS dataset for Viertel 10107 (Rheinauhafen) which is indicated in green. Building function according to the NRW-WFS dataset is as indicated.

In situations like this, in which the total number of buildings has increased from 2000 to 2019 but there are no buildings with unknown year of construction in 2019, we do not adjust the age distribution of the Viertel at this stage. Instead, we deal with inconsistencies in the age distribution later when assigning vulnerability classes based on year of construction, by modifying the theoretical distribution to fit the observations (i.e. in this case, by forcing the number of buildings constructed after 1990 to be 15).

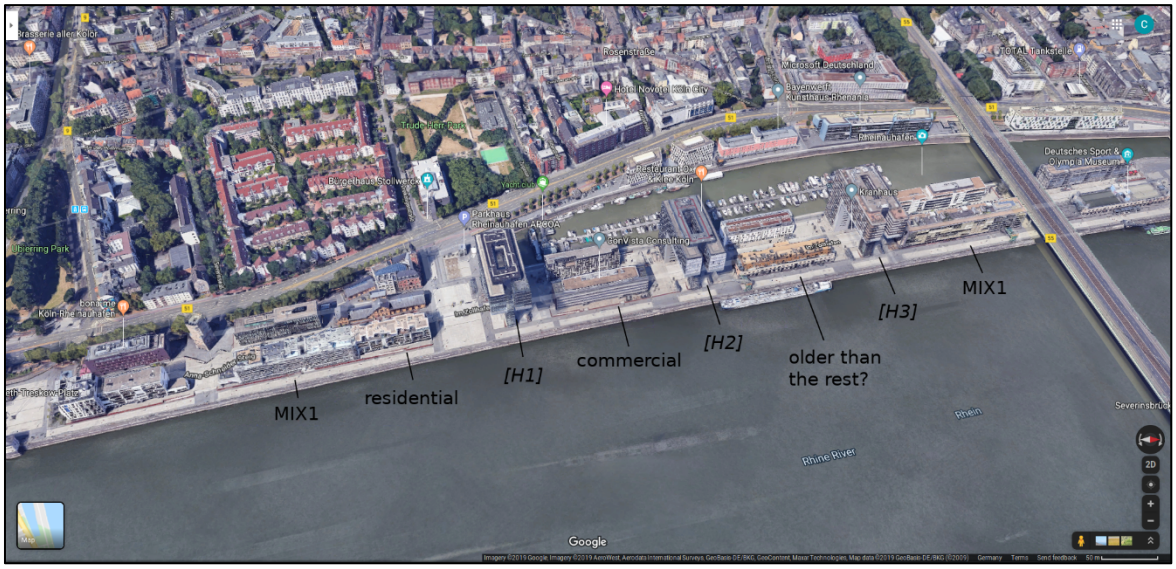

Figure 9.15: View of the waterfront from the river from east to west (Photo 1). Image taken from Google Maps 3D view.

STR 20/02. GFZ German Research Centre for Geosciences.
DOI: 10.2312/GFZ.b103-20026

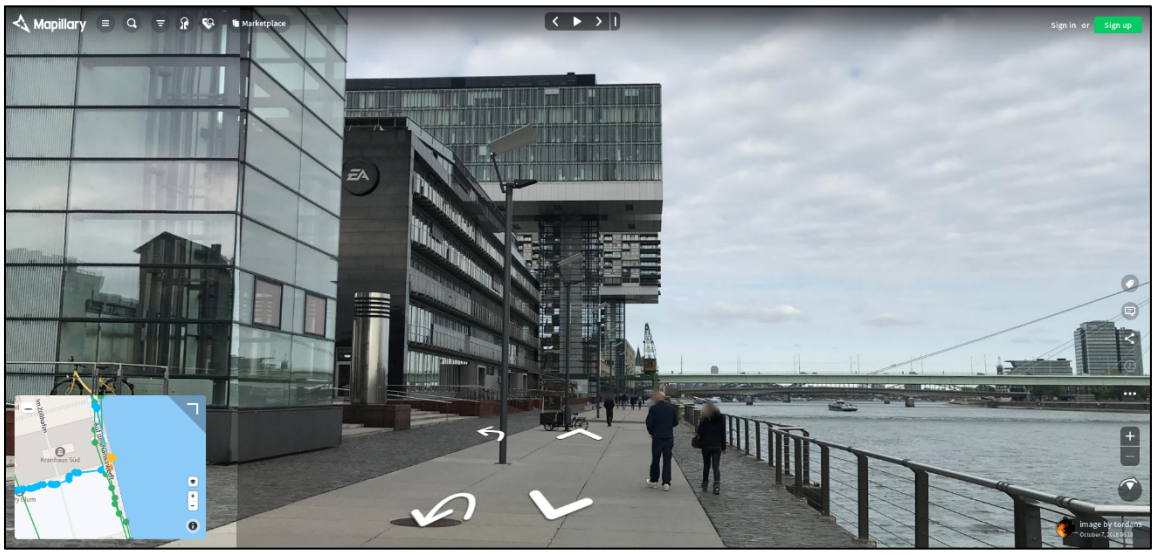

Figure 9.16: View of the waterfront from south to north (Photo 2). Photo by tordans at Mapillary, October 2018.

Figure 9.17: View of building in between H2 and H3 from north to south (Photo 3). Photo by tordans at Mapillary, October 2018.

STR 20/02. GFZ German Research Centre for Geosciences.
DOI: 10.2312/GFZ.b103-20026

Figure 9.18: View of building to the south of the bridge looking from west to east (Photo 4). Photo by tordans at Mapillary, October 2018.

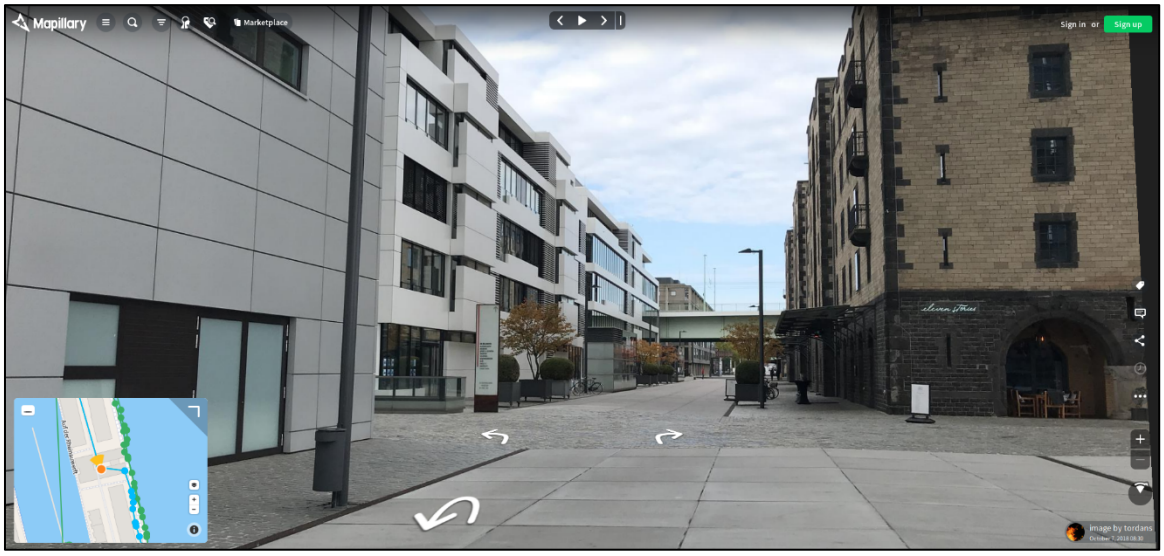

Figure 9.19: View of buildings close to the bridge from south to north (Photo 5). Photo by tordans at Mapillary, October 2018.

Case Study 2: Martins-Viertel (Viertel 10306)

In the case of Viertel 10306, there appear to be 46 buildings less in OBM than in the SM19 dataset, a decrease equivalent to 30.2% (Figure 9.20). Due to this and the fact that information on year of construction is available in OBM for over 20 buildings, the adopted theoretical distribution for this Viertel is the OBM one. It is, however, of interest to inspect the potential reasons for the seemingly large reduction in the number of buildings in time and the increase in the number of buildings built before 1948 as shown in the plot on the left of Figure 9.20. This increase in time of buildings built at an older age is a clear sign of inconsistencies across the datasets.

STR 20/02. GFZ German Research Centre for Geosciences.
DOI: 10.2312/GFZ.b103-20026

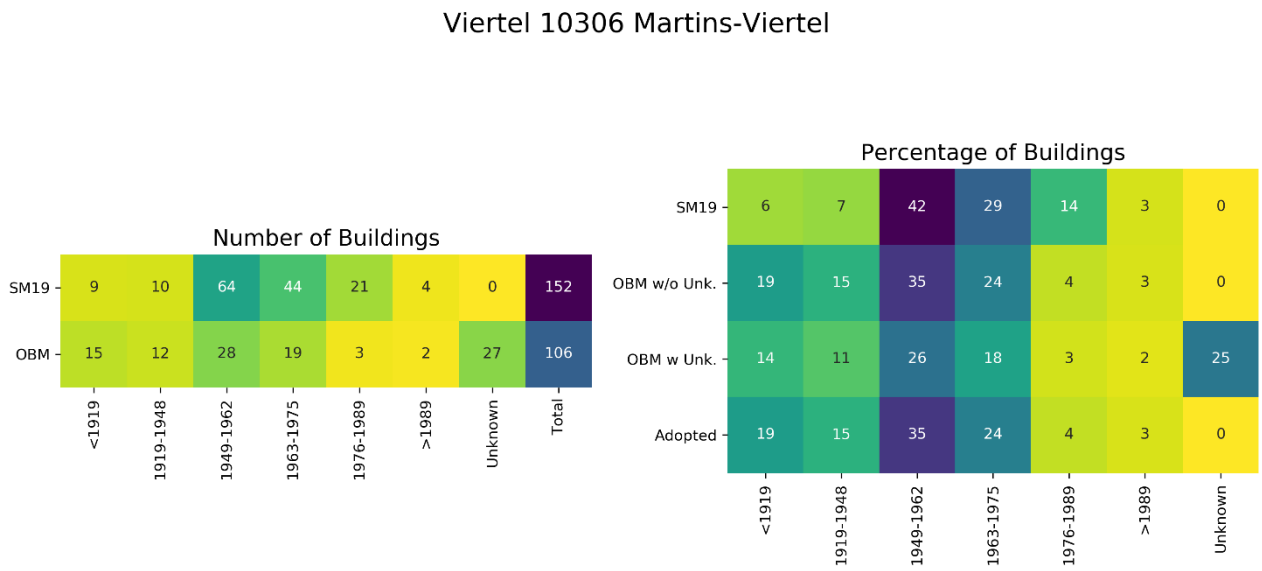

Figure 9.20: Number (left) and percentage (right) of OBM and SM19 buildings by category of year of construction for the Martins-Viertel. In the plot on the right, rows correspond, from top to bottom, to SM19, OBM buildings with known year of construction ("OBM w/o Unk."), all OBM buildings (including those with unknown year of construction; "OBM w Unk.") and the final adopted distribution ("Adopted").

Figure 9.21 shows two plans of the Viertel, one with all OBM buildings (left) and the other showing only those labelled as pre-1919. Figures 9.22 through 9.24 refer to the three cases marked in Figure 9.21 as A, B, and C. Case A refers to two OBM polygons that get associated with their corresponding NRW-WFS polygons, as shown in Figure 9.22. The most western polygon encloses two OKD points, one with date of construction 1900 and the other with 1952, each of them with a different address, and gets assigned 1900 as the year of construction following the criteria of selecting the older when two or more possibilities are found. The most eastern polygon encloses no OKD points and gets assigned the year 1900 as well since the address of the NRW-WFS polygon matches that of the OKD point with year 1900. From the Google Maps 3D view (Figure 9.22) it is not possible to define whether the two polygons are two separate structures or one. It may be that the original building dated from 1900 but its corner was destroyed during World War II and rebuilt in 1952 but this is a hypothesis that has not been verified. It is noted as well that the most eastern polygon is narrower than the most western polygon in both OBM and NRW-WFS but this appears to be the opposite in the Google Maps 3D view. If the SM19 dataset counted this building as two, one with date 1900 and the other with date 1952, then OBM results in more pre-1919 buildings in this case.

STR 20/02. GFZ German Research Centre for Geosciences.
DOI: 10.2312/GFZ.b103-20026

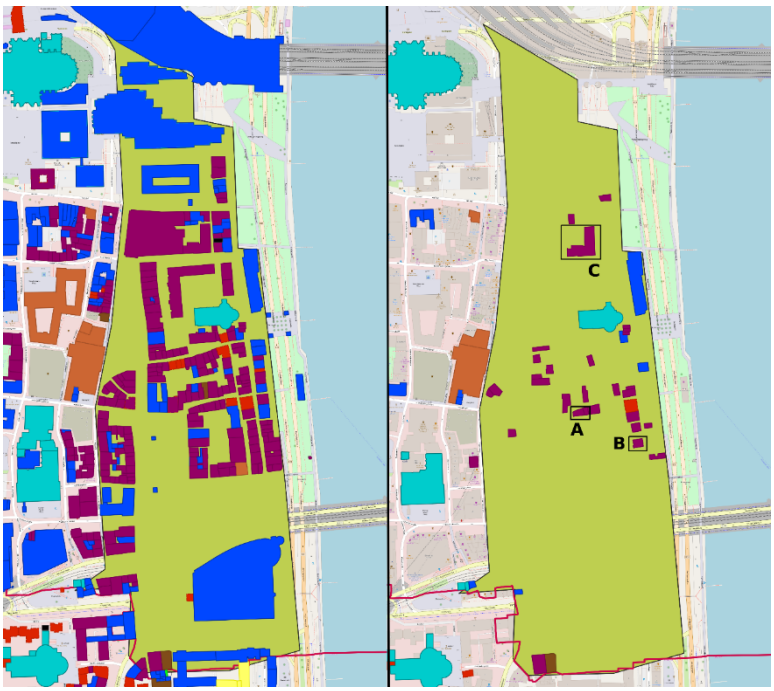

Figure 9.21: OBM buildings in Martins-Viertel: all (left) and only pre-1919 ones (right). Color scale indicates occupancy type (red: residential, blue: commercial, burgundy: mixed).

Figure 9.22: Viertel 10306, case A: superposition of OBM polygons (burgundy), NRW-WFS polygons (orange contours and text) and the OKD points (purple points, white text) (left) and Google Maps 3D view looking from north to south (right).

In Case B, one OBM polygon matches one NRW-WFS polygon and both enclose three OKD points with years of construction 1750, 1936 and 1992, as shown in Figure 9.23. From the Google Maps 3D view, it is not possible to understand why three points are associated with this one polygon.

STR 20/02. GFZ German Research Centre for Geosciences.
DOI: 10.2312/GFZ.b103-20026

Figure 9.23: Viertel 10306, case B: superposition of OBM polygons (burgundy), NRW-WFS polygons (orange contours and text) and the OKD points (purple points, white text) (left) and Google Maps 3D images looking from east to west (center) and west to east (right).

In Case C, an L-shaped OBM polygon matches an equally-shaped NRW-WFS polygon and both enclose four OKD points, three of which have 1895 as the year of construction while one corresponds to 1982. From the Google Maps 3D view (bottom of Figure 9.24) it is not clear why this is treated as one polygon in both OBM and NRW-WFS as it appears possible that this be three buildings instead. However, from photos on Mapillary, it would also appear that the balconies of both the red and the white corner buildings match from the architectural point of view, which could be a sign of the two being actually one building. What is of more relevance, nevertheless, is the fact that none of these buildings follow architectural styles to be expected for 1895. It is thus possible that these three buildings are treated separately in the SM19 dataset and have post-1919 dates, while they get merged into one pre-1919 building in OBM. This would result in a smaller number of buildings at present time.

STR 20/02. GFZ German Research Centre for Geosciences.
DOI: 10.2312/GFZ.b103-20026

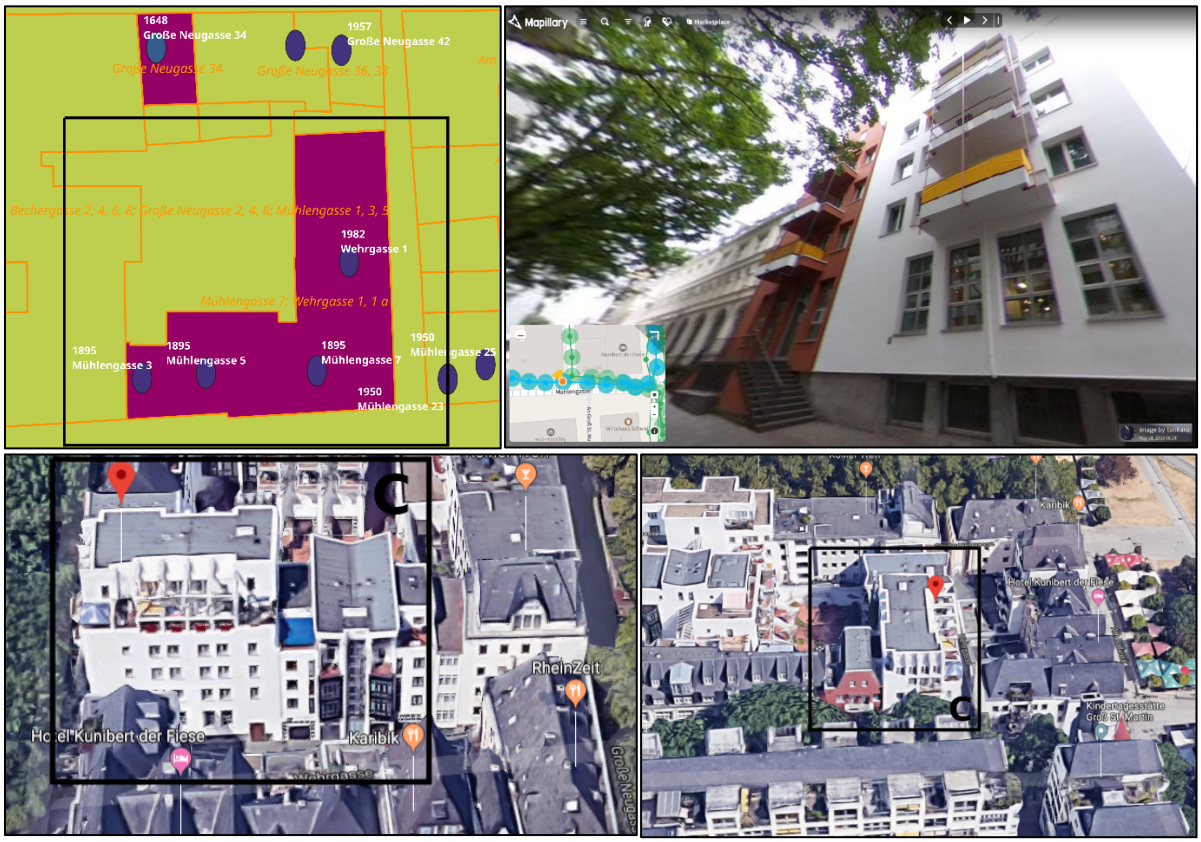

Figure 9.24: Viertel 10306, case C: superposition of OBM polygons (burgundy), NRW-WFS polygons (orange contours and text) and the OKD points (purple points, white text) (top left), photo of the south-eastern corner by tankaru at Mapillary (May 2018, top right) and Google Maps 3D views looking from east to west (bottom left) and south to north (bottom right).

Case D is an extreme example of the case in which several buildings get represented by one polygon in OBM and thus result in a lower number of buildings in the present time than in the SM19 dataset. It is not marked in Figure 9.21 because it does not correspond to pre-1919 buildings. As shown in Figure 9.25, a relatively large OBM polygon that matches a relatively large as well NRW-WFS polygon appears to correspond to several different buildings when looking at the Google Maps 3D view. Seven OKD points are enclosed by the OBM polygon, three of which indicate 1984 as the year of construction, the other four being 1895, 1957, 1985 and 1986. Given the repetition of 1984, this is the year finally adopted in the exposure model.

STR 20/02. GFZ German Research Centre for Geosciences.
DOI: 10.2312/GFZ.b103-20026

Figure 9.25: Viertel 10306, case D: superposition of OBM polygons (burgundy), NRW-WFS polygons (orange contours and text) and the OKD points (purple points, white text) (left) and Google Maps 3D view looking from south to north (right).

9.2.2.2. Distribution of year of construction and number of stories

When attempting to assign years of construction to buildings for which this information is not known in OBM, caution is needed to avoid non-realistic assignments. For example, it is highly unlikely that a 25-story building was built before 1918, and such an assignment of year of construction should be avoided. The relationship between year of construction and number of stories was retrieved from the buildings for which both these parameters are currently available (129,349 of the total 169,471 residential plus MIX1 buildings) and grouped in Table 9.7 according to the ranges of year of construction defined by Schwarz and Maiwald (2019) (see Table 9.2).

Table 9.7: Classification according to ranges of year of construction and number of stories of 129,349 buildings (residential plus MIX1 occupancy types) for which both parameters are available on OBM. Buildings in reddish areas have been visually inspected.

Year of construction	Number of stories									
	1	2	3	4	5	6	7	8	9	≥10
Before 1918	1388	3583	3020	2596	798	84	11	1	0	1
1919-1948	3591	10166	2452	1897	354	55	8	1	0	0
1949-1962	5729	13757	5230	4609	1455	376	125	45	43	15
1963-1975	4945	12800	3320	2653	1058	553	224	274	131	179
1976-1989	4197	8275	1335	981	432	182	69	22	11	41
After 1990	5624	13655	3558	2092	979	259	81	19	2	8

The existence of a few relatively tall old buildings in Table 9.7 (marked in red) is striking and prompted a manual verification of potential outliers. We identified one building with over 10 stories that has been built before 1919. This building is depicted in Figure 9.26 and it gets assigned 1890 as year of construction from its matching

STR 20/02. GFZ German Research Centre for Geosciences.
DOI: 10.2312/GFZ.b103-20026

ODK point, and 12 stories from its matching NRW-WFS polygon. However, as shown in Figure 9.26, it is clearly much more modern than indicated in the ODK dataset. Moreover, notwithstanding the limitations associated with observing images from Google Maps 3D view, it is possible that it may be 13 and not 12 storeys. As this is not a real case of a pre-1919 building taller than 10 stories, it was removed from the table.

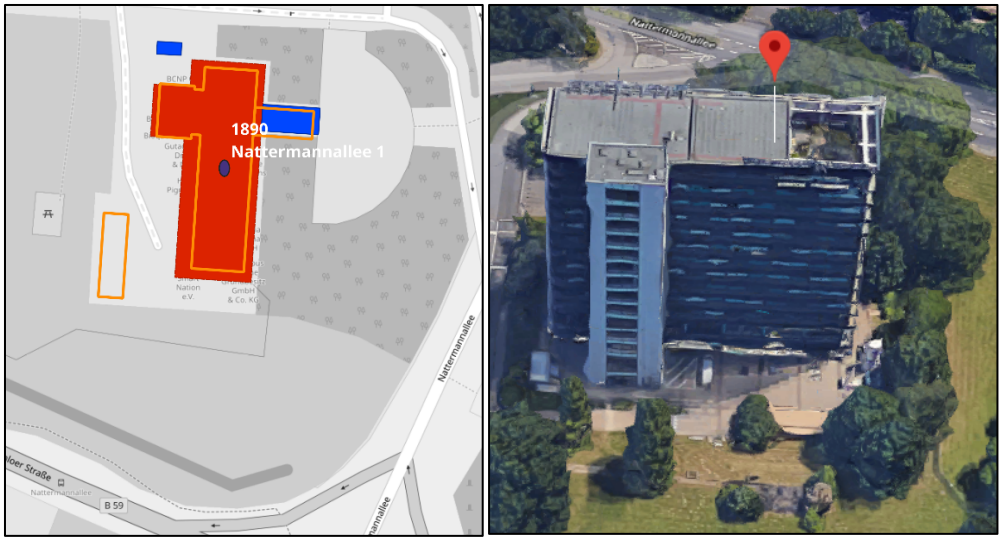

Figure 9.26: OSM building with ID 46837033 (red), NRW-WFS polygons (orange contours) and ODK points (left) and the same building according to Google Maps 3D view (right).

Another pre-1919 building is identified as having 8 stories, the latter number stemming from the associated NRW-WFS polygon. According to the ODK dataset, its year of construction is 1898. However, it is clear from Google Maps 3D view that the year of construction may actually be much more recent (Figure 9.27). The 8 stories appear to match what can be observed. As this is most likely not a real case of a pre-1919 building with 8 stories, it was removed from the table.

STR 20/02. GFZ German Research Centre for Geosciences.
DOI: 10.2312/GFZ.b103-20026

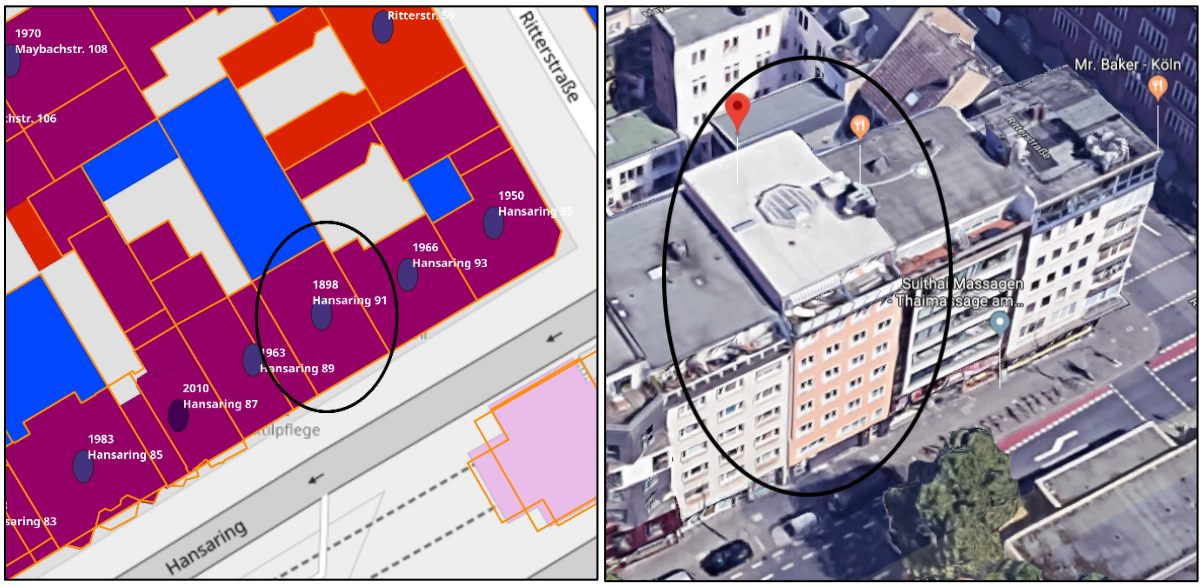

Figure 9.27: OSM building with ID 82103255 (red), NRW-WFS polygons (orange contours) and ODK points (left) and the same building according to Google Maps 3D view (right).

There is only one 8-story building attributed to the period 1919-1948. According to the ODK dataset, this building was built in 1929. However, the images from Google Maps 3D view (Figure 9.28) suggest not only that it is more modern but also that it is likely to be a twin of a building whose date of construction in the ODK dataset is 1970. As in this case the likely year of construction can be deduced as 1970, the building is not eliminated from the table but reallocated to the 1963-1975 period. From the Google images it would appear that both buildings are 9 stories instead of 8.

Figure 9.28: OSM building with ID 135232595 (red), NRW-WFS polygons (orange contours) and ODK points (left) and the same building according to Google Maps 3D view (right).

STR 20/02. GFZ German Research Centre for Geosciences.
DOI: 10.2312/GFZ.b103-20026

The eleven buildings classified as having seven stories and having been built before 1919 were investigated as well. As described above for the other buildings, seven of these eleven cases were removed from the table and four were kept. The table resulting from all these changes is shown in Table 9.8 and the associated proportions of numbers of stories per range of year of construction that were adopted are shown in Table 9.9.

Table 9.8: Adopted version of Table 9.7 after accounting for outliers as described in the text.

Year of construction	Number of stories									
	1	2	3	4	5	6	7	8	9	≥10
Before 1918	1388	3583	3020	2596	798	84	4	0	0	0
1919-1948	3591	10166	2452	1897	354	55	8	0	0	0
1949-1962	5729	13757	5230	4609	1455	376	125	45	43	15
1963-1975	4945	12800	3320	2653	1058	553	224	275	131	179
1976-1989	4197	8275	1335	981	432	182	69	22	11	41
After 1990	5624	13655	3558	2092	979	259	81	19	2	8

Table 9.9: Adopted distribution (%) of number of stories per range of year of construction. Note that each row adds up to 100% (the purpose of this table is not to serve as an age distribution but to indicate the number of stories associated to each age group).

Year of construction	Number of stories									
	1	2	3	4	5	6	7	8	9	≥10
Before 1918	12.1	31.2	26.3	22.6	6.96	0.73	0.03	0.00	0.00	0.00
1919-1948	19.3	54.8	13.2	10.2	1.91	0.30	0.04	0.00	0.00	0.00
1949-1962	18.2	43.8	16.6	14.6	4.64	1.20	0.40	0.14	0.14	0.05
1963-1975	18.9	48.9	12.7	10.1	4.05	2.12	0.86	1.05	0.50	0.68
1976-1989	27.0	53.2	8.59	6.31	2.78	1.17	0.44	0.14	0.07	0.26
After 1990	21.4	51.9	13.5	7.96	3.73	0.99	0.31	0.07	0.01	0.03

9.2.2.3. Procedure for assigning a vulnerability class

While the assignment of vulnerability classes needed to be done for the whole of Cologne, it was the buildings for which no information on year of construction was available that represented a challenge. For the rest, the distributions from Table 9.2 were directly applied.
In order to benefit from the information available regarding the age distribution per Viertel described above, the process described herein was applied on a Viertel-by-Viertel basis. For each Viertel, the procedure was as follows

STR 20/02. GFZ German Research Centre for Geosciences.
DOI: 10.2312/GFZ.b103-20026

1) Create four subsets of buildings within the district:
   1.1) those with both year of construction and number of stories,
   1.2) those only with year of construction,
   1.3) those only with number of stories,
   1.4) those with none of the two.
2) Create a table with the distribution of buildings by year of construction and number of stories for the Viertel using the age structure of the Viertel (label "B" in Figure 9.29) and Table 9.9 (label "A" in Figure 9.29). Keep the age structure adopted as explained above and distribute the subtotal per year of construction across the different number of stories, as exemplified in Figure 9.29 (label "C"). Note that in this and subsequent figures the categories of year of construction and number of stories have been simplified for illustrative purposes.

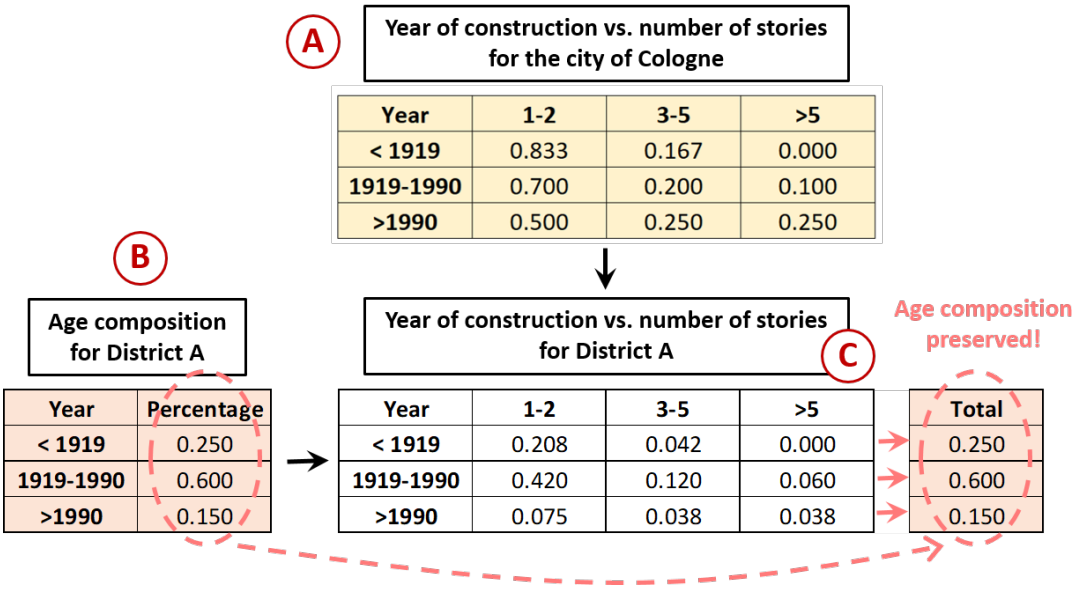

Figure 9.29: Example of how the distribution of the buildings of a district in terms of year of construction and number of stories is generated. The categories of both parameters have been simplified for illustrative purposes.

3) Multiply the table obtained in step (2) by the total number of buildings in the Viertel to obtain a theoretical number of buildings per year of construction and number of stories.
4) Use the table obtained in step (2) to randomly assign a number of stories to those buildings for which only the year of construction is known. For this, use the distribution of number of stories of the corresponding year of construction.
5) Classify buildings for which both year of construction and number of stories are known (including those from step (4); subsets i and ii of step (1)) according to their year of construction and number of stories.
6) Compare the theoretical number of buildings from step (3) (label "D" in Figure 9.30) against the counts from step (5) (label "E" in Figure 9.30). If there are

STR 20/02. GFZ German Research Centre for Geosciences.
DOI: 10.2312/GFZ.b103-20026

any cases in which the number of buildings counted is larger than the theoretical one, adjust the theoretical numbers by fixing the larger counts to the observations and re-distributing the rest proportionally to the theoretical distribution. In this way, the theoretical age composition is maintained as much as possible while still allowing to account for what is observed in OBM. The adjustment process is illustrated in Figure 9.30.

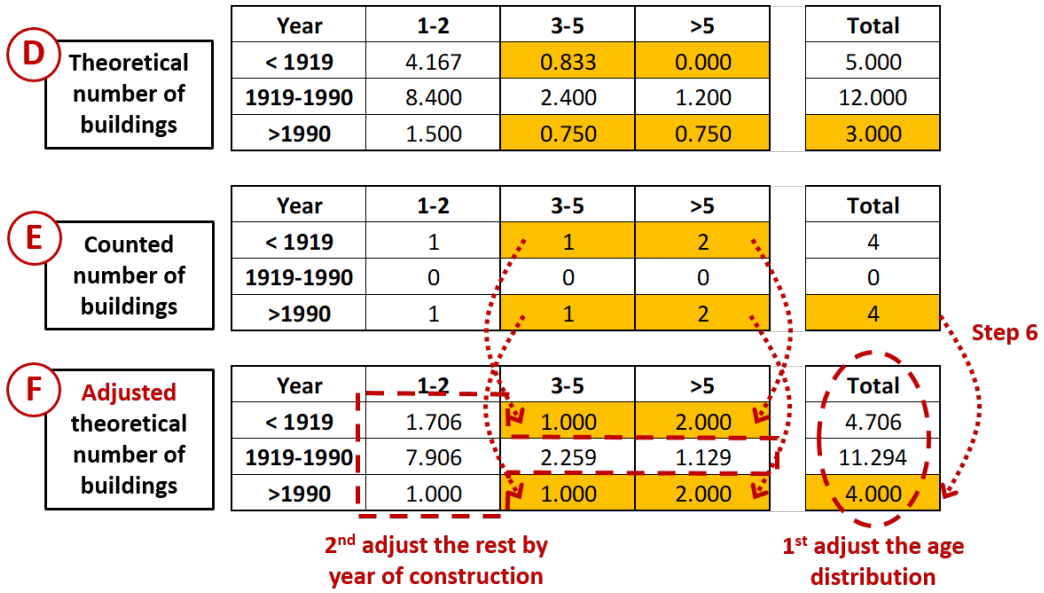

Figure 9.30: Example of how the distribution of the buildings of a district in terms of year of construction and number of stories is adjusted based on counts of buildings from OBM.

7) From the adjusted table just generated (label "F" in Figure 9.30), remove the buildings for which both year of construction and number of stories are known. This new table (label "G" in Figure 9.31) represents only the buildings for which only the number of stories is known and those for which no information is available (subsets iii and iv of step (1)).
8) Compare this last table (label "G" in Figure 9.31) against the number of buildings for which only the number of stories is known (label "H" in Figure 9.31). If the number of observations exceeds the theoretical number in any case, adjust the table by fixing the larger counts to the observations (in terms of totals per category of number of stories) and re-distributing within each category of number of stories as shown in Figure 9.31. If the number of observations is non-zero for a certain category of number of stories but the summation of the theoretical buildings for that category is zero, the distribution of years of construction for the whole of the entire table of virtual buildings to distribute is used for that category.
   A check is carried out against Table 9.9 to force to zero any numbers associated with unlikely old tall buildings (i.e. the final distribution for that category of

STR 20/02. GFZ German Research Centre for Geosciences.
DOI: 10.2312/GFZ.b103-20026

number of stories stems from considering both the distribution of years of construction for the whole of the entire table of virtual buildings to distribute and the distribution of years of construction by number of stories of Table 9.9).

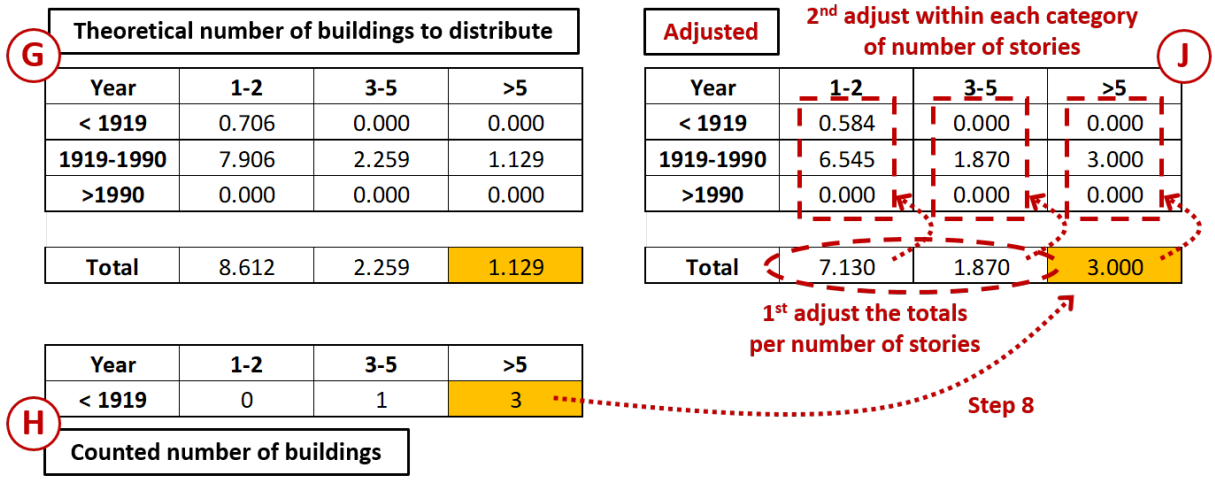

Figure 9.31: Example of adjustment of the table of buildings to distribute amongst those for which only the number of stories is known and those with neither number of stories nor year of construction based on counts of buildings from OBM for which only the number of stories is known.

9) Round the adjusted number of buildings obtained in step (8) (label "J" in Figures 9.31 and 9.32) into integers. Adjust by adding/subtracting buildings to cells with the greatest discrepancy between the integer and the real number if the total number of buildings differs from the one of step (8), as exemplified in Figure 9.32. Do this first by category of number of stories comparing against buildings for which only the number of stories is known and then for the whole table comparing against the total number of buildings from subsets iii and iv of step (1).

STR 20/02. GFZ German Research Centre for Geosciences.
DOI: 10.2312/GFZ.b103-20026

J **Real**

Year	1-2	3-5	>5	
< 1919	0.584	0.000	0.000	
1919-1990	6.545	1.870	3.000	
>1990	0.000	0.000	0.000	Σ=12

Integers

Year	1-2	3-5	>5	
< 1919	1	0	0	
1919-1990	7	2	3	
>1990	0	0	0	Σ=13

Difference Real vs Integer

Year	1-2	3-5	>5
< 1919	0.416	0.000	0.000
1919-1990	0.455	0.130	0.000
>1990	0.000	0.000	0.000

K **Adjusted Integers**

Year	1-2	3-5	>5	
< 1919	1	0	0	
1919-1990	6	2	3	
>1990	0	0	0	Σ=12

Figure 9.32: Example of adjustment of the integer table of buildings to distribute.

10) Go one by one through all the buildings for which only the number of stories is known and randomly assign them a range of year of construction based on the distribution for their corresponding number of stories (according to the table labelled "K" in Figure 9.32). Each time a building is assigned, it is eliminated from the table containing the combinations of number of stories-years of construction still to distribute.
11) Go one by one through all the buildings for which neither the year of construction nor the number of stories is known and randomly assign them a range of year of construction and number of stories based on the whole table that is left over from step (10). Each time a building is assigned, it is eliminated from the table containing the combinations of number of stories-years of construction still to distribute.
12) Assign the distribution of vulnerability classes to all buildings based on their year of construction (Table 9.2).

The possible combinations of random assignments of years of construction and/or number of stories described in steps (10) and (11) is very large. The importance of assigning a particular combination of years of construction and number of stories to each building is given by the spatial variability of ground-motions and, therefore, intensities, as different locations of these buildings can lead to different kinds of damage. We thus addressed the issue of the large number of possible combinations by means of a Monte Carlo simulation, in which steps (4) through (10) were repeated 200 times. For each realization, the order in which the buildings were assigned years of construction and/or number of stories was random, too, and the probability of occurrence of each damage grade was calculated as indicated in Chapter 9.1.4. Damage calculations were carried out only once for those buildings for which the year of construction was known. For the remaining buildings, the average (across all Monte Carlo realizations) of the probability of occurrence of each damage grade was adopted

STR 20/02. GFZ German Research Centre for Geosciences.
DOI: 10.2312/GFZ.b103-20026

as the corresponding final value.
As the fragility curves recommended by Schwarz and Maiwald (2019) provide coefficients both considering and not considering the number of stories (see Chapter 9.1.3), assigning a number of stories to buildings for which this information is not available was not strictly necessary. However, as the number of stories is being used herein to avoid assigning non-realistic years of construction, it was deemed reasonable to sample number of stories as well when needed. Moreover, as the number of stories is known for 96.6% of all the buildings in Cologne, we made the decision in order to take advantage of this information.

9.2.2.4. Resulting exposure model

The exposure model that results from the procedure and data described in Chapter 9.2 is based on a building-by-building definition of vulnerability. For the subset of buildings for which both year of construction and number of stories is known, and the subset for which only the year of construction is known and to which random numbers of stories are assigned, the exposure model indicates the year of construction, the number of stories and the resulting probability distribution of vulnerability classes (as per Table 9.2). No year of construction is univocally assigned in the model to each building of the subset for which only the number of stories is known, as neither of the two parameters are assigned to the subset for which nothing is known, as this assignment is done at each iteration of the Monte Carlo simulation. However, as the random assignment stems from the combination of theoretical and observed distributions of year of construction and number of stories, it is still possible to generate the equivalent of Table 9.7 for the whole set of buildings. The resulting table is shown in Table 9.10. The cases of buildings built before 1949 with 8 stories or more shown in Table 9.10 correspond to those discussed above which were removed from the adopted distribution (Tables 9.8 and 9.9) for corresponding to more modern buildings that are assigned an older year of construction in the ODK dataset. They appear in Table 9.10 because this removal was only carried out for the definition of the distribution of number of stories per range of year of construction, but the buildings are still present in the dataset.
The final distribution of number of stories per range of year of construction is shown, in turn, in Table 9.11. As can be observed, the tendencies of Table 9.9 have been overall preserved. Differences are due to the existence of buildings for which the number of stories is known (but not the year of construction) and the assumptions regarding buildings with no year of construction data having been built after 1990.

STR 20/02. GFZ German Research Centre for Geosciences.
DOI: 10.2312/GFZ.b103-20026

Table 9.10: Final distribution of year of construction and number of stories for the total 169,471 residential plus MIX1 buildings.

Year of construction	Number of stories									
	1	**2**	**3**	**4**	**5**	**6**	**7**	**8**	**9**	**≥10**
Before 1918	2022	4140	3578	3068	950	97	14	1	0	1
1919-1948	5099	10777	2719	2177	490	103	36	1	0	0
1949-1962	7468	14633	5562	5001	1705	446	145	60	46	19
1963-1975	6368	13524	3652	2996	1184	595	243	294	144	189
1976-1989	4763	8515	1436	1116	543	204	76	24	14	44
After 1990	18976	21324	6200	4394	1674	441	125	36	3	16

Table 9.11: Final distribution (%) of number of stories per range of year of construction (each row adds up to 100%) for the total 169,471 residential plus MIX1 buildings.

Year of construction	Number of stories									
	1	**2**	**3**	**4**	**5**	**6**	**7**	**8**	**9**	**≥10**
Before 1918	14.5	29.8	25.7	22.1	6.85	0.70	0.10	0.01	0.00	0.01
1919-1948	23.8	50.3	12.7	10.1	2.29	0.48	0.17	0.00	0.00	0.00
1949-1962	21.2	41.7	15.8	14.2	4.86	1.27	0.41	0.17	0.13	0.05
1963-1975	21.8	46.3	12.5	10.2	4.06	2.04	0.83	1.01	0.49	0.65
1976-1989	28.4	50.8	8.58	6.67	3.24	1.22	0.45	0.14	0.08	0.26
After 1990	35.6	40.0	11.6	8.26	3.15	0.83	0.24	0.07	0.01	0.03

Combining the total number of buildings per range of year of construction and the distribution of vulnerability classes per range of year of construction (Table 9.2) allows for the calculation of the overall aggregated distribution of vulnerability classes in the whole city of Cologne as depicted in Figure 9.33. The plot on the left refers only to the buildings for which the year of construction is known while that on the right refers to the complete set of RES plus MIX1 buildings. As can be observed, over 70% of the building stock is classified as vulnerability class C and around 20% is classified as B. These proportions are in overall agreement with those observed by Schwarz et al. (2004) for a reduced test area. The largest contribution of vulnerability classes CD and D with respect to that shown by Schwarz et al. (2004) is likely due to the assumptions applied regarding the passage of time and construction of new buildings (note the 15-year difference between the aforementioned study and the present work).

STR 20/02. GFZ German Research Centre for Geosciences.
DOI: 10.2312/GFZ.b103-20026

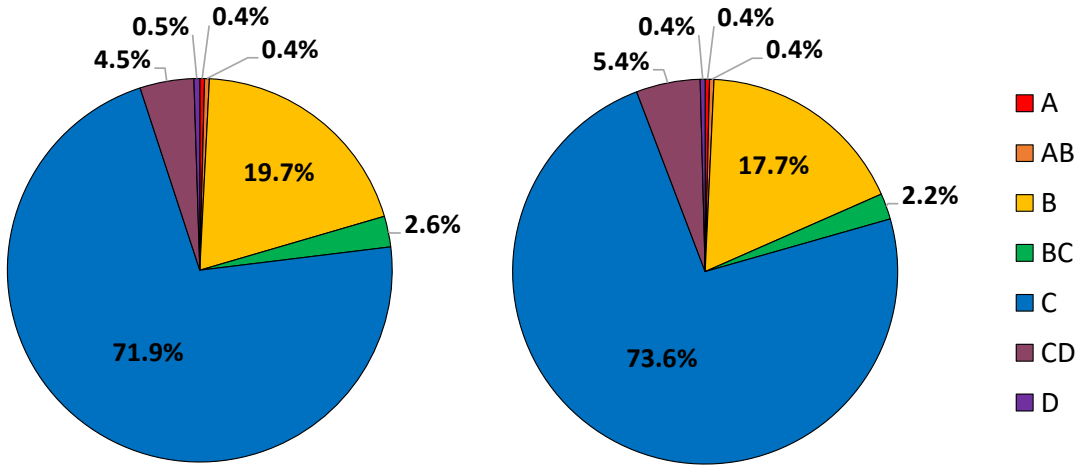

Figure 9.33: Aggregated distribution of vulnerability classes for Cologne: buildings for which the year of construction is known (left) and whole city after the enrichment of the exposure model with aggregated statistics (right).

In order to understand how much the theoretical distributions of years of construction per Viertel were kept or altered along the process, Figure 9.34 gathers a comparison between the theoretical and the final proportions for each range. The differences between the two stem from the adjustment of the theoretical distributions to fit the observations from the OBM values as described in steps 6 and 8 of the procedure. In Figure 9.34, every point represents a Viertel and all Viertel are represented in all ranges of years of construction. As can be observed, the points lie reasonably aligned with the 1:1 diagonal that would indicate that the theoretical and final proportions are the same.
Two sets of points that could be classified as outliers were investigated in more detail: (i) those with large final proportions of buildings of a certain range of year of construction but smaller corresponding proportions in the adopted theoretical distribution (defined in practical terms as > 90% and < 70%, respectively) and (ii) those with the opposite relation between final and theoretical proportions (defined in practical terms as < 5% and > 30%). Most of these cases correspond to Viertel with very few buildings (i.e. Viertel in which each building represents a large proportion of the total), most of which have known years of construction in OBM. At least one case was identified as a potential issue of many OBM polygons representing what appears to be one structure.
The maps in Figures 9.35 through 9.40 depict the resulting proportion of buildings from each range of year of construction per Viertel. These maps do not show the 4,455 buildings (2.6%) classified as not belonging to any of these Viertel ("Nicht zugewiesen" group).

STR 20/02. GFZ German Research Centre for Geosciences.
DOI: 10.2312/GFZ.b103-20026

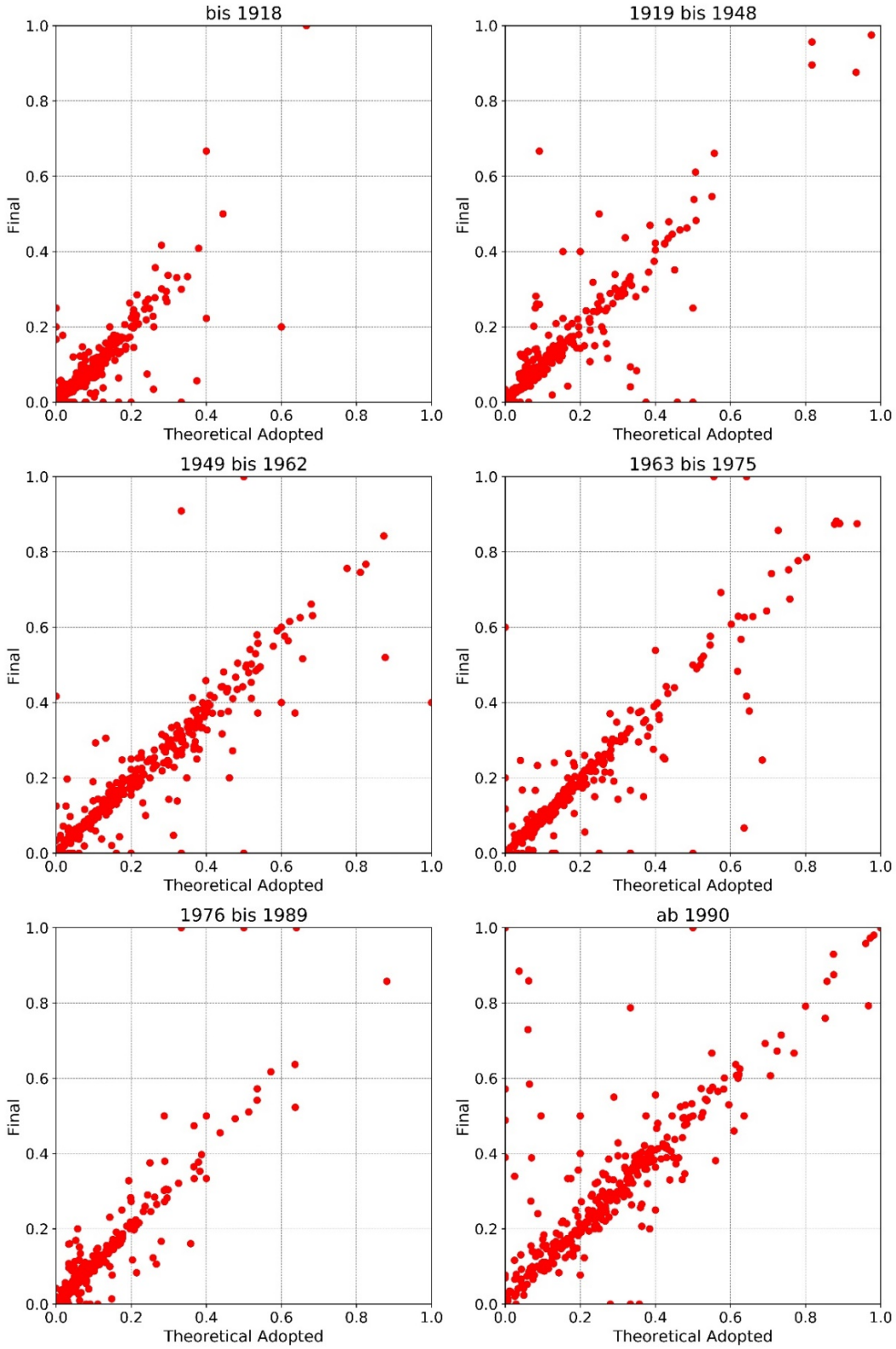

Figure 9.34: Final versus theoretical proportion of each range of year of construction for the whole of Cologne.

STR 20/02. GFZ German Research Centre for Geosciences.
DOI: 10.2312/GFZ.b103-20026

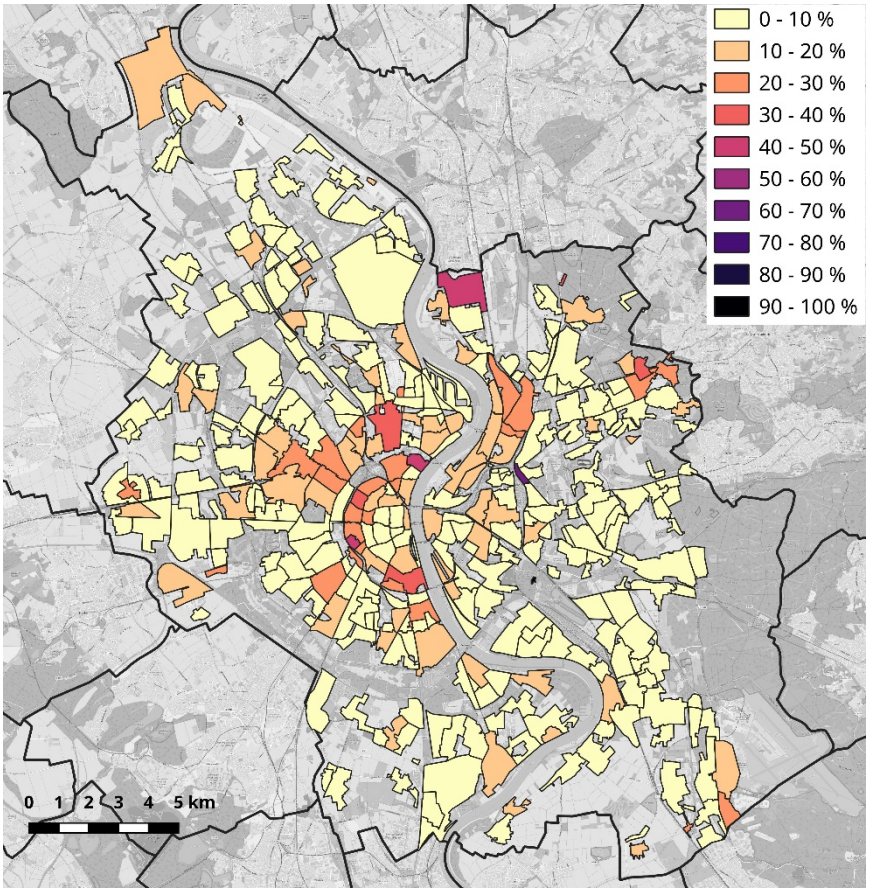

Figure 9.35: Final proportion of buildings built before 1919 per Viertel.

STR 20/02. GFZ German Research Centre for Geosciences.
DOI: 10.2312/GFZ.b103-20026

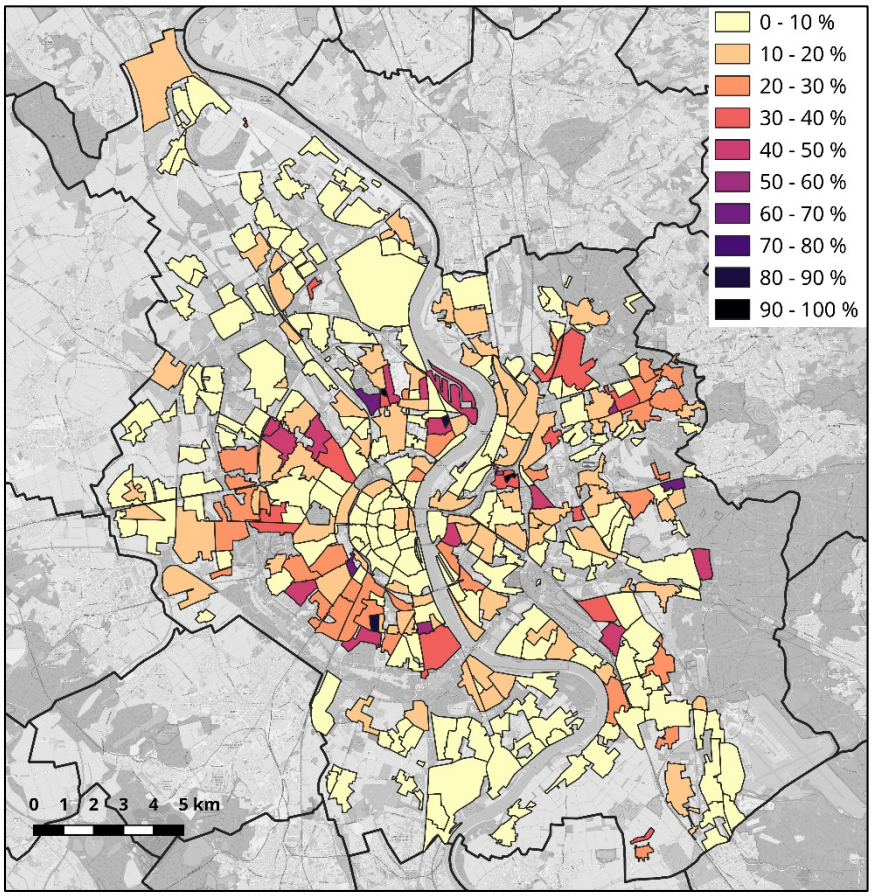

Figure 9.36: Final proportion of buildings built in the period 1919-1948 per Viertel.

STR 20/02. GFZ German Research Centre for Geosciences.
DOI: 10.2312/GFZ.b103-20026

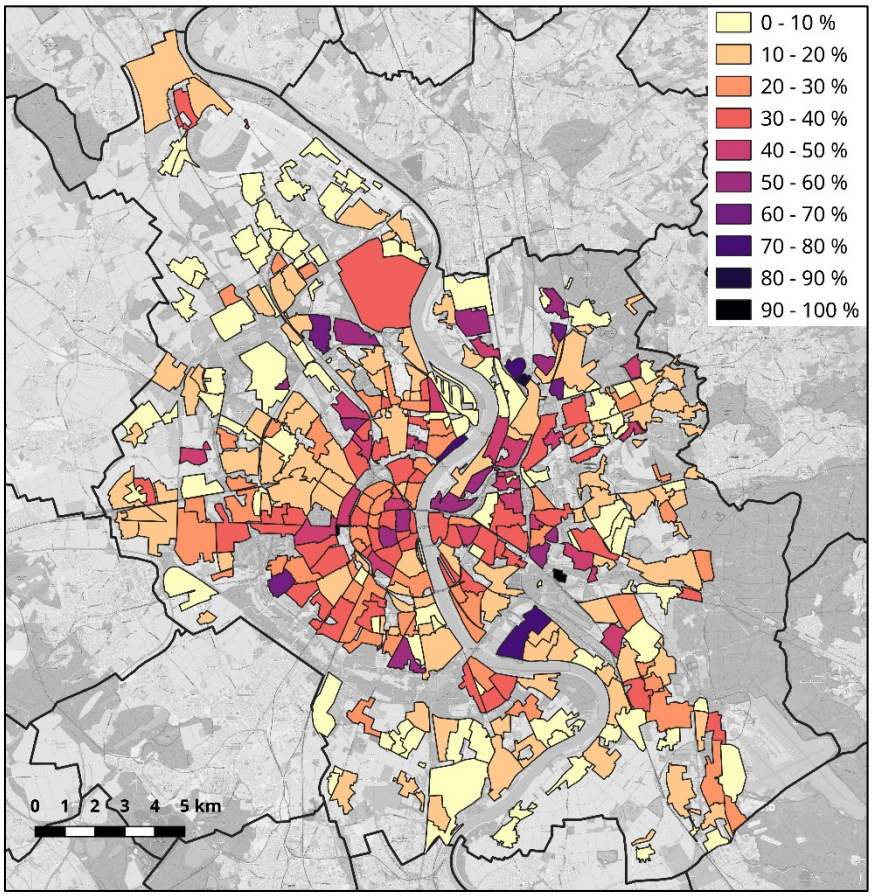

Figure 9.37: Final proportion of buildings built in the period 1949-1962 per Viertel.

STR 20/02. GFZ German Research Centre for Geosciences.
DOI: 10.2312/GFZ.b103-20026

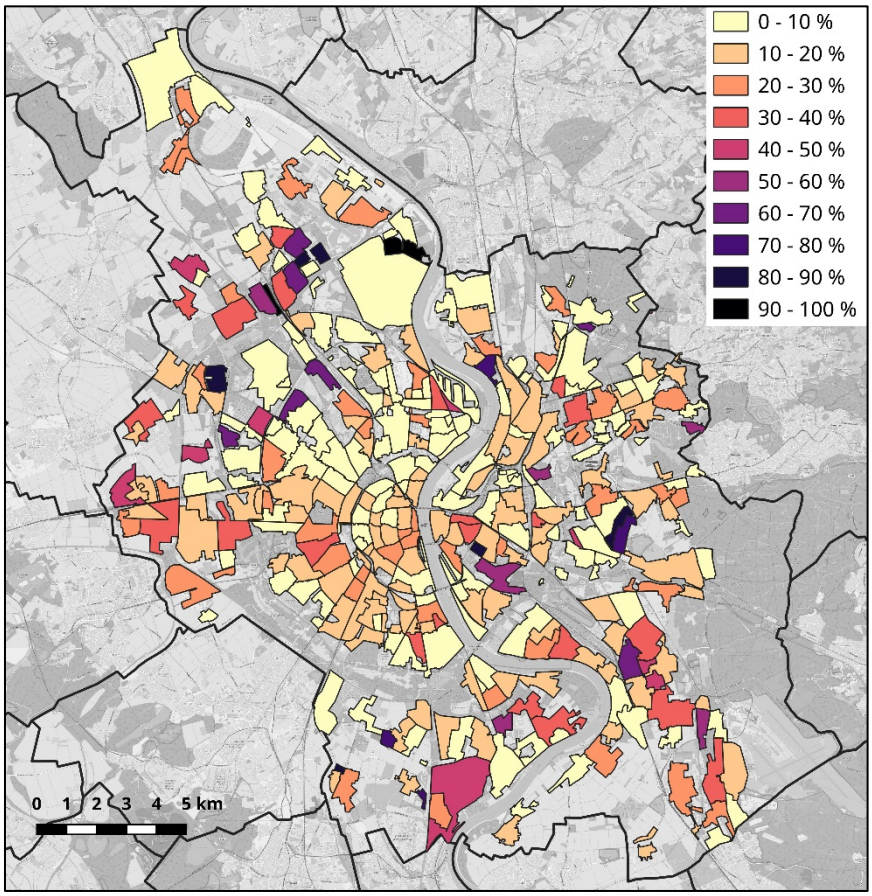

Figure 9.38: Final proportion of buildings built in the period 1963-1975 per Viertel.

STR 20/02. GFZ German Research Centre for Geosciences.
DOI: 10.2312/GFZ.b103-20026

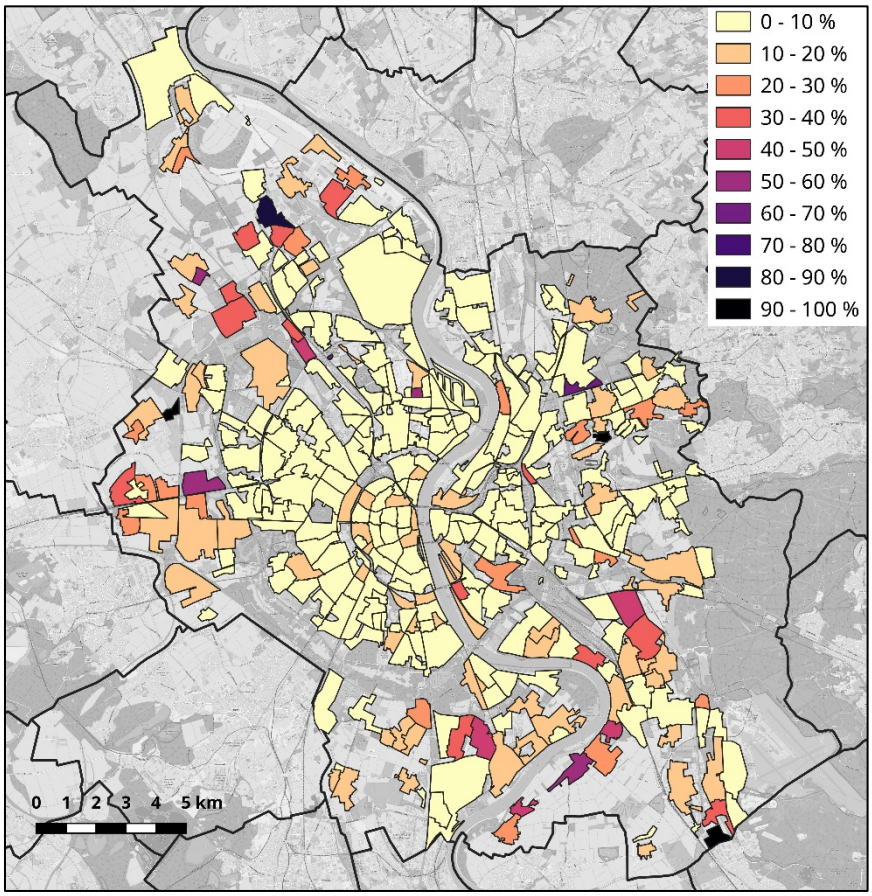

Figure 9.39: Final proportion of buildings built in the period 1976-1989 per Viertel.

STR 20/02. GFZ German Research Centre for Geosciences.
DOI: 10.2312/GFZ.b103-20026

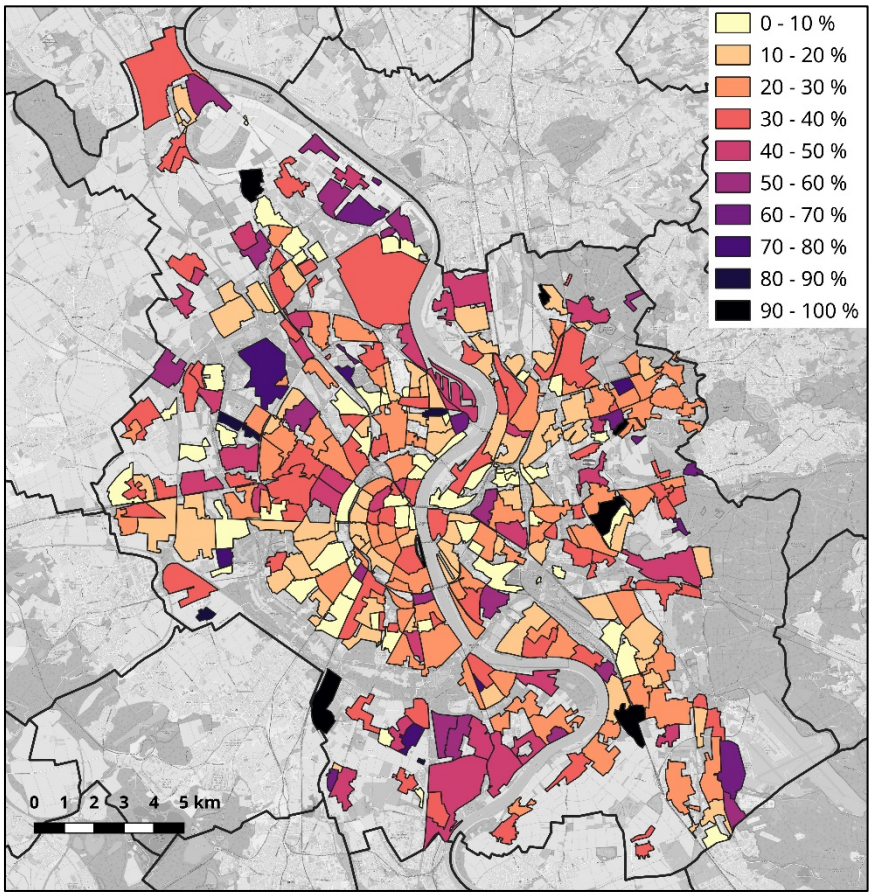

Figure 9.40: Final proportion of buildings built from 1990 onward per Viertel.

9.3. Results

9.3.1. Intensity

Macroseismic intensity is, by nature, a measure of the observed consequences of an earthquake as a whole and not an indicator of the damage suffered by any particular building. This is evident in the definition of the EMS-98 intensity scale which indicates (in qualitative terms) broad proportions of buildings of each vulnerability class that suffer from particular damage grades. Such proportions can only be defined within a collection of buildings and not for individual structures. Nevertheless, as we derived the intensity field from the peak ground acceleration field by means of conversion equations, it can be deemed to represent the severity of the shaking at any particular location. It is under this last perspective that the results shown in Table 9.12 are presented.

Table 9.12 shows the number of buildings subject to each EMS-98 intensity level, making the distinction between residential (understood as all residential plus MIX1-mixed residential and commercial occupancy-classes) and non-residential buildings. Intensity levels are herein defined as bins whose edge and mean values are shown in the "Interval" and "Mean" columns of the table. As can be observed, the proportions are very similar for residential and non-residential buildings, with around 70% of buildings subject to EMS-98 intensities of 7 and most of the remaining ones

STR 20/02. GFZ German Research Centre for Geosciences.
DOI: 10.2312/GFZ.b103-20026

subject to intensity 7.5. Less than 0.5% of the buildings are subject to intensities smaller than 7 or equal to or larger than 8.

Table 9.12: Number of buildings located in areas indicated as having EMS-98 intensity levels in the ranges shown.

EMS-98 intensity		**Occupancy type**					
Mean	**Interval**	**Residential**		**Non-residential**		**Total**	
		Num.	**%**	**Num.**	**%**	**Num.**	**%**
6.5	6.25-6.75	652	0.38	567	0.49	1,219	0.43
7.0	6.75-7.25	118,662	70.02	75,837	64.87	194,499	67.92
7.5	7.25-7.75	50,087	29.55	40,452	34.60	90,539	31.62
8.0	7.75-8.25	70	0.04	46	0.04	116	0.04
Total		169,471		116,902		286,373	

9.3.2. Damage

We express damage of each building as the probability of the building suffering a damage grade (DG0–DG5). The maps in Figures 9.41 to 9.46 depict these probabilities, while Tables 9.13 and 9.14 condense this information in terms of numbers and proportions of buildings that have a certain probability of being affected by a particular damage grade. As can be observed, around half of the total number of residential plus MIX1 buildings have a 20–30% chance of suffering from DG1 (no structural damage, slight non-structural damage), while a further 36% have a 30–40% chance of suffering the same damage. In turn, around half of the buildings have less than a 10% chance of suffering from DG2 (slight structural damage, moderate non-structural damage), while a further 35% and 15% have 10–20% and 20–30% probability of the same damage grade. With increasing damage grades the proportion of buildings with less than 10% chance of observing such damage increases drastically. In the case of DG5, almost all buildings actually have less than 5% such chance.

STR 20/02. GFZ German Research Centre for Geosciences.
DOI: 10.2312/GFZ.b103-20026

Table 9.13: Number of buildings classified according to their probability of observing a certain damage grade (note that the summation of each row is 169,471 because all buildings have some probability of suffering from each damage grade).

DG	Probability of occurrence (%)									
	0-10	10-20	20-30	30-40	40-50	50-60	60-70	70-80	80-90	90-100
DG0	1483	6942	9714	14911	22475	39518	43665	27552	3211	0
DG1	2	14389	93816	61264	0	0	0	0	0	0
DG2	85829	58462	25180	0	0	0	0	0	0	0
DG3	147086	16307	6078	0	0	0	0	0	0	0
DG4	163775	5330	365	1	0	0	0	0	0	0
DG5	169426	45	0	0	0	0	0	0	0	0

Table 9.14: Proportion of buildings classified according to their probability of observing a certain damage grade (note that the summation of each row is 100% because all buildings have some probability of suffering from each damage grade).

DG	Probability of occurrence (%)									
	0-10	10-20	20-30	30-40	40-50	50-60	60-70	70-80	80-90	90-100
DG0	0.88	4.10	5.73	8.80	13.26	23.32	25.77	16.26	1.89	0.00
DG1	0.00	8.49	55.36	36.15	0.00	0.00	0.00	0.00	0.00	0.00
DG2	50.65	34.50	14.86	0.00	0.00	0.00	0.00	0.00	0.00	0.00
DG3	86.79	9.62	3.59	0.00	0.00	0.00	0.00	0.00	0.00	0.00
DG4	96.64	3.15	0.22	0.00	0.00	0.00	0.00	0.00	0.00	0.00
DG5	99.97	0.03	0.00	0.00	0.00	0.00	0.00	0.00	0.00	0.00

The maps in Figures 9.41 to 9.46 show a tendency for the likelihood of higher degrees of damage to be concentrated around the central and western areas of the city. While all six maps should be considered simultaneously when making such a statement, the probabilities of damage grade 0 larger than 70% depicted in Figure 9.41 along the eastern side of the city are first hints in this direction.

STR 20/02. GFZ German Research Centre for Geosciences.
DOI: 10.2312/GFZ.b103-20026

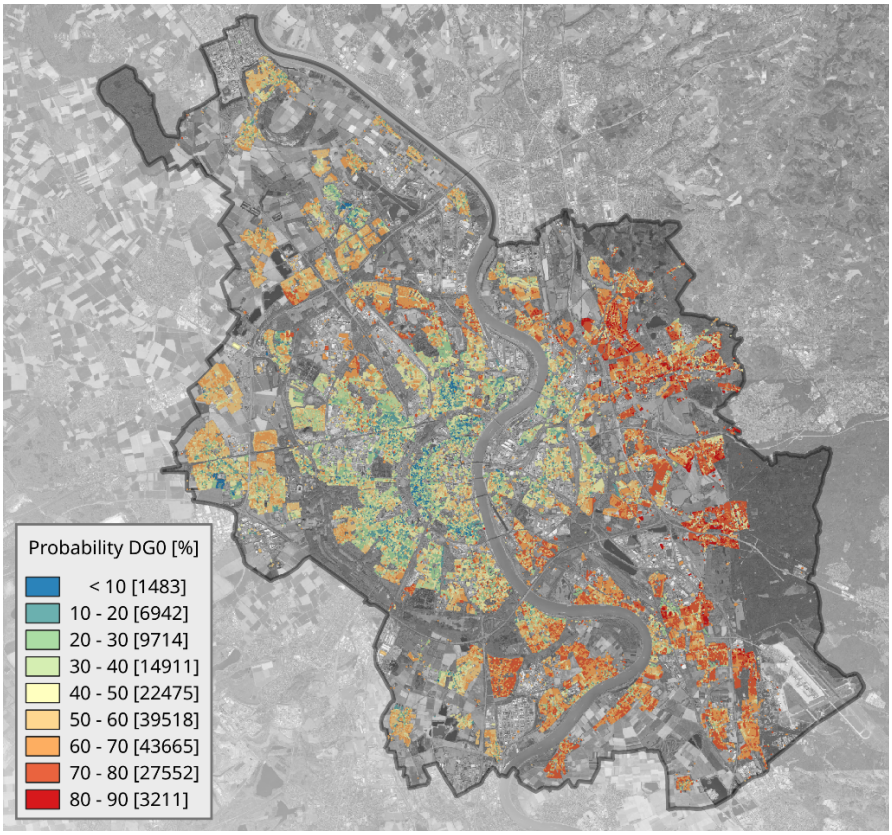

Figure 9.41: Probability of occurrence of damage grade 0 per building.

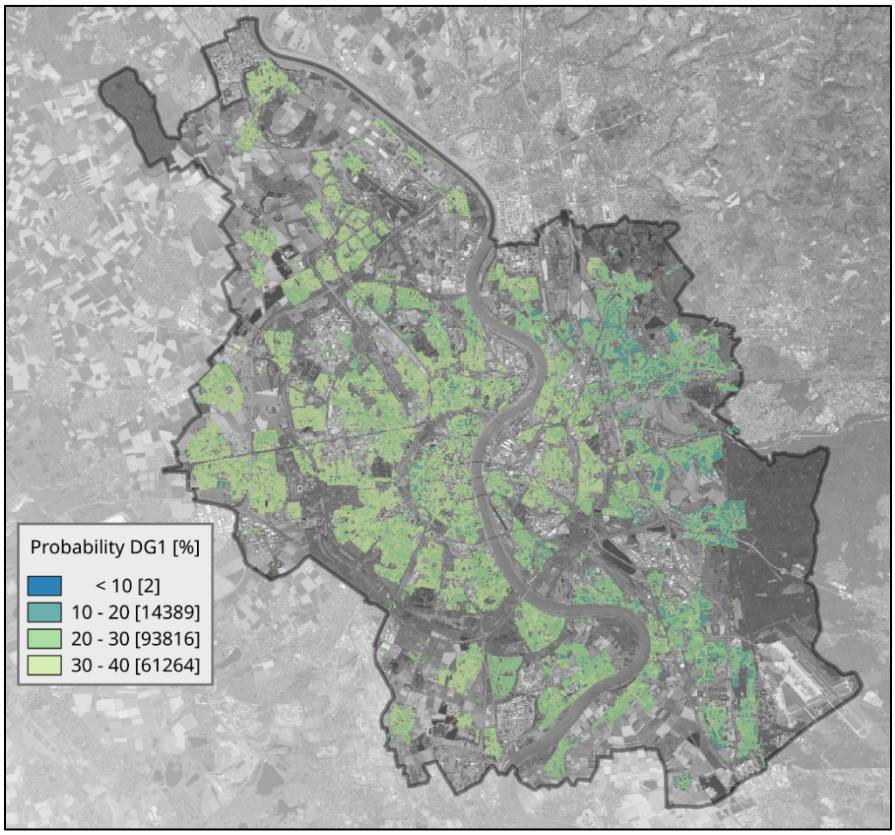

Figure 9.42: Probability of occurrence of damage grade 1 per building.

STR 20/02. GFZ German Research Centre for Geosciences.
DOI: 10.2312/GFZ.b103-20026

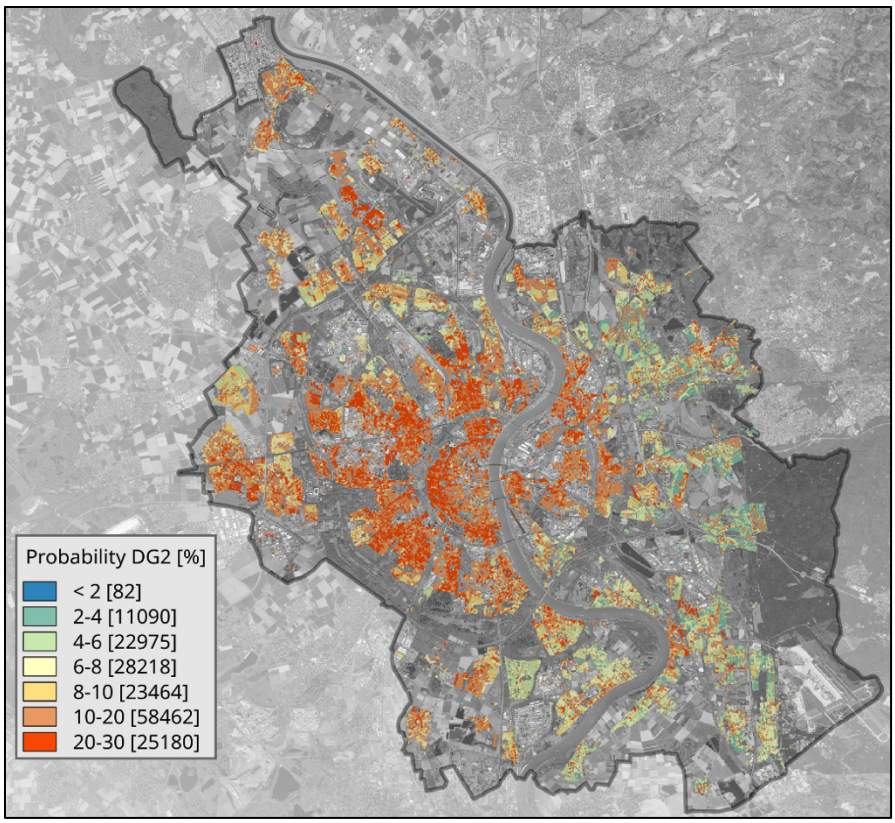

Figure 9.43: Probability of occurrence of damage grade 2 per building.

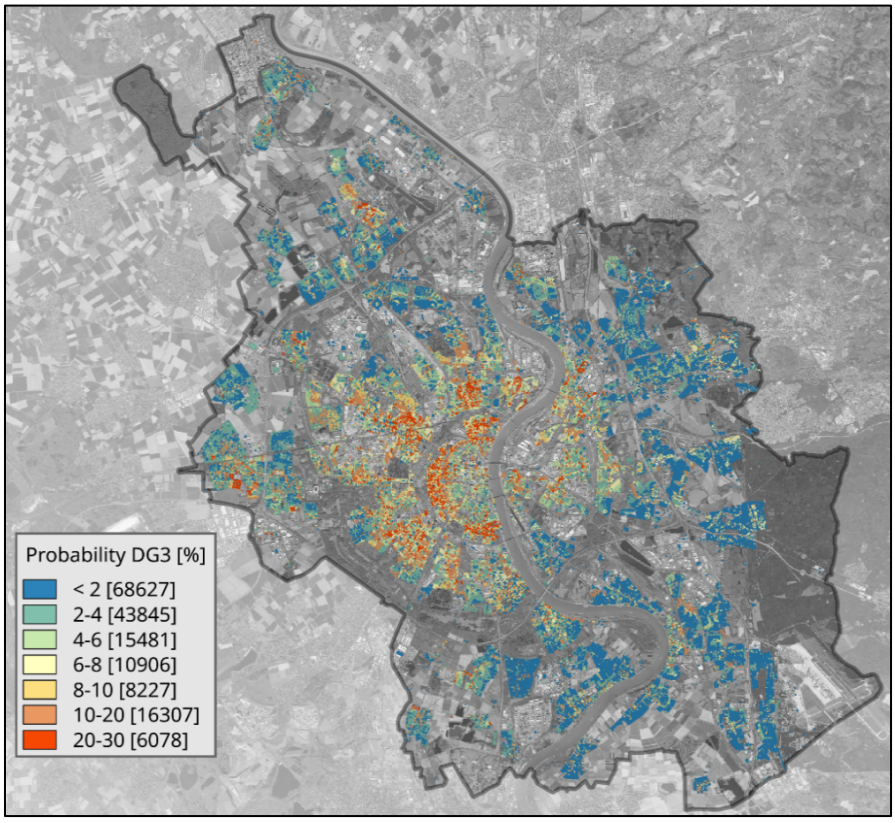

Figure 9.44: Probability of occurrence of damage grade 3 per building.

STR 20/02. GFZ German Research Centre for Geosciences.
DOI: 10.2312/GFZ.b103-20026

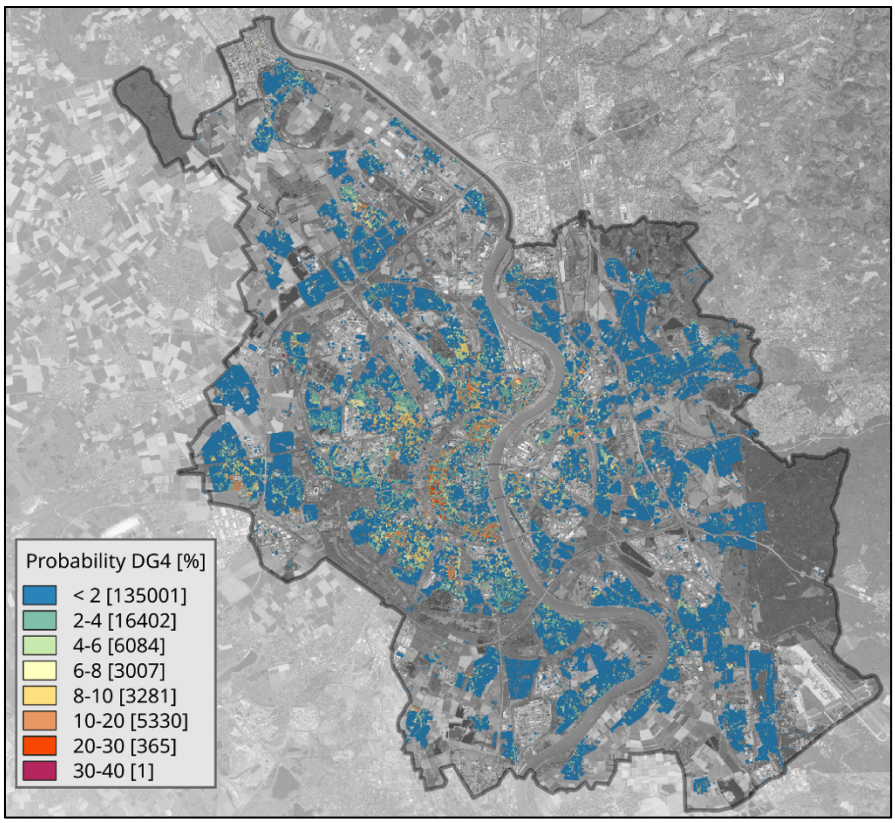

Figure 9.45: Probability of occurrence of damage grade 4 per building.

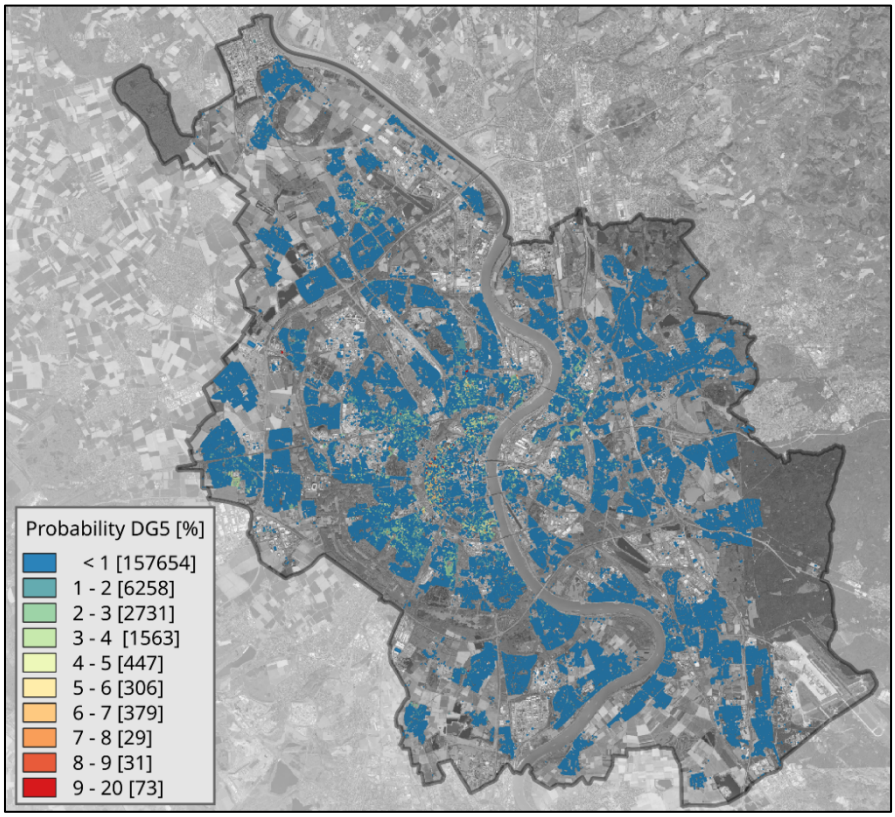

Figure 9.46: Probability of occurrence of damage grade 5 per building.

STR 20/02. GFZ German Research Centre for Geosciences.
DOI: 10.2312/GFZ.b103-20026

We show a very useful representation of results in Figure 9.47, which depicts the percentage of buildings with probability of exceedance of each damage grade (PoE: the probability of observing a particular damage grade or worse) equal to or larger than the values plotted along the horizontal axis. As can be seen

- all buildings have at least a 10% probability of exceeding DG1.
- 64.0% of the buildings have at least a 10% probability of exceeding DG2.
- 19.2% of the buildings have at least a 10% probability of exceeding DG3.
- 5.0% of the buildings have at least a 10% probability of exceeding DG4.
- 0.03% of the buildings have at least a 10% probability of exceeding DG5.

When considering 20% instead of 10% as a relevant threshold, then

- 98.1% of the buildings have at least a 20% probability of exceeding DG1.
- 29.7% of the buildings have at least a 20% probability of exceeding DG2.
- 8.1% of the buildings have at least a 20% probability of exceeding DG3.
- 0.7% of the buildings have at least a 20% probability of exceeding DG4.
- 0.0% of the buildings have at least a 20% probability of exceeding DG5.

From these numbers we conclude that the possibility of observing very heavy damage (DG4) cannot be ruled out and the possibility of observing substantial to heavy damage (DG3) is not negligible at all.

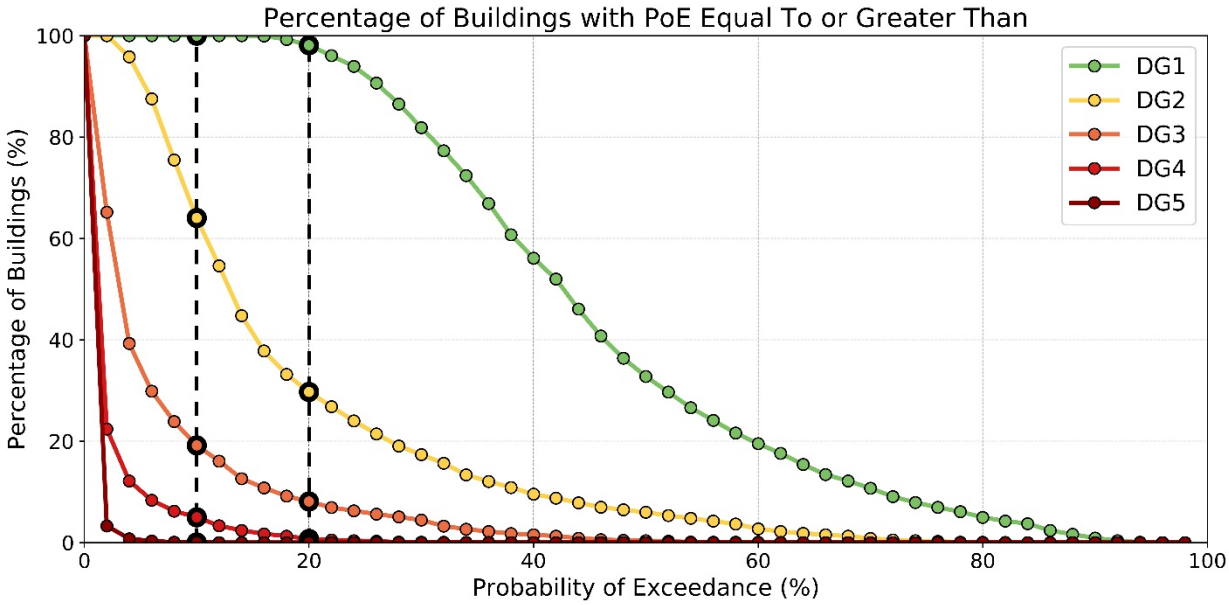

Figure 9.47: Proportion of buildings with probability of exceedance (PoE) of each damage grade (color scale) equal to or greater than indicated in the horizontal axis. DG corresponds to the respective damage grade.

The maps in Figures 9.48 to 9.57 present the same information as Figure 9.47 but in terms of numbers of buildings per Viertel for which the probability of exceedance of each damage grade is above the 10% or 20% thresholds discussed above. These maps do not show the 4,455 buildings (2.6%) classified as not belonging to any of these Viertel ("Nicht zugewiesen" group).

STR 20/02. GFZ German Research Centre for Geosciences.
DOI: 10.2312/GFZ.b103-20026

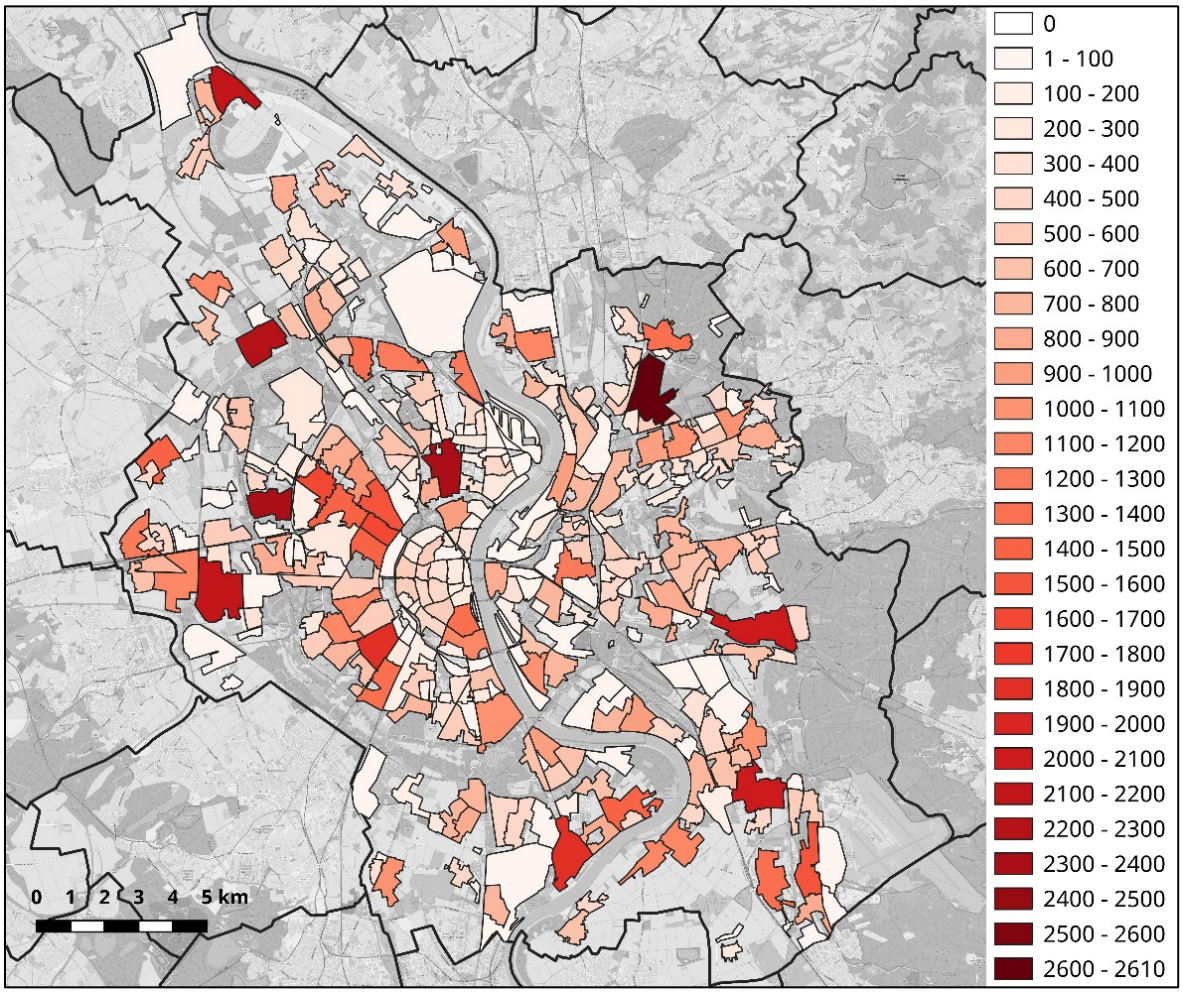

Figure 9.48: Number of buildings per Viertel with a probability of exceedance of EMS-98 damage grade 1 of 10% or higher.

STR 20/02. GFZ German Research Centre for Geosciences.
DOI: 10.2312/GFZ.b103-20026

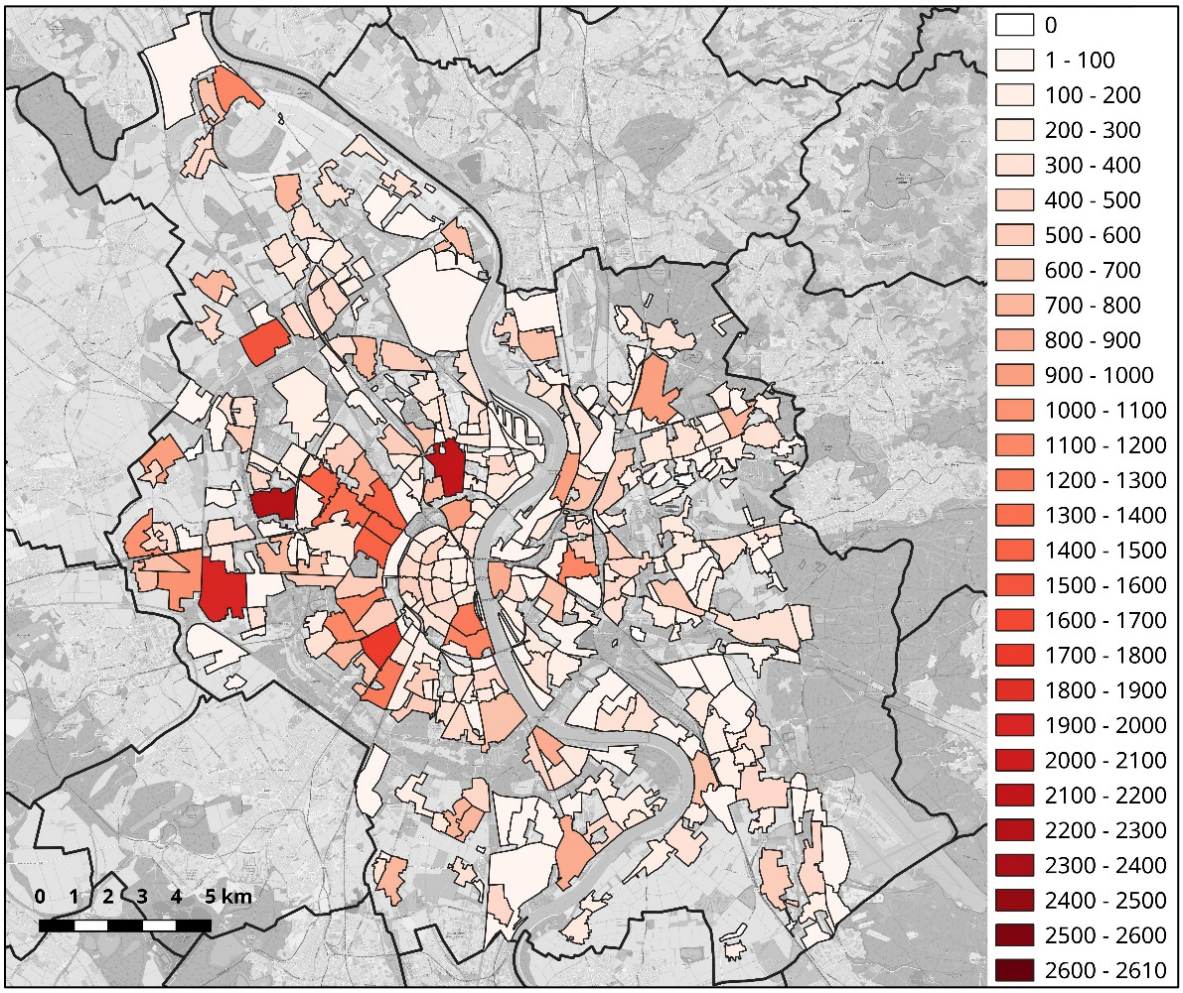

Figure 9.49: Number of buildings per Viertel with a probability of exceedance of EMS-98 damage grade 2 of 10% or higher.

STR 20/02. GFZ German Research Centre for Geosciences.
DOI: 10.2312/GFZ.b103-20026

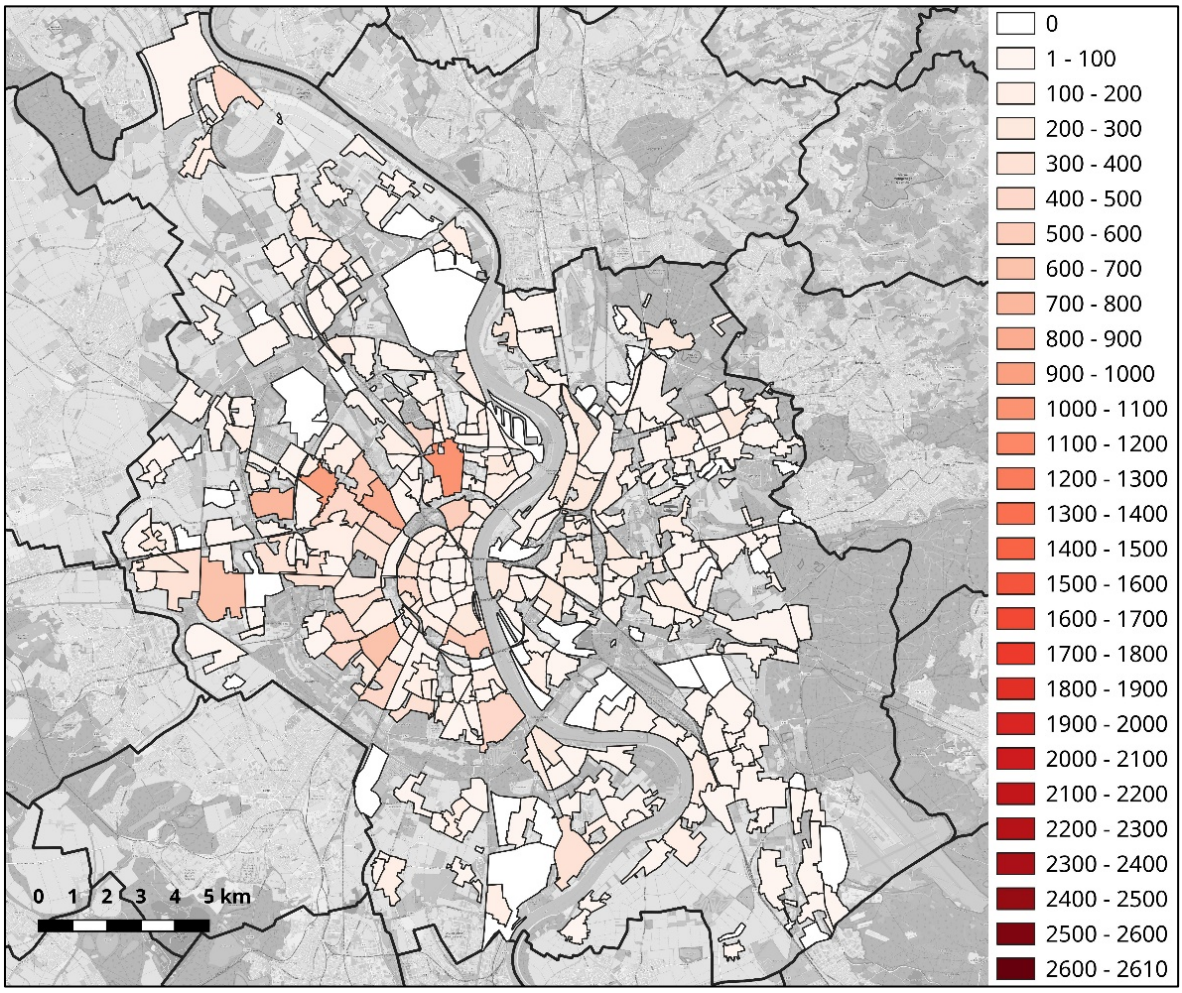

Figure 9.50: Number of buildings per Viertel with a probability of exceedance of EMS-98 damage grade 3 of 10% or higher.

STR 20/02. GFZ German Research Centre for Geosciences.
DOI: 10.2312/GFZ.b103-20026

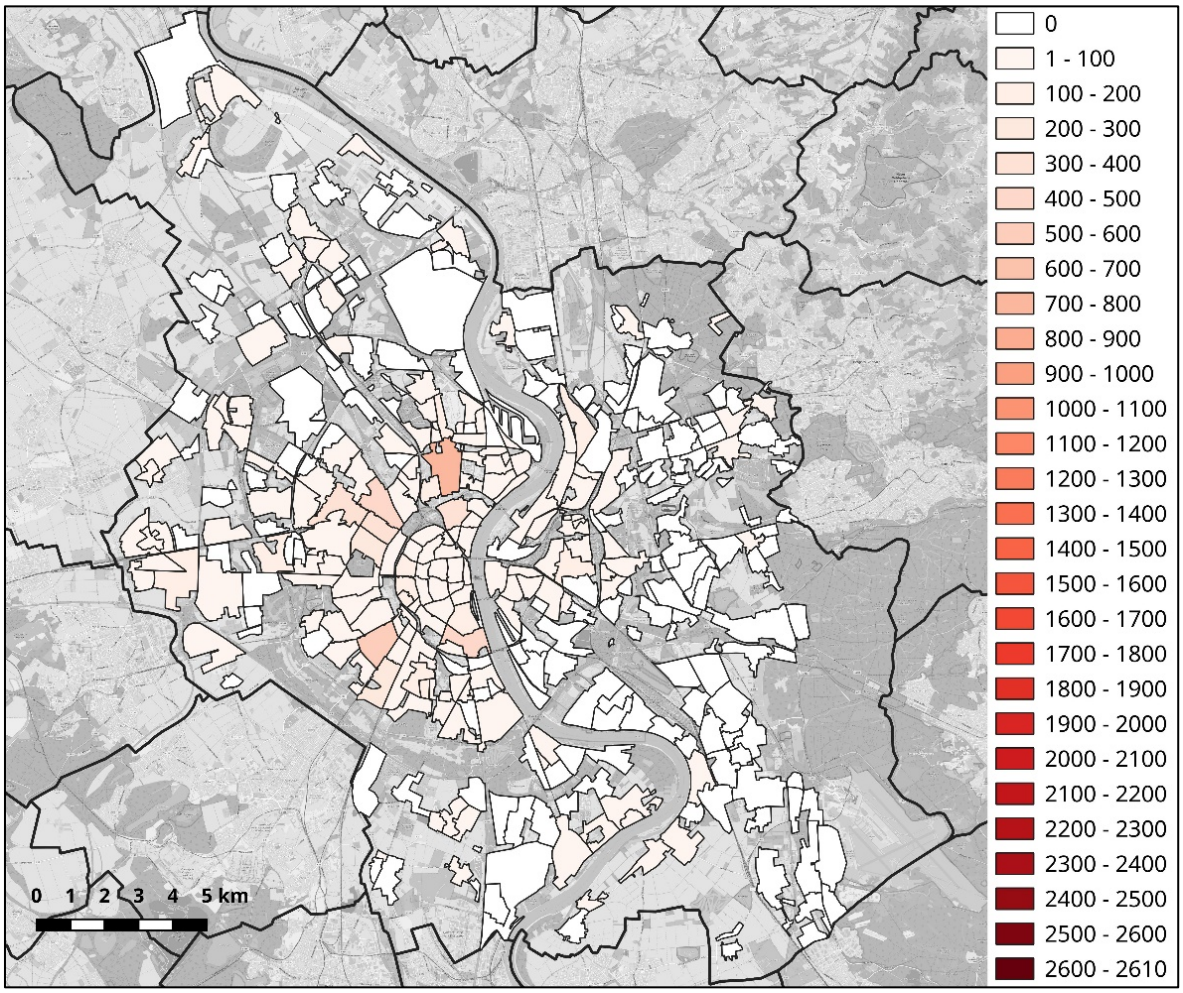

Figure 9.51: Number of buildings per Viertel with a probability of exceedance of EMS-98 damage grade 4 of 10% or higher.

STR 20/02. GFZ German Research Centre for Geosciences.
DOI: 10.2312/GFZ.b103-20026

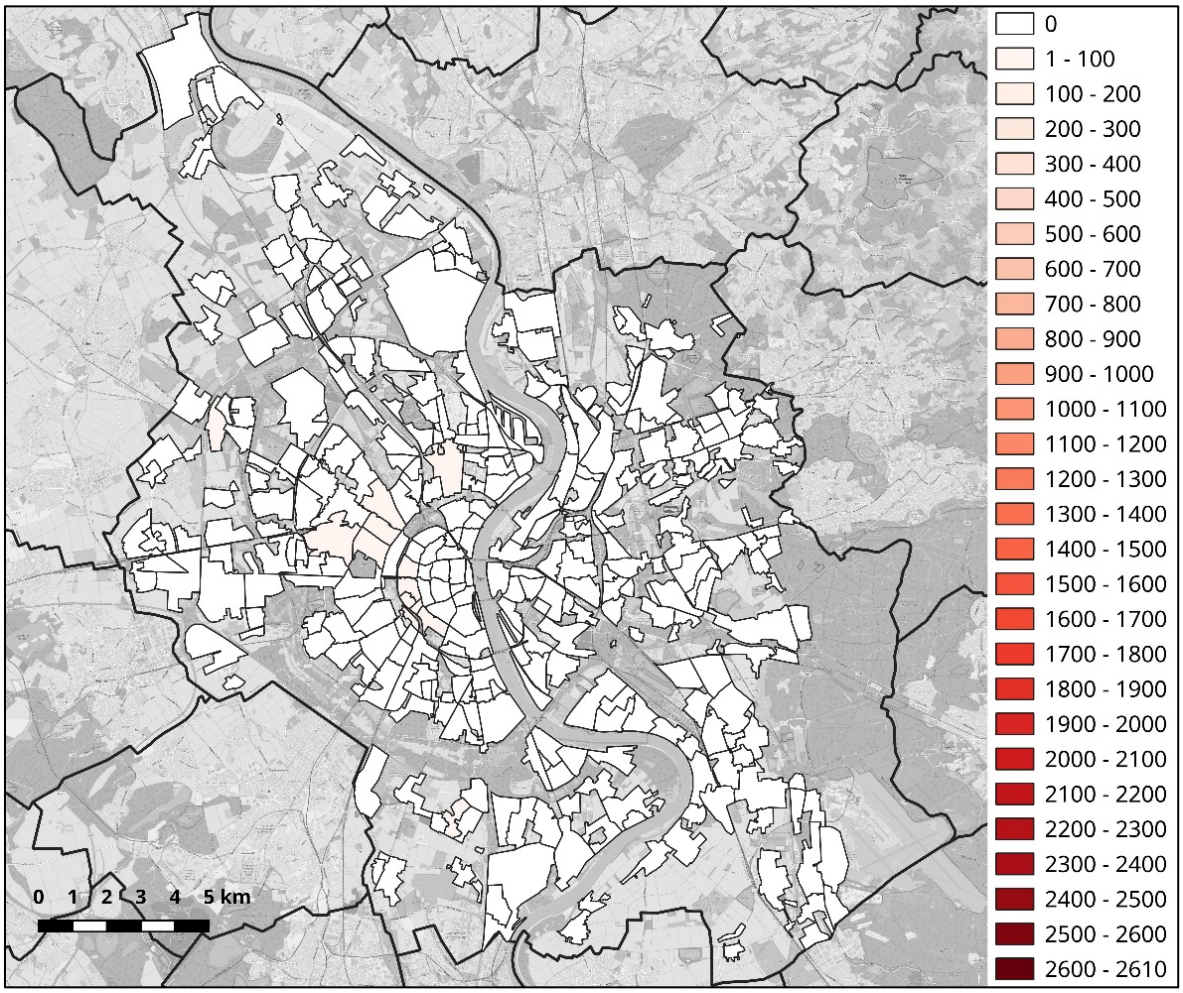

Figure 9.52: Number of buildings per Viertel with a probability of exceedance of EMS-98 damage grade 5 of 10% or higher.

STR 20/02. GFZ German Research Centre for Geosciences.
DOI: 10.2312/GFZ.b103-20026

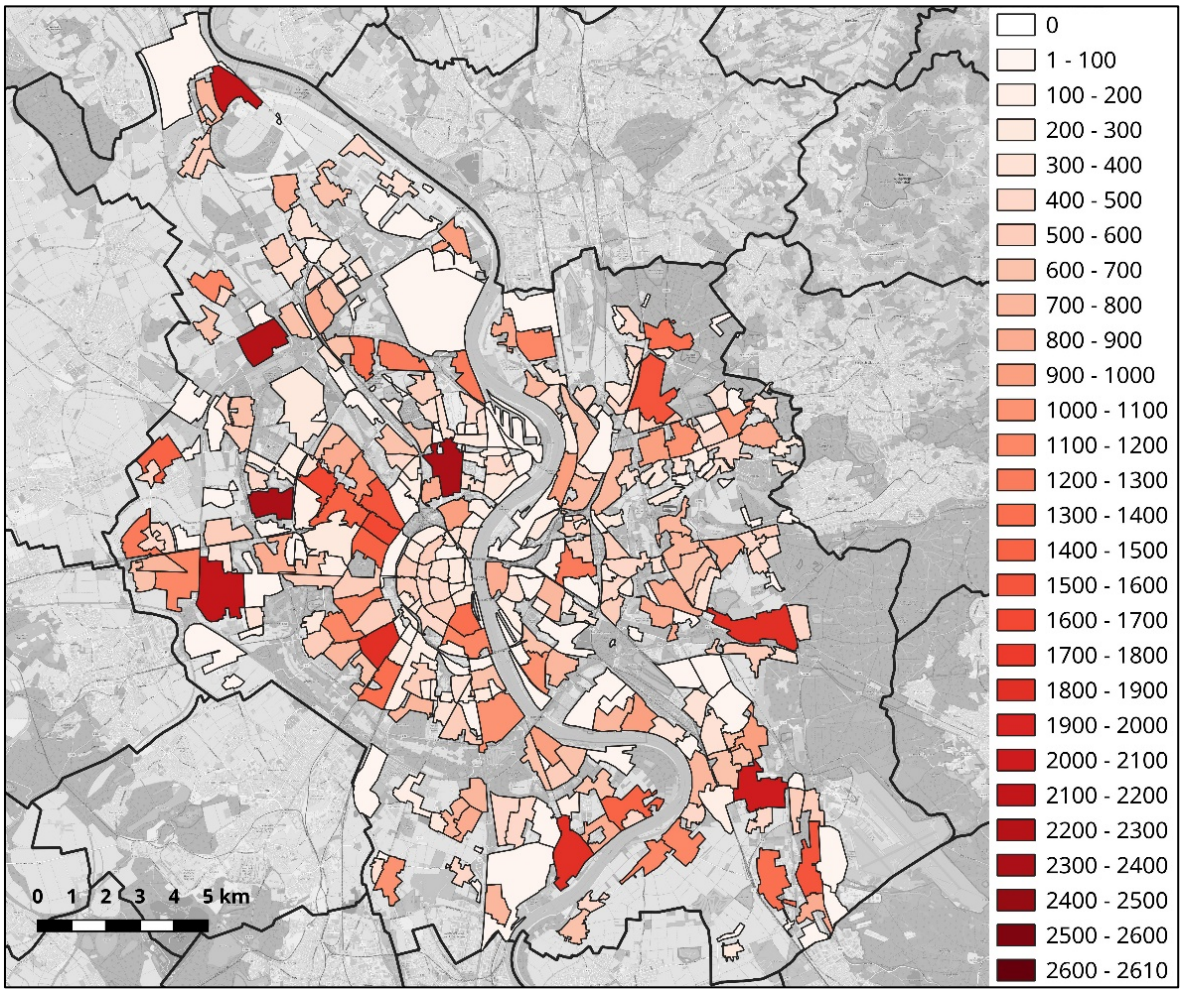

Figure 9.53: Number of buildings per Viertel with a probability of exceedance of EMS-98 damage grade 1 of 20% or higher.

STR 20/02. GFZ German Research Centre for Geosciences.
DOI: 10.2312/GFZ.b103-20026

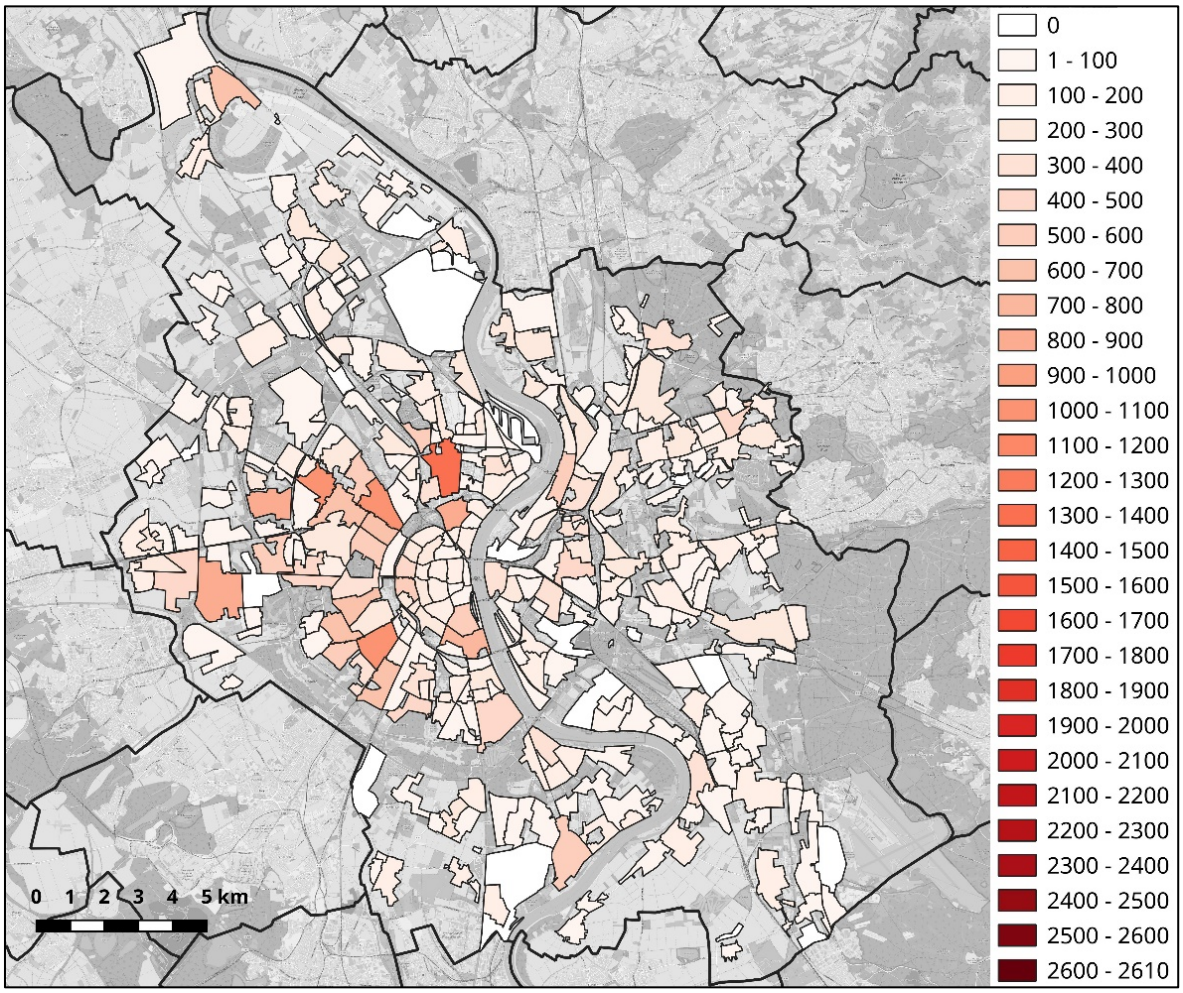

Figure 9.54: Number of buildings per Viertel with a probability of exceedance of EMS-98 damage grade 2 of 20% or higher.

STR 20/02. GFZ German Research Centre for Geosciences.
DOI: 10.2312/GFZ.b103-20026

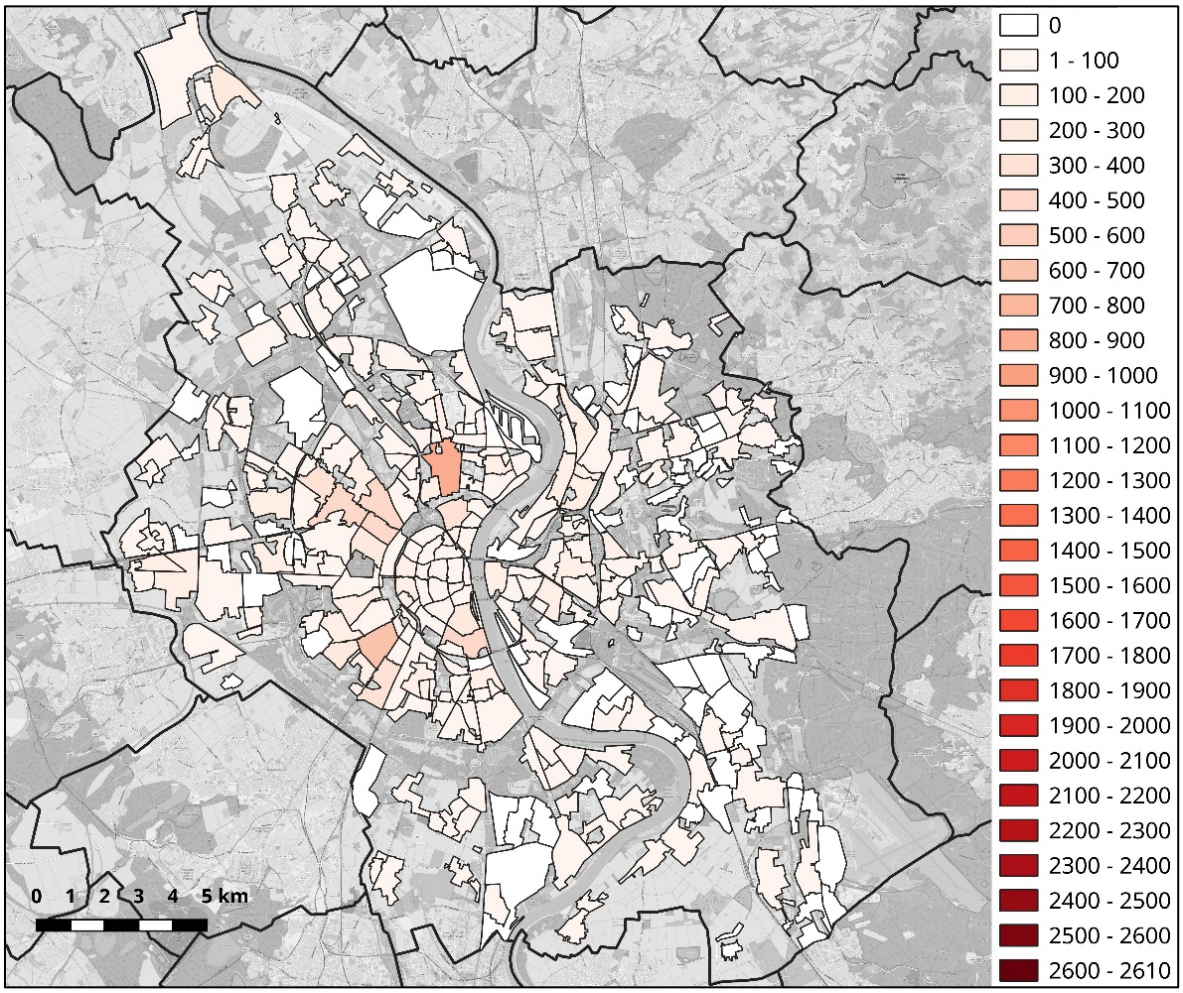

Figure 9.55: Number of buildings per Viertel with a probability of exceedance of EMS-98 damage grade 3 of 20% or higher.

STR 20/02. GFZ German Research Centre for Geosciences.
DOI: 10.2312/GFZ.b103-20026

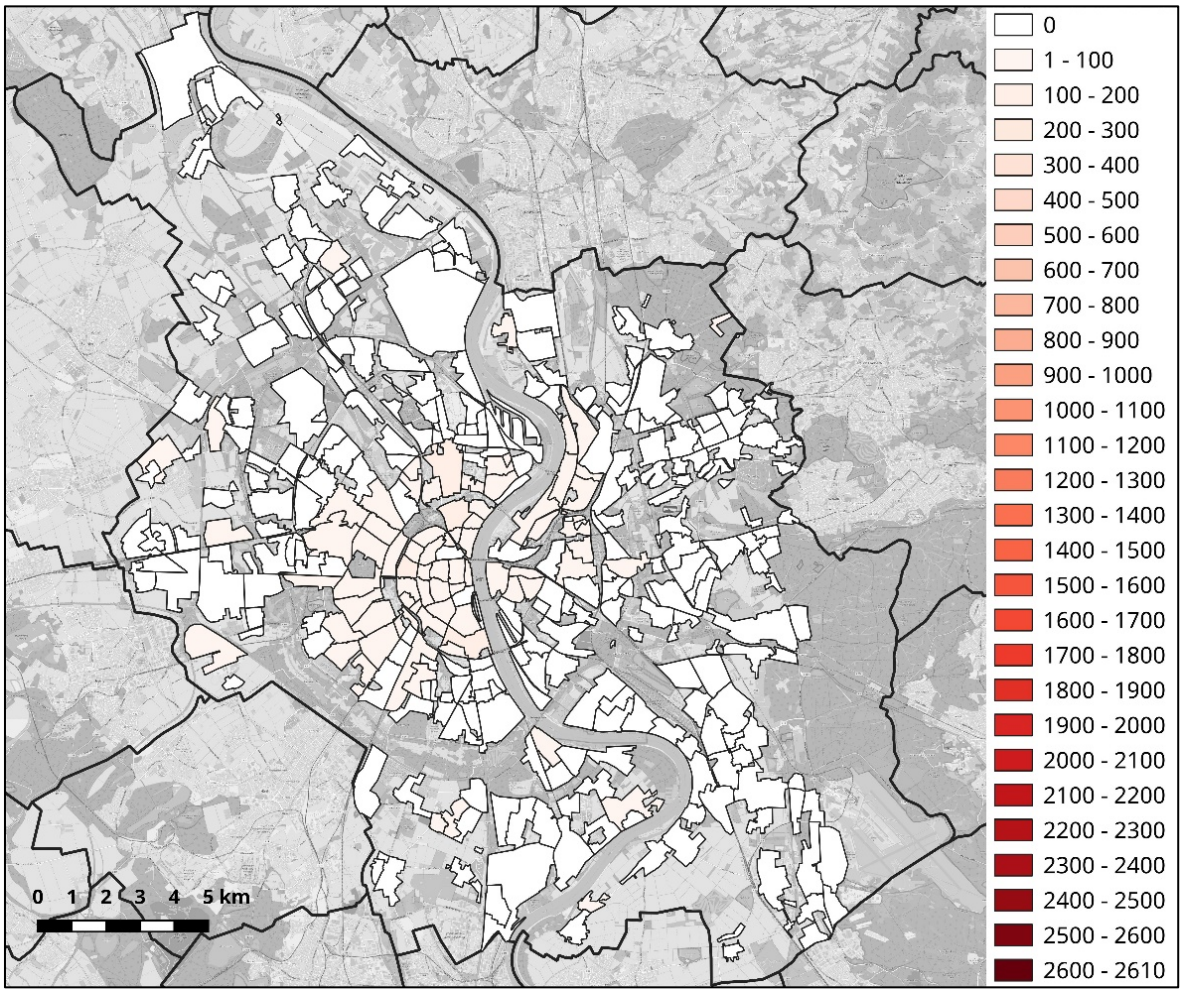

Figure 9.56: Number of buildings per Viertel with a probability of exceedance of EMS-98 damage grade 4 of 20% or higher.

STR 20/02. GFZ German Research Centre for Geosciences.
DOI: 10.2312/GFZ.b103-20026

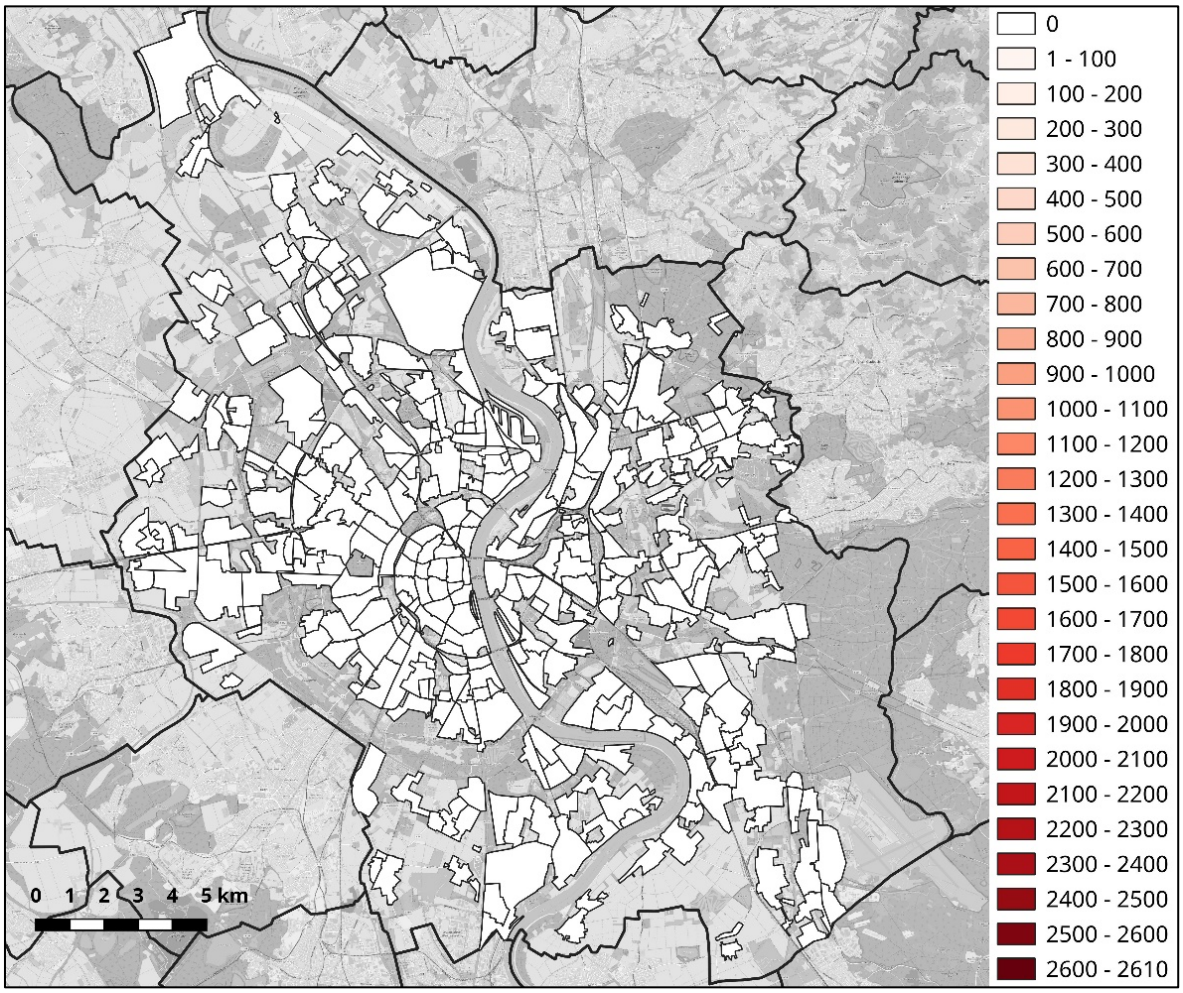

Figure 9.57: Number of buildings per Viertel with a probability of exceedance of EMS-98 damage grade 5 of 20% or higher.

A fundamental difference between using aggregated or building-by-building exposure models is the way in which the resulting damage can be presented and interpreted. When using aggregated exposure models, that is, models in which only a distribution of building classes is known for an area of interest, the probability of observing each damage grade is usually interpreted as representing the proportion of buildings of a particular class that is expected to suffer from such damage grade. For example, we may say that 70% of the buildings in an area are characterised by EMS-98 vulnerability class C and that such buildings, when subject to the ground shaking that can be deemed to represent the area of interest, have a 25% probability of not being damaged (DG0), 30% probability of DG1, 25% probability of DG2, 15% probability of DG3, 4% probability of DG4 and 1% probability of DG5. If there are 100,000 buildings in the area, then 70,000 would be of vulnerability class C, and these results could be interpreted as an expectation that, of these 70,000 buildings, 17,500 will be undamaged, 21,000 will suffer DG1, 17,500 will suffer DG2, 10,500 will suffer DG3, 2,800 will suffer DG4 and 700 will suffer DG5. However, when using a building-by-building exposure model like it was done herein, each of these 70,000 buildings will be assigned probabilities of 25%, 30%, 25%, 15%, 4% and 1% of observing DG0

STR 20/02. GFZ German Research Centre for Geosciences.
DOI: 10.2312/GFZ.b103-20026

through DG5 and it is not possible to assign any particular damage grade to any particular building. However, following the same logic as that of an aggregated model, we can treat the fractions of buildings (e.g. 0.15 of a building) as buildings we can add up to obtain overall aggregated statistics. For each of these 70,000 buildings, we would then say that 0.25 building is undamaged, 0.30 building will suffer DG1, and so on.
The summation of all these fractions for the 70,000 buildings will yield the same numbers discussed above. The results of applying this process to the present case are depicted in Table 9.15, which shows that, in an aggregated sense, around half of the residential buildings in Cologne are not expected to suffer any damage. 46,356 (27.4%) buildings are likely to suffer from DG1 (no structural damage, slight non-structural damage), 19,704 (11.6%) are likely to suffer from DG2 (slight structural damage, moderate non-structural damage), 7,947 (4.7%) from DG3 (moderate structural damage, heavy non-structural damage), 2,691 (1.6%) from DG4 (heavy structural damage, very heavy non-structural damage), and 444 (0.3%) may suffer from DG5 (very heavy structural damage and/or destruction). From the maps in Figures 9.41 to 9.46 it appears that these extreme cases of damage are more likely to occur around the central area, to the west of the river, and further west. While estimates for all damage grades are subject to uncertainties inherent to the grouping of individual buildings into classes, variability of material and structural properties, characterization of ground-shaking intensity measures, etc., experience on the derivation of fragility models for non-structural damage (such as the cracking of plaster of the walls) is limited (Crowley et al. 2019). As a consequence, an estimate of around 50% of undamaged buildings should never be interpreted as a certainty over the complete absence of any kind of damage for those buildings. It cannot be overemphasized that caution is needed in the interpretation of estimates regarding all damage grades.

Table 9.15: Number and proportion of buildings (residential plus MIX1) with probability of occurrence and exceedance of different damage grades, obtained by treating results in an aggregated manner.

Damage grade	Occurrence		Exceedance	
	Number	%	Number	%
DG0	92,328.6	54.5%	169,471.0	100.0%
DG1	46,356.3	27.4%	77,142.4	45.5%
DG2	19,703.5	11.6%	30,786.1	18.2%
DG3	7,947.3	4.7%	11,082.6	6.5%
DG4	2,691.3	1.6%	3,135.4	1.9%
DG5	444.1	0.3%	444.1	0.3%

9.3.3. Comparison with the 1978 Albstadt Earthquake

The 1978 Albstadt (Baden-Württemberg) earthquake is one of the most damaging earthquakes to have occurred in Germany. It occurred on 3rd September 1978 at

STR 20/02. GFZ German Research Centre for Geosciences.
DOI: 10.2312/GFZ.b103-20026

05:08 UTC and had a moment magnitude M_w of 5.2. The Albstadt districts of Tailfingen, Onstmettingen and Ebingen were the most affected. While having a much smaller magnitude than the M_w 6.5 considered herein for Cologne, its rupture appears to have been located much closer to the affected sites. A representation of the fault to which the Albstadt earthquake is attributed can be found in the European Database of Seismogenic Faults (EDSF, see Basili et al. 2013), developed for the SHARE project (Woessner et al. 2015). The causative fault is known as the Albstadt fault (DECS009). A best-fitting rupture from this fault was selected to match as closely as possible the hypocenter calculated by Leydecker (2011), assuming a rupture area as per Wells and Coppersmith (1994) and the hypocenter location at the centroid of the fault plane. The selected rupture yields Joyner-Boore distances of around 1 to 3km to Tailfingen and Onstmettingen, the two districts for which detailed statistics on damage are available from Beinersdorf et al. (2013) (reinterpretation of damage descriptions from the time of the earthquake). The Joyner-Boore distance to the center of Cologne is, under the scenario considered herein, around 15 to 20km instead. In order to understand whether or not a comparison between the two earthquakes would be of relevance, we calculated the response spectra of both scenarios using the Boore et al. (2014) ground-motion model and values of V_{s30} and Z1 deemed to be representative of the corresponding sites (decisions based on information from Schwarz et al. 2008, Lang and Schwarz 2006, and the characterization of site conditions in Cologne from the present study).
As shown in Figure 9.58, spectral acceleration values tend to be higher for the Albstadt scenario at the shorter periods and for the Cologne scenario at the longer periods, with the crossing point lying at a period of around 0.4 seconds. Based on the kind of buildings observed in Cologne in the present work (predominance of 1- and 2-story buildings, with relatively large presence of 3- and 4-story buildings as well, assumption of masonry and infilled reinforced concrete structures) and the classes reported by Beinersdorf et al. (2013) for Albstadt, in combination with the summary of relations between building height/number of stories and fundamental period of vibration reported by Martins and Silva (2018), we decided to put emphasis in the 0.1 to 1.0 second range for the sake of comparison herein. Median spectral accelerations at 0.1s are around 0.25g for Cologne, 0.53g for Tailfingen and 0.45g for Onstmettingen. At 0.4s, the values are around 0.32g for Cologne, 0.27g for Tailfingen and 0.25g for Onstmettingen. At 1.0s, they are around 0.15g for Cologne, 0.08g for Tailfingen and 0.06g for Onstmettingen. These values suggest that the expected ground-motions from the two earthquakes are not so dissimilar, particularly when considering the uncertainty around these median values and the spatial distribution of buildings (only one set of coordinates considered here per city/district). In terms of building vulnerability, Beinersdorf et al. (2013) estimate around 14.7% of the building stock of Tailfingen and Onstmettingen to have corresponded to EMS-98 vulnerability class B, 45.9% to class BC, 31.1% to class C, 1.4% to class CD and 6.3% to class D. While the proportion of vulnerability class B is comparable in both earthquakes (14.7 as opposed to 17.7%, see Figure 9.33), the proportion of BC plus C is comparable only as an ensemble and not individually (77.0% vs 75.8%), as is that of CD plus D (7.7% as opposed to 5.8%). These considerations and the earlier ones regarding ground-motions indicate that, broadly speaking and notwithstanding the differences in the affected building stocks, a comparison of damage from the two earthquakes may be pertinent.

STR 20/02. GFZ German Research Centre for Geosciences.
DOI: 10.2312/GFZ.b103-20026

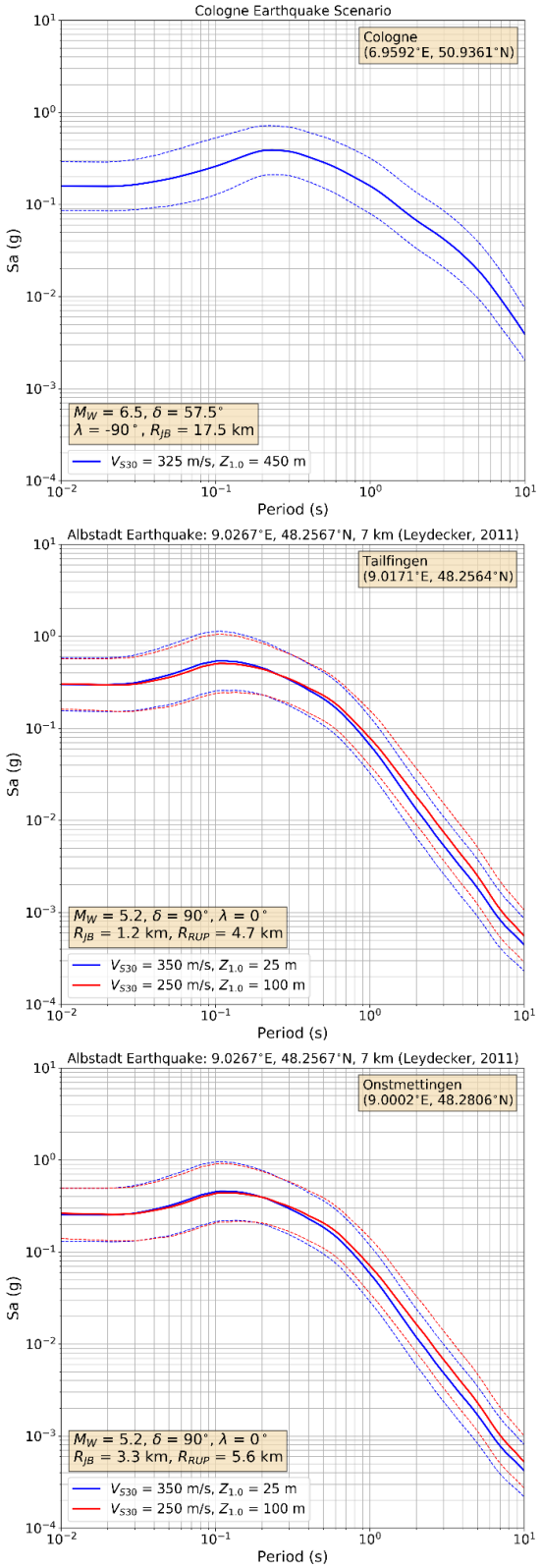

Figure 9.58: Response spectra for a site in the center of Cologne under the earthquake scenario studied herein (top) and for the center of the Albstadt districts of Tailfingen (center) and Onstmettingen (bottom) under a scenario reproducing the 1978 Mw 5.2 Albstadt earthquake calculated using the Boore et al. (2014) ground-motion model.

STR 20/02. GFZ German Research Centre for Geosciences.
DOI: 10.2312/GFZ.b103-20026

Figure 9.59 shows the comparison between the aggregated results for Cologne (pie chart of the values shown in Table 9.15) and the proportions of EMS-98 damage grades reported by Beinersdorf et al. (2013) for the Albstadt districts of Tailfingen and Onstmettingen. The latter do not include the district of Ebingen, which was affected as well. As can be observed, results obtained for Cologne speak of greater damage than that observed for the Albstadt earthquake, though the overall consistency of proportions suggests that the results obtained for Cologne may be reasonable. This comparison is not intended as a "validation" of the results presented herein for Cologne but is carried out simply as a good consistency check, given that the expected ground-motions and the distribution of building vulnerability classes are not so dissimilar for the two events.

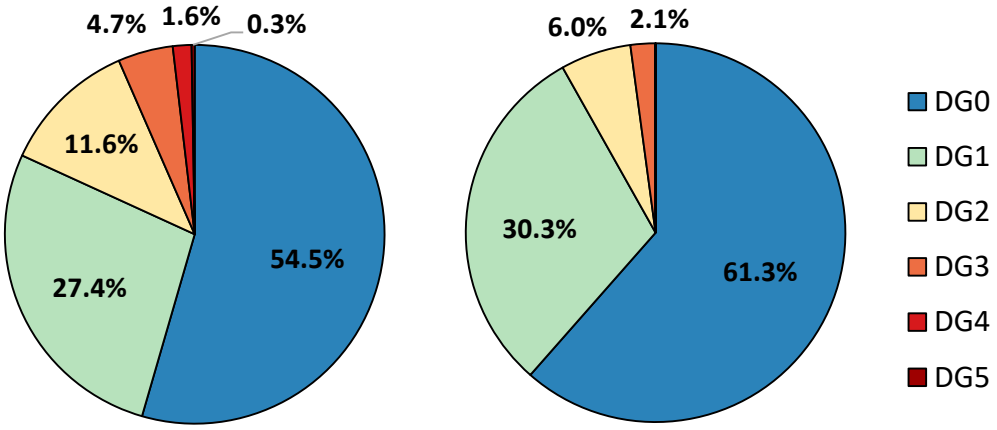

Figure 9.59: Comparison between the distribution of EMS-98 damage grades calculated for the city of Cologne under the earthquake scenario studied herein (left, aggregated results) and the proportions reported by Beinersdorf et al. (2013) for the Albstadt districts of Tailfingen and Onstmettingen (right).

9.4. Discussion

We carried out the assessment of building damage in the city of Cologne due to the mainshock considered herein by means of

- a building-by-building exposure model, developed combining three main sources of open data, in which each building is characterised by its year of construction, number of stories and occupancy type.
- a Monte Carlo simulation approach that integrates the building-by-building exposure model and available aggregated statistics in order to assign years of construction and/or numbers of stories to buildings for which this information was not available.
- a relationship between the year of construction and a distribution of likely EMS-98 vulnerability classes for the city of Cologne, from a previous study.
- fragility curves yielding the probability of exceedance of EMS-98 damage grades as a function of EMS-98 intensity, EMS-98 vulnerability class and number of stories, from a previous study.

STR 20/02. GFZ German Research Centre for Geosciences.
DOI: 10.2312/GFZ.b103-20026

- a conversion of the field of peak ground accelerations into an EMS-98 intensity fields using an existent empirical model.

While the exposure model covers all kinds of occupancy types, the estimation of damage focused herein on residential and mixed residential-commercial classes (169,471 buildings), for which appropriate fragility curves were available. The behaviour of industrial and commercial classes is, in general, less broadly studied than that of their residential counterparts, as is that of historical constructions and monuments, which can sometimes be so peculiar that a specific analysis is warranted. Nevertheless, median EMS-98 intensity values have been estimated for all 286,373 buildings in the exposure model, and it has been observed that the proportions of buildings located within areas corresponding to particular levels of EMS-98 intensities are very similar for residential and non-residential buildings. Around 70% of buildings are subject to EMS-98 intensities of 7 and most of the remaining ones are subject to intensity 7.5, with less than 0.5% of the buildings being subject to intensities smaller than 7 or equal to or larger than 8. However, these numbers should be taken only as a broad indication of the ground shaking to which buildings could be subjected, as they stem from the application of empirical conversion equations to peak ground acceleration values. Moreover, correlation between peak ground acceleration and damage is only observed for very low-period structures, while spectral acceleration is more appropriate for inferring damage inflicted to structures with longer periods of vibration.

Results on damage consist on a building-by-building distribution of the probability of the building suffering from damage grades 0 through 5 when subject to the earthquake scenario. Maps with spatial distribution of these results suggest a tendency for the likelihood of higher degrees of damage to be concentrated around the central and western areas of the city. Results can be presented in a variety of ways, but perhaps one of the most useful ones is to state the percentage of buildings with probability of exceedance of each damage grade equal to or larger than a certain (arbitrary) threshold:

- all buildings have at least a 10% probability of exceeding DG1.
- 64.0% of the buildings have at least a 10% probability of exceeding DG2.
- 19.2% of the buildings have at least a 10% probability of exceeding DG3.
- 5.0% of the buildings have at least a 10% probability of exceeding DG4.
- 0.03% of the buildings have at least a 10% probability of exceeding DG5.

These proportions of probabilities of exceedance indicate that the possibility of observing very heavy damage (DG4) cannot be ruled out, and the possibility of observing substantial to heavy damage (DG3) is not negligible at all. Figure 9.60 shows examples of two German buildings classified as suffering from EMS-98 DG3 after the 1978 M_w 5.1 Albstadt (Baden-Württemberg) earthquake by Schwarz et al. (2010), while Figure 9.61 depicts a third building classified as suffering from EMS-98 DG2 after the same earthquake, according to Grünthal (1998).

When aggregating results, it becomes possible to interpret probabilities of occurrence of each damage grade for each building as proportions of a collective of buildings. Doing so yields around 46,356 (27.4%) buildings being likely to suffer from DG1, 19,704 (11.6%) likely to suffer from DG2, 7,947 (4.7%) from DG3 , 2,691 (1.6%) from DG4, and 444 (0.3%) likely to suffer from DG5. A brief comparison against damage grades observed for the 1978 Albstadt earthquake (reinterpretation of damage descriptions from the time) suggests that the results obtained for Cologne are reasonable. This comparison is not intended as a “validation” of the results

STR 20/02. GFZ German Research Centre for Geosciences.
DOI: 10.2312/GFZ.b103-20026

presented herein for Cologne but was carried out simply as a good consistency check, given that the expected ground-motions and the distribution of building vulnerability classes are not so dissimilar for the two events.

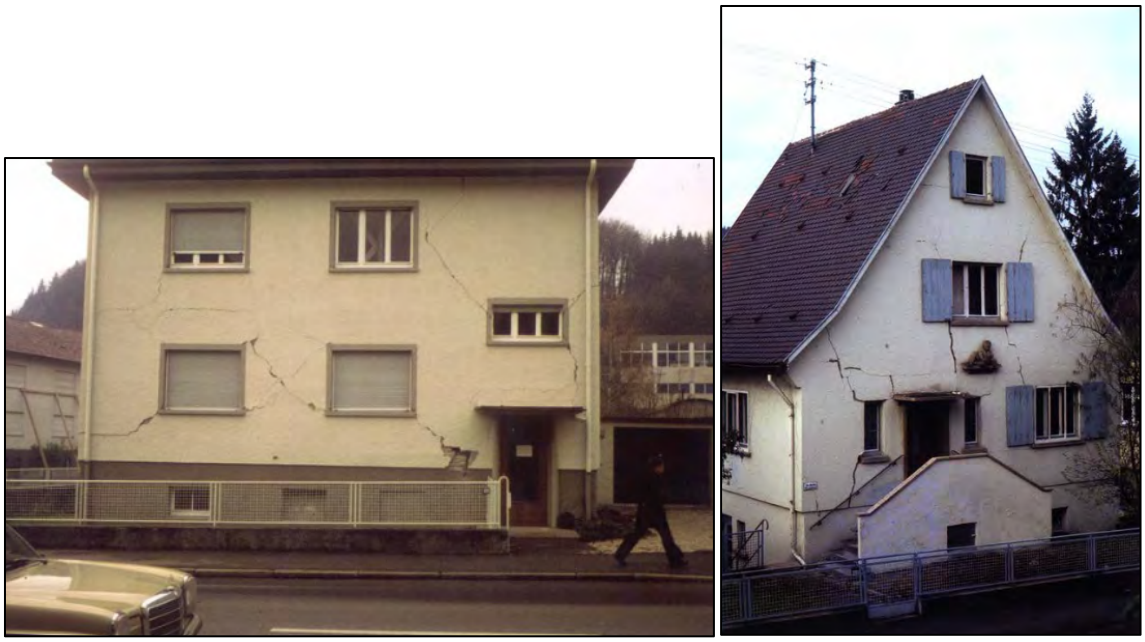

Figure 9.60: Buildings classified as suffering from EMS-98 damage grade 3 after the 1978 M_w 5.1 Albstadt (Baden-Württemberg) earthquake. Photos and damage assessment taken from Schwarz et al. (2010).

Figure 9.61: Building classified as suffering from EMS-98 damage grade 2 after the 1978 M_w 5.1 Albstadt earthquake. Photo and damage assessment from Grünthal (1998).

STR 20/02. GFZ German Research Centre for Geosciences.
DOI: 10.2312/GFZ.b103-20026

The results presented herein are subject to the limitations inherent to the method applied. Regarding building exposure and vulnerability, these are:

- The years of construction and number of stories available from the ODK and NRW-WFS datasets are of undetermined reliability. Visual inspection of a limited number of cases suggests the existence of both agreement and disagreement with what can be inferred from photos available from Google Street View or Mapillary.
- Comparison and merging of different datasets is challenging, as inconsistencies unfailingly arise due to spatial mismatch of associated polygons and points, different addresses associated to one polygon, etc.
- It has been established that cases exist in which it is not clear why two separate polygons appear to be representing one building, and vice-versa, as judged from photos available from Google Street View or Mapillary. This can lead to potentially erroneous building counts.
- Available verbal descriptions used to infer building occupancy types are not always detailed enough to fully and unequivocally interpret their meaning and implications from the structural point of view.
- Statistics available on the year of construction of the buildings in each Viertel are in many cases inconsistent with the values available from the merging of the datasets used to build the exposure model. This can be due to different ways of determining what one building is (*e.g.*, one structure, one address?), the occurrence of demolitions and building of new structures, the difficulties associated with classifying buildings according to their occupancy type, and errors in either the statistics or the datasets.
- The years of construction of around one quarter of the buildings were randomly assigned based on statistical information available at the Viertel level. These years of construction, and the subsequent assignment of probability distributions of EMS-98 vulnerability classes, are subject to the same limitations as the data used to assign them.
- A more precise characterization of the fragility of the buildings could be achieved if more details on the structures were to be known and, consequently, more specific fragility models could be applied.

The final distribution of vulnerability classes in an aggregated sense across all residential buildings of Cologne are in overall agreement with those observed by Schwarz et al. (2004) for a reduced test area.

Limitations and assumptions associated with other steps of the process that may have an influence in the damage results are:

- The conversion of peak ground acceleration into EMS-98 intensity was carried out by a conversion equation based on Italian earthquakes, and the relation between the two parameters might be potentially different for Germany. Moreover, the correlation between peak ground acceleration and damage is only observed for very low-period structures, while spectral acceleration is more appropriate for inferring damage inflicted to structures with longer periods of vibration.
- EMS-98 intensity has been calculated only at specific points and subsequently interpolated at the centroids of the buildings. This procedure assumes a

STR 20/02. GFZ German Research Centre for Geosciences.
DOI: 10.2312/GFZ.b103-20026

smooth variation of soil properties and cannot account for potential small-scale irregularities.

- The ground-motion and intensity fields used do not take into account spatial correlation. They can, however, be deemed to represent the average of a large number of ground-motion fields that do account for spatial correlation.

STR 20/02. GFZ German Research Centre for Geosciences.
DOI: 10.2312/GFZ.b103-20026

10. Estimation of casualties

We estimated the number of casualties applying the PAGER (Prompt Assessment of Global Earthquakes for Response) empirical method (Jaiswal and Wald 2010) taking into account the population of the Regierungsbezirk of Köln. This method is intensity-based and is thus independent of the damage calculations.
The PAGER empirical method uses a two-parameter lognormal cumulative distribution to model the median fatality rate as a function of Modified Mercalli Intensity (MMI). These two parameters are empirical and country-dependent. The median fatality rate is the expected ratio between the number of deaths and the number of people exposed to the corresponding intensity level. The PAGER empirical model further provides a quantification of uncertainty that allows us to calculate the probability of the number of fatalities falling in a particular range. According to Jaiswal and Wald (2010), comparisons of their PAGER empirical method against data on fatalities from past earthquakes yield an overall agreement within one order of magnitude. We assumed a 1:1 equivalence between MMI and EMS-98 (Musson et al. 2010).
For the case of Germany and other countries with scarce to null data on fatalities resulting from past earthquakes, the parameters were derived by Jaiswal and Wald (2010) based on a global regionalizationz scheme that associated countries with similar vulnerability. Under this scheme, Germany was grouped together with northern and western Europe in general, as well as Greece. Figure 4.1 shows the mean fatality rate for Germany (and other countries) according to this model, using version 2.0 of the coefficients provided by the authors at the USGS website. According to the plot, the population exposed to MMI VII are expected to have a mortality rate of 0.002% The similarity between the models for Germany and Greece is due to the two countries being grouped together by Jaiswal and Wald (2010).

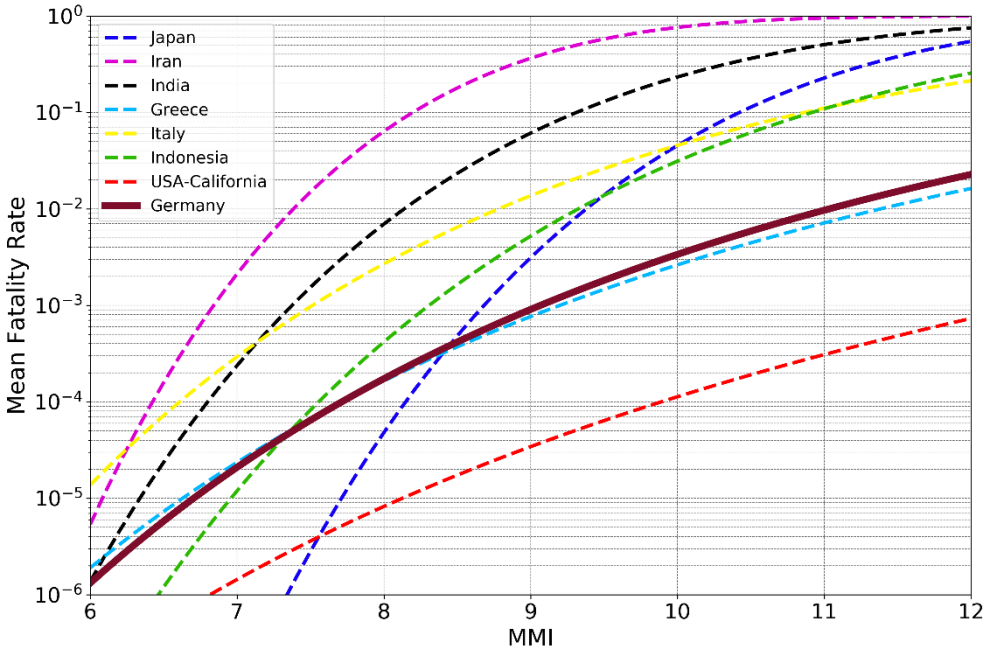

Figure 10.1: Mean fatality rates for Germany and other countries according to the PAGER empirical model of Jaiswal and Wald (2010).

STR 20/02. GFZ German Research Centre for Geosciences.
DOI: 10.2312/GFZ.b103-20026

10.1. Population exposure

The estimation of casualties was carried out for the whole of the Regierungsbezirk of Köln. This corresponds to a region of level 2 according to the Nomenclature of Territorial Units for Statistics (NUTS), a European system of geographical hierarchies. The NUTS levels are three, and in Germany these correspond to the Bundesländer (NUTS 1), the Regierungbezirke (NUTS 2), and the Kreise (NUTS 3). After the NUTS 3 level come the local administrative units (LAUs), which correspond to the German Gemeinden. For further details, please refer to Eurostat (2020).
The population data was gathered at different administrative levels for the Kreisfreie Stadt of Cologne, Bonn and Aachen than for the rest of the NUTS 3 subdivisions of the Regierungsbezirk of Köln. While for the latter we gathered data at the level of the LAUs, for the former we retrieved information at the neighborhood (Viertel) and district (Bezirk) levels. It is noted that both Stadt Köln and Stadt Bonn are at the same time Kreise (NUTS 3) and Gemeinde (LAU), while Stadt Aachen is a LAU within the Städteregion Aachen (NUTS 3), which contains other LAUs as well. For each sub-group of administrative units considered, we used the following population data (Table 10.1):

- Köln Kreisfreie Stadt: Viertel level. The data were retrieved from Stadt Köln (2019a) for 31 December 2017.
- Bonn Kreisfreie Stadt: district (Bezirk) level. The data were retrieved from Esri Deutschland (2018) for 31 December 2017.
- Aachen Kreisfreie Stadt: district (Bezirk) level. The population data were retrieved from Offene Daten Aachen (2019). The shapefiles were obtained at the Viertel level from Offene Daten Aachen (2017) and combined to retrieve the corresponding districts.
- The rest of the NUTS 3 subdivisions: municipality (Gemeinde) level. The data were obtained from Information und Technik Nordrhein-Westfalen (2018) for 31 December 2017.

This last source suggests that the population reported for 31 December 2017 was calculated based on the 2011 census though it is not clear if the reported values are extrapolations or if they were estimated by considering births, deaths and migration (in German: "Fortschreibung auf Basis des Zensus 2011"). The source indicates as well that difficulties were encountered when considering the number of asylum seekers that arrived to Germany around the year 2016. Small discrepancies can be observed when comparing these population values against those resulting from aggregating data at the Viertel and/or Bezirk level, as shown in Table 10.2. For small differences in terms of percentage, we performed no adjustment. The final values adopted are those stemming from aggregating data from the Viertel/Bezirk levels, as shown in the map of Figure 10.2, which depicts the population at the LAU level. The total population of the Regierungsbezirk (NUTS 2) of Köln adds up to 4,459,638 people. Figures 10.3 through 10.5 show the population by Viertel/Bezirk in Köln, Aachen and Bonn. As can be observed, the match between the polygons from each of the datasets enumerated above and those available from the GADM database (V3.4) is not perfect. However, this is not a major problem for the scope of the present work.

STR 20/02. GFZ German Research Centre for Geosciences.
DOI: 10.2312/GFZ.b103-20026

Table 10.1. Data sources used to build the population exposure model for Cologne.

Source	Contents	Last accessed
Stadt Köln (2019a)	Population of 31 December 2017 per Viertel of Cologne	9 July 2019
Esri Deutschland (2018)	Population of 31 December 2017 per Bezirk of Bonn	18 Sept 2019
Offene Daten Aachen (2019)	Population of 31 December 2017 per Bezirk of Aachen	18 Sept 2019
Information und Technik Nordrhein-Westfalen (2018)	Population of 31 December 2017 per LAU level of Nordrhein-Westfalen	17 Sept 2019

Table 10.2: Comparison of population values according to different sources.

NUTS 3	Population		
	NUTS 4	From Viertel/Bezirk	Difference (%)
Köln Kreisfreie Stadt	1,080,394	1,073,680	-0.6%
Bonn Kreisfreie Stadt	325,490	327,919	0.7%
Aachen Kreisfreie Stadt	246,272	255,967	3.9%

As can be easily inferred, basing the fatalities estimation on the census population per administrative unit is implicitly assuming that the whole population is present at the time of the earthquake (e.g. nobody is travelling) and that nobody who normally inhabits elsewhere needs to be added, or, alternatively, that these two numbers counterbalance each other.

STR 20/02. GFZ German Research Centre for Geosciences.
DOI: 10.2312/GFZ.b103-20026

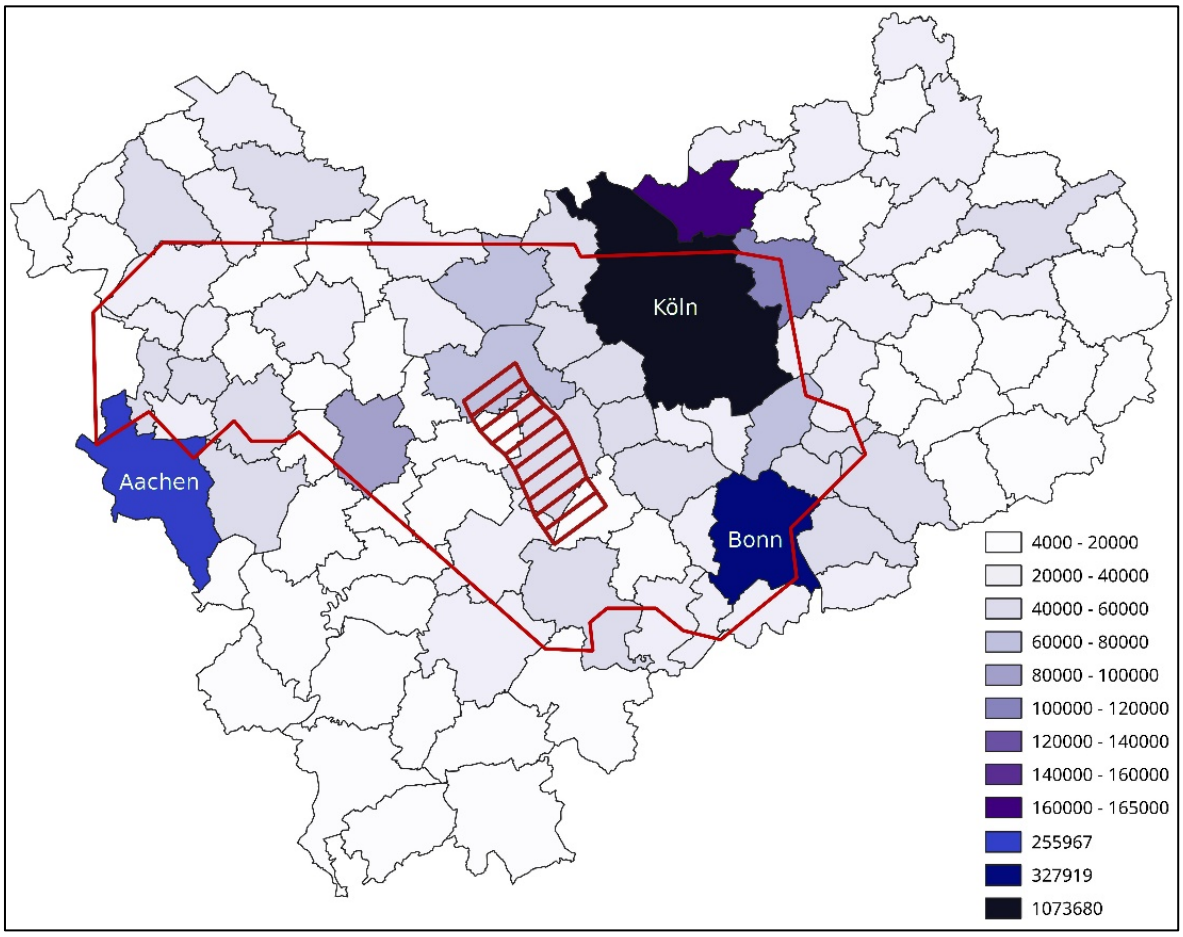

Figure 10.2: Population by 31 December 2017 at the LAU (Gemeinde) level according to Information und Technik Nordrhein-Westfalen (2018), except for Cologne, Bonn and Aachen, for which the values result from aggregating data at the Viertel/Bezirk level. Shapefiles of administrative units of Germany are taken from the GADM database version 3.4. The smaller red polygon indicates the surface projection of the multi-planar geometry of the causative fault, while the larger red polygon encloses the (approximate) area for which data on site amplification are available. Calculations outside this area were carried out by means of extrapolation.

STR 20/02. GFZ German Research Centre for Geosciences.
DOI: 10.2312/GFZ.b103-20026

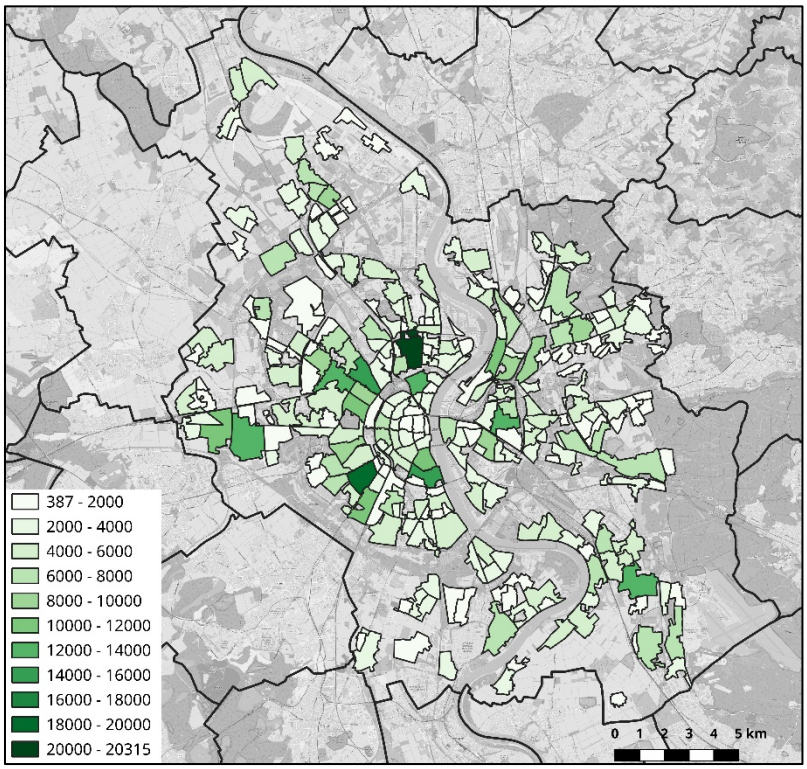

Figure 10.3: Population of Köln per Viertel according to Stadt Köln (2019a). Background from OpenStreetMap.

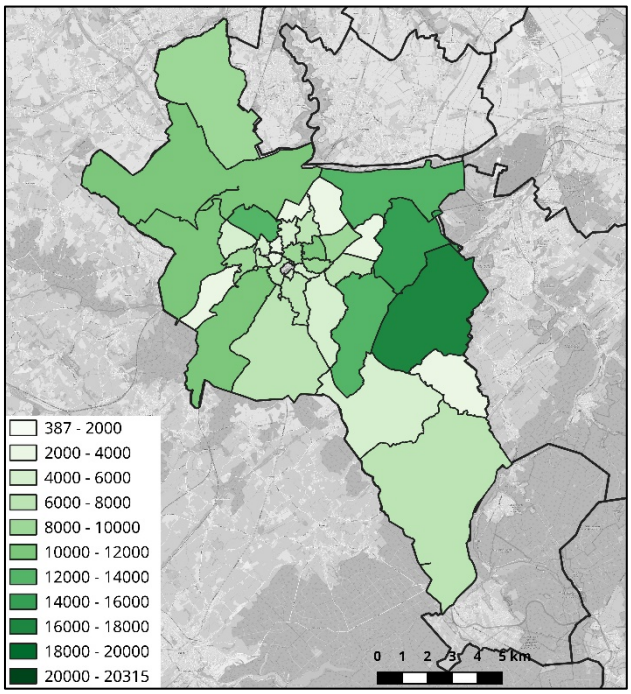

Figure 10.4: Population of Aachen per Bezirk according to Offene Daten Aachen (2017, 2019). Background from OpenStreetMap.

STR 20/02. GFZ German Research Centre for Geosciences.
DOI: 10.2312/GFZ.b103-20026

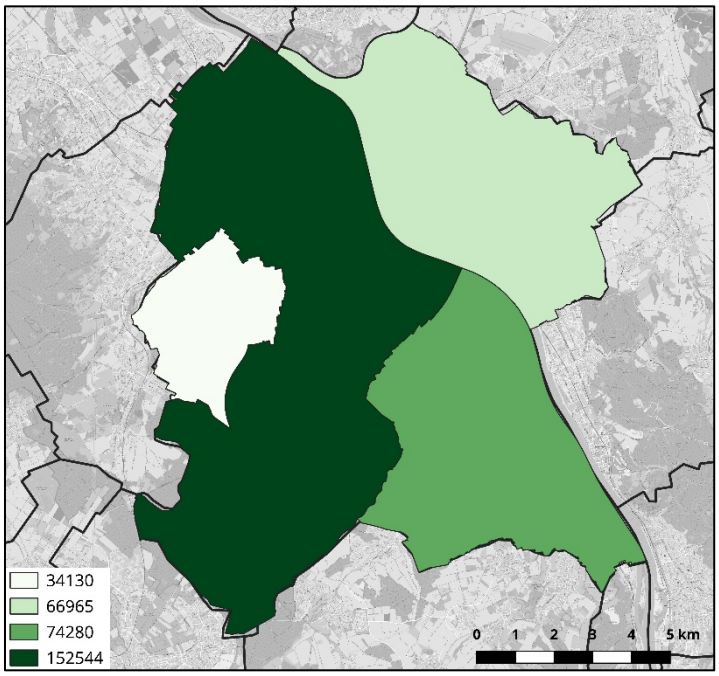

Figure 10.5: Population of Bonn per Bezirk according to Esri Deutschland (2018). Background from OpenStreetMap.

10.2. Methodology

The median EMS-98 intensities were retrieved for each Viertel, Bezirk and NUTS 4 administrative unit following two different approaches, depending on the size of the administrative unit. As explained above, the final intensity field adopted is defined in a 30-arc sec grid. Whenever two or more points of this grid were enclosed by the contour of an administrative unit, the average of the median EMS-98 intensities across all enclosed points was adopted, while the value corresponding to the centroid of the administrative unit was used otherwise. The latter were determined through linear interpolation within the 30-arc sec grid. The map in Figure 10.6 indicates which approach was adopted in each administrative unit.

The discrimination into these cases was prompted by the fact that several administrative units have too large geographical extension for the value read at the corresponding centroid to be representative of the whole area. This is the case of the Bezirke of Bonn and many of the NUTS 4 administrative units. Moreover, some of the latter are located directly above the rupture or very close to it (see Figure 10.2), which results in them being associated with relatively variable intensity levels, as the gradient of the ground-motion attenuation changes fast in the near field. It is clear that taking the average of all points enclosed by each administrative unit does not necessarily yield the same results as estimating fatalities at each point. However, the population values are only known per administrative unit, and the distribution within each unit is undetermined from the available data. As a consequence, estimating fatalities per point assuming a particular distribution of the population within the administrative unit would not necessarily increase the precision of the estimations.

As can be observed from Figure 10.6, all cases in which we adopted intensities at the centroids were adopted correspond either to Viertel of Cologne or Bezirke of Aachen. These are not only quite small but also lie within areas in which median intensities

STR 20/02. GFZ German Research Centre for Geosciences.
DOI: 10.2312/GFZ.b103-20026

do not change so much within short distances.

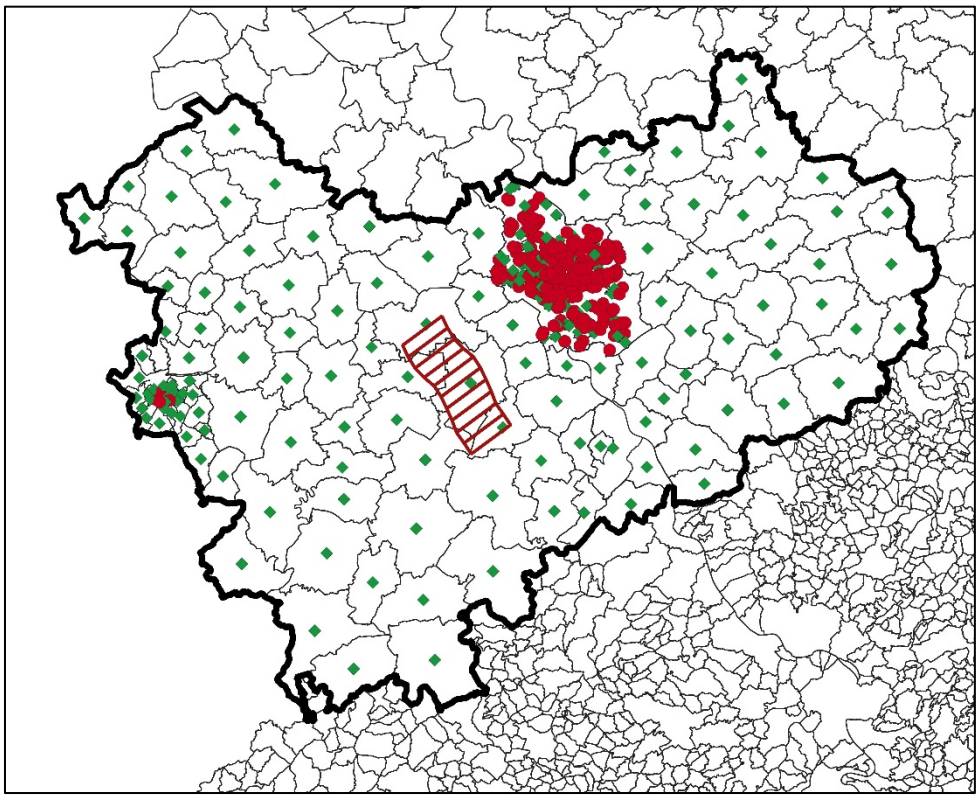

Figure 10.6: Centroids of the administrative units used for the estimation of casualties. Green diamonds and red circles indicate cases in which the average of the points within the administrative unit and the values at the centroid were adopted, respectively.

According to Jaiswal and Wald (2010), the PAGER empirical method was developed combining data on fatalities from past earthquakes with the estimation of population exposure to different levels of macroseismic intensity, making sure that the summation of estimated deaths from all intensity levels matched the total observed for the earthquakes. From this and further explanations in Jaiswal and Wald (2010), the method is meant to be applied by bands of intensity levels, and that the summation of median deaths expected at each intensity band should provide the total estimation for the earthquake. In view of this, the different administrative units were grouped according to their median intensities (determined as described above) using bins of intensities of width equal to half a unit. This half-unit width was selected as indicated in the publication of Jaiswal and Wald (2010). Bins were defined with edges at 4.25, 4.75, 5.25, …, 8.75, 9.25, 9.75 and corresponding midpoints 4.5, 5.0, …, 9.0, 9.5. These bins cover all average (per administrative unit) median intensities of interest for the scenario mainshock.
For each intensity band, the midpoint of the intensity bin was used to determine the fatality rate, which was in turn multiplied by the population associated with the band to obtain the corresponding median fatalities. We calculated the total number of fatalities expected for the earthquake (F_{tot}) as the sum of these median fatalities per intensity band (Equation 2 of Jaiswal and Wald 2010). To estimate the final

STR 20/02. GFZ German Research Centre for Geosciences.
DOI: 10.2312/GFZ.b103-20026

distribution of the probability of observing fatalities within pre-defined ranges of interest, we used the logarithm of this final value as the mean of a normal distribution whose standard deviation (ζ) is given by the PAGER empirical model. The probability that the number of fatalities *d* lies between thresholds *a* and *b* is given by Equation 14, where Φ is the standard normal cumulative distribution function.

$$P[a < d \leq b] = \Phi\left[\frac{ln(b) - ln(F_{tot})}{\zeta}\right] - \Phi\left[\frac{ln(a) - ln(F_{tot})}{\zeta}\right] \qquad (14)$$

Focusing only on the Regierungsbezirk (NUTS 2) of Köln, results obtained herein do not necessarily represent the final total for the earthquake but only for this region. This is equivalent to assuming either that the population beyond these administrative units is null or that the intensity beyond its boundaries is so low that any contribution from other administrative units would be negligible. None of these assumptions is true in reality.
While incorporating the uncertainty in intensity would be desirable, the PAGER empirical method has not been developed to do so explicitly. By defining intensity bands both in its derivation and application, the method is, by nature, grouping areas under the same band that have a range of mean intensities and not the single value used to represent them. Moreover, the derivation of the method was carried out using estimations of intensity and the population exposed to different intensity levels, and not observations, calibrating the parameters for the overall sum of fatalities from each earthquake for which data was available. From this point of view, the model could be thought of implicitly incorporating some level of uncertainty in the intensity field. Trying to incorporate uncertainty by, for example, discretizing the distribution of intensity, determining the fatality rate for each bin and calculating the final fatality rate as the weighted average of the contributions from each bin, would be inconsistent with the way the method was derived.

10.3. Results

Figure 10.7 shows the classification of the administrative units considered for the estimation of fatalities into bands of (median) EMS-98 intensity. Results obtained for each of the intensity bands are presented in Table 10.3. As can be observed, the largest proportions of the population fall within the bands of intensity 7.0, 6.5 and 7.5, in this order, although the largest number of expected fatalities stems from the bands of intensity 8.0 and 8.5. Only bands in which population exists within the Regierungsbezirk (NUTS 2) of Köln are shown.

STR 20/02. GFZ German Research Centre for Geosciences.
DOI: 10.2312/GFZ.b103-20026

Table 10.3: Population, fatality rate and expected fatalities for each intensity band.

Intensity			Population	Fatality rate	Fatalities
Mid-point	**Range**				
5.5	5.25	5.75	111,939	2.385E-07	0.0
6.0	5.75	6.25	273,465	1.322E-06	0.4
6.5	6.25	6.75	1,108,950	5.791E-06	6.4
7.0	6.75	7.25	1,697,836	2.093E-05	35.5
7.5	7.25	7.75	769,397	6.446E-05	49.6
8.0	7.75	8.25	355,037	1.735E-04	61.6
8.5	8.25	8.75	143,014	4.167E-04	59.6
Total			4,459,638	-	213.1

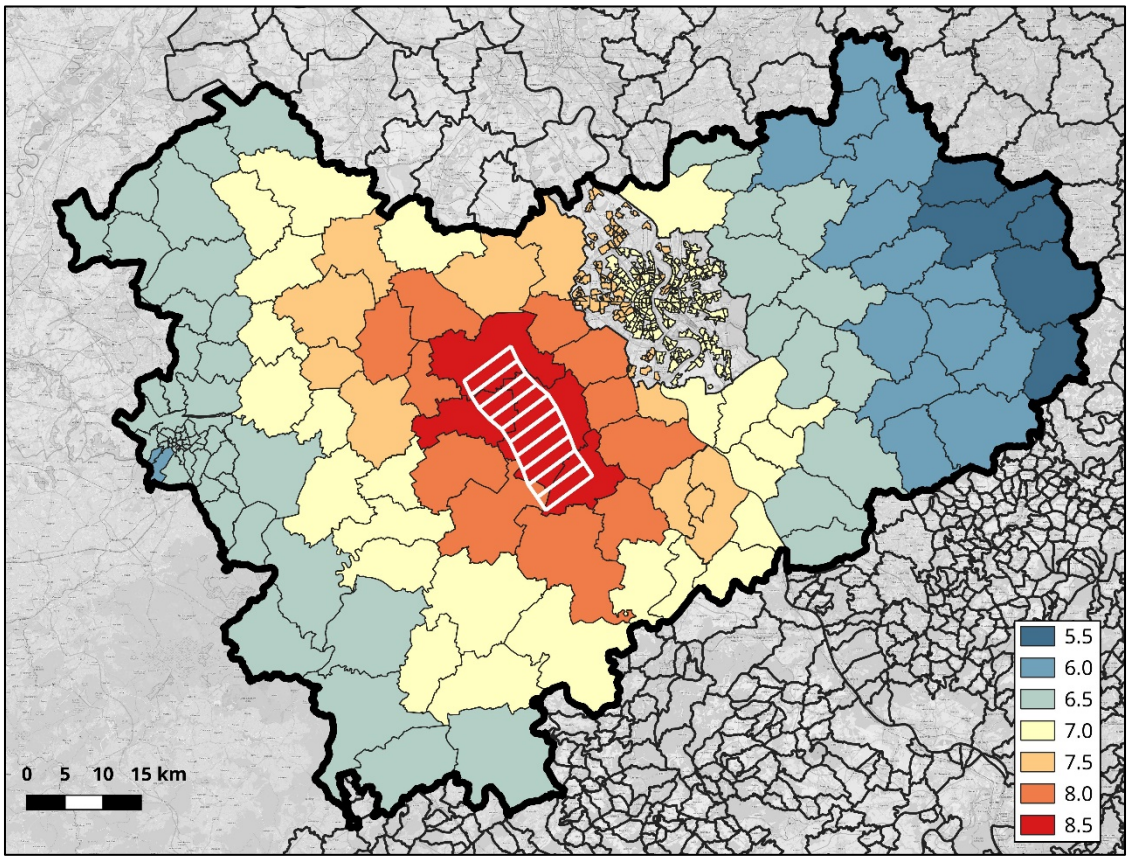

Figure 10.7: Classification of administrative units into bands of median EMS-98 intensity. Gray areas within the city of Cologne are not considered to be part of neighborhoods (Viertel) in the Shapefile of boundaries (courtesy of Schwarz and Maiwald 2019) but they correspond to parks and other such areas.

STR 20/02. GFZ German Research Centre for Geosciences.
DOI: 10.2312/GFZ.b103-20026

The total expected fatalities for the whole of the Regierungsbezirk (NUTS 2) of Köln (F_{tot}) results from the summation of the individual values, and amounts to 213 of the total of 4,459,638 people. Introducing this value in Equation 14 results in the probability of observing fatalities within pre-defined ranges of interest, as shown in Figure 10.8. The logarithmic scale is chosen for the bins, as Jaiswal and Wald (2010) indicate that the observed precision of the method is within one order of magnitude. As can be observed, while the median expected value is 213, there is a 60% probability of observing 100 to 1,000 deaths, and over 10% probability of having more than 1,000 deaths.

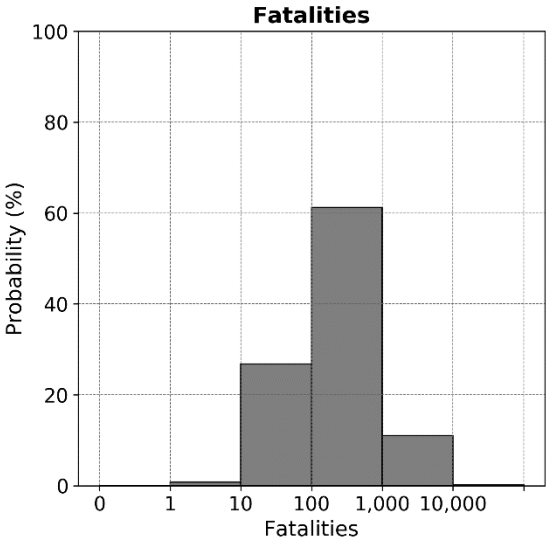

Figure 10.8: Probability of observing fatalities within predefined ranges in the Regierungsbezirk of Köln.

Carrying out the same calculations for each administrative unit yields slightly different results if the median intensity values for each unit are used to determine the fatality rate instead of using 0.5-unit intensity bins. The summation of median fatalities across all LAU (Gemeinde) level regions yields 198 fatalities instead of the 213 calculated using intensity bands. Nevertheless, the agreement between the two numbers is quite good. The map in Figure 10.9 shows the median values obtained per administrative unit.

STR 20/02. GFZ German Research Centre for Geosciences.
DOI: 10.2312/GFZ.b103-20026

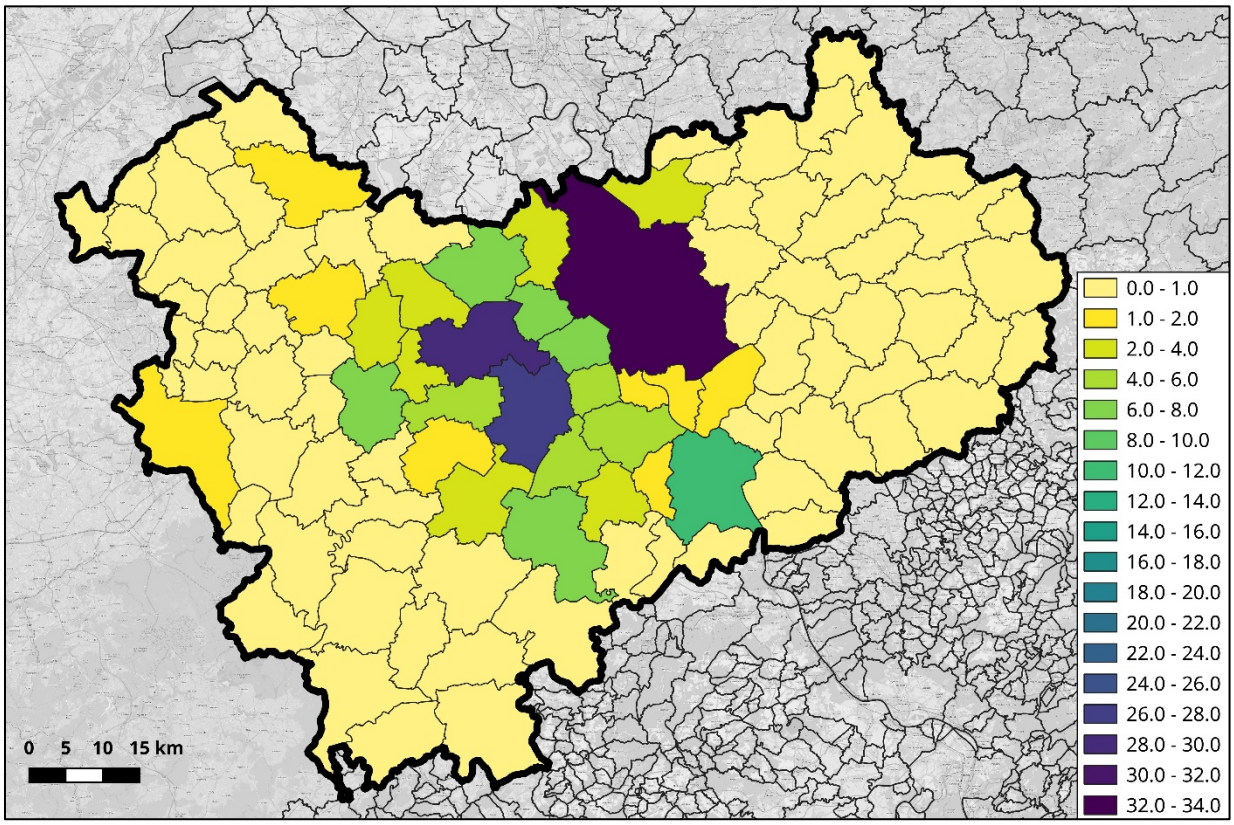

Figure 10.9: Median estimated fatalities per LAU (Gemeinde) level.

Further small discrepancies can be observed when using population at the Viertel level in Cologne and the Bezirk level in Bonn and Aachen. While these three cities are associated with 34.6, 10.9 and 1.4 median fatalities when carrying out the calculation at the LAU level (Figure 10.9), the summation of medians from Viertel/Bezirk yield the slightly different values of 33.0, 10.1 and 1.2. Figures 10.10 through 10.12 show the results obtained for each Viertel/Bezirk. As can be observed, at this level we are talking of less than one death per Viertel/Bezirk, and a color scale to display fractions of a person is used only for the purpose of distributing the overall number of expected fatalities in space. With the levels of expected intensities not varying greatly within the city of Cologne, the pattern of fatalities depicted in Figure 10.10 follows in general terms the distribution of the population (Figure 10.3).
While deaths are, in reality, integers, they are treated as real numbers herein because the method is meant to estimate aggregates of deaths and not deaths at such small spatial units. The work of Jaiswal and Wald (2010) provides no guidance regarding the rounding of fatalities to integers but from the method it is inferred that estimates for each intensity band are intended to be added as floating point numbers, as they represent only intermediate results and the model was derived to match total numbers of deaths of past earthquakes, not by intensity band. Similarly, the standard deviation that allows to estimate the overall probability distribution of fatalities (Equation 14, Figure 10.8) was calculated for the total number of deaths in an earthquake. The procedure used to derive the method implies as well that unevenness in the distribution of the population around earthquake sources is implicitly present in the emerging model. In other words, the fatality rates of the model account for the fact that some areas might be uninhabited while others are

STR 20/02. GFZ German Research Centre for Geosciences.
DOI: 10.2312/GFZ.b103-20026

not. Therefore, the results presented herein at such a level of detail as those shown in Figures 10.10 through 10.12 should be handled with care and it is the plot on the left of Figure 10.8 and the total estimate of 213 fatalities for the whole area that should be regarded as the most realistic outcome of this calculation (constrained by not including NUTS 2 areas other than the Regierungsbezirk of Köln.

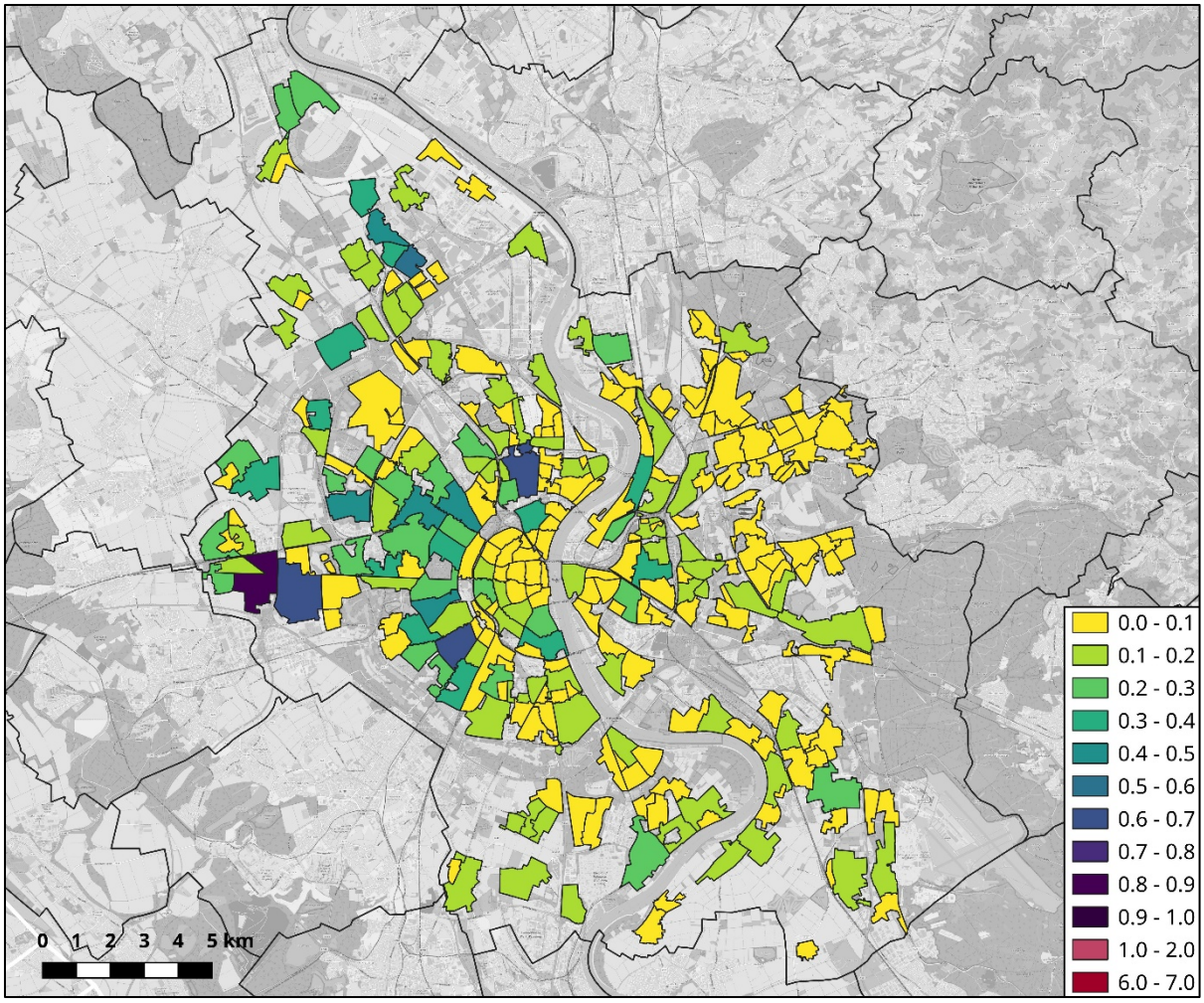

Figure 10.10: Median estimated fatalities per Viertel of Cologne.

STR 20/02. GFZ German Research Centre for Geosciences.
DOI: 10.2312/GFZ.b103-20026

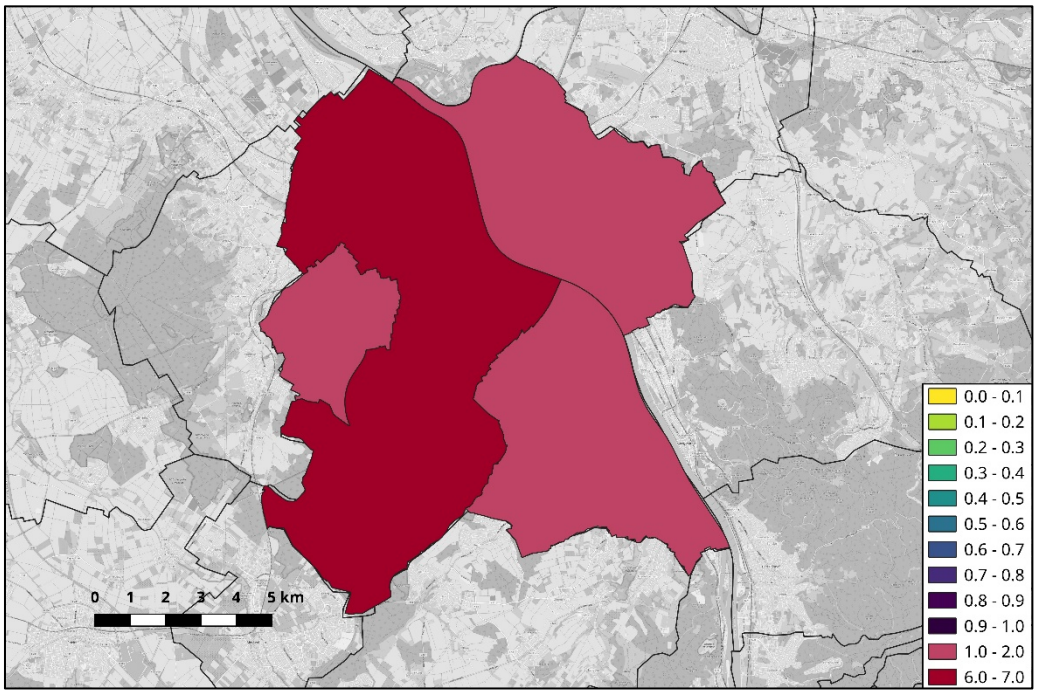

Figure 10.11: Median estimated fatalities per Bezirk of Bonn.

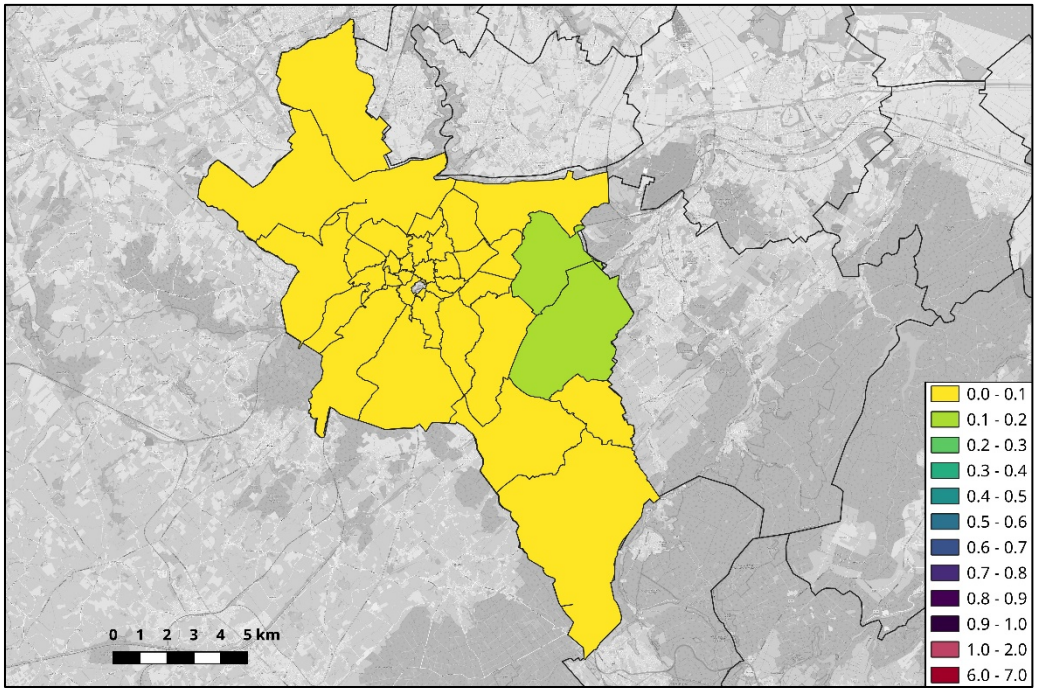

Figure 10.12: Median estimated fatalities per Bezirk of Aachen.

STR 20/02. GFZ German Research Centre for Geosciences.
DOI: 10.2312/GFZ.b103-20026

10.4. Discussion

Having applied the PAGER empirical method of Jaiswal and Wald (2010), the median expected number of fatalities due to the main shock is around 200 people of the total 4,459,638 people that live in the Regierungsbezirk (NUTS 2) of Köln. The largest proportions of the population fall within the bands of EMS-98 intensity 7.0, 6.5 and 7.5, in this order, although the largest number of expected fatalities stems from the bands of intensity 8.0 and 8.5. With the observed precision of the method being within one order of magnitude, it is, however, safer to speak in terms of probability of occurrence of ranges of fatalities. As has been shown, the method estimates a 60% probability of the main shock resulting in 100-1,000 fatalities and over 25% chance of the number of fatalities lying in the range 10-100 instead. A probability of around 10% of the figures rising up to the 1,000-10,000 range is indicated by the results as well. Focusing only on the Regierungsbezirk (NUTS 2) of Köln, these values do not necessarily represent the final total for the earthquake but only for this region. This is equivalent to assuming either that the population beyond these administrative units is null or that the intensity beyond its boundaries is so low that any contribution from other administrative units would be negligible. None of these assumptions is true in reality.
Further assumptions/limitations behind these results are

- A one-to-one relationship between EMS-98 and MM intensities as suggested by Musson et al. (2010).
- The whole census population is present in the region at the time of the earthquake and nobody who normally inhabits elsewhere needs to be added (no traveling, no visiting), or, alternatively, that the balance of absent residents and present visitors adds up to zero at the time of the earthquake.
- The population is grouped in intensity bins that depend on the average intensity within each administrative unit. This does not account for uneven distribution of the population or the intensity levels within the administrative unit. However, the problem of uneven distribution is implicit in the derivation of the method by Jaiswal and Wald (2010).
- The uncertainty in intensity cannot be explicitly accounted for within the PAGER empirical method. However, the way in which the method was derived could be thought of implicitly incorporating some (unspecified) level of uncertainty in the intensity field. This could be done by estimating the intensity and the population exposed to different intensity levels, and not observations, grouping the exposed population in intensity bands, and calibrating the parameters for the overall sum of fatalities from each earthquake.
- The global regionalization scheme used by Jaiswal and Wald (2010) to derive the model for Germany (and other countries with scarce to null data on fatalities resulting from past earthquakes) can really represent the situation in Cologne.
- The conversion of peak ground acceleration into EMS-98 intensity was carried out by means of a conversion equation based on Italian earthquakes, and the relation between the two parameters might be potentially different for Germany.

STR 20/02. GFZ German Research Centre for Geosciences.
DOI: 10.2312/GFZ.b103-20026

- Detailed shear-wave velocity profiles are available only for a limited region. As a consequence, the intensity fields used for the estimation of fatalities stem from combining peak ground acceleration values obtained from both detailed velocity profiles and the slope-derived proxy V_{s30} values of Wald and Allen (2007).

While the PAGER empirical method is intensity-based and, thus, independent of the damage calculations, it is of interest to relate these results with those presented in Chapter 9. From the estimation of damage to residential buildings, it appears that EMS-98 damage grades up to 3 are the most likely. Instances of physical damage associated to damage grades 1 through 3 that may result in injury or death include (Table 9.1):

- the fall of small-to-large pieces of plaster
- the fall of loose stones, bricks and roof tiles from buildings
- the partial or total collapse of chimneys, gable walls, etc.

Notwithstanding the relevance of the role of partial and total collapses in the aftermath of fatalities of an earthquake, deaths due to falling debris are not uncommon during seismic events. Moreover, the proportions of probabilities of exceedance obtained in Chapter 9 indicate that the possibility of observing very heavy damage of grades 4 and 5 (including partial and total collapses) cannot be ruled out, with around 2,691 and 444 buildings estimated to be likely to experience these two more extreme instances of damage, respectively.

Apart from the fragility of buildings, factors that may have a large influence on the number of fatalities and injuries include, for example:

- whether or not a foreshock that causes the population to be alert occurs shortly before the main shock, giving people sufficient time to evacuate buildings and search for safe open-air locations;
- the time of the day at which the earthquake occurs, with more people being inside or outside of buildings at different hours, and the potential difference of fragility of residential buildings versus commercial or industrial ones;
- whether the population has been educated or not on how to react and protect themselves in case of an earthquake;
- whether the population has been educated or not on how to anchor furniture and other kinds of components so as to prevent injury due to the motion of such elements.

STR 20/02. GFZ German Research Centre for Geosciences.
DOI: 10.2312/GFZ.b103-20026

11. Conclusions and recommendations

The northern Lower Rhine area in central Europe represents an active intraplate rift system with a moderate level of seismicity. However, there is a significant lack of public and political awareness of the potential seismic risk due to the rareness of damaging earthquakes.
Taking advantage of a large amount of various studies and geophysical data collected in the area, we created a harmonized 3D model of seismic velocities and attenuation parameters for the southern Lower Rhine Embayment. Over a wide area between the cities of Cologne, Bonn and Aachen, the model maps seismic velocities, density and attenuation on a 2 km grid. Beneficially, a significantly higher spatial resolution is available in and around the city of Cologne. This model serves as a basis for calculating theoretical 1D SH amplification functions for quantifying the impact of the geological layering and the geological discontinuities of the deep and extended basin on ground-motion amplification. Since no significant lateral discontinuities at depth are found across the Lower Rhine Embayment, the influence of 3D site effects has been considered only minor.
Using available ground-motion models for active shallow crustal earthquakes, ground-motion is modeled for a scenario event. As the ground shaking in the investigated region must be well represented by the chosen ground-motion model, we assessed its suitability by comparing modeling results with the observations of previous events in the Lower Rhine Embayment. Overall, ground-motion modeling provides a quantitative understanding of the salient (linear) site effects accounting for non-negligible lateral variations of ground-motion which cannot be captured without explicitly incorporating site-effect features in ground-motion models.
The ground-motion scenario further allows a scenario-based risk analysis for the city of Cologne and the Lower Rhine Embayment to be carried out. Results indicate that for the city of Cologne, a city actually located in a low to moderate seismic hazard region, significant consequences are possible. Expected macroseismic intensity levels categorizing the severity of ground shaking for the city of Cologne range around VII for the scenario event, meaning that moderate to large damage could be expected for large parts of the building stock in the city. We carried out the damage assessment using a building-by-building exposure model generated through the combination of three main sources of open data in which each building is characterized by its year of construction, number of stories and occupancy type. The damage assessment benefitted from previous studies providing a relationship between the year of construction and a distribution of most likely vulnerability class as well as fragility curves yielding the probability of exceedance of a given damage grade as a function of macroseismic intensity. It should, however, be noted that the monetary impact of an earthquake like the one studied herein is not limited to the extent of structural damage alone. Damage to non-structural components, such as ceilings, partition walls etc. can often amount to non-negligible monetary sums and pose a significant hazard to the population, even if the structural elements are preserved intact.
Having applied the empirical PAGER method for assessing the number of casualties shows that the median expected number due to the scenario event is around 200 people of a total of more than 4 million inhabitants in the Regierungsbezirk Köln. With the observed precision of the method being within one order of magnitude, a probability of slightly over 60% is observed for the scenario event resulting in 100 to 1,000 fatalities, with a probability of around 10% of falling in the 1,000-10,000 range instead. However, these numbers can change dramatically with the collapse of even

STR 20/02. GFZ German Research Centre for Geosciences.
DOI: 10.2312/GFZ.b103-20026

a very limited number of structures. For example, of the 185 individuals killed in the 2011 M 6.3 Canterbury (New Zealand) event, more than 60 percent (i.e. 115) were killed in the collapse of a single building only.

Although previous studies have provided precious information both on the soil characteristics and on the building environment, uncertainties are still large. This work and further results following the 1978 Albstadt earthquake have shown the necessity of an updated (re-)evaluation of the German building stock and the corresponding infrastructure. On the one hand, the German building stock in regions with a high level of seismic hazard has not yet been systematically investigated with regard to its vulnerability and the resulting risk. On the other hand, the building stock has seen significant recent changes (e.g. increased vulnerability due to large openings in new buildings, largely reduced stabilizing elements) and these changes have not yet been included. Field work and detailed on-site investigations as well as a comprehensive synopsis with further damage indicators is therefore required.

Additionally, for critical infrastructure such as hospitals or bridges, it is often not possible to make universally valid recommendations since for these facilities, structure-specific information is required. It is particularly recommended that additional efforts should be spent on school buildings. Collapses of school buildings during the Molise earthquake in Italy in 2002 and the Wenchuan earthquake in China in 2008 claimed large numbers of victims with a strong negative impact on the public opinion. With a relatively minor investment, significant improvements could be made. The canton of Basel-Stadt in Switzerland has already launched research activities and corresponding retrofitting for school buildings. With respect to school buildings it is further important to highlight that the power of preparedness and education in minimizing the number of victims should not be underestimated.

Finally, in cooperation with legally trained personnel, it should be investigated whether and how such regional hazard and risk modeling, partially based on crowd-sourcing data, can be legally disseminated at the individual building level.

STR 20/02. GFZ German Research Centre for Geosciences.
DOI: 10.2312/GFZ.b103-20026

References

Abrahamson, N. A., Silva, W. J., Kamai, R. (2014). Summary of the ASK14 ground-motion relation for active crustal regions. *Earthquake Spectra*, 30, 1025-1055. DOI: https://doi.org/10.1193/070913EQS198M

Al Atik, L., Kottke, A., Abrahamson, N., Hollenback, J. (2013). Kappa (κ) scaling of ground-motion prediction equations using an inverse random vibration theory approach. *Bulletin of the Seismological Society of America*, *104*(1), 336-346. DOI: https://doi.org/10.1785/0120120200

Basili R., Kastelic V., Demircioglu M. B., Garcia Moreno D., Nemser E. S., Petricca P., Sboras S. P., Besana-Ostman G. M., Cabral J., Camelbeeck T., Caputo R., Danciu L., Domac H., Fonseca J., García-Mayordomo J., Giardini D., Glavatovic B., Gulen L., Ince Y., Pavlides S., Sesetyan K., Tarabusi G., Tiberti M. M., Utkucu M., Valensise G., Vanneste K., Vilanova S., Wössner J. (2013). The European Database of Seismogenic Faults (EDSF) compiled in the framework of the Project SHARE. http://diss.rm.ingv.it/share-edsf/, DOI: https://doi.org/10.6092/INGV.IT-SHARE-EDSF

Bazzurro, P., Cornell, C. (1999). Disaggregation of seismic hazard. *Bulletin of the Seismological Society of America*, *89*(2), 501-520.

Beinersdorf, S., J. Schwarz, T. Langhammer (2013). Vulnerability assessment of a building stock and reliability considerations on the basis of observed damage grades: reconstruction of the September 3, 1978 Albstadt earthquake. Proceedings of the Vienna Congress on Recent Advances in Earthquake Engineering and Structural Dynamics (VEESD), August 28-30, Vienna, Austria.

Bommer, J. J., Stafford, P. J., Alarcón, J. E. (2009). Empirical equations for the prediction of the significant, bracketed, and uniform duration of earthquake ground-motion. *Bulletin of the Seismological Society of America*, *99*(6), 3217-3233. DOI: https://doi.org/10.1785/0120080298

Boore, D. M., Stewart, J. P., Seyhan, E., Atkinson, G. M. (2014). NGA-West2 equations for predicting PGA, PGV, and 5% damped PSA for shallow crustal earthquakes. *Earthquake Spectra*, *30*(3), 1057-1085.
DOI: https://doi.org/10.1193/070113EQS184M

Bozorgnia, Y., Abrahamson, N. A., Atik, L. A., Ancheta, T. D., Atkinson, G. M., Baker, J. W., Darragh, R. (2014). NGA-West2 research project. *Earthquake Spectra*, *30*(3), 973-987. DOI: https://doi.org/10.1193/072113EQS209M

Bradley, B. A., Pettinga, D., Baker, J. W., Fraser, J. (2017). Guidance on the utilization of earthquake-induced ground motion simulations in engineering practice. *Earthquake Spectra*, *33*(3), 809-835.
DOI: https://doi.org/10.1193/120216eqs219ep

STR 20/02. GFZ German Research Centre for Geosciences.
DOI: 10.2312/GFZ.b103-20026

Breddin, H. (1954). Ein neuartiges hydrogeologisches Kartenwerk für die südliche Niederrheinische Bucht. Zeitschrift der Deutschen Gesellschaft für Geowissenschaften, Band 106, 94-112.

Breddin, H., Brühl, H. Dieler, H. (1963). Das Blatt Aachen-NW der praktischgeologischen Grundkarte 1:5000. Geol. Mitt., 1, 251-428.

Brüstle, W. Stange, S. (1999). Vorstudie zum Forschungsvorhaben: Karte der geologischen Untergrundklassen für DIN 4149 (neu). Landesamt für Geologie, Rohstoffe und Bergbau Baden-Württemberg.

Brzev, S., C. Scawthorn, A.W. Charleson, L. Allen, M. Greene, K. Jaiswal, V. Silva (2013). GEM Building Taxonomy Version 2.0. GEM Technical Report 2013-02 V1.0.0, 188 pp., GEM Foundation, Pavia, Italy, https://www.globalquakemodel.org/gempublications/GEM-building-taxonomy-version-2.0

BSSC, Building Seismic Safety Council (2003). NEHRP Recommended Provisions for Seismic Regulations for New Buildings and Other Structures, FEMA-450, 2003 revision, Federal Emergency Management Agency, Washington D.C.

Budny, M. (1984). Seismische Bestimmung der Bodendynamischen Kennwerte von oberflächennahen Schichten in Erdbebengebieten der Niederrheinischen Bucht und ihre ingenieurseismologische Anwendung. Sonderveröff. Geol. Inst. Uni. Köln, 57, 208.

Campbell, K. W., Bozorgnia, Y. (2014). NGA-West2 ground-motion model for the average horizontal components of PGA, PGV, and 5% damped linear acceleration response spectra. *Earthquake Spectra*, 30, 1087-1115.
DOI: https://doi.org/10.1193/062913EQS175M

Cartwright, D. E., Longuet-Higgins, M. S. (1956). The statistical distribution of the maxima of a random function. *Proceedings of the Royal Society of London. Series A. Mathematical and Physical Sciences*, *237*(1209), 212-232.
DOI: https://doi.org/10.1098/rspa.1956.0173

CEN, European Committee for Standardization, (2003). Eurocode 8: Design of structures for earthquake resistance - Part 1: General rules, seismic actions and rules for buildings.", European Committee for Standardization, Brussels.

Chi-Miranda, M. A., Montejo, L. A. (2017). A numerical comparison of random vibration theory and time histories based methods for equivalent-linear site response analyses. *International Journal of Geo-Engineering*, *8*(1), 22.
DOI: https://doi.org/10.1186/s40703-017-0059-6

Chiou, B. S. J., Youngs, R. R. (2014). Update of the Chiou and Youngs NGA model for the average horizontal component of peak ground-motion and response spectra. *Earthquake Spectra*, *30*, 1117-1153.
DOI: https://doi.org/10.1193/072813EQS219M

Coburn A.W., R.J.S. Spence, A. Pomonis (1992). Factors determining casualty levels in earthquakes: Mortality prediction in building collapse. Proceedings of the 10th World Conference in Earthquake Engineering, Madrid, Spain.

Crowley, H., R. Pinho, J. van Elk, J. Uilenreef (2019). Probabilistic damage assessment of buildings due to induced seismicity. Bulletin of Earthquake Engineering 17(8), 4495-4516. DOI: https://doi.org/10.1007/s10518-018-0462-1

Cua, G., Wald, D. J., Allen, T. I., Garcia, D., Worden, C. B., Gerstenberger, M., Marano, K. (2010). *Best practices" for using macroseismic intensity and ground-motion-intensity conversion equations for hazard and loss models in GEM1* (p. 4). GEM Technical Report 2010-4, GEM Foundation, Pavia, Italy.

Delavaud E., Cotton F., Akkar S., Scherbaum F., Danciu L., Beauval C., Drouet S., Douglas J., Basili R., Sandikkaya M.A., Segou M., Faccioli E., Theodoulidis N. (2012). Toward a ground-motion logic tree for probabilistic seismic hazard assessment in Europe. Journal of Seismology 16(3): 451-473.
DOI: https://doi.org/10.1007/s10950-012-9281-z

Despotaki, V., V. Silva, S. Lagomarsino, I. Pavlova, J. Torres (2018). Evaluation of seismic risk on UNESCO cultural heritage sites in Europe. International Journal of Architectural Heritage 12(7-8), 1231-1244.
DOI: https://doi.org/10.1080/15583058.2018.1503374

Douglas, J. (2019). GMPE compendium, available at http://www.gmpe.org.uk/ , last accessed 10 December 2019.

Edwards B., Cauzzi C., Danciu L., Fäh D. (2016). Region-Specific Assessment, Adjustment, and Weighting of Ground-Motion Prediction Models: Application to the 2015 Swiss Seismic-Hazard Map, Bulletin of the Seismological Society of America 106, 1840-1857. DOI: https://doi.org/10.1785/0120150367

Esri Deustchland (2018).
https://opendata-esri-de.opendata.arcgis.com/datasets/b554b6a4155441279862a389b88934d7_0. Last accessed 18 September 2019.

European Environmental Agency (EEA). CORINE Land Cover project. Available online at: https://land.copernicus.eu/pan-european/corine-land-cover. Last accessed: 21 October 2019.

Eurostat (2020). NUTS – Nomenclature of Territorial Units for Statistics. Available online at: https://ec.europa.eu/eurostat/web/nuts/background. Last accessed: 27 January 2020.

Faenza, L., Michelini, A. (2010). Regression analysis of MCS intensity and ground-motion parameters in Italy and its application in ShakeMap. *Geophysical Journal International*, *180*(3), 1138-1152.
DOI: https://doi.org/10.1111/j.1365-246X.2009.04467.x

Fäh, D., Kind, F., Giardini, D. (2001). A theoretical investigation of average H/V ratios. *Geophysical Journal International*, *145*(2), 535-549. DOI: https://doi.org/10.1046/j.0956-540x.2001.01406.x

Fäh, D., Gisler, M., Jaggi, B., Kästli, P., Lutz, T., Masciadri, V., Tauber, J. (2009). The 1356 Basel earthquake: an interdisciplinary revision. *Geophysical Journal International*, *178*(1), 351-374. DOI: https://doi.org/10.1111/j.1365-246X.2009.04130.x

GADM database. https://www.gadm.org/, last accessed: 18. September 2019.

Gamba, P. (2014). Global Exposure Database: Scientific Features. GEM Technical Report 2014-10 V1.0.0, 46 pp., GEM Foundation, Pavia, Italy, DOI: 10.13117/GEM.EXP---MOD.TR2014.10.

Gasparini, D., Vanmarcke, E. H. (1976). SIMQKE: A program for artificial motion generation. *Department of Civil Engineering, Massachusetts Institute of Technology, Cambridge, MA*.

Gregor, N., Abrahamson, N. A., Atkinson, G. M., Boore, D. M., Bozorgnia, Y., Campbell, K. W., Silva, W. (2014). Comparison of NGA-West2 GMPEs. *Earthquake Spectra*, *30*(3), 1179-1197. DOI: https://doi.org/10.1193/070113EQS186M

Grinstead, C.M., J. Laurie Snell (1997). Introduction to Probability. Chapter 7: Sums of Independent Random Variables. A publication of the American Mathematical Society. ISBN 978-0-8218-9414-9. Available online https://www.dartmouth.edu/~chance/teaching_aids/books_articles/probability_book/Chapter7.pdf, last accessed 30 September 2019.

Grünthal, G. (1998). European Macroseismic Scale 1998 (EMS-98). European Seismological Commission, Subcommission on Engineering Seismology, Working Group Macroseismic Scales. Conseil de l'Europe. *Cahiers du Center Européen de Géodynamique et de Séismologie*, *15*.

Grünthal, G., Wahlström, R. (2012). The European-Mediterranean earthquake catalogue (EMEC) for the last millennium. Journal of Seismology, 16(3), 535-570. DOI: https://doi.org/10.1007/s10950-012-9302-y

Grünthal G, Wahlström R, Stromeyer D (2009) The unified catalogue of earthquakes in central, northern, and northwestern Europe (CENEC)—updated and expanded to the last millennium. Journal of Seismology 13(4):517–541.
DOI: https://doi.org/10.1007/s10950-008-9144-9

Grünthal, G., Stromeyer, D., Bosse, C., Cotton, F., Bindi, D. (2018). The probabilistic seismic hazard assessment of Germany—version 2016, considering the range of epistemic uncertainties and aleatory variability. *Bulletin of Earthquake Engineering*, 1-57. DOI: https://doi.org/10.1007/s10518-018-0315-y

Grützner, C., Fischer, P., Reicherter, K. (2016). Holocene surface ruptures of the Rurrand Fault, Germany—insights from palaeoseismology, remote sensing and

shallow geophysics. *Geophysical Journal International*, *204*(3), 1662-1677. DOI: https://doi.org/10.1093/gji/ggv558

Hanks, T. C., Kanamori, H. (1979). A moment magnitude scale. *Journal of Geophysical Research: Solid Earth*, *84*(B5), 2348-2350. DOI: https://doi.org/10.1029/JB084iB05p02348

Haskell, N. A. (1953). The dispersion of surface waves on multilayered media. *Bulletin of the seismological Society of America*, *43*(1), 17-34.

Hilden, H.D. (1988a). Devon-Geologie am Niederrhein, Geologisches Landesamt Nordrhein-Westfalen, Krefeld, 14-16.

Hilden, H.D. (1988b). Karbon-Geologie am Niederrhein, Geologisches Landesamt Nordrhein-Westfalen, Krefeld, 16-18.

Idriss, I. M. (2014). An NGA-West2 empirical model for estimating the horizontal spectral values generated by shallow crustal earthquakes. *Earthquake Spectra*, *30*, 1155-1177. DOI: https://doi.org/10.1193/070613EQS195M

Information und Technik Nordrhein-Westfalen (2018). Bevölkerung in Nordrhein-Westfalen am 30. Juni 2018 (Gemeindeergebnisse). Available online at: https://www.it.nrw/nrw-einwohnerzahl-lag-auch-mitte-dieses-jahres-bei-179-millionen-93832. Last accessed: 17 September 2019.

Jaiswal, K., D. Wald (2010). An empirical model for global earthquake fatality estimation. Earthquake Spectra 26(4), 1017-1037. Model coefficients available online: https://pubs.usgs.gov/of/2009/1136/.

Kaestli P., Fäh D. (2006). Rapid estimation of macroseismic effects and ShakeMaps using macroseismic data, First European Conference on Earthquake Engineering and Seismology, Geneva, Switzerland.

Keintzel, E. (2005). Über den Weg zur neuen deutschen Erdbebennorm DIN 4149: 2005-04. *Bautechnik*, *82*(8), 475-485.
DOI: https://doi.org/10.1002/bate.200590164

Kempton, J. J., Stewart, J. P. (2006). Prediction equations for significant duration of earthquake ground-motions considering site and near-source effects. *Earthquake Spectra*, 22, 985-1013. DOI: https://doi.org/10.1193/1.2358175

Knapp, G. (1988). Trias-Geologie am Niederrhein, Geologisches Landesamt Nordrhein-Westfalen, Krefeld, 23-27.

Knauff, W. (1988). Jura-Geologie am Niederrhein, Geologisches Landesamt Nordrhein-Westfalen, Krefeld, 27-28.

Knopoff, L. (1964). A matrix method for elastic wave problems. *Bulletin of the Seismological Society of America*, *54*(1), 431-438.

Kottke, A., Rathje, E. M. (2008). A semi-automated procedure for selecting and scaling recorded earthquake motions for dynamic analysis. *Earthquake Spectra*, *24*(4), 911-932. DOI: https://doi.org/10.1193/1.2985772

Kottke, A. R., Rathje, E. M. (2013). Comparison of time series and random-vibration theory site-response methods. *Bulletin of the Seismological Society of America*, *103*(3), 2111-2127. DOI: https://doi.org/10.1785/0120120254

Lang, D.H., J. Schwarz (2006). Instrumental subsoil classification of Californian strong motion sites based on single-station measurements. Proceedings of the 8th U.S. National Conference on Earthquake Engineering (NCEE), April 22-26, San Francisco, Unites States.

Leonard, M. (2010). Earthquake fault scaling: Self-consistent relating of rupture length, width, average displacement, and moment release. *Bulletin of the Seismological Society of America*, *100*(5A), 1971-1988.
DOI: https://doi.org/10.1785/0120090189

Leydecker, G. (2011). Erdbebenkatalog für Deutschland mit Randgebieten für die Jahre 800 bis 2008, Geologisches Jahrbuch, E 59, 198 S. BGR, Hannover.

Mai, P. M., Spudich, P., Boatwright, J. (2005). Hypocenter locations in finite-source rupture models. *Bulletin of the Seismological Society of America*, *95*(3), 965-980. DOI: https://doi.org/10.1785/0120040111

Mak, S., Cotton, F., Gerstenberger, M., Schorlemmer, D. (2018). An Evaluation of the Applicability of NGA-West2 Ground-Motion Models for Japan and New ZealandAn Evaluation of the Applicability of NGA-West2 GMMs for Japan and New Zealand. *Bulletin of the Seismological Society of America*, *108*(2), 836-856.
DOI: https://doi.org/10.1785/0120170146

Mapillary. https://www.mapillary.com/.

Mason et al. (2004). List of the largest explosive eruptions on earth. http://www.volcano.geog.cam.ac.uk/database/list.html, last accessed 30 November 2018.

McGuire, R. K. (1995). Probabilistic seismic hazard analysis and design earthquakes: closing the loop. *Bulletin of the Seismological Society of America*, *85*(5), 1275-1284.

Musson, R.M.W., G. Grünthal, M. Stucchi (2010). The comparison of macroseismic intensity scales. *Journal of Seismology* 14(2), 413-428.
DOI: https://doi.org/10.1007/s10950-009-9172-0

Nordrhein-Westfalen Web Feature Service (2019).
https://www.wfs.nrw.de/geobasis/wfs_nw_alkis_vereinfacht?request=GetCapabilities&service=WFS&NAMESPACES=xmlns%28ave,http://repository.gdi-de.org/schemas/adv/produkt/alkis-vereinfacht/2.0%29, last accessed 18 August 2019.

Offene Daten Aachen (2017). Stimmbezirke der Stadt Aachen für die Landtags- und Bundestagswahl 2017. Available online at: http://offenedaten.aachen.de/dataset/stimmbezirke-stadt-aachen, last accessed 18 September 2019.

Offene Daten Aachen (2019). Einwohnerstatistik allgemein nach Statistischen Bezirken. Available online at: http://offenedaten.aachen.de/dataset/einwohnerstatistik, last accessed: 18 September 2019.

Pagani, M., Monelli, D., Weatherill, G., Danciu, L., Crowley, H., Silva, V., Simionato, M. (2014). OpenQuake engine: An open hazard (and risk) software for the global earthquake model. *Seismological Research Letters*, *85*(3), 692-702. DOI: https://doi.org/10.1785/0220130087

Parolai, S., Bormann, P., Milkereit, C. (2001). Assessment of the natural frequency of the sedimentary cover in the Cologne area (Germany) using noise measurements. *Journal of Earthquake Engineering*, *5*(04), 541-564. DOI: https://doi.org/10.1080/13632460109350405

Parolai, S., Bormann, P., Milkereit, C. (2002). New relationships between Vs, thickness of sediments, and resonance frequency calculated by the H/V ratio of seismic noise for the Cologne area (Germany). *Bulletin of the Seismological Society of America*, *92*(6), 2521-2527. DOI: https://doi.org/10.1785/0120010248

Parolai, S., Richwalski, S. M., Milkereit, C., Fäh, D. (2006). S-wave velocity profiles for earthquake engineering purposes for the Cologne area (Germany). *Bulletin of Earthquake Engineering*, *4*(1), 65-94. DOI: https://doi.org/10.1007/s10518-005-5758-2

Raschke, M. (2003). Die Korrelation zwischen Erdbebenschaden und Erdbebenstärke und deren Anwendung in der Erdbebenrisikoanalyse. Dissertation Bauhaus-Universität Weimar.

Rathje, E. M., Kottke, A. R., Ozbey, M. C. (2005). Using inverse random vibration theory to develop input Fourier amplitude spectra for use in site response. In *16th International Conference on Soil Mechanics and Geotechnical Eningeering: TC4 Earthquake Geotechnical Engineering Satellite Conference* (pp. 160-166).

Reamer, S. K., Hinzen, K. G. (2004). An Earthquake Catalog for the Northern Rhine Area, Central Europe (1975-2002). *Seismological Research Letters*, *75*(6), 713-725. DOI: https://doi.org/10.1785/gssrl.75.6.713

Rodriguez-Marek, A., Rathje, E. M., Bommer, J. J., Scherbaum, F., Stafford, P. J. (2014). Application of single-station sigma and site-response characterization in a probabilistic seismic-hazard analysis for a new nuclear site. *Bulletin of the Seismological Society of America*, *104*(4), 1601-1619. DOI: https://doi.org/10.1785/0120130196

Schneider, H. Thiele, S. (1965). Geohydrologie des Erftgebietes. Schriftenreihe Min. Ernähr., Landwirtsch. u. Forsten Land Nordrh.-Westf., 186 S., Düsseldorf

Schwarz, J., H. Maiwald (2019). Bevölkerungsschutz Bund – Risikoanalyse 2019 – Szenario "Erdbeben": Vorschlag zur Schadenmodelierung im Referenzgebiet Köln (inklusive Anlage zur Altersstruktur). Bauhaus-Universität Weimar, Earthquake Damage Analysis Center (EDAC). Internal report.

Schwarz, J., H. Maiwald, M. Raschke (2004). Erdbebenszenarien für deutsche Großstadträume und Quantifizierung der Schadenpotentiale. Deutsches Forschungsnetz Naturkatastrophen (DFNK) Abschlussbericht, edited by Merz B. and H. Apel, 188-200.

Schwarz, J., S. Beinersdorf, T. Swain, T. Langhammer, M. Leipold, C. Kaufmann, T. Wenk (2008). Realistic vulnerability and displacement functions for masonry structures derived from damaging earthquakes in Central Europe. Proceedings of the 14th World Conference on Earthquake Engineering, October 12-17, Beijing, China.

Schwarz, J., S. Beinersdorf, H. Meidow, L. Ahorner (2010). Magnitudenorientierter Erdbebenkatalog für deutsche und angrenzende Gebiete EKDAG – erweiterter Ahorner-Katalog (version 1.0). Bauhaus University, Weimar, Germany. Available at: https://www.edac.biz/projekte/erdbebenkatalog/kontakt-download/, last accessed 10 July 2019.

Silva, V., C. Yepes-Estrada, J. Dabbeek, L. Martins, S. Brzev (2018). GED4ALL - Global Exposure Database for Multi-Hazard Risk Analysis – Multi-Hazard Exposure Taxonomy. GEM Technical Report 2018-01, GEM Foundation, Pavia, Italy.

So, E.K.M., A. Pomonis (2012). Derivation of globally applicable casualty rates for use in earthquake loss estimation models. Proceedings of the 15th World Conference in Earthquake Engineering, Lisbon, Portugal.

Stadt Köln (2016). Statistisches Jahrbuch 2016, 93. Jahrgang. 302 pp. Available online at: https://www.stadt-koeln.de/mediaasset/content/pdf15/statistik-jahrbuch/statistisches_jahrbuch_2016_ksn_2_2016.pdf, last accessed 8 July 2019.

Stadt Köln (2019a). Offene Daten Köln: Einwohner Statistik Köln Stadtviertel. Available online at: https://www.offenedaten-koeln.de/dataset/einwohner-statistik-koeln , last accessed 9 July 2019.

Stadt Köln (2019b). Offene Daten Köln: OSM Hausnummern (MapServer). Available online at: https://geoportal.stadt-koeln.de/arcgis/rest/services/Statistische_Daten/OSM_Hausnummern/MapServer/0l last accessed 9 July 2019.

Statistische Ämter des Bundes und der Länder (2018). Zensus 2011. Results available online at: https://ergebnisse.zensus2011.de , last accessed 8 July 2019.

STR 20/02. GFZ German Research Centre for Geosciences.
DOI: 10.2312/GFZ.b103-20026

Stromeyer, D., Grünthal, G. (2009). Attenuation relationship of macroseismic intensities in Central Europe. *Bulletin of the Seismological Society of America*, *99*(2A), 554-565. DOI: https://doi.org/10.1785/0120080011

Stromeyer, D., Grünthal, G. (2015). Capturing the uncertainty of seismic activity rates in probabilistic seismic-hazard assessments. *Bulletin of the Seismological Society of America*, 105, 580-589. DOI: https://doi.org/10.1007/s10518-018-0398-5

Thomson, W. T. (1950). Transmission of elastic waves through a stratified solid medium. *Journal of applied Physics*, *21*(2), 89-93.
DOI: https://doi.org/10.1063/1.1699629

Vanmarcke, E. H. (1975). On the distribution of the first-passage time for normal stationary random processes. *J. of Appl. Mech.*, 42, 215-220.
DOI: https://doi.org/10.1115/1.3423521

Vanmarcke, E. H., Gasparini, D. A. (1976). A program for artificial motion generation, user's manual and documentation. *Department of Civil Engineering, Massachusetts Institute of Technology*.

Vanneste, K., Camelbeeck, T., Verbeeck, K. (2013). A Model of Composite Seismic Sources for the Lower Rhine Graben, Northwest Europe. A Seismic Source Model for the Lower Rhine Graben. *Bulletin of the Seismological Society of America*, *103*(2A), 984-1007.

Von Kamp, H. (1986). Geologische Karte von Nordrhein-Westfalen, 1:100.000, Geologisches Landesamt Nordrhein-Westfalen, Krefeld.

Wald, D. J., Allen, T. I. (2007). Topographic slope as a proxy for seismic site conditions and amplification. *Bulletin of the Seismological Society of America*, *97*(5), 1379-1395. DOI: https://doi.org/10.1785/0120060267

Wang, X., Rathje, E. M. (2016). Influence of peak factors on site amplification from random vibration theory based site-response analysis. *Bulletin of the Seismological Society of America*, *106*(4), 1733-1746. DOI: https://doi.org/10.1785/0120150328

Weber, B. (2007). Bodenverstärkung in der südlichen Niederrheinischen Bucht, Doktorarbeit, Universität zu Köln, 205 S.

Wells, D. L., Coppersmith, K. J. (1994). New empirical relationships among magnitude, rupture length, rupture width, rupture area, and surface displacement. *Bulletin of the seismological Society of America*, *84*(4), 974-1002.

Woessner, J., D. Giardini, H. Crowley, F. Cotton, G. Grünthal, G. Valensise, R. Arvidsson, R. Basili, M. B. Demircioglu, S. Hiemer, C. Meletti, R. W. Musson, A. N. Rovida, K. Sesetyan, M. Stucchi The SHARE Consortium (2015). The 2013 European Seismic Hazard Model: Key Components and Results. Bulletin of Earthquake Engineering 13(12), 3553–3596. DOI: https://doi.org/10.1007/s10518-015-9795-1

Xia, J., Xu, Y., Miller, R. D., Ivanov, J. (2012). Estimation of near-surface quality factors by constrained inversion of Rayleigh-wave attenuation coefficients. *Journal of Applied Geophysics*, *82*, 137-144.
DOI: https://doi.org/10.1016/j.jappgeo.2012.03.003

Yepes-Estrada, C., V. Silva, J. Valcárcel, A.B. Acevedo, N. Tarque, M.A. Hube, G. Coronel, H. Santa María (2017). Modeling the residential building inventory in South America for seismic risk assessment. Earthquake Spectra 33(1), 299-322. DOI: https://doi.org/10.1193/101915eqs155dp

Zaccarelli, R., Bindi, D., Strollo, A., Quinteros, J., Cotton, F. (2019). Stream2segment: An Open-Source Tool for Downloading, Processing, and Visualizing Massive Event-Based Seismic Waveform Datasets. *Seismological Research Letters*, DOI: https://doi.org/10.1785/0220180314

Zaccarelli, Riccardo (2018). Stream2segment: a tool to download, process and visualize event-based seismic waveform data. V 2.7.3, GFZ Data Services, DOI: https://doi.org/10.5880/GFZ.2.4.2019.002

Glossary

Epicenter (German: Epizentrum): point on the earth's surface vertically above the hypocenter, a point in the crust where a seismic rupture begins.

Fault (German: Verwerfung): a fracture along which the blocks of crust on either side have moved relative to one another parallel to the fracture.

Fault plane (German: Bruchfläche): planar (flat) surface along which there is slip during an earthquake.

Fragility (German: Fragilität): probability of exceedance / occurrence of a set of thresholds of damage conditional on the occurrence of a particular level of ground motion (PGA, SA, macroseismic intensity).

Hypocenter (German: Hypozentrum): point within the earth where an earthquake rupture starts.

Intensity (German: Intensität): macroseismic intensity is an integer number (generally written as a Roman numeral) describing the severity of an earthquake in terms of its effects on the earth's surface and on humans and their structures.

Joyner-Boore distance R_{JB} (German: Joyner-Boore-Entfernung): shortest distance from a site to the surface projection of the rupture surface.

Liquefaction (German: Bodenverflüssigung): process by which water-saturated sediment temporarily loses strength and acts as a fluid, like when you wiggle your toes in the wet sand near the water at the beach. This effect can be caused by earthquake shaking.

Moment magnitude Mw (German: Momentenmagnitude): Because of the limitations of all three different magnitude scales, a more uniformly applicable extension of the magnitude scale, known as moment magnitude was developed. The seismic moment is a physical quantity proportional to the slip on the fault multiplied by the area of the fault surface that slips; it is related to the total energy released in the earthquake.

Peak ground acceleration PGA (German: maximale Bodenbeschleunigung): amplitude of the largest absolute acceleration recorded on an accelerogram at a site during a particular earthquake.

Quality factor Q (German: Gütefaktor): The dimensionless Q factor is defined as the ratio of elastic energy stored at maximum stress and strain to energy lost in one cycle or wavelength. The quality factor is inverse proportional to the attenuation factor.

Recurrence period (German: Wiederkehrperiode): average time span between earthquake occurrences on a fault or in a source zone.

Return period (German: mittlere Wiederholungsperiode): the inverse of the annual probability of exceedance for a certain level of seismic hazard. This value represents

STR 20/02. GFZ German Research Centre for Geosciences.
DOI: 10.2312/GFZ.b103-20026

the average number of years it takes to get an exceedance.

Seismic noise (German: seismisches Rauschen / Umgebungsrauschen): describes the relatively persistent vibration of the ground due to a multitude of causes, either natural (frequencies below 1 Hz caused by tides, wind and other atmospheric phenomena) and artificial (frequencies above 1 Hz, caused by human activities) sources.

Spectral acceleration (also Peak spectral acceleration, German: maximale Spektralbeschleunigung): measure of the maximum force experienced by a mass on top of a rod having a particular natural period of resonance.

Vulnerability (German: Verletzbarkeit): Probability distribution of loss (or loss ratio) given a particular level of ground-motion (PGA, SA, macroseismic intensity). Vulnerability functions result from combining fragility functions with consequence functions.

STR 20/02. GFZ German Research Centre for Geosciences.
DOI: 10.2312/GFZ.b103-20026

Appendix

A1. Data sources

Data	Data source	Last accessed
Model for V_P, V_S, Q and density for the Lower Rhine Embayment	Data have been provided by Bernd Weber. A description of the data set can be found in Weber, B. (2007). Bodenverstärkung in der südlichen Niederrheinischen Bucht, PhD thesis, University of Cologne, pp. 205.	
Model for V_P and V_S around the city of Cologne and the Rhein-Erft-Kreis	Data are available at GFZ Potsdam. A description of the data sets can be found in Parolai, S., Bormann, P., Milkereit, C. (2001). Assessment of the natural frequency of the sedimentary cover in the Cologne area (Germany) using noise measurements. *Journal of Earthquake Engineering*, *5*(04), 541-564 and in Parolai, S., Richwalski, S. M., Milkereit, C., Fäh, D. (2006). S-wave velocity profiles for earthquake engineering purposes for the Cologne area (Germany). *Bulletin of Earthquake Engineering*, *4*(1), 65-94.	
Earthquake data for previous events in and around the Lower Rhine Embayment	Data have been retrieved from http://eida.gfz-potsdam.de/webdc3/	3 March 2019
Topography for the Lower Rhine Embayment	Data have been retrieved from https://www.gebco.net/data_and_products/gridded_bathymetry_data/gebco_30_second_grid/	10 March 2019
Footprints, location, occupancy type of buildings. Buildings represented as polygons.	Data have been retrieved from OpenStreetMap	20 August 2019
Years of construction and addresses of buildings	Offene Daten Köln (Stadt Köln 2019b)	24 August 2018
Number of stories, occupancy type and addresses of buildings	Nordrhein-Westfalen Web Feature Service (2019)	20 August 2019

STR 20/02. GFZ German Research Centre for Geosciences.
DOI: 10.2312/GFZ.b103-20026

Buildings represented as polygons		
Number of buildings in the city of Cologne in the year 2011	German National Census 2011	6 October 2018
Distribution of ranges of year of construction per Viertel of Cologne, based on data from the city of Cologne for the year 2000	Data taken from Schwarz and Maiwald (2019)	
3D models and photos of buildings	Google Maps / Google Earth / Google Street View	
Photos of buildings	Mapillary	
Population of 31 December 2017 per Viertel of Cologne	Stadt Köln (2019a)	9 July 2019
Population of 31 December 2017 per Bezirk of Bonn	Esri Deutschland (2018)	18 Sept 2019
Population of 31 December 2017 per Bezirk of Aachen	Offene Daten Aachen (2019)	18 Sept 2019
Population of 31 December 2017 per LAU level	Information und Technik Nordrhein-Westfalen (2018)	17 Sept 2019

STR 20/02. GFZ German Research Centre for Geosciences.
DOI: 10.2312/GFZ.b103-20026

A2. Mapping of occupancy strings into occupancy classes

The adopted mapping of NRW-WFS occupancy strings into occupancy classes was the following

- **'AGR': # Agriculture and Forestry**
  - 0: 'Agriculture': 'Gebäude für Land- und Forstwirtschaft', 'Land- und forstwirtschaftlich', 'Landwirtschaft', 'Forstwirtschaft', 'forstwirtschaftlich', 'Windmühle', 'Wassermühle', 'Mühle'
  - 1: 'Agricultural storage': 'Silo', 'Speichergebäude'
  - 2: 'Animal shelter': 'Scheune und Stall', 'Scheune', 'Stall', 'Stall für Tiergroßhaltung', 'Reithalle', 'Stall im Zoo'
  - 3: 'Agricultural processing': 'Farmgebäude', 'Land- und forstwirtschaftliches Betriebsgebäude', 'Treibhaus, Gewächshaus', 'Gewächshaus, verschiebbar', 'Wirtschaftsgebäude', 'Gärtnerei', 'Treibhaus', 'Gartenhaus', 'Gewächshaus (Botanik)', 'Gewächshaus', 'Pflanzenschauhaus'
- **'ASS': # Assembly**
  - 0: 'Assembly': 'Gemeinbedarf', 'Zusammenkunft', 'Empfangsgebäude'
  - 1: 'Religious gathering': 'Gebäude für religiöse Zwecke', 'Gemeindehaus', 'religiös', 'Gotteshaus', 'Kirche', 'Tempel', 'Kloster', 'Kapelle', 'Kirchturm', 'Glockenturm', 'Synagoge', 'Moschee'
  - 2: 'Arena': 'Arena', 'Stadion', 'Gebäude im Stadion', 'Zuschauertribüne', 'Zuschauertribüne, überdacht', 'Tribüne'
  - 3: 'Auditorium': 'Auditorium', 'Kino', 'Konzerthalle', 'Konzertgebäude', 'Theater, Oper', 'Theater', 'Oper', 'Veranstaltungsgebäude', 'Festsaal'
  - 5: 'Club house': 'Freizeit-, Vereinsheim, Dorfgemeinschafts-, Bürgerhaus', 'Clubgebäude', 'Vereinsheim', 'Seniorenfreizeitstätte', 'Jugendfreizeitheim'
  - 6: 'Cemetery': 'Friedhofsgebäude', 'Trauerhalle', 'Krematorium', 'Friedhof'
  - 7: 'Exhibition': 'Ausstellung, Messe', 'Ausstellungshalle', 'Messehalle'
- **'COM': # Commercial and public**
  - 0: 'Commercial': 'Gebäude für Wirtschaft oder Gewerbe', 'Gebäude für Gewerbe und Industrie', 'Sonstiges Gebäude für Gewerbe und Industrie', 'Wirtschaft oder Gewerbe', 'kommerziell', 'Wirtschaft', 'Gewerbe', 'Atelier', 'Gebäude für Fernmeldewesen', 'Funk- u. Fernmeldewesen', 'Rundfunk-, Fernsehen', 'Kommunikation', 'Telekommunikation', 'Rundfunk', 'Television', 'Fernmeldewesen'
  - 1: 'Retail trade': 'Gebäude für Handel und Dienstleistungen', 'Handel und Dienstleistungen', 'Einzelhandel', 'Kaufhaus', 'Einkaufszentrum', 'Mall', 'Markthalle', 'Supermarkt', 'Geschäftsgebäude', 'Geschäft', 'Laden', 'Kiosk', 'Store', 'Apotheke'
  - 2: 'Wholesale trade': 'Lagerhalle, Lagerschuppen, Lagerhaus', 'Gebäude für Vorratshaltung', 'Kühlhaus', 'Großhandel', 'Lagerhaus', 'Vorratshaltung', 'Speditionsgebäude', 'Lager', 'Warenhaus', 'Deposit'
  - 3: 'Offices and services': 'Bürogebäude', 'Büro', 'Versicherung', 'Dienstleistung', 'Werkstatt', 'Wartehalle', 'Fahrzeughalle', 'Zahnarzt', 'Arztpraxis'

STR 20/02. GFZ German Research Centre for Geosciences.
DOI: 10.2312/GFZ.b103-20026

- 5: 'Entertainment': 'Freizeit- und Vergnügungsstätte', 'Unterhaltung', 'Vergnügungsstätte', 'Spielhalle', 'Kegel-, Bowlinghalle', 'Bowling', 'Kasino', 'Spielkasino'
- 6: 'Public building': 'Gebäude für öffentliche Zwecke', 'öffentlich', 'Bibliothek, Bücherei', 'Bibliothek', 'Touristisches Informationszentrum', 'touristisch', 'Tourist', 'Museum', 'Bücherei', 'Gebäude für kulturelle Zwecke', 'kulturell', 'historisch', 'Burg, Festung', 'Burg', 'Festung', 'Schloss', 'Schloss-, Burgturm', 'Burgturm', 'Stadtmauer', 'Befestigung (Burgruine)', 'Torturm', 'Stadtturm'
- 7: 'Parking': 'Gebäude zum Parken', 'Tiefgarage', 'Parkdeck', 'Parkhaus', 'Fahrzeughalle', 'Parken'
- 8: 'Bus station': 'Bushaltestelle', 'Busbahnhof'
- 9: 'Railway station': 'S-Bahnhof', 'Bahnhofsgebäude', 'Bahnstation', 'Bahnhof'
- 10: 'Airport': 'Flughafen'
- 11: 'Recreation and leisure': 'Sport-, Turnhalle', 'Gebäude für Sportzwecke', 'Sportzwecke', 'Turnhalle', 'Fitnesscenter', 'Sporthalle', 'Freizeitgestaltung', 'Gebäude zur Freizeitgestaltung', 'Freizeit', 'Gebäude für Erholungszwecke', 'Gebäude für andere Erholungseinrichtung', 'Erholungszwecke', 'Erholungseinrichtung', 'Empfangsgebäude des Zoos', 'Zoo', 'Gebäude im Zoo', 'Gebäude im Freibad', 'Gebäude- u. Freifläche Erholung, Zoologie', 'Sportplatz', 'Gebäude zum Sportplatz', 'Sprungschanze', 'Freibad', 'Badegebäude', 'Hallenbad', 'Tierschauhaus', 'Empfangsgebäude des botanischen Gartens', 'botanischen Garten', 'botanischer Garten', 'Gebäude im botanischen Garten', 'Gebäude- u. Freifläche Erholung, Botanik', 'Aquarium, Terrarium, Voliere', 'Aquarium', 'Terrarium', 'Voliere', 'Campingplatzgebäude', 'Gebäude- u. Freifläche Erholung, Camping', 'Wochenend- und Ferienhausfläche'
- 12: 'Harbor': 'Hafen'
- 13: 'Subway station': 'U-Bahnhof'
- 14: 'Hotel': 'Gebäude für Beherbergung', 'Hotel, Motel, Pension', 'Jugendherberge', 'Hütte (mit Übernachtungsmöglichkeit)', 'Hotel', 'Motel', 'Hostel', 'Pension', 'Beherbergung'
- 15: 'Restaurant': 'Gebäude für Bewirtung', 'Gaststätte, Restaurant', 'Restaurant', 'Catering', 'Bewirtung', 'Kantine', 'Cafeteria', 'Gaststätte'
- 16: 'Bank': 'Bankfiliale', 'Bank', 'Kreditinstitut', 'Finanzdienstleistung'
- 17: 'Post': 'Post'
- 18: 'Gas station': 'Waschstraße, Waschanlage, Waschhalle', 'Tankstelle', 'Waschstraße, Waschanlage, Waschhalle', 'Waschstraße', 'Waschanlage', 'Waschhalle'

- **'EDU': # Education and research**
  - 0: 'Education and research': 'Bildung'
  - 1: 'Pre-school': 'Kinderkrippe, Kindergarten, Kindertagesstätte', 'Vorschule', 'Kinderkrippe', 'Kindertagesstätte', 'Krippe', 'Kindergarten'
  - 2: 'School': 'Schule', 'Klassenraum', 'Allgemeinbildende Schule', 'Allgemein bildende Schule'
  - 3: 'College and university': 'Gebäude für Bildung und Forschung', 'Bildung und Forschung', 'Hochschulgebäude (Fachhochschule, Universität)', 'Berufsschule',

STR 20/02. GFZ German Research Centre for Geosciences.
DOI: 10.2312/GFZ.b103-20026

'Berufsbildende Schule', 'Hochschulgebäude', 'Fachhochschule', 'Hochschule', 'Universität'
  - 4: 'Research': 'Forschung', 'Forschungsinstitut', 'Labor', 'Gebäude für Forschungszwecke', 'Forschungszwecke'
- **'EME': # Emergency**
  - 0: 'Emergency': 'Notfall', 'Gebäude für Sicherheit und Ordnung', 'Sicherheit und Ordnung'
  - 1: 'Police': 'Polizei', 'Polizeistation', 'Polizeiwache'
  - 2: 'Fire': 'Feuerwehr', 'Feuerwachturm'
- **'GOV': # Government**
  - 0: 'Government': 'Regierung', 'Behörde', 'Bezirksregierung', 'Kreisverwaltung'
  - 1: 'Administration': 'Verwaltungsgebäude', 'Administration', 'administrativ'
  - 3: 'Townhall': 'Rathaus'
  - 4: 'Diplomatic mission': 'Botschaft, Konsulat', 'Botschaft', 'Konsulat'
  - 5: 'Parliament': 'Parlament'
  - 6: 'Court house': 'Gerichtsgebäude', 'Gericht'
  - 7: 'Tax and customs': 'Zollamt', 'Zoll', 'Finanzamt'
  - 8: 'Prison': 'Gefängnis', 'Justizvollzugsanstalt'
- **'IND': # Industrial**
  - 0: 'Industrial': 'industriell', 'Industrie'
  - 1: 'Heavy industrial': 'Schwerindustrie', 'Kühlturm', 'Gebäude zur Gasversorgung', 'Gebäude und Freifläche Versorgungsanlage, Gas', 'Gaswerk', 'Gasversorgung', 'Gasometer', 'Sägewerk', 'Hochofen', 'Grundstoffgewinnung', 'Gebäude zur Grundstoffgewinnung', 'Gebäude für Grundstoffgewinnung', 'Grundstoff', 'Saline', 'Gradierwerk', 'Bergwerk', 'Förderturm', 'Mine'
  - 2: 'Light industrial': 'Leichtindustrie', 'Gebäude zur Versorgung', 'Gebäude zur Versorgungsanlage', 'Fabrik', 'Brennerei', 'Brauerei', 'Produktionsgebäude'
  - 3: 'Company building': 'Betriebsgebäude'
  - 6: 'Container': 'Tank', 'Container', 'Wasserbehälter', 'Kesselhaus'
  - 8: 'Crane': 'Laufkran, Brückenlaufkran', 'Brückenlaufkran', 'Laufkran', 'Portalkran', 'Drehkran', 'Kran'
  - 9: 'Shipyard': 'Werft (Halle)', 'Werft'
- **'LIF': # Buildings related to lifelines**
  - 0: 'Lifelines': 'Gebäude an unterirdischen Leitungen', 'Gebäude- und Freifläche Versorgungsanlage', 'Versorgungsanlage', 'Versorgung'
  - 1: 'Water': 'Wasserversorung', 'Gebäude zur Wasserversorgung', 'Gebäude- und Freifläche Versorgungsanlage, Wasser', 'Pumpwerk (nicht für Wasserversorgung)', 'Wasserturm', 'Wasserwerk', 'Pumpstation', 'Pumpwerk', 'Turbinenhaus', 'Schöpfwerk'
  - 2: 'Electricity': 'Gebäude zur Energieversorgung', 'Gebäude zur Elektrizitätsversorgung', 'Gebäude- und Freifläche Versorgungsanlage, Elektrizität', 'Energieversorgung', 'Energie', 'Elektrizitätsversorgung', 'Elektrizitätswerk', 'Elektrizität', 'Kraftwerk', 'Kohlekraftwerk', 'Atomkraftwerk', 'Reaktorgebäude', 'Gebäude- und Freifläche Versorgungsanlage, Wärme', 'Heizwerk', 'Biogasanlage', 'Windturbine', 'Windrad', 'Solarzellen', 'photovoltaisch', 'Umformer', 'Umspannwerk', 'Transfomer', 'Umwandler'

STR 20/02. GFZ German Research Centre for Geosciences.
DOI: 10.2312/GFZ.b103-20026

  - 3: 'Communications': 'Wetterstation', 'Funkturm', 'Funkmast', 'Fernmeldeturm'
  - 4: 'Sewage treatment': 'Gebäude der Kläranlage', 'Gebäude zur Abwasserbeseitigung', 'Abwasseraufbereitung', 'Abwasserbeseitigung', 'Kläranlage', 'Entsorgung'
  - 5: 'Waste disposal': 'Gebäude zur Entsorgung', 'Gebäude- und Freifläche Entsorgungsanlage', 'Müllbunker', 'Gebäude zur Müllverbrennung', 'Gebäude der Abfalldeponie', 'Gebäude zur Abfallbehandlung', 'Müllkippe', 'Abfalldeponie', 'Abfallbehandlung', 'Müllverbrennung', 'Müllbunker'
- **'MIL': # Military**
  - 0: 'Military': 'Militär'
- **'MED': # Healthcare**
  - 0: 'Healthcare': 'Gebäude für Gesundheitswesen', 'Badegebäude für medizinische Zwecke', 'medizinisch', 'Gesundheitswesen'
  - 1: 'Hospital': 'Krankenhaus', 'Klinik', 'Ärztehaus, Poliklinik', 'Polyklinik', 'Poliklinik', 'Rettungsstelle', 'Ärztehaus'
  - 2: 'Sanitorium': 'Heilanstalt, Pflegeanstalt, Pflegestation', 'Nervenheilanstalt', 'Heilanstalt', 'Pflegeanstalt', 'Pflegestation', 'Sanatorium', 'Gebäude für Kurbetrieb', 'Kurbetrieb', 'Kur'
- **'RES': # Residential**
  - 0: 'Residential': 'Wohngebäude', 'Wohngebäude mit Gemeinbedarf', 'Land- und forstwirtschaftliches Wohngebäude', 'Farmhaus', 'Bauernhaus', 'Wohn- und', 'mit Wohnen', 'Wohnen', 'Wohn'
  - 1: 'Single dwelling': 'Wohnhaus', 'Einfamilienhaus', 'Hütte', 'Almhütte'
  - 2: 'Multi-unit': 'Mehrfamilienhaus'
  - 3: 'Temporary': 'Sommerhaus', 'Ferienhaus', 'Wochenendhaus', 'vorübergehende Unterkunft', 'Schuppen', 'Schutzhütte', 'Schutzbunker', 'Hütte (ohne Übernachtungsmöglichkeit)', 'Jagdhaus, Jagdhütte', 'Jagdhaus', 'Jagdhütte', 'Forsthaus'
  - 4: 'Institutional housing': 'institutionelles Wohnen', 'Studenten-, Schülerwohnheim', 'Altenheim', 'Seniorenheim', 'Obdachlosenheim', 'Studentenwohnheim', 'Schülerwohnheim', 'Schwesternwohnheim', 'Kinderheim', 'Asylbewerberheim', 'Wohnheim', 'Schullandheim', 'Kaserne'
  - 5: 'Mobile home': 'Wohnwagen'
- **'TRA': # Buildings related to traffic and transportation**
  - 0: 'Traffic and transportation': 'Verkehrsanlagen', 'Betriebsgebäude zu Verkehrsanlagen (allgemein)', 'Verkehr'
  - 1: 'Maritime traffic': 'Schiffsverkehr', 'Betriebsgebäude für Schiffsverkehr', 'Empfangsgebäude Schifffahrt', 'Gebäude und Freifläche zu Verkehrsanlagen, Schifffahrt', 'Werft (Halle)', 'Dock (Halle)', 'Schleuse', 'Betriebsgebäude zur Schleuse'
  - 2: 'Bus traffic': 'Gebäude zum Busbahnhof', 'Busdepot'
  - 3: 'Railway traffic': 'Gebäude zum S-Bahnhof', 'Gebäude- und Freifläche zu Verkehrsanlagen, Schiene', 'Betriebsgebäude für Schienenverkehr', 'Betriebsgebäude des Güterbahnhofs', 'Schienenverkehr', 'Güterbahnhof', 'Bahnwärterhaus', 'Stellwerk, Blockstelle', 'Stellwerk', 'Lokschuppen,

STR 20/02. GFZ German Research Centre for Geosciences.
DOI: 10.2312/GFZ.b103-20026

Wagenhalle', 'Blockstelle', 'Gebäude- und Freifläche zu Verkehrsanlagen, Schiene', 'Schiene'
  - 4: 'Subway line': 'Gebäude zum U-Bahnhof', 'U-Bahn'
  - 5: 'Flight traffic': 'Betriebsgebäude für Flugverkehr', 'Flugverkehr', 'Gebäude- und Freifläche zu Verkehrsanlagen, Luftfahrt', 'Flughafengebäude', 'Flugzeughalle', 'Hangar', 'Kontrollturm'
  - 6: 'Road': 'Betriebsgebäude für Straßenverkehr', 'Gebäude- und Freifläche zu Verkehrsanlagen, Straße', 'Straßenverkehr', 'Straße', 'Straßenmeisterei'
  - 7: 'Ropeway': 'Seilbahn', 'Betriebsgebäude zur Seilbahn', 'Spannwerk zur Drahtseilbahn'
- **'OTH': # Other occupancy type**
  - 1: 'Non-occupied': 'leerstehend', 'Denkmal', 'Gedenkstätte', 'Denkstein', 'Standbild', 'Stange', 'Mast', 'Schornstein, Schlot, Esse', 'Schornstein', 'Schlot', 'Esse', 'Aussichtsplattform', 'Aussichtsturm', 'Wachturm', 'Warte'
  - 2: 'Garage': 'Garage', 'Bootshaus', 'Carport', 'überdacht', 'Überdachung', 'Dach'
- **'UNK': # Unknown**
  - 'Quellenlage nicht zu spezifizieren', 'anders', 'unbekannt', 'sonstiges', 'nicht zu spezifizieren', 'betrieblich', 'Betrieb', 'Gebäude für soziale Zwecke', 'Gebäude für betriebliche Sozialeinrichtung', 'sozial', 'Sozialdienst', 'soziale Einrichtung', 'Sozialeinrichtung', 'Toilette'

STR 20/02. GFZ German Research Centre for Geosciences.
DOI: 10.2312/GFZ.b103-20026

ISSN 2190-7110